

https://dspace.org/

The distribution of germanium in polymetallic sulphide assemblages: case studies from Kipushi and Tsumeb

Stewart, Caitlin Nesta

2020

https://hdl.handle.net/10539/31015

Downloaded from a DSpace repository. https://dspace.org/

THE DISTRIBUTION OF GERMANIUM IN POLYMETALLIC SULPHIDE ASSEMBLAGES: CASE STUDIES FROM KIPUSHI AND TSUMEB



Caitlin Nesta Stewart

A dissertation submitted to the Faculty of Science, University of the Witwatersrand, Johannesburg, in fulfilment of the requirements for the degree of Master of Science.

Johannesburg, 2020

Declaration

I, Caitlin Stewart, declare that this dissertation is my own, unaided work. It is being submitted for the degree of Master of Science at the University of the Witwatersrand, Johannesburg. It has not been submitted before for any degree or examination at any other University.



_____

Caitlin Stewart

On this the 5th day of August 2020 at Olivedale, Johannesburg.

Abstract

Germanium (Ge) is considered a critical raw material within the EU and USA, as it is becoming more valuable and in demand as its technological uses increase. Ge is used to create solar panels, and is used in fibre optics, and infra-red optics. Two African deposits contain the highest known grades of Ge globally, Kipushi in the DRC and Tsumeb in Namibia. Both are Pb-Zn-Cu deposits that have been mined in the past. Both of these deposits are referred to as 'Kipushi-type' deposits; these are epigenetic, carbonate-hosted polymetallic pipe-like ore bodies. Most of the Ge in these deposits is hosted in the Ge-bearing sulphides, renierite and germanite; however, Ge has also been found to concentrate into some of the other sulphides. Past studies suggest that Ge concentrates into the sphalerite in various sulphide ore deposits, by substituting with the Zn, as these two elements have the same ionic radius and ionic charge. A Tescan Integrated Mineral Analyser (TIMA) was used to determine the distribution of the Ge within the Kipushi and Tsumeb deposits. Element maps show that the Ge is not concentrated in the sphalerite, but is rather concentrated in the galena and tennantite in both Kipushi and Tsumeb. This suggests that the Ge is substituting for Pb in the galena ($Ge^{2+} \leftrightarrow Pb^{2+}$; $Ge^{4+} \leftrightarrow Pb^{4+}$), as these two elements have the same ionic charge, but do not have the same ionic radius, this substitution is possible at high temperatures. The Ge has substituted for Cu in the tennantite ($Ge^{2+} \leftrightarrow Cu^{2+}$) as these two elements have the same ionic radius and charge. Ge will concentrate into these mineral phases when the Ge-bearing sulphides are both present and absent in the sulphide assemblages. Knowing where the Ge is concentrated will assist in the best possible extraction of the element for the future mining of these deposits, making more Ge available to the electronics market.

Dedication

I dedicate this dissertation to myself. For all my hardships and prosperity through some of the most difficult months of my life. I never gave up, and I too have now lived this adventure.

“I am and always will be the optimist. The hoper of far-flung hopes and dreamer of improbable dreams.” – The Doctor

Acknowledgements

The greatest of thanks go out to my amazing supervisors, Professors Paul Nex and Judith Kinnaird. Without their continued guidance and enthusiasm this project would not have made it.

The support of the DST-NRF Centre of Excellence for Integrated Mineral and Energy Resource Analysis (DST-NRF CIMERA) towards this research is hereby acknowledged. Opinions expressed and conclusions arrived at are those of the authors, and are not necessarily to be attributed to the Centre. This project would not have been possible without their support.

Thank you to Wirsam Scientific: Vicky Wagner, Jere Classe and the rest of the Wirsam team for the use of the TIMA before it was moved to Wits, and their constant support and making me feel welcome at their offices in Richmond, Johannesburg. Thank you to Louis Coetzee for teaching me how to operate the TIMA with confidence.

Thank you to Solly Theron for helping me with the TIMA side of things for the corrections of the dissertation.

Thank you to Mary Evans for supporting me during the first year of my MSc while I worked a full-time job in her laboratory.

A huge thanks goes to my Wits dads, Caiphas Majola and Sam Tshabalala for their support and the making of all my polished hand specimens, ore blocks and thin sections, even when the thin sections gave them a very hard time.

Thank you to Brayner Nelwalani, from Wits School of Chemical and Metallurgical Engineering, for running the SEM with such efficiency, and allowing time for me in both of our working schedules. Thank you to Alexander Ziegler for teaching me how to use the EPMA, and assisting when it provided great problems.

A huge thank you to Griff Gigler for collecting a sample from the Kipushi ‘Big Zinc’ section during his visit to the DRC for his Masters, and to George Henry for providing me with a sample from Tsumeb from his own personal collection for analysis.

To Erin, thank you for editing my work, making sure all my grammar was correct, and for being a welcome distraction when the work got too much.

To my ‘Cool Kids Gangue’, Kimi, Priyanka and Sarah, you three kept me sane during this tough time. Thank you for being there for me, through the depression and anxiety, and teaching me I can come out on top if I just believe in myself. A big thank you to Sarah, for photographing my polished hand specimens while I was out of the country. A special thanks to Kimi, for helping me improve my writing skills, and believing in me. Another thanks go out to Thomas Jones, Matthew Hales, Kirsten Youlton, and everyone else in G120 for all the encouragement and scientific conversations.

To my human rocks, Mom and Victor, you two have provided me with unconditional love and support through all this craziness. Thank you for all the laughs and the shoulders to cry on, as well as words of encouragement when I needed them most. Thank you for pushing me when I wasn’t feeling motivated, and most of all, thank you for believing in me, when I couldn’t believe in myself.

Table of Contents

Declaration ..... **i**
Abstract ..... **ii**
Dedication ..... **iii**
Acknowledgements ..... **iii**
Table of Contents ..... **v**
List of Figures ..... **vii**
List of Tables ..... **xii**
Chapter 1 ..... **1**
Introduction **1**
Germanium 3
Kipushi 4
Tsumeb 7
Chapter 2 ..... **11**
Sampling and Analytical Methodologies **11**
Petrography 11
X-Ray Diffraction (XRD) 13
Whole Rock Geochemical Analysis 13
Scanning Electron Microscope (SEM) 13
Tescan Integrated Mineral Analyser (TIMA) 14
Electron Probe Micro-Analysis (EPMA) 15
Chapter 3 ..... **18**
Germanium in the Kipushi Deposit **18**
Petrography 18
X-Ray Diffraction 31
Whole Rock Geochemical Analysis 31
Scanning Electron Microscopy and Mineral Analysis 37
Element Maps 38
TIMA Semi-Quantitative Analysis 49
Quantitative Analysis by Electron Microprobe 51
EPMA 51
Chapter 4 ..... **55**
Germanium in the Tsumeb Deposit **55**

Petrography....55
X-Ray Diffraction....65
Whole Rock Geochemical Analysis....65
Scanning Electron Microscopy and Mineral Analysis....70
Element Maps....71
TIMA Semi-Quantitative Analysis....78
Quantitative Analysis by Electron Microprobe....80
Chapter 5....82
Discussion....82
Petrography and Mineral Assemblages....82
Kipushi....82
Tsumeb....83
Whole Rock Trace Element Geochemical Analysis....84
Kipushi....84
Tsumeb....84
Electron Microscopy....84
Kipushi....85
Tsumeb....88
Synthesis....89
Chapter 6....91
Conclusion....91
References....93
Appendix A....98
Appendix B....125
Appendix C....130
Appendix D....206
Appendix E....236
Appendix F....241

List of Figures

Figure 1.1: Map of south-central Africa showing the location of the Kipushi mine within the Lufilian Arc in the DRC, and the location of the Tsumeb mine within the Damara Orogenic Belt of Namibia (modified after Schneider et al., 2007). 3
Figure 1.3: The Kipushi ore body (pink), shown in relation to the Formations from the Nguba Group and the Kipushi fault zone (red dotted line) (inset). Kipushi mine shown in relation to the anticline. (modified after Turner et al., 2018) 5
Figure 1.4: Geological map of the Otavi Mountainland showing the location of the Tsumeb mine (pink star), near-by towns and surrounding mines (yellow stars) (modified after Melcher, 2003). 8
Figure 1.5: Geological cross-section of the Tsumeb deposit's pipe-like ore body cross-cutting the different formations (modified after Melcher, 2003). 9
Figure 3.1: Photomicrograph of sample KP1 in reflected light, showing a bornite-dominant assemblage of massive bornite with chalcocite veining, betekhtinite and renierite, with gangue (black). 20
Figure 3.2: Mineral textures from the bornite-dominant assemblage in reflected light. (a) shows the incomplete replacement with remnant bornite (bn) globules within chalcocite (ccc), and chalcocite veins leading from it from sample KP1. There is also betekhtinite (bt) within bornite. (b) shows the concentrated areas of chalcopyrite (ccp) within bornite, as well as blebby galena (gn) from sample 586a. (c) shows the bi-directional chalcopyrite within bornite from sample KP16. (d) shows blebby renierite (rn), tennantite (tn) and sphalerite (sp) within bornite from sample KP12. .. 21
Figure 3.3: Mineral textures from the bornite-chalcopyrite-dominant assemblage in reflected light. (a) shows the bi-directional chalcopyrite (ccp) laths and sphalerite (sp) within bornite (bn) from sample KP13. (b) shows the network of chalcopyrite as well as tennantite (tn) and sphalerite blebs within bornite from sample 6547. 22
Figure 3.4: Large chalcocite (ccc) veins with the remnant globules of bornite (bn) within chalcocite hosting slightly smaller, blebby renierite (rn) (outlined) veins, all within a base of bornite, from sample 15453b, in reflected light. 22
Figure 3.5: Mineral textures from the chalcopyrite-pyrite-dominant assemblage in reflected light. (a) shows pyrite (py) and much smaller arsenopyrite (aspy) within chalcopyrite (ccp) from sample S2801c. (b) shows the unknown dusty brown grey mineral in sample S2801c. 23
Figure 3.6: Massive chalcopyrite (ccp) and gangue from sample 12492b in reflected light. 23
Figure 3.7: Minerals and their textures from the sphalerite-dominant assemblage in reflected light. (a) shows small chalcopyrite (ccp) blebs within the massive sphalerite (sp) from sample KP11. (b) shows tennantite (tn) as a vein in sample KP11. (c) shows galena (gn) blebs and chalcopyrite forming along a vein in sample KP11. (d) shows arsenopyrite (aspy) within the chalcopyrite, as well as tennantite (tn) and galena veining from sample KP11. 24

Figure 3.8: Photomicrograph of sample 12492f in reflected light, showing massive sphalerite (grey) with an extensive chalcopyrite (yellow) network, with gangue (black). 26
Figure 3.9: Minerals and textures from the sphalerite-chalcopyrite-dominant assemblage in reflected light. (a) shows a small network of galena (gn) among sphalerite (sp) and chalcopyrite (ccp) from sample 6548. Chalcopyrite can be seen to have replaced the gangue. (b) shows the dusty brown-grey mineral among sphalerite and chalcopyrite from sample 6548. 26
Figure 3.10: Minerals and their textures from the sphalerite-bornite-dominant assemblage in reflected light. (a) shows sphalerite (sp) within bornite (bn) alongside blebby renierite (rn), tennantite (tn) and galena (gn) from sample KP2. (b) shows sphalerite within bornite and galena, as well as renierite blebs from sample KP2. (c) shows many tennantite blebs surrounding betekhtinite (bt) in sample KP2. 28
Figure 3.11: Ternary diagram showing where the analysed samples fall with respect to Pb, Zn and Cu. Grey represents the Zn-dominant assemblage-type, purple the Cu-dominant assemblage-type and the brown is the mineralised country rock with bornite veining. 33
Figure 3.12: Graphical representation of trace elements within 10 samples from the Kipushi ore deposit. Sphalerite- and bornite-dominant assemblages are rich in As. Most sphalerite-dominant assemblages have a high concentration of Cd. Ge is more abundant in the bornite-dominant assemblage, and to a lesser extent in the sphalerite-dominant assemblage, and to a much lesser extent in the mineralised country rock. Ag occurs in the bornite-dominant assemblages as well in the bornite rich country rock. 34
Figure 3.13: Ge, in ppm, plotted against Pb, in ppm, showing a slight correlation between the two elements. 35
Figure 3.14: Ge, in ppm, plotted against Ga, in ppm, showing a slight correlation between the two elements. 35
Figure 3.15: Ge, in ppm, plotted against As, in ppm, showing a general correlation between these two elements. 36
Figure 3.16: Ge, in ppm, plotted against Zn, in ppm, showing no correlation between the elements. 36
Figure 3.17: Sb, in ppm, plotted against As, in ppm, showing a general correlation. 37
Figure 3.18: Cd, in ppm, plotted against Zn, in ppm, showing an excellent correlation. 37
Figure 3.19 Full polished thin section image in reflected light showing bornite-dominant sample KP12 and the area selected for TIMA analysis (red circle). 38
Figure 3.20: False colour primary phase map (a) showing sphalerite, bornite and renierite, backscatter electron image and element maps for Zn, Cu, Ge and Fe from sample KP12. These images were all obtained using the TIMA. Ge is concentrated into renierite. 39
Figure 3.21: Full ore block image in reflected light showing bornite-chalcopyrite sample 1216 and the area selected for TIMA analysis (red circle). 40

Figure 3.22: False colour primary phase map (a) showing sphalerite, bornite and quartz (qz), backscatter electron image and element maps for Cu, Zn, Ge and Fe from sample 1216. These images were all obtained using the TIMA. No Ge concentration in any of these phases. 41
Figure 3.23: Full polished thin section image in reflected light showing sphalerite-chalcopyrite-dominant sample 1058 and the area selected for TIMA analysis (red circle). 42
Figure 3.24: False colour primary phase map (a) showing sphalerite, galena, chalcopyrite, bornite, tennantite and renierite, backscatter electron image and element maps for Pb, Cu, Fe, As, Ge and Ga from sample 1058. These iages were all obtained using the TIMA. Ge concentrates into renierite and galena. There is more Ge in renierite than in galena. Galena contains As and Ga, and tennantite contains Pb. 43
Figure 3.25: Full polished thin section image in reflected light showing sphalerite-chalcopyrite-dominant sample 6548 and the areas selected for SEM analysis (red circles). 44
Figure 3.26: Backscatter electron image showing sphalerite, chalcopyrite and tennantite and element maps of Zn, Cu, Fe, Ge and As from sample 6548. These images were all obtained using the SEM. Ge is concentrated into tennantite. 45
Figure 3.27: Backscatter electron image showing sphalerite, galena and chalcopyrite and element maps of Zn, Cu, Fe, Ge and As from sample 6548. These images were all obtained using the SEM. Ge and Ag concentrate into galena. 46
Figure 3.28: Full polished thin section image in reflected light showing sphalerite-dominant sample KP11c and the area selected for TIMA analysis (red circle). 47
Figure 3.29: False colour primary phase map (a) showing quartz (qz), sphalerite, tennantite, galena, chalcopyrite, pyrite and arsenopyrite, backscatter electron image and element maps for Pb, S, Cu, Fe, Ge and As from sample KP11c. These images were all obtained using the TIMA. Ge is concentrated into galena, as is As. The Fe-rich phases, chalcopyrite, pyrite and arsenopyrite all contain Co. 48
Figure 4.1: Photomicrograph of the entire ore block of sample 263 in reflected light, showing massive bornite with chalcocite veins and minor tennantite and galena, and one euhedral pyrite grain with gangue (black). 56
Figure 4.2: Mineral textures from the bornite-dominant assemblage in reflected light. (a) shows small chalcocite (ccc) veins and larger masses of chalcocite all surrounding a tennantite (tn) bleb from sample 263. (b) shows chalcocite veins and two blebs of renierite (rn) from sample 263. (c) shows a large bleb of betekhtinite (bt) in sample 477. (d) shows many blebs of germanite (gm) interspersed with renierite, chalcocite and sphalerite (sp) from sample TS 8 57
Figure 4.3: Mineral textures from the tennantite-dominant assemblage in reflected light. (a) shows a vein of sphalerite (sp) cross-cutting massive tennantite (tn) from sample 470. (b) shows renierite (rn), germanite (gm), digenite (dig) and galena (gn) within the massive tennantite from sample TS7. 58

Figure 4.4: Photomicrograph of entire ore block of sample 8 in reflected light, showing sphalerite, tennantite, bornite and digenite in massive galena, with a single pyrite grain and with gangue (black). 59
Figure 4.5: Mineral textures from the galena-dominant assemblage in reflected light. (a) shows sphalerite (sp) and pyrite (py) from sample 91. (b) shows blebby tennantite (tn) within the massive galena (gn) from sample 253a. (c) shows digentite (dig) within the tennantite from sample 253a. (d) shows small sections of arsenopyrite (aspy) next to tennantite blebs and bornite (bn) TS11. 60
Figure 4.6: Photomicrograph of sample 110 in reflected light, showing massive sphalerite, a galena network and minor digenite, tennantite, bornite, chalcocite and pyrite, with gangue (black). 61
Figure 4.7: Blebby pyrite (pale yellow) throughout the massive sphalerite (dark grey), with gangue (black) of sample 395 in reflected light. 62
Figure 4.8: Ternary diagram showing where the analysed samples fall with respect to Pb, Zn and Cu. Grey represents the Zn-dominant assemblage-type, purple the Cu-dominant assemblage-type, blue is the Pb-dominant assmeblage-type and the brown is the mineralised country rock with bornite veining. 67
Figure 4.9: Graphical representation of trace elements within 10 samples from the Tsumeb ore suite. All samples are rich in As. Ge is only seen in high concentrations in sample 99A, a Cu-dominant sample. Most samples contain high concentrations of Mo. 68
Figure 4.10: Ge, in ppm, plotted against Pb, in ppm, showing no correlation between the two elements. 69
Figure 4.11: Ge, in ppm, plotted against Zn, in ppm, showing no correlation. 69
Figure 4.12: As, in ppm, plotted against Sb, in ppm, showing a slight correlation between the two elements. 70
Figure 4.13: Cd, in ppm, plotted against Zn, in ppm, showing a correlation between the two elements. 70
Figure 4.14: Full polished ore block reflected light image showing sample TS3 and the area selected for TIMA analysis (red rectangle). 72
Figure 4.15: False colour primary phase map (a) showing renierite, galena, tennantite, pyrite and gangue, backscatter electron image and element maps for Pb, As, Ge, Sb, Zn and Ga from bornite-dominant sample TS3. These images were all obtained using the TIMA. 73
Figure 4.16: Full polished ore block reflected light image showing sample 110 and the area selected for TIMA analysis (red rectangle). 74
Figure 4.17: False colour primary phase map (a) showing galena, sphalerite, tennantite, digenite and pyrite, backscatter electron image and element maps for Pb, Zn, Ge, As, Cu, Fe, Co and Ga from sphalerite-dominant sample TS 3. These images were all obtained using the TIMA. 75
Figure 4.18 Full polished ore block reflected light image showing galena-dominant sample TS11 and the area selected for TIMA analysis (red rectangle). 76
Figure 4.19: False colour primary phase map (a) showing galena, tennantite, betekhtinite chalcocite and quartz, backscatter electron image and element maps for

Pb, Cu, Ge, As, Ag and Zn from sample TS11. These images were all obtained using the TIMA. 77
Figure 4.20: Mineral spectrum for unknown grey mineral. Cu, Fe and S suggest it could be betekhtinite, as does this mineral being found within the Tsumeb deposit in the past. 78
Figure 5.1: Ionic radii plotted against ionic charge for various elements found within the Kipushi sulphide mineral assemblages. Data extracted from Shannon (1976)… 87
Figure 6.1: Schematic diagrams, not to scale, of various sulphide mineral assemblages from Kipushi and Tsumeb. The key to the mineralogy for all the minerals used in the other diagrams is shown in (a); gm (germanite), bn (bornite), rn (renierite), bt (betekhtinite), ccp (chalcopyrite), py (pyrite), ccc (chalcocite), gn (galena), tn (tennantite) and sp (sphalerite). (b) shows a renierite-present assemblage from the Kipushi deposit with elements partitioning into the relevant minerals; Ge into renierite, galena and tennantite, in order of abundance, Co into chalcopyrite, and Ag and Ga into the galena. (c) shows a renierite absent assemblage from the Kipushi deposit. Here the Ge partitions into the galena and tennantite. Co still partitions into the chalcopyrite and Ga and Ag into the galena. (d) shows a germanite and renierite-present assemblage from the Tsumeb deposit. The Ge partitions into the germanite, renierite, galena and tennantite, in order of abundance. Ga and Ag also partition into the galena, and Co concentrates into the pyrite. 92

List of Tables

Table 1.1: Major and minor Ge-bearing sulphide minerals from the Kipushi and Tsumeb deposits, with their chemical formula 2
Table 1.2: Lithostratigraphic column representing the upper portion of the Katanga Supergroup. The Kipushi deposit is located within the carbonates of the Kaponda, Kakontwe and Kipushi Formations. 5
Table 1.3: Assemblages from De Vos et al. (1974) including dominant, accessory and trace minerals that defined each assemblage. 7
Table 1.4: Stratigraphic column of the Otavi Mountainland, Namibia. The Tsumeb deposit is located within the dolomites of the Elandshoek and Huttenberg Formations. 8
Table 2.1: Samples from the Hughes (1987) PhD sample suite with localities within the Tsumeb mine mentioned in Hughes (1987). 11
Table 2.2: Fist-sized hand-samples selected for polishing. Nine of the selected samples were Cu-dominant, eight of which were the bornite-dominant, and one which was the chalcopyrite-dominant. The one bornite-dominant and the chalcopyrite-dominant sample were mineralised country rocks. Three samples selected were sphalerite-dominant from the Zn-dominant assemblage type. 12
Table 2.3: Ore blocks made from the samples selected from the Kipushi and Tsumeb sample suites. The 14 polished ore blocks from Kipushi are Cu-dominant assemblage types, while the remaining 3 are mineralised country rock. Sixteen ore blocks were selected from the Cu-dominant assemblage type from the Tsumeb suite, 7 samples each from the Pb- and Zn-dominant assemblage types, and 11 mineralised country rocks. 12
Table 2.4: All the Kipushi samples used for this dissertation are detailed below. The tick indicates the methods each sample has undergone. Samples are colour-coded to the basic assemblage-type. Purple represents the Cu-dominant assemblage-type, grey the Zn-dominate assemblage-types and brown is the mineralised country rock. 16
Table 2.5: All the Tsumeb samples used for this dissertation are detailed below. The tick indicates the methods each sample has undergone. Samples are colour-coded to the basic assemblage-type. Purple represents the Cu-dominant assemblage-type, blue the Pb-dominant assemblage-type, grey is the Zn-dominate assemblage-type and brown is the mineralised country rock. 17
Table 3.1: Table detailing samples and sample assemblages examined for the Kipushi ore suite. Sample numbers in **bold** were examined using microbeam techniques. 18
Table 3.2: A comprehensive table showing the mineral assemblages for each sample. The purple background represents the Cu-dominant assemblage-type, grey represents the Zn-dominant assemblage-type and the brown represents the mineralised country rock. 30
Table 3.3 Results of XRD analysis showing the various mineral phases identified, as well as their weight % determined by the Rietveld methodology. 31

Table 3.4: Results from the whole rock analysis. Amount of each element is measured in ppm. Samples are colour-coded to the basic assemblage-type. Purple represents the Cu-dominant assemblage-type, grey the Zn-dominate assemblage-type, and the brown is the mineralised country rock. 32
Table 3.5: Mineral compositions extracted from the TIMA for bornite, sphalerite and chalcopyrite from sample KP 13, and for renierite from sample KP 2. 50
Table 3.6: Published mineral compositions for bornite, sphalerite, chalcopyrite and renierite compared to the average mineral compositions for the same minerals from the TIMA. (Bornite: Pessic and Olson, 1984; sphalerite: Mondillo et al., 2018; chalcopyrite: Lundstrom et al., 2005; renierite: Sclar and Geier, 1957). 50
Table 3.7: Mineral formula for bornite, sphalerite, chalcopyrite and renierite using the chemical composition obtained from the TIMA 51
Table 3.8: Weight percentage of Ni, Fe, Co, Cu, Zn, Ga, Ge, Ag, In, Zn, Pb and S analysed for 2 points on a renierite phase in sample KP12, and 3 points on a renierite phase in sample KP2. The average of all these analyses is shown in the last row of the table. 52
Table 3.9: Weight percent of S, Fe, As, Cu, Zn, Pb and Ge in a published renierite composition (from Sclar and Geier, 1957) and the average composition obtained from the EPMA from samples KP2 and KP12. 52
Table 3.10: Calculated formula from weight percent for each renierite analysis from the EPMA. 52
Table 3.11: Weight percentage of Ni, Fe, Co, Cu, Zn, Ga, Ge, Ag, In, Zn, Pb and S analysed for 3 points on a galena phase in sample KP2. The average of all these analyses is shown in the last row of the table. 53
Table 3.12: Weight percent of S, Fe, As, Cu, Zn, Pb and Ge in a published galena composition (from Peng et al., 2003) and the average composition obtained from the EPMA from sample KP2. 53
Table 3.13: Weight percentage of Ni, Fe, Co, Cu, Zn, Ga, Ge, Ag, In, Zn, Pb and S analysed for 3 points on a sphalerite phase in sample KP2. The average of all these analyses is shown in the last row of the table. 53
Table 3.14: Weight percent of S, Fe, As, Cu, Zn, Pb and Ge in a published sphalerite composition (Mondillo et al., 2018) and the average composition obtained from the EPMA from sample KP2. 54
Table 4.1: Table detailing samples and sample assemblages examined for the Tsumeb ore suite. Sample numbers in **bold** were examined using microbeam techniques. 55
Table 4.2: A comprehensive table showing the mineral assemblages for each sample. The purple background represents the Cu-dominant assemblage-type, blue represents the Pb-dominant assemblage-type and grey represents the Zn-dominant assemblage-type. 64
Table 4.3 Results of XRD analysis showing the various mineral phases identified, including weight % of each phase by Rietveld method 65
Table 4.4: Results from whole rock analysis. The amount of each trace element is measured in ppm. Samples are colour-coded to the basic assemblage-types. Brown

represents the mineralised country rock, grey represents the Zn-dominant assemblage-type, purple represents the Cu-dominant assemblage-type and blue represents the Pb-dominant assemblage-type. 66
Table 4.5: Mineral compositions extracted from the TIMA for bornite, sphalerite and renierite from sample 125, and for galena, renierite and germanite from sample TS 3. 79
Table 4.6: Published mineral compositions for bornite, sphalerite, galena, renierite and germanite compared to the average mineral compositions for the same minerals from the TIMA. (Bornite: Pessic and Olson, 1984; sphalerite: Mondillo et al., 2018; galena: Peng et al., 2003; renierite and germanite: Sclar and Geier, 1957) 80
Table 5.1: Sulphide mineral assemblages found within the Kipushi sample suite from this study. 82
Table 5.2: Sulphide mineral assemblages found in the Tsumeb deposit of this study. Purple represents the Cu-dominant assemblage-type, blue the Pb-dominant assemblage-type and grey represents the Zn-dominant assemblage-type. 83
Table 5.3: Average TIMA composition for renierite from the Kipushi suite. 87
Table 5.4: Average TIMA compositions for renierite and germanite from the Tsumeb suite. 89

Chapter 1

Introduction

The distribution and concentration of Ge within various sulphide mineral assemblages from the Kipushi and Tsumeb Pb-Zn-Cu deposits have been explored in this study. The results from this study will help determine where in these Pb-Zn-Cu deposits the Ge is found for extraction in high concentrations. The concentration of the Ge has been determined using inductively coupled plasma (ICP) mass spectrometry, while the distribution of the Ge within the various sulphide minerals was determined using element maps created by a scanning electron microscope (SEM) and a Tescan Integrated Mineral Analyser (TIMA).

Germanium (Ge) is a chemical element classified as a metalloid in Group 14 of the periodic table. Because Ge is transparent to infrared light, it is commonly used as lenses and windows for items such as night vision devices, as well as being used to create fibre optics and infra-red optics. (Holl, *et al*., 2007). It is also used within a variety of electronic devices, such as guidance systems, integrated circuit transistors, and thin-film solar cells which are used in satellites (Sinclair, 2014; Fortier, *et al*., 2018). Ge is also used as a catalyst to create polyethylene terephthalate (PET) plastics (Holl *et al*., 2007; Sinclair, 2014; Schultz *et al*., 2017).

Because of this Ge is currently regarded as a critical raw material within the European Union and the United States (Schulz *et al*., 2017; Binnemans *et al*., 2018). A critical raw material can be defined as one which is becoming more valuable and more in demand as technological uses for these metals increase (Graedel *et al*., 2014). They can also have a high economic importance for countries which consider them critical. For example, a raw material can be considered critical when it is at high risk of major supply disruption, which in turn would cause severe negative impacts on a country's economy (Binnemans *et al*., 2018).

The demand for Ge is expected to increase due to a greater demand for Ge in thin-film solar cells and transistors. With the current trend of 'green' technology, many governments are implementing alternative energy sources to carbon-based energy sources. This includes the increased use of solar panels. Ge-based thin-film solar cells

are currently the best performing films for solar panels as they are the most energy efficient cells making them a viable source for both large-scale energy generation and satellites (Fortier *et al*., 2018). According to Pillarisetty (2011) Ge transistors can operate at higher speeds than silicon-based transistors, while using less power. This therefore, makes Ge a more attractive element for future semiconductor technology.

Ge is found in trace amounts within the Kipushi and the Tsumeb deposits located in the Democratic Republic of the Congo and Namibia respectively (Figure 1.1). Ge is found in Ge-bearing minerals, as well as within other sulphide minerals (Table 1.1) in these two southern African deposits (De Vos *et al*., 1974; Melcher, 2003; Stewart, 2015). These two deposits contain the highest known grades of Ge globally (Bernstein, 1985; Melcher and Buchholz, 2014; Holl *et al*., 2007). Both of these deposits are epigenetic, carbonate-hosted polymetallic pipe-like ore bodies, which have been referred to as “Kipushi-type deposits” in the works of Holl *et al*. (2007) and Melcher *et al*. (2006). Kipushi-type deposits comprise polymetallic Pb-Zn-Cu ore that have replaced the carbonate host rock (Melcher *et al*., 2006; Schulz *et al*., 2017). They are different from strata-bound Pb-Zn deposits in that they have high a grade of Cu and As, as well as other uncommon trace elements: Ge, Ga, In and Ag.

Table 1.1: Major and minor Ge-bearing sulphide minerals from the Kipushi and Tsumeb deposits, with their chemical formula

Major Ge-bearing sulphide minerals	**Formula**
Renierite	$(Cu^{1+},Zn)_{11}Fe_4(Ge^{4+},As^{5+})_2S_{16}$
Briartite	$Cu_2(Fe,Zn)GeS_4$
Germanite	$Cu_{26}Fe_4Ge_4S_{32}$
Minor Ge-bearing sulphide minerals	
Galena	PbS
Tennantite	$Cu_6(Cu_4(Fe,Zn)_2)As_4S_{13}$
Sphalerite	ZnS

Ge trace-metal concentrations in both sulphide and coal deposits are not easily available from the literature, or, where available, are of poor quality. In order to rectify this, this study has investigated trace-metal concentrations and the distribution of Ge in polymetallic sulphide assemblages from two deposits in southern Africa. This will ultimately lead to better decision making for further exploration and potential mining of these deposits, as well as in similar deposits worldwide.

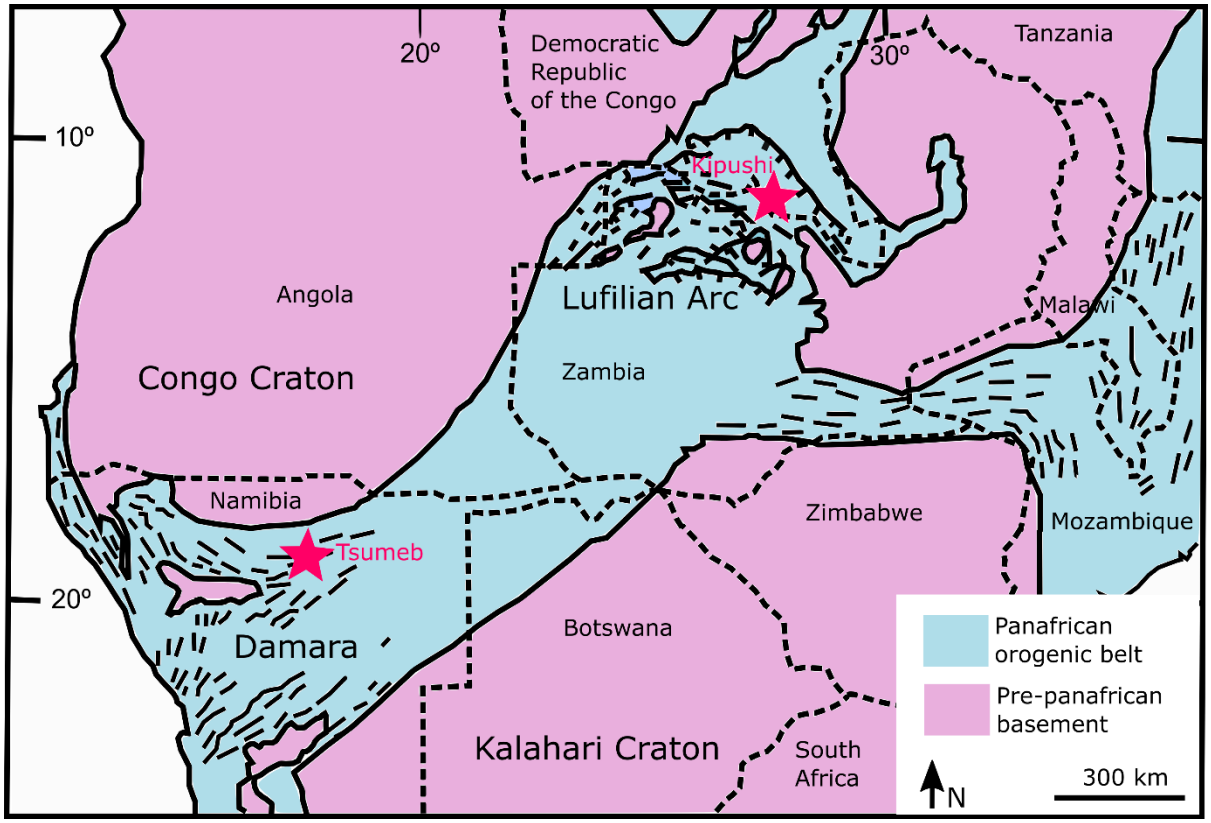

Figure 1.1: Map of south-central Africa showing the location of the Kipushi mine within the Lufilian Arc in the DRC, and the location of the Tsumeb mine within the Damara Orogenic Belt of Namibia (modified after Schneider et al., 2007).

Germanium

Ge, the 32nd element on the periodic table, was first discovered by Clemens Winkler in 1886 after he isolated it from the silver sulphide mineral argyrodite ($AgGeS_6$). Ge has an atomic weight of 72.64 u, putting it in period IVa on the periodic table, just below silicon. It is a grey-white, metallic metal that has electrical properties between that of a metal and an insulator (Holl, *et al.*, 2007).

Ge, when exposed to different environments, can be a lithophile, siderophile, chalcophile or an organophile element (Bernstein, 1985). There are a variety of minerals that contain essential Ge. These minerals fall into the sulphide, oxide, hydroxide, silicate and sulphate classes.

Ge can also occur within other minerals, substituting for other elements within the crystal lattice. Ge^{4+} is very similar chemically to Si^{4+}, therefore Ge is often found substituting for silica within various silicate minerals (Melcher, 2003; Holl *et al*., 2007). Ge is also known to substitute for Fe, Cu, Zn and Pb (Holl *et al*., 2007; Stewart, 2015) in various sulphide minerals. This suggests that Ge will be found in multiple sulphide minerals, not just in the minerals that contain essential Ge, within polymetallic sulphide deposits.

Ge has been found to occur dominantly in Zn sulphide ores (specifically those that contain sphalerite) and in coal and lignite deposits in China and Russia (Bernstein, 1985; Holl *et al*., 2007). Ge has been extracted from slags of Zn-Pb deposits, such as at Tsumeb (Holl *et al*., 2007). Hundreds of ppm of Ge have been found in iron-nickel meteorites, suggesting there is a Ge enrichment within the Earth's core (Bernstein, 1985).

Two massive Ge-rich sulphide deposits have been selected for this petrographic and analytical study.

Kipushi

The Kipushi deposit is located in the south of the Democratic Republic of the Congo, approximately 1 km from the Zambian border. It is about 30 km from the city of Lubumbashi, within the Katanga Province (Lhoest, 1995). Geologically the deposit is found within the Panafrican Lufilian Arc of the Central African Copperbelt (Figure 1.1), hosted in the shallow marine platform carbonates and dolomitic and sandy shales (Kampunzu, *et al.*, 2009) of the Kakontwe Formation of the lower Nguba Group that forms part of the Katanga Supergroup (Table 1.1) (Turner *et al*., 2018).

The deposit lies in the NE limb of the NW-trending Kipushi anticline (Figure 1.2) along a NNE-trending fault that has a ~70° west dip, known as the Kipushi Fault (Figure 1.2 inset) (Turner *et al.*, 2018).

Table 1.2: Lithostratigraphic column representing the upper portion of the Katanga Supergroup. The Kipushi deposit is located within the carbonates of the Kaponda, Kakontwe and Kipushi Formations.

Group	Subgroup	Formation	Lithology
Kundelungu	Ngule	Sampwe	Pelites, sandstones
		Kiubo	Sandstone, siltstone
		Mongwe	Pelites, sandstones
	Gombela	Lubudi	Limestone, carbonates
		Kanianga	Carbonate shales
		Lusele	Dolomite
		Kyandamu	Diamictite
Nguba	Bunkeya	Monwezi	Sandstone, siltstone
		Katete	Sandstone, siltstone
	Muombe	Kipushi	Dolomite
		Kakontwe	Carbonates
		Kaponda	Carbonate shales
		Mwale	Diamictite

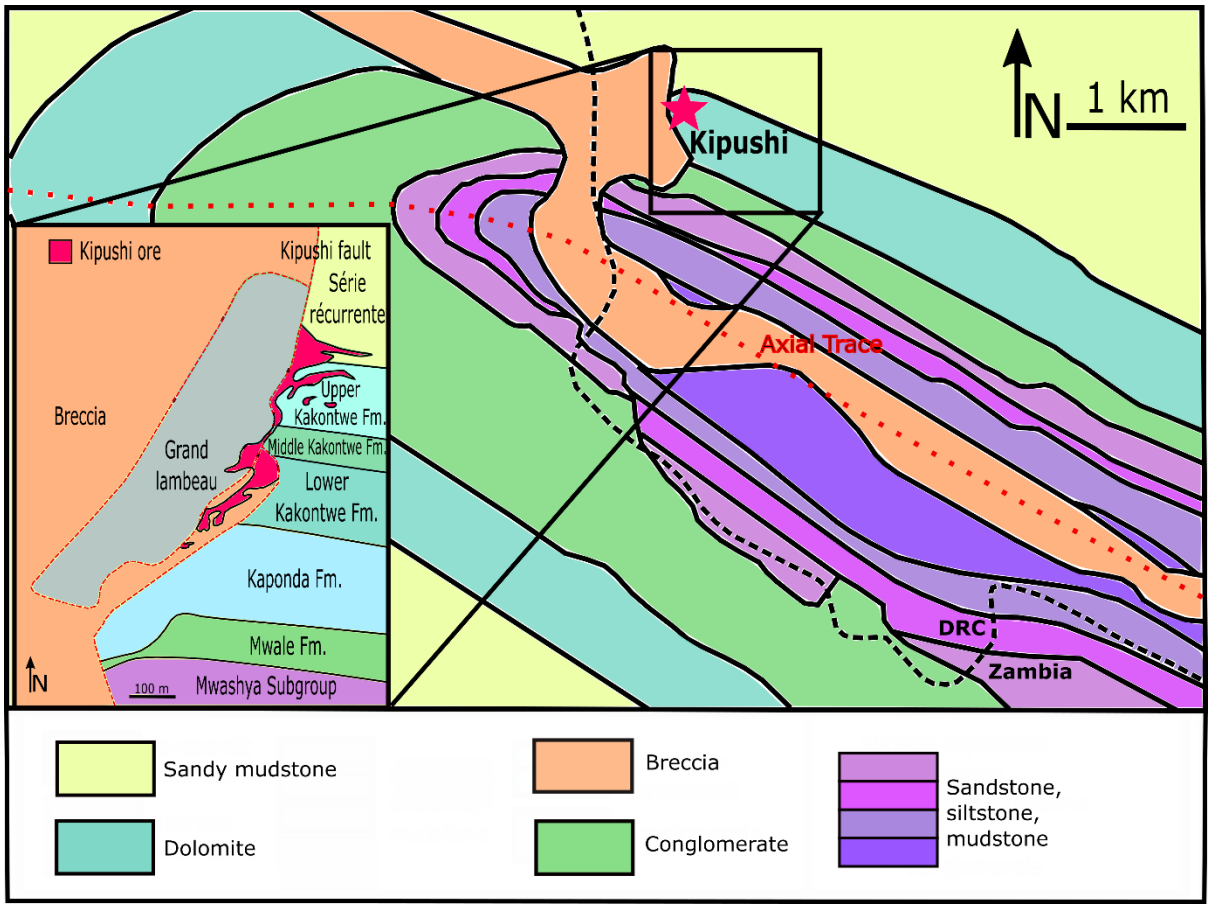

Figure 1.2: The Kipushi ore body (pink), shown in relation to the Formations from the Nguba Group and the Kipushi fault zone (red dotted line) (inset). Kipushi mine shown in relation to the anticline. (modified after Turner et al., 2018)

The mine was originally called the Prince Leopold Mine, until 1966 (Ivanhoe, 2014). The deposit was originally mined for Zn and Cu; however, Ge has been produced from this mine in the past (Ivanhoe, 2014). The mine stopped production in 1993 due to political instability in the country. Ivanhoe Mines Ltd. acquired majority shares of the mine in 2011 with an aim to advance drilling exploration (Ivanhoe, 2014).

The ore body itself is a massive, irregular, subvertical pipe-like body (Figure 1.2 inset) Bernstein, 1985 and Holl, *et al.*, 2007 divided the mine into three Cu-dominated zones, namely, the Fault Zone, the Nord-riche and the Série Récurrente, as well as some Zn-dominated zones, the most notable of which is the unmined Big Zinc (Turner *et al.*, 2018). The high-grade ore occurs as both massive and disseminated ore.

Kipushi is the type locality for Kipushi-type deposits and is also the type locality for the minerals renierite and briartite. Bornite, sphalerite, chalcopyrite, galena, tennantite, pyrite, arsenopyrite and chalcocite are the dominant sulphide minerals with renierite more abundant than briartite (Stewart, 2015). Bornite is usually accompanied by chalcopyrite, tennantite, galena, renierite, chalcocite, and in some cases sphalerite. Massive sphalerite is often found in an assemblage with chalcopyrite, minor galena, tennantite, pyrite and arsenopyrite (Stewart, 2015). Previous studies on the sulphide mineral assemblages at Kipushi divide the assemblages into two main types: Cu-bearing assemblages and Zn-bearing assemblages (De Vos *et al.*, 1974; Dimanche, 1974; Intiomale and Oosterbosch, 1974). These assemblages were each based on the dominant and accessory minerals within the ores (De Vos *et al.* 1974). These assemblages and their mineral constituents are shown in Table 1.2. Stewart (2015) determined there were more assemblages than those described by De Vos *et al.* (1974), due to different accessory minerals and a higher concentration of certain minerals in the samples.

In 2015 a preliminary study was conducted by Stewart (2015) which investigated the distribution and concentration of Ge and Ag within the different sulphide assemblages at Kipushi. This was done using scanning electron microscopy to create element maps that showed the distribution of Ge within the various sulphide minerals. The study found that when the Ge-bearing sulphide renierite was present in the assemblage, Ge concentrated into the renierite. Contrary to previous works, Ge was found to occur preferentially in galena and tennantite, when renierite was absent, rather than into

sphalerite, as suggested by Bernstein (1985), Holl *et al.* (2007), Kampunzu *et al.* (2009), Sinclair (2014) and Mondillo *et al.* (2018).

Table 1.3: Assemblages from De Vos et al. (1974) including dominant, accessory and trace minerals that defined each assemblage.

Type	Assemblage/Dominant Mineral	Accessory Minerals	Trace Minerals
Cu	Chalcopyrite, Pyrite	Arsenopyrite, sphalerite, tennantite, renierite	Marcasite, pyrrhotite, hematite, bismuth
	Chalcopyrite	Sphalerite, tennantite, bornite	Pyrite, arsenopyrite, digenite, renierite, galena
	Bornite	Sphalerite, chalcocite, tennantite, galena, betechtinite	Stromeyerite, covellite, digenite, renierite, shungite, arsenopyrite, linneite, molybdenite, mawsonite, tungstenite, V minerals
Zn	Sphalerite, Pyrite	Arsenopyrite, chalcopyrite, tennantite, galena	Shungite, briartite
	Sphalerite, Chalcopyrite	Arsenopyrite, tennantite, galena	Pyrite, shungite, briartite
	Sphalerite, Bornite	Sphalerite, chalcocite, tennantite, galena, betechtinite	Stromeyerite, covellite, digenite, renierite, shungite, arsenopyrite, linneite, molybdenite, mawsonite, tungstenite, V minerals

The range of sulphur isotopes values of $\delta^{34}S$ for Kipushi of -2.6 to +19.2 ‰, suggest that the possible source for the sulphur was from seawater sulphates (Kampunzu *et al.*, 2009). Rb-Sr and Re-Os isochron dating of sphalerite has determined a mineralisation age of approximately 450 Ma (Schneider, *et al.*, 2007).

Tsumeb

The Tsumeb deposit lies within the Oshikoto Province of Namibia, approximately 60 km from the town of Otavi (Figure 1.3). The deposit occurs within the Otavi Mountainland in Namibia and is hosted within the Damara Supergroup (Table 1.3).

The main ore body is hosted in the carbonates of the Tsumeb Subgroup of the Otavi Group (Figure 1.3) (Melcher, 2003). The Tsumeb deposit is a structurally controlled pipe-like ore body filled by carbonate breccia and sandstone that cross-cuts the dolomites (Figure 1.4) (Melcher, 2006).

Table 1.4: Stratigraphic column of the Otavi Mountainland, Namibia. The Tsumeb deposit is located within the dolomites of the Elandshoek and Huttenberg Formations.

Group	Subgroup	Formation	Lithology
Mulden		Kombat	Shale
		Tschudi	Arenite
Otavi	Tsumeb	Huttenberg	Dolomite, pelite
		Elandshoek	Chert, dolomite
		Maieberg	Limestone
		Ghaub	Diamictite
	Abneb	Gauss	Dolomite
		Berg Aukas	
		Chuos	Diamictite
Nosib		Askevold	Volcanics
		Nabis	Clastics
Grootfontein Basement Complex			

Tsumeb deposit

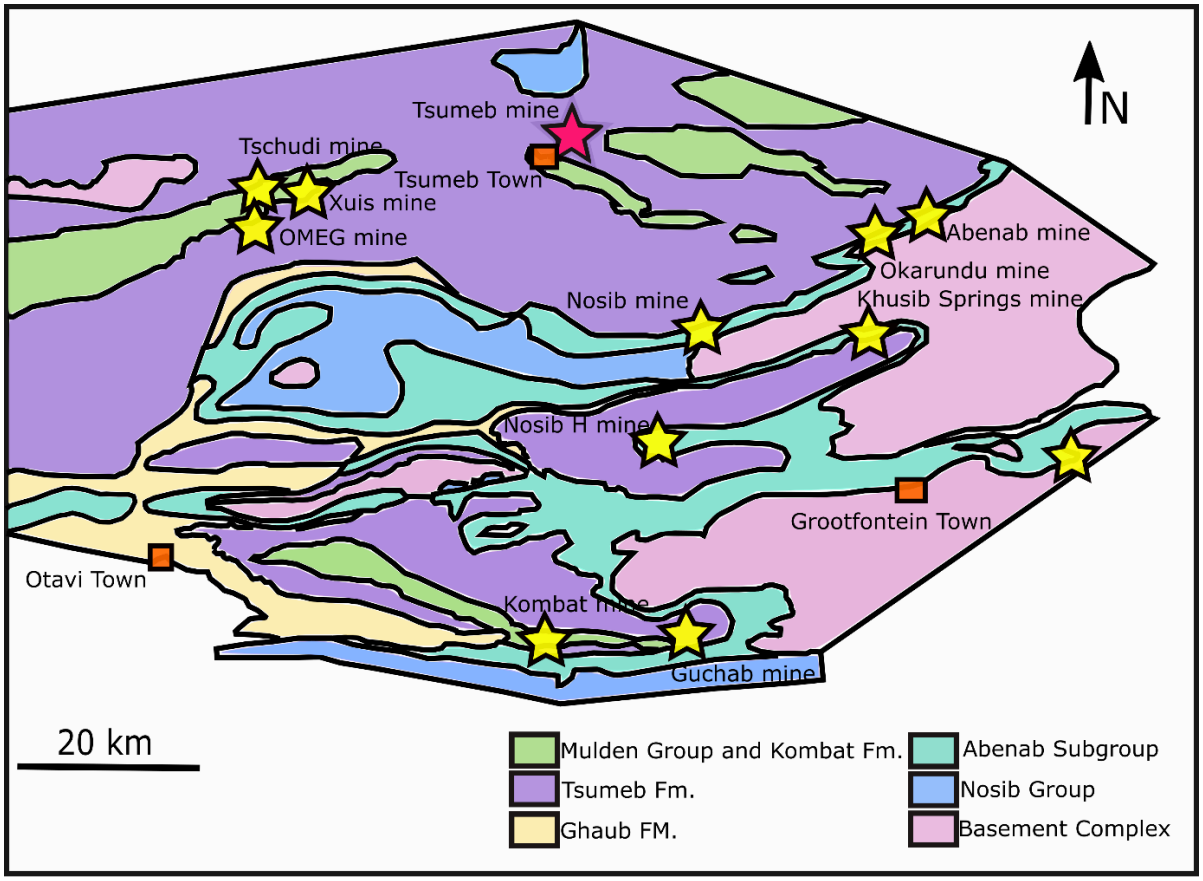

Figure 1.3: Geological map of the Otavi Mountainland showing the location of the Tsumeb mine (pink star), near-by towns and surrounding mines (yellow stars) (modified after Melcher, 2003).

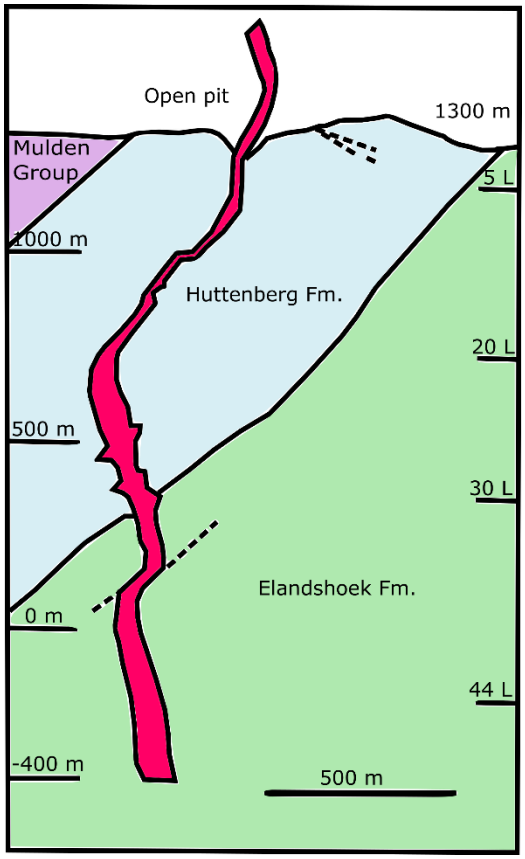

Figure 1.4: Geological cross-section of the Tsumeb deposit's pipe-like ore body cross-cutting the different formations (modified after Melcher, 2003).

The deposit was mined for Pb in the past (Söhnge, 1964), as well as for significant amounts of Zn and Cu (Melcher, 2003). Ge, Ag and Cd were also produced as by-products from the deposit (Söhnge, 1964). The German railway and mining company Otavi-Minen-und Eisenbahngesellschaft (OMEG) mined the deposit from 1907 to 1940. In 1947 the Tsumeb Corporation Limited (TCL) took over mining operations until 1996 (Melcher, 2003), after which time the mine was forced to close due to a major strike by miners and other staff. This downing of tools led to flooding inside the mine and a decision was later made that the mine was not worth draining due to the small amount of economic ore left inside the mine (von Bezing *et al*., 2014). In 2004, Ongopolo Mining and Processing Limited began dewatering the upper levels of the mine in the hope that mining could be resumed (von Bezing *et al*., 2014).

The ore body has zones of varying sulphide concentration and Pb-Zn-Cu grade, with the highest grade on the periphery of the pipe (Melcher, 2003). The major ore minerals found within the Tsumeb deposit are galena, sphalerite, tennantite, bornite, pyrite, digenite, enargite and chalcocite. Many primary Ge minerals have been noted, in fact,

Tsumeb is the type locality for germanite, a Ge-bearing sulphide mineral. Other Ge minerals found at this locality include renierite, and briartite (Melcher, 2003). The germanite and renierite often occur in association with tennantite, sphalerite, bornite, galena, enargite, pyrite and digenite. Renierite has only been uncovered below level 15 of the pipe (Melcher, 2003).

Previous sulphur isotope studies by Melcher (2003) show a $\delta^{34}S$ range of +17 to +27 ‰. This $\delta^{34}S$ range suggests an abiologic reduction process. Similar $\delta^{34}S$ from surrounding deposits suggest a common source of sulphur. Melcher (2003) has suggested this source may have been evaporite beds, possibly from the upper Nosib Group, or within the Tsumeb Subgroup itself.

George *et al.* (2016) states that “there is an abundance of published trace element data for sphalerite, galena and chalcopyrite in natural systems, yet for a co-crystallised assemblage comprising these base metal sulphides, there is no detailed understanding of the preferred host of many trace elements.” Both Kipushi and Tsumeb consist of assemblages with these base metal sulphides, and more. This study hopes to shine a light on the preferred hosts of trace elements within these sulphides.

Chapter 2

Sampling and Analytical Methodologies

Kipushi samples were obtained from the Beloch Geological Museum collection in the School of Geosciences, University of the Witwatersrand. The 29 selected samples were labelled and had accession details which referred to the Prince Leopold Mine, signifying the collection of these samples happened before 1924, from one of the upper levels of the mine. The 39 samples from Tsumeb were selected from the PhD collection of Hughes (1987). Table 2.1 shows the 5 samples with localities within the Tsumeb mine from Hughes (1987).

Table 2.1: Samples from the Hughes (1987) PhD sample suite with localities within the Tsumeb mine mentioned in Hughes (1987).

Sample	Location
TS 3	17L stope 1727 31/1/157
TS 6	2024 x/c S at 527 + 22 m S
TS 7	24L E19 stope S263-2
TS 8	W35/22? 10/8/159
TS 10	1300 1527 stope

Petrography

Thirteen approximately fist-sized samples were selected for polishing and analysis. These sample types are shown in Table 2.2. These samples were cut into approximately 2 cm thick slices, and one surface was polished. These samples were then thoroughly described (Appendix A).

Specific samples from the Kipushi suite were selected to be made into polished thin sections. Six of the 12 selected samples were characterised by a bornite-dominant assemblage and the remaining six samples with a sphalerite-dominant assemblage. A total of 25 polished thin sections were made. Duplicates of many samples were made due to issues during the thin section creation procedure. The rocks, once mounted onto the glass slides, kept breaking during cutting. To prevent this, samples were instead ground down once they had been glued onto the glass sides. The

samples were made to be between 50 and 100 µm, thicker than the average 30 µm thin section. Thin sections were originally chosen rather than a polished ore block because they cause less charge build-up on a scanning electron microscope compared to a polished ore block (Stewart, 2015).

Table 2.2: Fist-sized hand-samples selected for polishing. Nine of the selected samples were Cu-dominant, eight of which were the bornite-dominant, and one which was the chalcopyrite-dominant. The one bornite-dominant and the chalcopyrite-dominant sample were mineralised country rocks. Three samples selected were sphalerite-dominant from the Zn-dominant assemblage type.

Assemblage Type	Assemblage	Number of samples
Cu-dominant	Bornite-domiant	8
	Chalcopyrite-dominant	1
Zn-dominant	Sphalerite-dominant	3

In addition, 17 polished ore blocks were made from the Kipushi suite. A total of 41 polished ore blocks were made from the 39 selected samples from the Tsumeb suite Table 2.3).

Table 2.3: Ore blocks made from the samples selected from the Kipushi and Tsumeb sample suites. The 14 polished ore blocks from Kipushi are Cu-dominant assemblage types, while the remaining 3 are mineralised country rock. Sixteen ore blocks were selected from the Cu-dominant assemblage type from the Tsumeb suite, 7 samples each from the Pb- and Zn-dominant assemblage types, and 11 mineralised country rocks.

	Kipushi	Tsumeb
Assemblage Type	Number of ore blocks	Number of ore blocks
Cu-dominant	14	16
Pb-dominant		7
Zn-dominant		7
Mineralised country rock	3	11

Each of the polished thin sections were scanned and full-section images were created using the Olympus BX63 petrographic microscope available at the University of the Witwatersrand's Microscopy and Microanalysis Unit (MMU). Full-section images of the polished ore blocks were generated using the Olympus BX53 available in the School of Geoscience. Detailed descriptions, as well as small-scale photographs were taken using an Olympus BX 41 petrographic microscope. Detailed petrological descriptions and full-section scans are contained in Appendix A.

X-Ray Diffraction (XRD)

XRD analysis was conducted on 17 samples, 12 samples from Kipushi and 5 samples from Tsumeb. Samples were selected based on the diversity of mineral phases as well as the availability of material from the limited sample suites. Seven samples were selected from Kipushi's Cu-dominant assemblage-type, and 5 samples from the Zn-dominant assemblage-type. A total of 3 samples were selected from the Cu-dominant assemblage-type of the Tsumeb deposit, as well as 1 Zn-dominant and one Pb-dominant assemblage-type. The methodology for the XRD analysis can be found within Appendix F.

Whole Rock Geochemical Analysis

Ten samples from Kipushi and ten samples from Tsumeb were sent to Intertek Genalysis for trace element analysis. Samples could not be analysed at the Wits Earth Lab due to the massive nature of the sulphides; and a specialised method was needed. Samples with similar assemblages from Kipushi and Tsumeb were selected to allow for an adequate comparison of the results. This included bornite-dominant assemblages, some with chalcocite veins, as well as sphalerite-dominant assemblages. One mineralised country rock with a bornite assemblage was selected from each suite. A massive galena sample and a massive tennantite/tetrahedrite sample was selected from the Tsumeb samples to get an accurate Ge concentration for each.

Inductively coupled plasma-optical emission spectroscopy (ICP-OES) and inductively coupled plasma-mass spectrometry (ICP-MS) was used to obtain the whole rock composition for 26 different trace elements. The ICP-MS method was used to detect Ag, As, Be, Bi, Cd, Co, Ga, Ge, In, Li, Mo, Pb, Rb, Re, Sb, Sc, Se, Te, and Tl. The ICP-OES method was used for Cr, Cu, Mn, Na, Ni, and Zn. More details on the methods used can be found in Appendix B.

Scanning Electron Microscope (SEM)

A Zeiss Gemini SEM at the School of Chemical and Metallurgical Engineering at the University of the Witwatersrand was used to create backscatter electron images and element maps for four polished thin sections from the Kipushi sample suite. Samples

with the highest number of minerals were selected, with both renierite-present and renierite-absent assemblages. Polished thin sections were coated in 30 nm of carbon at the MMU.

Element maps for Fe, Cu, Zn, As, Pb, S, Co, Ge, Sb, In and Ga were created for each area of the selected samples. Each area in four of the samples was left to scan for 30 minutes to achieve higher quality maps. Backscatter electron and secondary electron images can be found in Appendix C.

After the analysis of these five samples, access to an improved micro-beam analyser was granted, and used in place of the SEM, so no further samples were analysed using this method.

Tescan Integrated Mineral Analyser (TIMA)

The TIMA was used for extensive analyses on samples from both Kipushi and Tsumeb. Element maps of 17 samples from Kipushi, and 18 samples from Tsumeb were acquired. The same polished thin sections that were analysed on the SEM were re-analysed on the TIMA. Samples were selected from both the bornite-dominant and sphalerite-dominant assemblages, both with and without renierite, as well some galena-dominant and tennantite/tetrahedrite-dominant samples from Tsumeb. Mineralised country rocks from both suites were also analysed. Samples containing galena and sphalerite were given preference, to provide a better comparison of the Ge distribution.

The TIMA is a SEM based auto mineralogy system that identifies minerals by composition, and aids in the quantification of mineral proportions, size and textures. More details on the TIMA can be found in Appendix D.

The TIMA was first used at Wirsam Scientific in Richmond, Johannesburg. The TIMA was later moved to the University of the Witwatersrand, School of Geosciences and used there. Samples were all coated in a 30 nm thick layer of carbon, done at the MMU, and later coated in the Wits Automated Mineralogy Lab (WAM Lab). Multiple areas on each sample were scanned using the high-resolution liberation analysis feature of the TIMA. A pixel size of 2 µm and a working distance of 15 mm were used for each sample.

Backscatter electron images (BSE), false colour primary phase maps, and element maps for Ge, Zn, Pb, Fe, Cu, S, As, Ag, Co, Ga, Sb and In were obtained for each analysis area on the samples. Element maps obtained from the TIMA were in greyscale, and later coloured using Fiji ImageJ software (Schindelin, *et al.*, 2012; Rueden, *et al.*, 2017).

Sample processing was done both online and offline. Unknown phases were identified by comparing the spectra to the TIMA software's database. Once all mineral phases were adequately identified, the same scheme of identified phases was applied to each sample. This allowed for each phase to be identified for the false colour primary phase map.

A normalised weight percent composition was obtained for bornite, sphalerite, chalcopyrite, galena, renierite and germanite. Bornite, chalcopyrite, galena and sphalerite were used as a baseline to indicate the reliability of the analysis.

Electron Probe Micro-Analysis (EPMA)

Five polished thin sections were selected for analysis on the Electron Probe Micro-Analyser (EPMA) at the MMU in order to gather compositional data for each mineral. Initially, while the polished thin sections from Kipushi fitted into the holder, the 3 ore blocks from Tsumeb did not fit into the sample mount holder, and therefore had to be cut down to 25 mm. Samples that contain galena, tennantite/tetrahedrite and sphalerite were analysed, as well as some samples with renierite. Renierite, galena, tennantite/tetrahedrite, and sphalerite were selected for multi-point analysis to determine a weight percent composition.

The full suite of samples and the methods conducted on each sample are outlined for the Kipushi samples (Table 2.4) and the Tsumeb samples (Table 2.5). Each sample is colour-coded to show what assemblage it falls into. Purple represents the Cu-dominant assemblage-type, grey the Zn-dominate assemblage-type, brown is the mineralised country rock and blue the Pb-dominant assemblage-type. Each sample also has its specific assemblage noted.

Table 2.4: All the Kipushi samples used for this dissertation are detailed below. The tick indicates the methods each sample has undergone. Samples are colour-coded to the basic assemblage-type. Purple represents the Cu-dominant assemblage-type, grey the Zn-dominate assemblage-types and brown is the mineralised country rock.

Sample Number	Assemblage-type	Assemblage	Petrography	Whole Rock	SEM	TIMA	EMPA
KP 3	Cu	bn	✓			✓	
KP 12		bn	✓		✓	✓	✓
15452a		bn	✓	✓			
15452b		bn	✓		✓	✓	✓
586a		bn	✓	✓			
586b		bn	✓			✓	
586c		bn	✓			✓	
12492Aa		bn	✓	✓		✓	
12492Ab		bn	✓				
12492Ac		bn	✓				
KP 1		bn	✓				
KP 16		bn	✓				
KP 4		bn	✓				
6547		bn	✓			✓	
587		bn + ccp	✓			✓	
KP 13a		bn +ccp	✓				
KP 13b		bn + ccp	✓			✓	
1216		bn + ccp	✓			✓	
1213		bn + ccp		✓			
15453a		bn + ren	✓	✓			
15453b		bn + ren	✓				
12492a		ccp + py	✓	✓			
S2801c		ccp + py	✓		✓	✓	
12492b		ccp	✓				
KP 11a	Zn	sp	✓	✓		✓	
KP 11b		sp	✓				
KP 11c		sp	✓			✓	
KP 18		sp	✓				
1058a		sp + ccp	✓	✓			
1058b		sp + ccp	✓			✓	✓
6548		sp + ccp	✓		✓	✓	
S2801a		sp + ccp	✓	✓			
12492c		sp + ccp	✓				
12492d		sp + ccp	✓				
12492e		sp + ccp	✓				
12492f		sp + ccp	✓			✓	✓
S2801b		sp + ccp	✓				
KP 17a		sp + bn	✓				
KP 17b		sp + bn	✓				
KP 17c		sp + bn	✓		✓	✓	
KP 2		sp + bn	✓			✓	✓
KP 5a		sp + bn	✓				
KP 5b		sp + bn	✓				
KP 8	Mineralised country	ccp	✓				
KP 6		ccp	✓	✓		✓	
KP 7		bn	✓				

Table 2.5: All the Tsumeb samples used for this dissertation are detailed below. The tick indicates the methods each sample has undergone. Samples are colour-coded to the basic assemblage-type. Purple represents the Cu-dominant assemblage-type, blue the Pb-dominant assemblage-type, grey is the Zn-dominate assemblage-type and brown is the mineralised country rock.

Sample Number	Assemblage-type	Assemblage	Petrography	Whole Rock	TIMA	EMPA
107	Cu	bn	✓			
263		bn	✓		✓	
333		bn	✓		✓	
337		bn	✓			
434 a		bn	✓			
434 b		bn	✓			
477 a		bn	✓	✓		
477 b		bn	✓			
523		bn	✓			
265 C		bn	✓			
99 A a		bn	✓	✓	✓	
99 A b		bn	✓			
717		bn	✓		✓	
TS 7		tn	✓		✓	✓
TS 1		tn	✓	✓		
470		tn	✓	✓		
8	Pb	gn	✓			
259		gn	✓	✓	✓	
560		gn	✓			
91		gn	✓	✓		
340		gn	✓	✓		
423		gn	✓		✓	
TS 11		gn	✓		✓	
110	Zn	sp	✓	✓	✓	
149		sp	✓	✓		
735		sp	✓		✓	
272 A		sp	✓		✓	
519		sp + py	✓			
268		sp + py	✓		✓	
395		sp + py	✓			
125	Mineralised country	bn	✓	✓	✓	
253 b		bn	✓		✓	
TS 6		bn	✓			
TS 8		bn	✓		✓	
TS 9		bn	✓			
TS 10		bn	✓			
TS 3		bn	✓		✓	
TS 4		gn	✓			
TS 5		gn	✓		✓	✓
90		gn	✓			
253 a		gn	✓		✓	✓

The number of samples used in this study was limited due to the availability of samples from the Beloch Geological Museum collection.

Chapter 3

Germanium in the Kipushi Deposit

The Kipushi deposit is an epigenetic, hydrothermal massive sulphide system comprising bornite, chalcopyrite, galena and sphalerite and an abundance of minor sulphides. One of these less abundant sulphide minerals is renierite, a Ge-essential mineral whose type locality is the Kipushi Mine (Gait, 2002). This chapter presents the results of petrology, whole-rock chemistry and SEM studies investigating the presence of Ge in other sulphide minerals of this deposit.

Petrography

The samples from Kipushi have been divided into two main assemblage-types: Cu-dominant and Zn-dominant, which can be broken down into various assemblages (Table 3.1). The Cu assemblages include bornite-dominant, bornite-chalcopyrite-dominant, chalcopyrite-pyrite-dominant and chalcopyrite-dominant. The Zn assemblages include sphalerite-dominant, sphalerite-chalcopyrite-dominant and sphalerite-bornite-dominant. These assemblages have been previously defined in the work of Stewart (2015), based on the work of De Vos *et al.* (1974). All samples were examined under reflected light using a petrographic microscope and images of complete polished thin sections and ore blocks were acquired using an Olympus BX53 microscope and an Olympus BX63 microscope (Appendix A.2.1).

*Table 3.1: Table detailing samples and sample assemblages examined for the Kipushi ore suite. Sample numbers in **bold** were examined using microbeam techniques.*

Assemblage type	Dominant Sulphide	Sample #
Copper	Bornite	**586, 6547, 12492 A**, KP 1, KP 3, KP 4, KP 7, **KP 12**, KP 16
	Bornite-chalcopyrite	**587, 1216, KP 13**
	Bornite-renierite	**15453**
	Chalcopyrite-pyrite	12492a, **S280, 1 c**
	Chalcopyrite	**KP 6,** KP 8, 12492 b
Zinc	Sphalerite	KP 18, **KP 11**
	Sphalerite-chalcopyrite	**1058, 6548, 12492** c-**f**, S2801 a,b
	Sphalerite-bornite	**KP 2**, KP 5, **15452, KP 17**

Cu Assemblages

Bornite-dominant

Most of the Kipushi samples exhibit a bornite-dominant assemblage which also contains various other Cu-sulphides. A photomicrograph of the entire ore block of sample KP1 shows the bornite-dominant assemblage (Figure 3.1). This comprises massive bornite with chalcocite veins, an unknown grey mineral and renierite. Chalcocite veins replacing bornite are very common in this assemblage, and incomplete replacement is shown by remnant globules of bornite within chalcocite (Figure 3.2a). Areas with a high concentration of chalcopyrite are found within some of these samples (Figure 3.2b). Another sample (KP16) has bi-directional chalcopyrite laths within bornite, possibly showing replacement processes (Figure 3.2c). This assemblage also contains occasional renierite, galena and tennantite. Both renierite and tennantite occur as large to small blebs (Figure 3.2c, d). Galena usually forms blebs within chalcopyrite and bornite, suggesting that it is a late replacement of most minerals (Figure 3.2b). Rounded sphalerite can also be found in this assemblage (Figure 3.2d). In some cases, an unknown grey mineral that is anisotropic pinkish brown to grey in crossed polars, is seen (Figure 3.2a). After SEM analysis, this phase was identified to be most likely betekhtinite ($Cu_{10}(Fe,Pb)S6$), as this is a previously identified mineral within the Kipushi deposit. In some samples, such as 587, carrollite has also been noted.

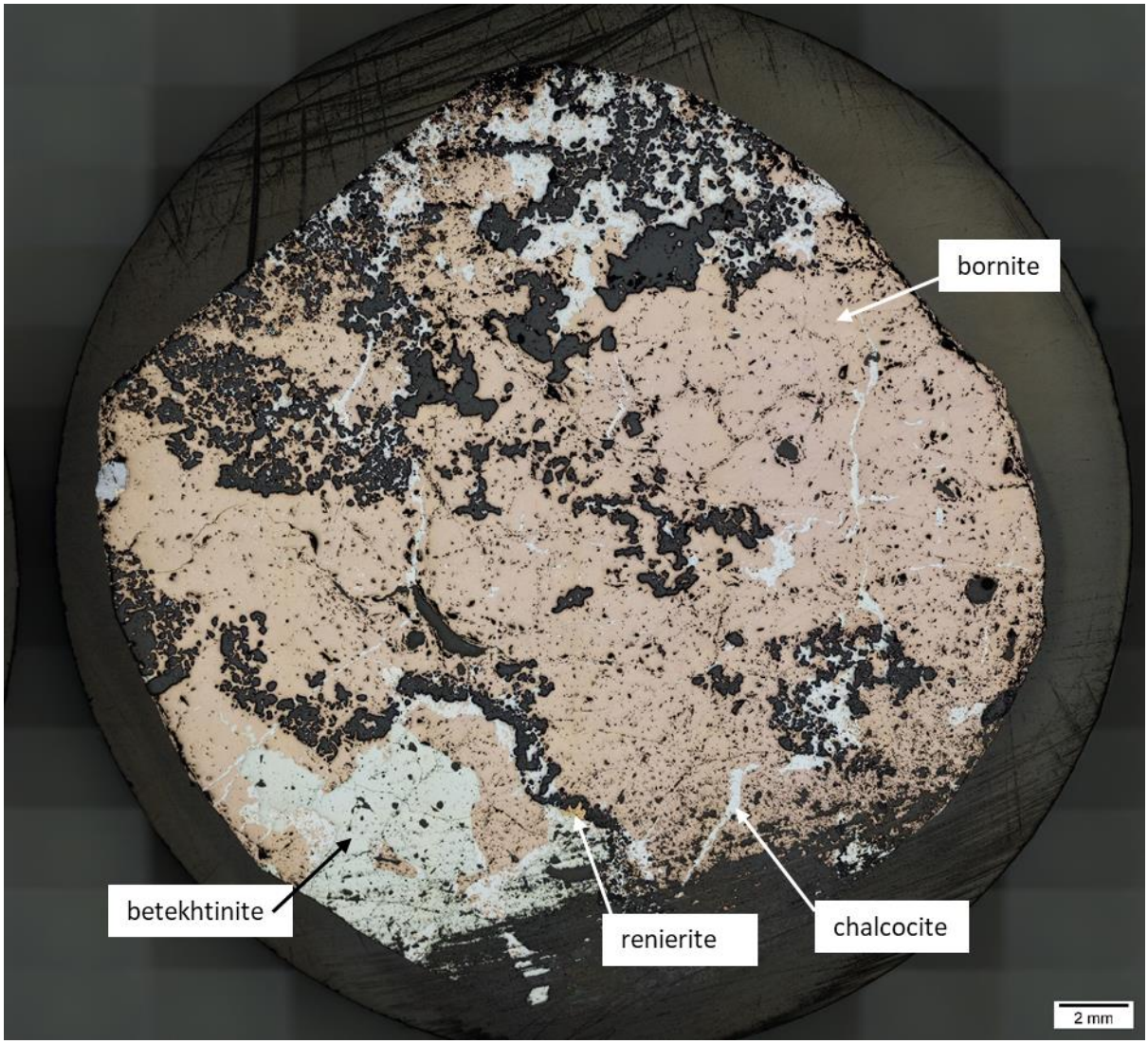

Figure 3.1: Photomicrograph of sample KP1 in reflected light, showing a bornite-dominant assemblage of massive bornite with chalcocite veining, betekhtinite and renierite, with gangue (black).

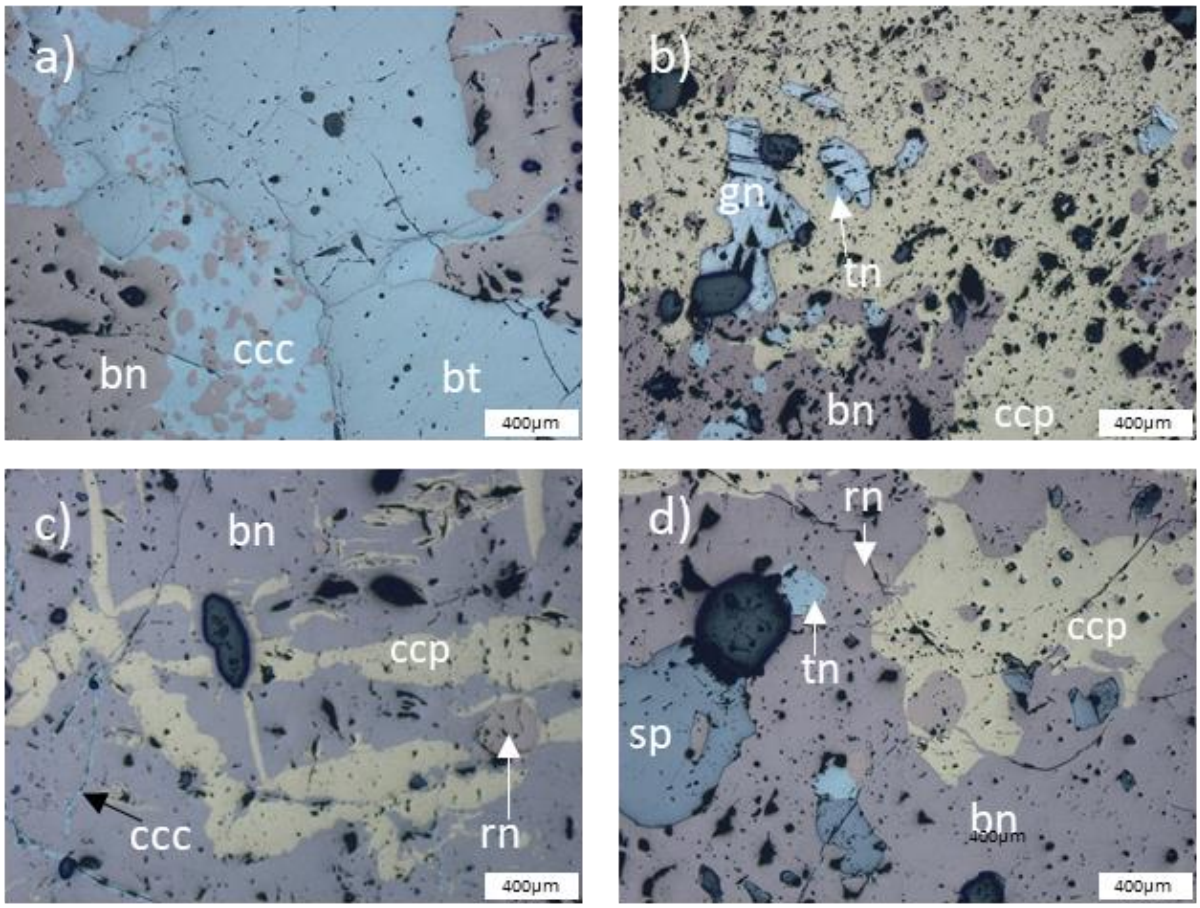

Figure 3.2: Mineral textures from the bornite-dominant assemblage in reflected light. (a) shows the incomplete replacement with remnant bornite (bn) globules within chalcocite (ccc), and chalcocite veins leading from it from sample KP1. There is also betekhtinite (bt) within bornite. (b) shows the concentrated areas of chalcopyrite (ccp) within bornite, as well as blebby galena (gn) from sample 586a. (c) shows the bi-directional chalcopyrite within bornite from sample KP16. (d) shows blebby renierite (rn), tennantite (tn) and sphalerite (sp) within bornite from sample KP12.

Bornite-chalcopyrite-dominant

This assemblage contains almost equal amounts of bornite and chalcopyrite. Chalcopyrite usually occurs as bi-directional laths within bornite (Figure 3.3a) similar to that seen in the bornite-dominant assemblage. Chalcopyrite can be seen creating a network among bornite (Figure 3.3b). Renierite, tennantite, sphalerite and galena show a similar occurrence to that in the bornite-dominant assemblage. Less chalcocite occurs within bornite in this assemblage compared to that in the bornite-dominant assemblage.

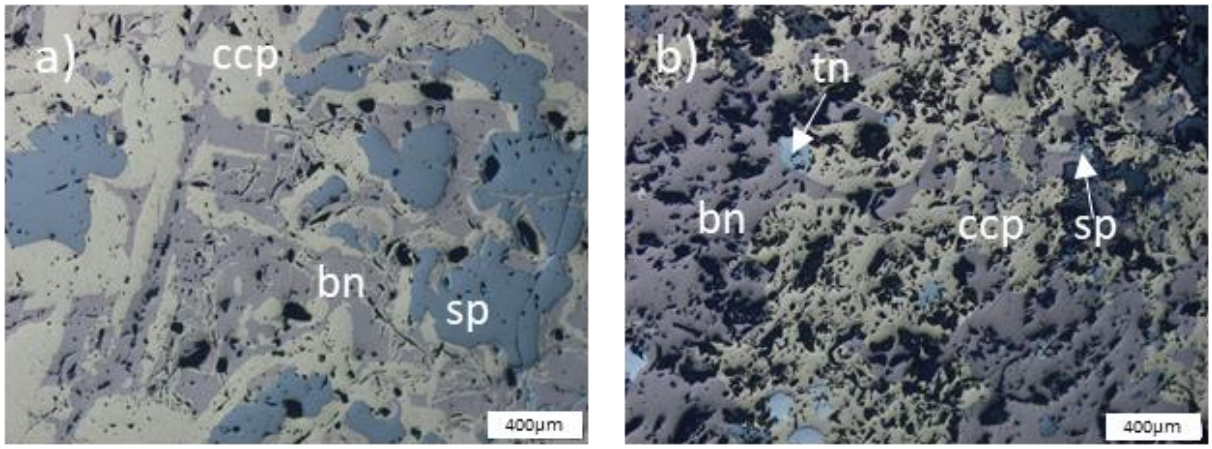

Figure 3.3: Mineral textures from the bornite-chalcopyrite-dominant assemblage in reflected light. (a) shows the bi-directional chalcopyrite (ccp) laths and sphalerite (sp) within bornite (bn) from sample KP13. (b) shows the network of chalcopyrite as well as tennantite (tn) and sphalerite blebs within bornite from sample 6547.

Bornite-renierite-dominant

Only one sample was found to fall into this assemblage. This sample is dominantly bornite (40%), with a much larger amount of renierite (30%) compared to all other samples and assemblages. Chalcocite veins are larger in this sample, spreading out across the whole sample. Chalcocite also forms with remnant globules of bornite within it (Figure 3.4). Renierite occurs as large veins within chalcocite (Figure 3.4). Minor blebby betekhtinite can also be found in this sample.

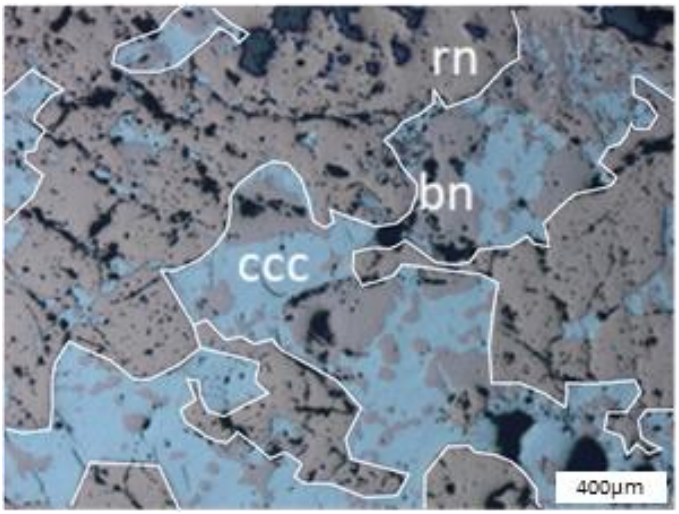

Figure 3.4: Large chalcocite (ccc) veins with the remnant globules of bornite (bn) within chalcocite hosting slightly smaller, blebby renierite (rn) (outlined) veins, all within a base of bornite, from sample 15453b, in reflected light.

Chalcopyrite-pyrite-dominant

This assemblage occurs primarily of massive chalcopyrite with inclusions of euhedral to subhedral grains of pyrite that range from 400 to 1000 µm amongst gangue minerals (Figure 3.5a). Very small grains of arsenopyrite that are tens of microns in size are dispersed throughout this assemblage (Figure 3.5a). Disseminated sphalerite also occurs within this assemblage and an unknown dusty brown-grey mineral that is anisotropic black-grey to light grey in crossed polars is also found in these samples (Figure 3.5b).

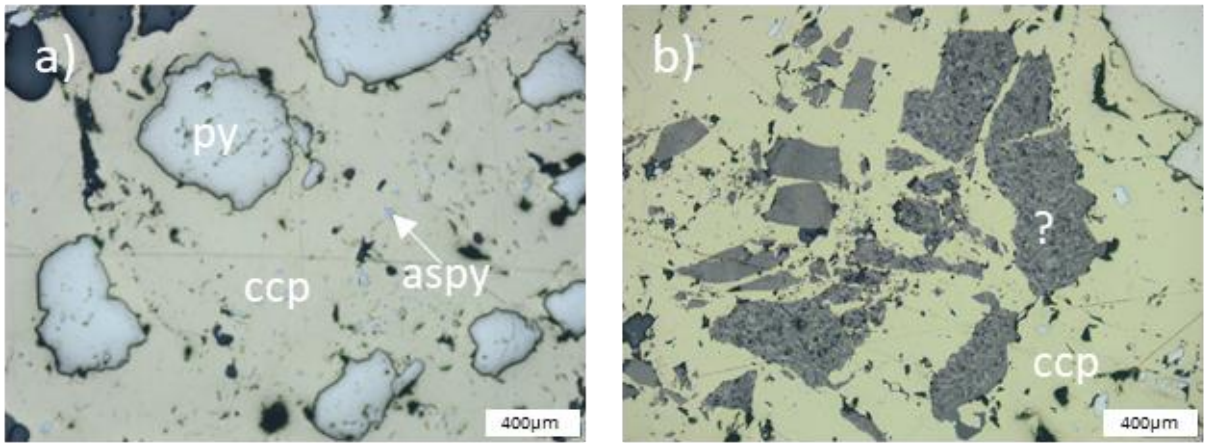

Figure 3.5: Mineral textures from the chalcopyrite-pyrite-dominant assemblage in reflected light. (a) shows pyrite (py) and much smaller arsenopyrite (aspy) within chalcopyrite (ccp) from sample S2801c. (b) shows the unknown dusty brown grey mineral in sample S2801c.

Chalcopyrite-dominant

Massive chalcopyrite makes up the bulk of this assemblage (Figure 3.6). Occasional subhedral pyrite grains of roughly 100 microns occur, as well as disseminated blebs of sphalerite.

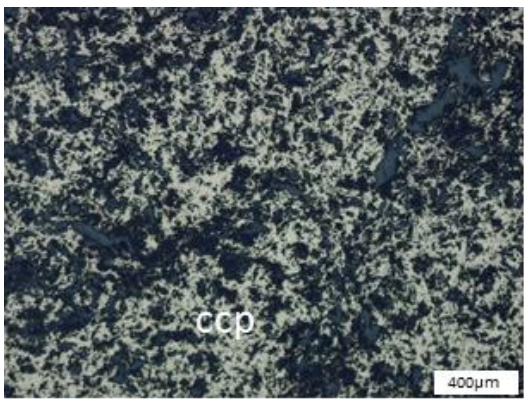

Figure 3.6: Massive chalcopyrite (ccp) and gangue from sample 12492b in reflected light.

Zn Assemblages

Sphalerite-dominant

This assemblage comprises massive sphalerite with minor chalcopyrite, the unknown brown mineral, tennantite, galena, pyrite and arsenopyrite. Chalcopyrite occurs as small 100 μm blebs within sphalerite (Figure 3.7a). The unknown dusty brown-grey mineral occurs as small veins. Chalcopyrite and tennantite also occur as veins (Figure 3.7b, c). Arsenopyrite occurs within chalcopyrite (Figure 3.7d). Galena also occurs as a small vein associated with tennantite, chalcopyrite and arsenopyrite (Figure 3.7d).

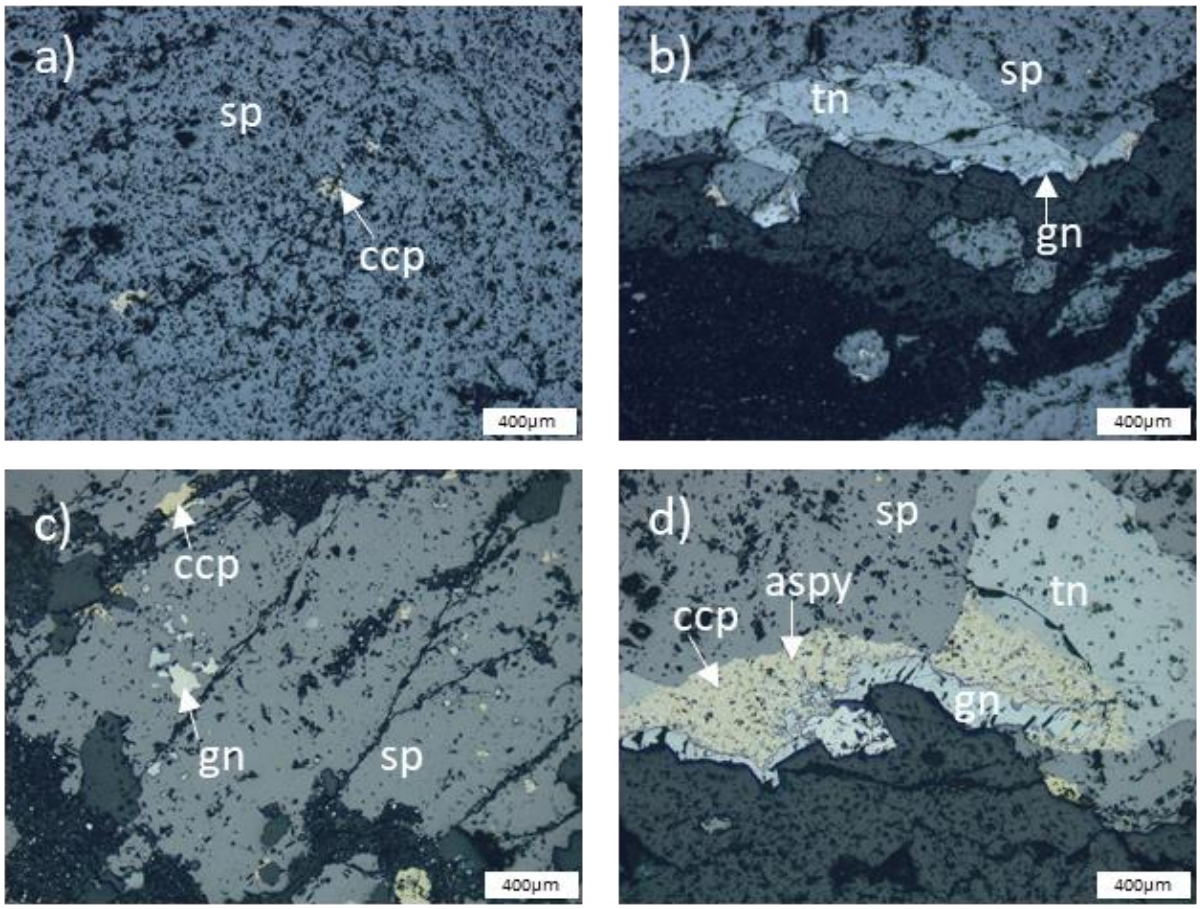

Figure 3.7: Minerals and their textures from the sphalerite-dominant assemblage in reflected light. (a) shows small chalcopyrite (ccp) blebs within the massive sphalerite (sp) from sample KP11. (b) shows tennantite (tn) as a vein in sample KP11. (c) shows galena (gn) blebs and chalcopyrite forming along a vein in sample KP11. (d) shows arsenopyrite (aspy) within the chalcopyrite, as well as tennantite (tn) and galena veining from sample KP11.

Sphalerite-chalcopyrite-dominant

This assemblage consists of massive sphalerite with an extensive network of chalcopyrite. A photomicrograph of the entire thin section of sample 12492f shows a typical sphalerite-chalcopyrite-dominant assemblage of massive sphalerite and chalcopyrite (Figure 3.8). In many cases, chalcopyrite is found to have replaced gangue (Figure 3.9a). The unknown dusty brown-grey mineral is prevalent within this assemblage (Figure 3.9b). A small network of galena is found in some of these samples (Figure 3.9a). Small blebs of bornite, renierite and tennantite can occur within sphalerite. Some samples contain small blebs of pyrite or arsenopyrite.

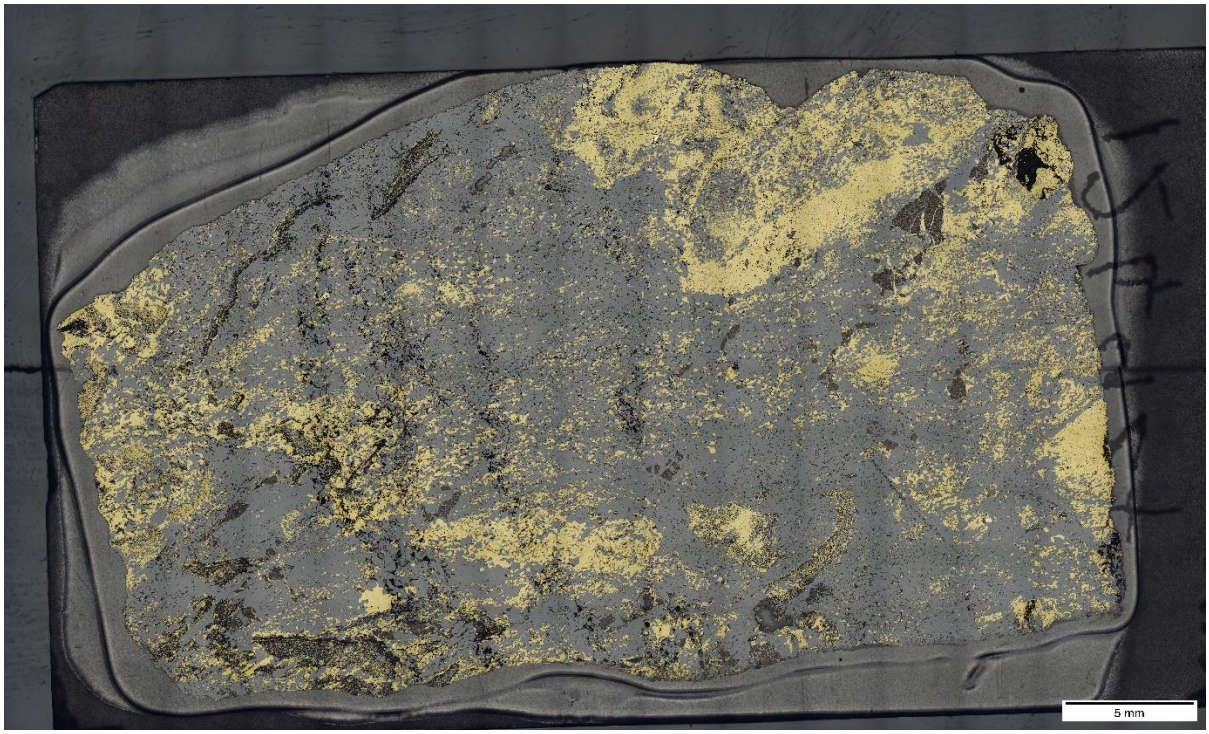

Figure 3.8: Photomicrograph of sample 12492f in reflected light, showing massive sphalerite (grey) with an extensive chalcopyrite (yellow) network, with gangue (black).

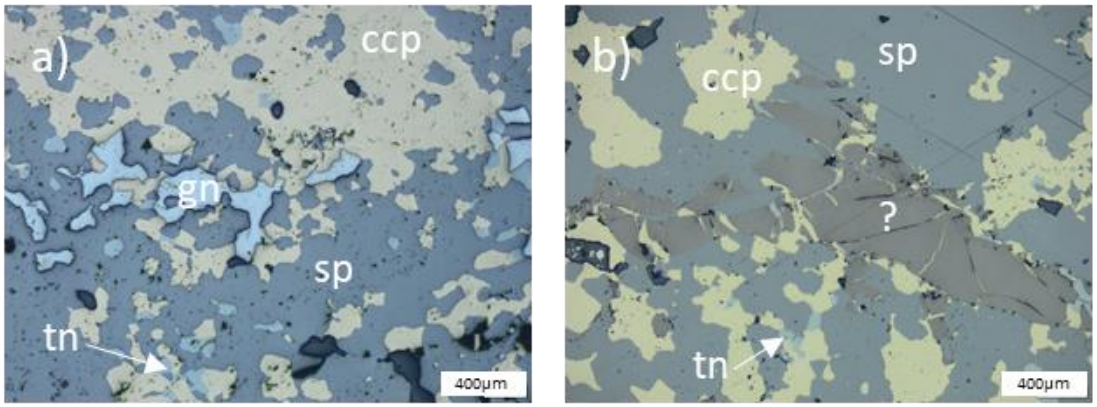

Figure 3.9: Minerals and textures from the sphalerite-chalcopyrite-dominant assemblage in reflected light. (a) shows a small network of galena (gn) among sphalerite (sp) and chalcopyrite (ccp) from sample 6548. Chalcopyrite can be seen to have replaced the gangue. (b) shows the dusty brown-grey mineral among sphalerite and chalcopyrite from sample 6548.

Sphalerite-bornite-dominant

This assemblage contains massive sphalerite that has replaced what was once massive bornite, suggested by the remnants of bornite within sphalerite. The other Cu sulphide minerals present have similar textures to that of the bornite-dominant assemblage. Chalcocite occurs as veins and has remnant globules of bornite within it.

Areas rich in chalcopyrite, as well as smaller chalcopyrite blebs, occur within bornite and sphalerite. Tennantite and renierite occur as large to small blebs (Figure 3.10a). Galena forms as irregular blebs to small networks, as it has also assisted in replacing bornite (Figure 3.10 a,b). Betekhtinite also occurs as blebs (Figure 3.10c).

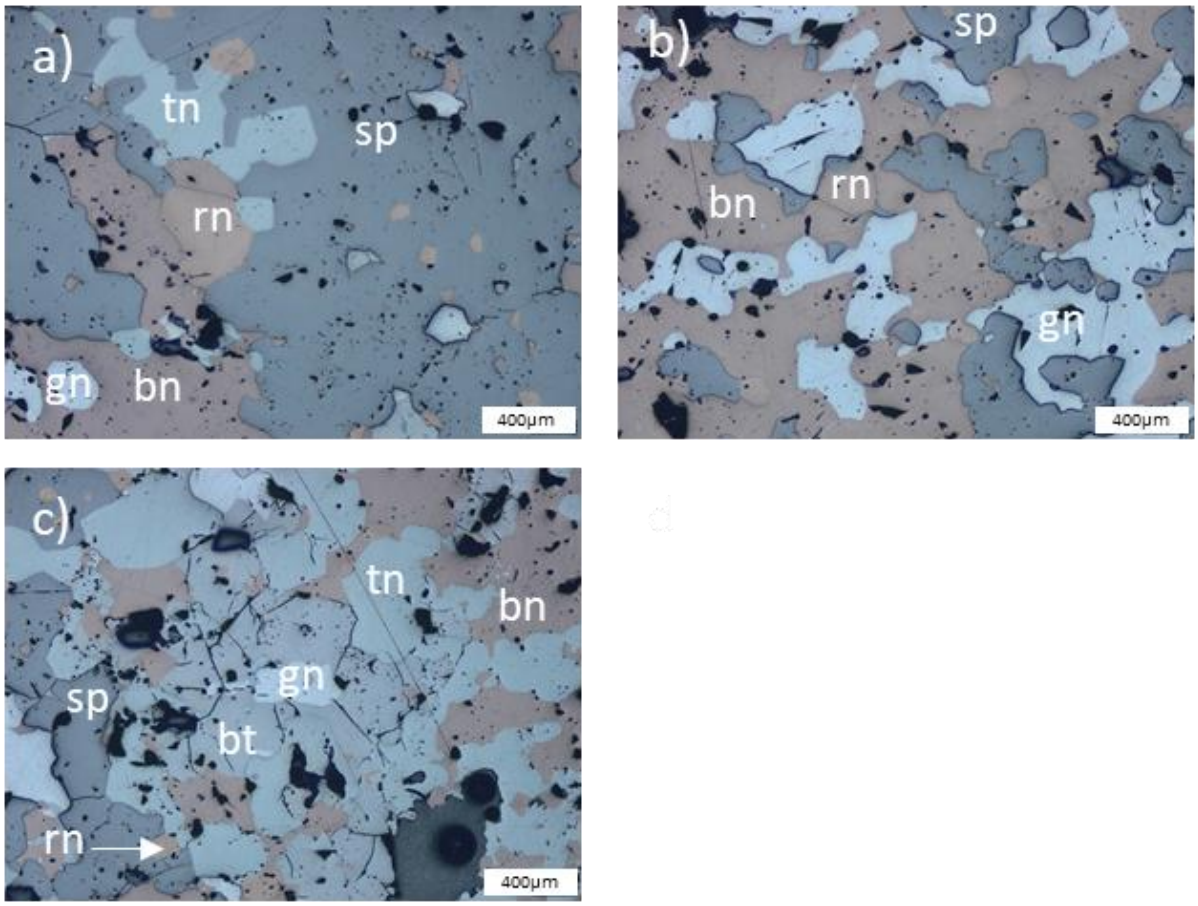

Figure 3.10: Minerals and their textures from the sphalerite-bornite-dominant assemblage in reflected light. (a) shows sphalerite (sp) within bornite (bn) alongside blebby renierite (rn), tennantite (tn) and galena (gn) from sample KP2. (b) shows sphalerite within bornite and galena, as well as renierite blebs from sample KP2. (c) shows many tennantite blebs surrounding betekhtinite (bt) in sample KP2.

Petrological summary

Most of the 26 samples that contain renierite are from the Cu-dominant assemblage-type (Table 3.2). Tennantite and galena are also more prevalent within the Cu-dominant assemblage-type. Chalcocite only occurs in the Cu-dominant assemblage-type, while chalcopyrite is abundant within the Cu-dominant assemblage-type, it also occurs in every sample of the Zn-dominant assemblage-type. Pyrite is more abundant in the Zn-dominant assemblage-type.

Paragenesis

Bornite appears to have been replaced by several other phases, thus suggesting it was the first phase to form. Chalcocite forms veins within the bornite, and has replaced the bornite in such a way that it has left remnant blebs of bornite within it. This suggests

the chalcocite was second to form. Chalcopyrite and sphalerite were the next phases to form, creating blebs that appear to replace the bornite and chalcocite. After that, tennantite, betekhtinite and renierite formed as blebs that replaced all the previous phases. Galena was the next phase to form, as indicated by the galena forming along the rims of all the other minerals or replacing them. Finally, carrollite, pyrite and arsenopyrite formed, as can be seen by these phases coating the underlying, earlier phases.

Heijlen *et al.* (2008) suggests that sphalerite, chalcopyrite, tennantite and renierite (along with briartite and germanite) all formed together, first, followed by bornite and chalcocite, with late stage sphalerite and chalcopyrite.

Samples were selected for further study based on the complexity of the mineral assemblages and their textures. Areas that contained sphalerite, and areas with galena, as well as areas with renierite were given preference for further analyses. Areas with silicates were looked at, however these were not given preference as the study focused on polymetallic sulphide minerals. These areas were polished thoroughly.

Table 3.2: A comprehensive table showing the mineral assemblages for each sample. The purple background represents the Cu-dominant assemblage-type, grey represents the Zn-dominant assemblage-type and the brown represents the mineralised country rock.

Sample Number	Bn	Sp	Ccp	Tn-Td	Ren	Gn	Py	Aspy	Cc
1216	✓	✓	✓	✓	✓	✓		✓	
KP 2	✓	✓		✓	✓	✓			
KP 5a	✓	✓	✓	✓		✓			
KP 5b	✓	✓	✓	✓	✓	✓			
KP 3	✓	✓	✓		✓	✓			✓
KP 12	✓	✓	✓	✓	✓	✓			✓
15452a	✓	✓	✓	✓	✓	✓			
15452b	✓	✓	✓	✓	✓	✓		✓	✓
586a	✓	✓	✓	✓	✓				✓
586b	✓			✓	✓	✓			✓
586c	✓				✓	✓			✓
12492Aa	✓			✓					✓
12492Ab	✓				✓				✓
12492Ac	✓				✓				✓
KP 17a	✓	✓		✓	✓				✓
KP 17b	✓	✓		✓	✓	✓			✓
587	✓	✓	✓			✓	✓		✓
6547	✓	✓	✓	✓		✓			
KP 13a	✓	✓	✓		✓				✓
KP 13b	✓	✓	✓	✓	✓		✓		✓
15453a	✓				✓	✓			✓
15453b	✓				✓	✓			✓
KP 1	✓				✓				✓
KP 16	✓		✓		✓		✓		✓
KP 4	✓		✓		✓				✓
KP 17c	✓	✓	✓	✓	✓			✓	✓
KP 11a	✓	✓	✓	✓		✓	✓		
KP 11b		✓	✓	✓		✓	✓		
KP 11c		✓	✓	✓		✓	✓	✓	
1058a	✓	✓	✓	✓	✓	✓			
1058b	✓	✓	✓	✓	✓	✓			
KP 18		✓	✓	✓					
6548		✓	✓	✓	✓	✓		✓	
S2801a		✓	✓				✓		
S2801b		✓	✓				✓	✓	
S2801c		✓	✓				✓	✓	
12492a		✓	✓				✓		
12492b		✓	✓				✓		
12492c		✓	✓						
12492d		✓	✓						
12492e		✓	✓				✓		
12492f		✓	✓						
KP 8			✓						
KP 7	✓				✓			✓	✓
KP 6	✓	✓							

X-Ray Diffraction

Mineral phases that were identified using petrography have been confirmed using XRD. The results of the XRD include the weight % of each identified phase (Table 3.3) by Rietveld analysis (Post and Bish, 1989). The weight % of each phase confirms most of the assemblages identified by petrography. However, sample 15453, identified by petrography as a bornite-renierite sample, contains no renierite above detection limits according to the XRD. Sample KP 7 is dominated by dolomite as it is a mineralised country rock. There are two bornite phases identified by XRD. 'Bornite high' is refers to bornite that has formed at high temperatures, while 'bornite' refers to bornite that formed at lower temperatures (Putnis and Grace, 1976; Grguric *et al.*, 1998). This suggests two phases of bornite deposition. However, only one bornite phase was identified using petrographical methods.

Table 3.3 Results of XRD analysis showing the various mineral phases identified, as well as their weight % determined by the Rietveld methodology.

Kipushi	Dolomite	Bornite	Tennantite	Quartz	Renierite	Chalcopyrite	Galena	Sphalerite	Bornite high	Pyrite	Total
1058	0	3.6	5.8	1.9	6.2	14.6	6.1	60	1.9	0	100.1
1213	0	6.5	0.2	8.5	3.4	65.2	0	3.1	10.9	2.3	100.1
12492	0	0	0.8	2	0	97.1	0	0.2	0	0	100.1
12492A	0	84.2	1	13.1	0	0	0	1.8	0	0	100.1
15453	0	7.8	16.8	2.1	0	25.3	0	5.6	42.3	0	99.9
6548	0	2.9	0.3	2.8	4.9	5.8	0	81.1	2.2	0	100
15452	0	8.1	1.1	5.2	0	0.4	0.3	31.1	53.7	0	99.9
586	0	7.1	4	12.8	0	0.3	0.9	21.7	53.2	0	100
KP1	0	13.8	0	0	0	0	0	1.7	81.2	3.3	100
KP11	0	3.8	0	9.4	6.2	0.7	0	76.1	3.9	0	100.1
KP7	87.5	2.9	1	1.4	0	0	0.7	2.3	3.1	1	99.9
S2801	0.8	0	0.4	2.3	0	94.5	0	0.2	0	1.7	99.9

Whole Rock Geochemical Analysis

Specific samples were chosen for whole rock geochemical analysis at Intertek Genalysis laboratories using ICP-MS and ICP-OES. Multiple samples from each assemblage-type were selected to obtain an indication of the variation of Ge concentration within the different assemblage-types. One mineralised country rock with bornite veining was chosen to see if the gangue had concentrations of Ge. Four samples were selected from the Zn-dominant assemblage-type and five samples from the Cu-dominant assemblage-type for trace element analysis. Details of analytical methods and element accuracies and precisions are contained in Appendix B. Samples were analysed for Ag, As, Be, Bi, Cd, Co, Cr, Cs, Cu, Ga, Ge, In, Li, Mn, Mo,

Na, Ni, Pb, Rb, Re, Sb, Sc, Se, Tl and Zn (Table 3.4). Although this is a limited data set, due to the limited number of samples, it can prove indicative of trace element relationships within different minerals.

Table 3.4: Results from the whole rock analysis. Amount of each element is measured in ppm. Samples are colour-coded to the basic assemblage-type. Purple represents the Cu-dominant assemblage-type, grey the Zn-dominate assemblage-type, and the brown is the mineralised country rock.

	Country	Zn				Cu				
Sample # / Element	KP 7	KP 11	1058	S2801	12492	586	12492 A	15453	15452	1213
Ag	2942	9.99	198.8	18.51	78.1	839	896	1477	1075	829
As	23.6	688.5	3780.6	2665.7	1546.9	2341.1	69.1	7188.9	1628.6	892.8
Be	0	0.22	0	0	0	0	0	0	0	0
Bi	0.08	0.1	0.67	8.85	7.87	1.59	39.25	0.28	0.24	2.37
Cd	8.43	4694	3347	2060	22.2	2386	9.59	156.67	950.61	29.79
Co	0.6	2.3	91.4	19.4	6.8	55.7	28	29.5	39.8	9
Cr	0	17	0	0	0	0	6	6	0	0
Cs	0	0.41	0	0	0	0.16	0	0	0	0
Cu	192900	1326	106900	116700	311900	298400	495500	460700	431500	467800
Ga	2.12	3.35	621.36	3.27	1.77	186.97	2.99	92.08	118.5	51.02
Ge	49	39.6	1845	25	7.1	387.8	21.5	>2000	474.9	137.9
In	0.28	0	3.16	4.77	2.44	3.64	0.18	0.81	1.55	0.3
Li	3.9	26.7	5.7	4	5	5.5	0.9	1	1.6	0.7
Mn	467	125	136	75	913	102	26	34	45	24
Mo	0.7	9.4	1.9	0.8	1.3	1.2	8.3	2.7	0.3	17.2
Na	265	149	579	27	0	430	0	124	164	0
Ni	3	4	20	14	15	3	8	13	6	9
Pb	3083.4	3042.5	112500	319.9	722.8	32700	126600	3324.1	53000	4551.5
Rb	0.8	16.02	0.47	2.42	2.92	0.43	1.09	0.39	0.18	0.46
Re	0.007	0.006	0.017	0.003	0.006	0.002	0.628	0.022	0.006	0.004
Sb	0.52	7.72	66.59	3.88	3.54	33.85	2.28	50.73	22.32	30.22
Sc	0.2	2.9	0	0.3	0.3	0	0	0	0	0
Se	5.7		63.7	5.4	2.2	92.1	47.1	45.4	105.2	5.4
Te	0	0	0	0	0	0	0	0	0	0
Tl	0.02	0.32	0.17	0.16	0.09	0.05	0.25	0.07	0.08	0.08
Zn	1046	525200	420500	336600	2823	305200	1147	14499	108500	1843

All samples were plotted in a ternary diagram of Pb, Zn and Cu (Figure 3.11). This shows that the mineralised country rock is extremely rich in Cu, as are two of the Cu-dominant samples and one Zn-dominant sample. This suggests a high bornite or chalcopyrite concentration within these samples. Two of the other Cu-dominant samples are less rich in Cu, while one sample is poor in Cu. One Zn-dominant sample is extremely rich in Zn, while two others have less Zn, but are still rich in Zn. These Zn-rich samples have a high sphalerite content.

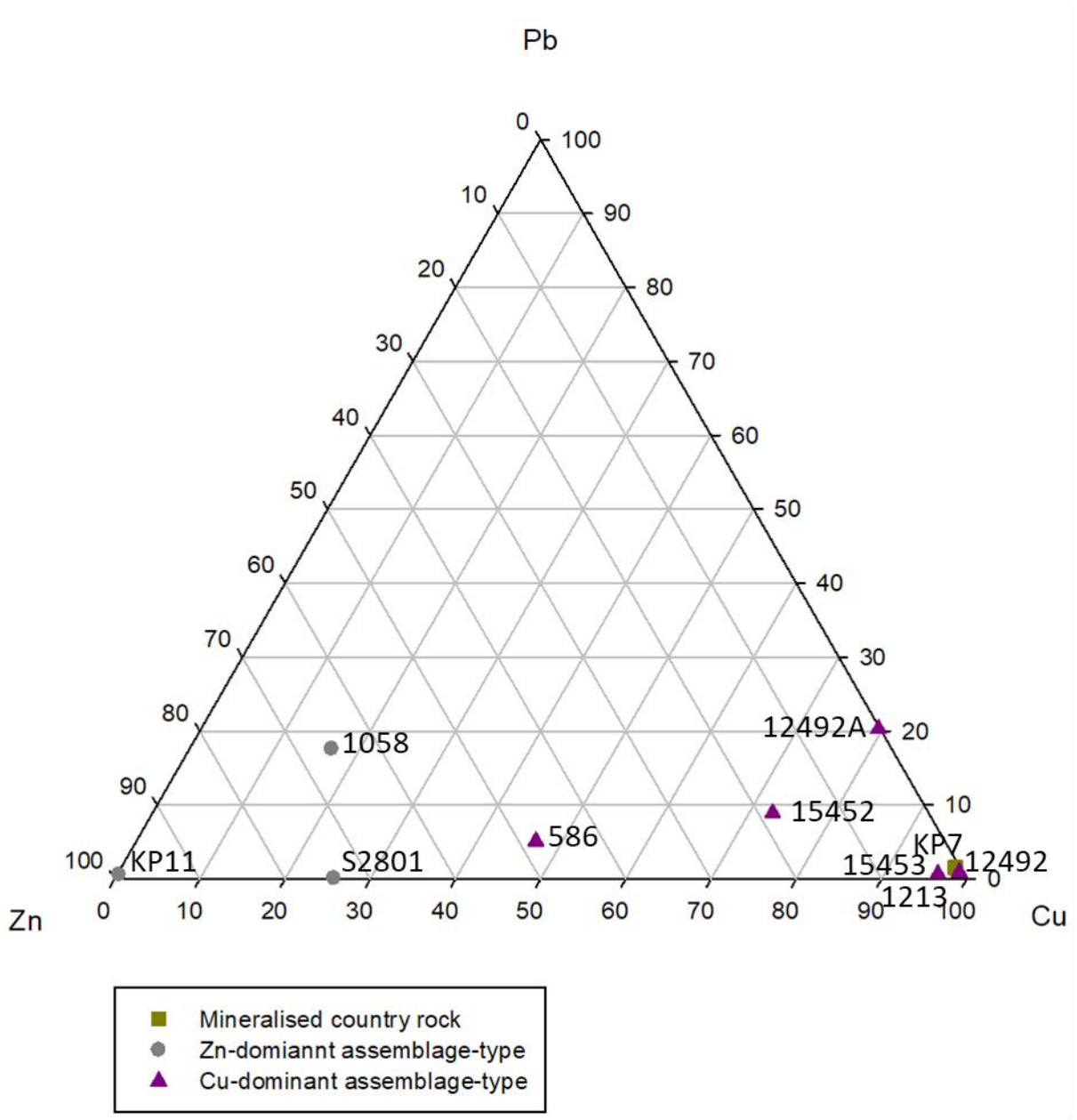

Figure 3.11: Ternary diagram showing where the analysed samples fall with respect to Pb, Zn and Cu. Grey represents the Zn-dominant assemblage-type, purple the Cu-dominant assemblage-type and the brown is the mineralised country rock with bornite veining.

None of the samples contained detectable Te. All samples contained very little Be, Cs, Cr, In, Li, Rb, Re and Tl. However, they are enriched in Cu, Pb and Zn, in bornite- and sphalerite-bearing samples, with greater Cu in the samples containing bornite. Most samples contained moderately high quantities of Ag, As, Cd, Ga, and Ge (Table 3.4 and Figure 3.12). Cu, Zn and Pb can be considered essential elements within these samples due to the presence of galena, sphalerite and bornite. Trace elements within these samples, excluding the essential elements, show Ge to be present within all the

Cu-dominant samples, and only in one Zn-dominant sample (Figure 3.12). The country rock sample contains low Ge, As and Cd, but is rich in Ag. Ge and Ag are preferentially enriched in the bornite-dominant samples, however there appears to be significant Ge within sphalerite-bearing sample 1058. The sphalerite-bearing samples are enriched in Cd, however sample 12492 seems anomalous, this could be attributed to the high concentration of chalcopyrite in this sample.

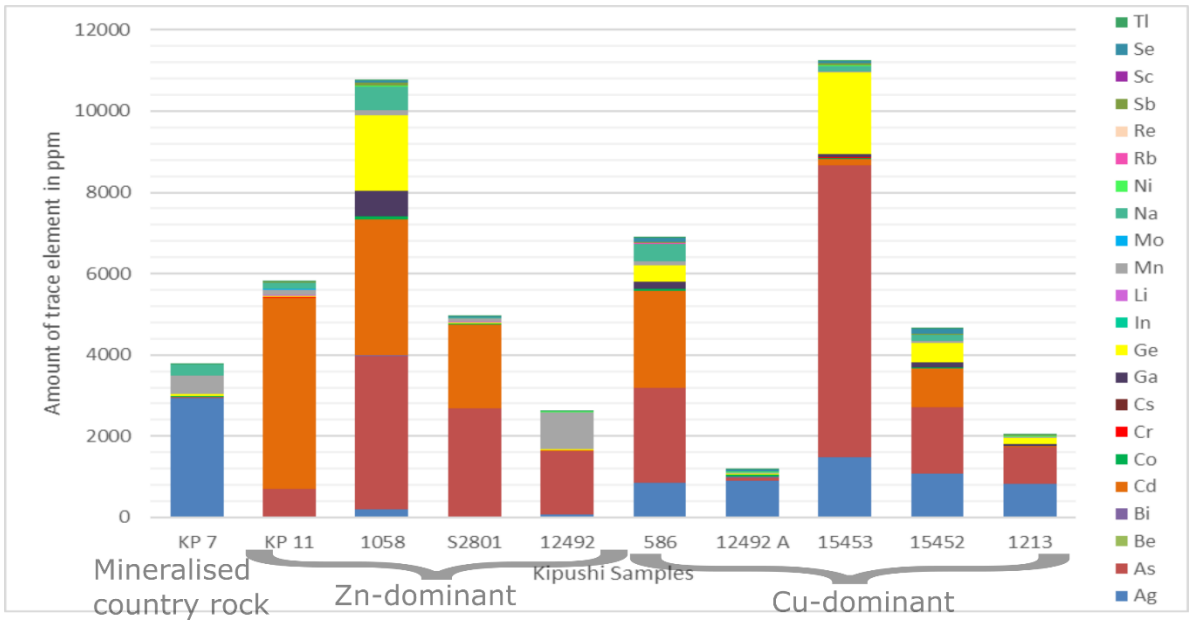

Figure 3.12: Graphical representation of trace elements within 10 samples from the Kipushi ore deposit. Sphalerite- and bornite-dominant assemblages are rich in As. Most sphalerite-dominant assemblages have a high concentration of Cd. Ge is more abundant in the bornite-dominant assemblage, and to a lesser extent in the sphalerite-dominant assemblage, and to a much lesser extent in the mineralised country rock. Ag occurs in the bornite-dominant assemblages as well in the bornite rich country rock.

Pb and Ge appear to correlate (Figure 3.13). In general, the more Ge within the sample, the more Pb there is present. This suggests a relationship between galena and Ge. There are two outliers in this graph; sample 15453, which contains little Pb, but high Ge, and sample 12492A, which contains little Ge, but is enriched in Pb. This could be due to little galena and abundant Ge-essential renierite in sample 15453. Sample 12492A would have mostly bornite with galena, and possibly little renierite in this sample.

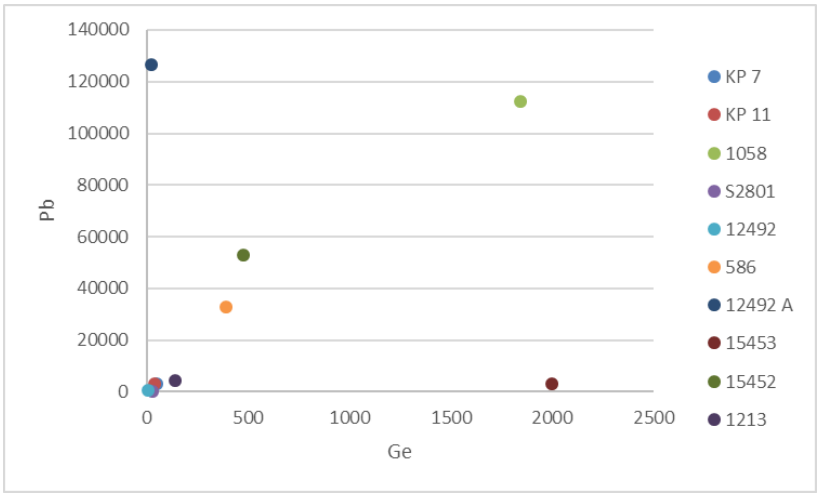

Figure 3.13: Ge, in ppm, plotted against Pb, in ppm, showing a slight correlation between the two elements.

Ga and Ge show a general correlation (Figure 3.14). As Ga increases, so does Ge. However, there is an outlier; sample 15453 contains more Ge than Ga. This sample is a bornite-renierite-dominant sample, which accounts for the enrichment in Ge.

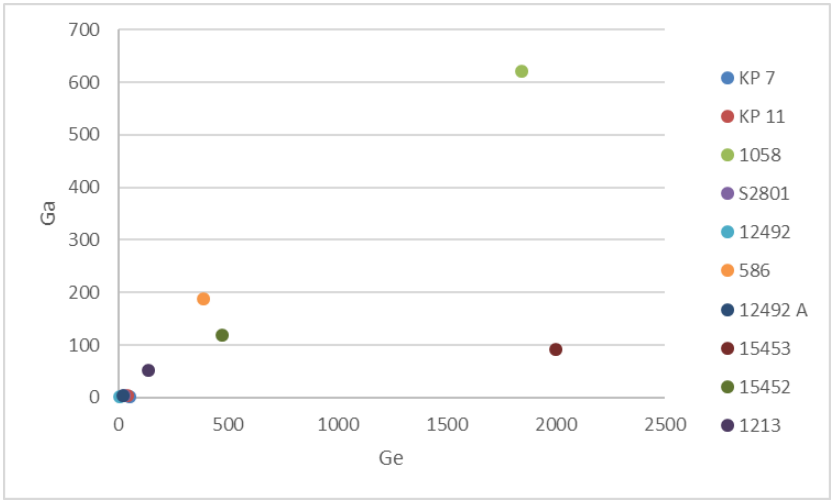

Figure 3.14: Ge, in ppm, plotted against Ga, in ppm, showing a slight correlation between the two elements.

As and Ge show a general correlation (Figure 3.15). As Ge increases, so does As. There are samples (12492A and KP7) with no Ge or As in them. These are bornite-dominant samples with little renierite and tennantite. Samples 12492 and S2801 have low Ge content as these samples lack renierite.

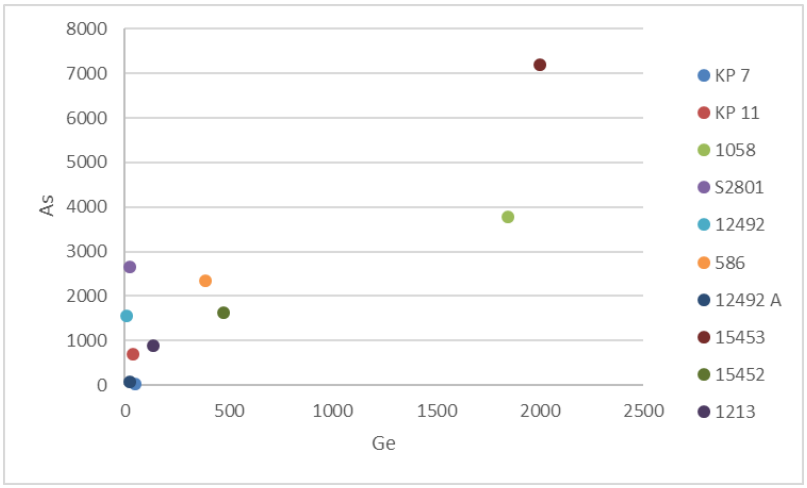

Figure 3.15: Ge, in ppm, plotted against As, in ppm, showing a general correlation between these two elements.

Zn and Ge show no obvious correlation (Figure 3.16). This suggests that there is little to no Ge within sphalerite.

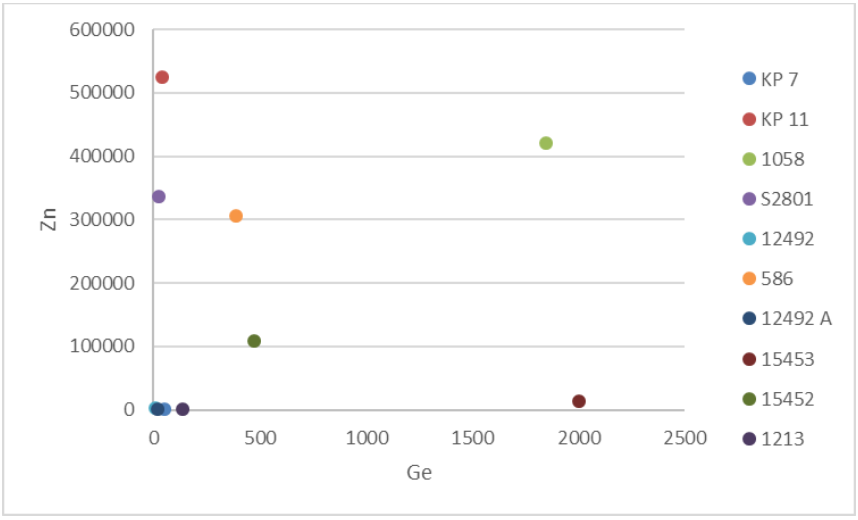

Figure 3.16: Ge, in ppm, plotted against Zn, in ppm, showing no correlation between the elements.

As and Sb appear to correlate (Figure 3.17). There are two outliers; sample 15453 and S2801. These samples have more Sb than As, whereas all the other samples have more As than Sb.

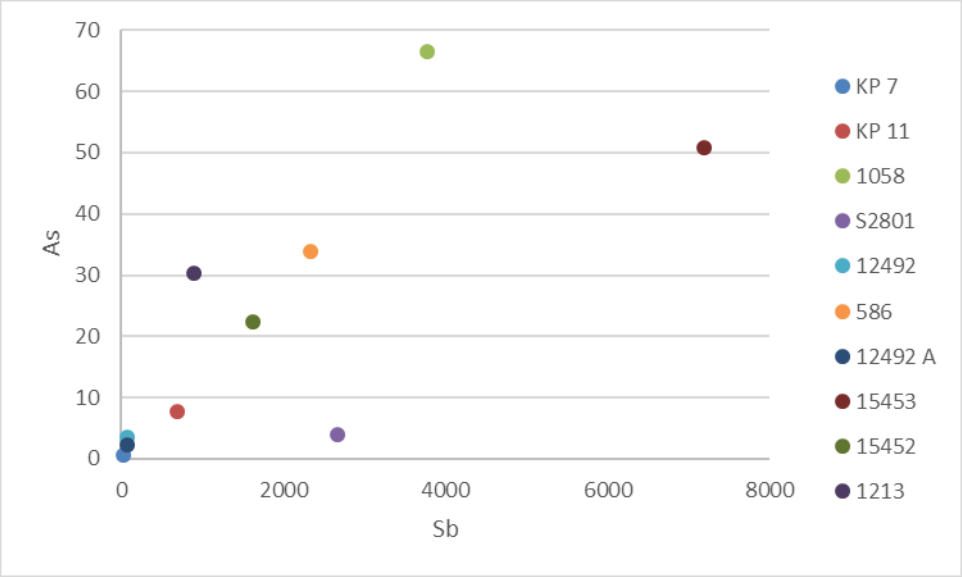

Figure 3.17: Sb, in ppm, plotted against As, in ppm, showing a general correlation.

Zn and Cd show an almost perfect correlation. (Figure 3.18). As Zn increases, so does Cd. This suggests a relationship between Cd and sphalerite.

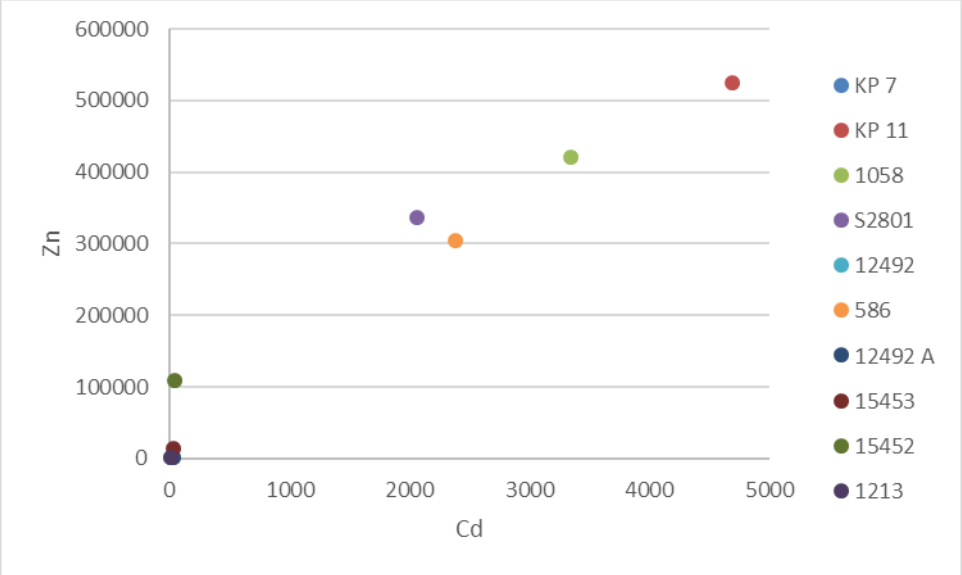

Figure 3.18: Cd, in ppm, plotted against Zn, in ppm, showing an excellent correlation.

Scanning Electron Microscopy and Mineral Analysis

Two semi-quantitative SEMs were used to obtain mineralogical information, element maps and mineral compositional data for the Kipushi samples. A Zeiss Gemini SEM and a Tescan Integrated Mineral Analyser (TIMA) were used. Multiple areas on each sample were selected for analysis. These areas were chosen based on the minerals

present in the assemblages, and their texture. Areas with and without renierite were selected, to see if Ge concentrates solely into renierite when renierite is present. Areas containing both sphalerite and galena were given preference to evaluate the partitioning of Ge between them. Sphalerite was chosen as literature references suggest Ge should be concentrated in sphalerite (Bernstein, 1985; Holl *et al*., 2007). A comprehensive set of element maps together with BSE images and false colour primary phase maps can be found in Appendix C.

Element Maps

An area consisting of bornite, sphalerite and renierite was chosen for analysis from bornite-dominant sample KP12 (Figure 3.19) to examine the distribution of Ge within this assemblage. The element maps of Zn, Cu, Ge and Fe for this area show Ge concentrating within Ge-essential renierite (Figure 3.20). This was evident for every sample that was examined that contains renierite. It should be noted that there is no detectable Ge within sphalerite in this area.

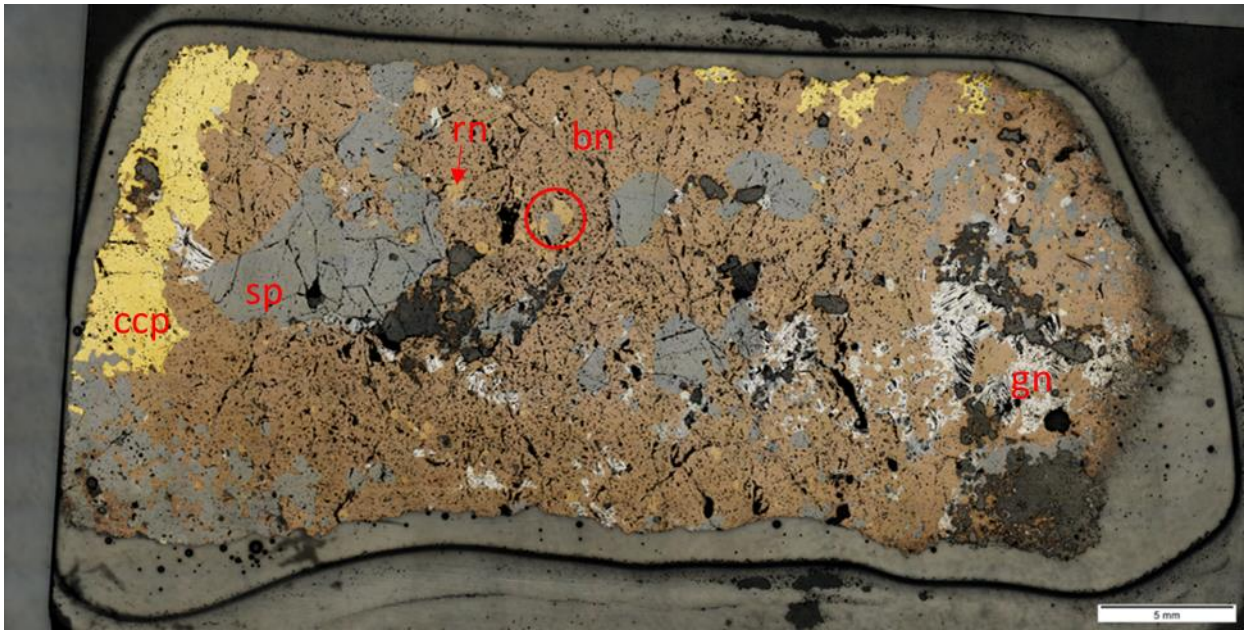

Figure 3.19 Full polished thin section image in reflected light showing bornite-dominant sample KP12 and the area selected for TIMA analysis (red circle).

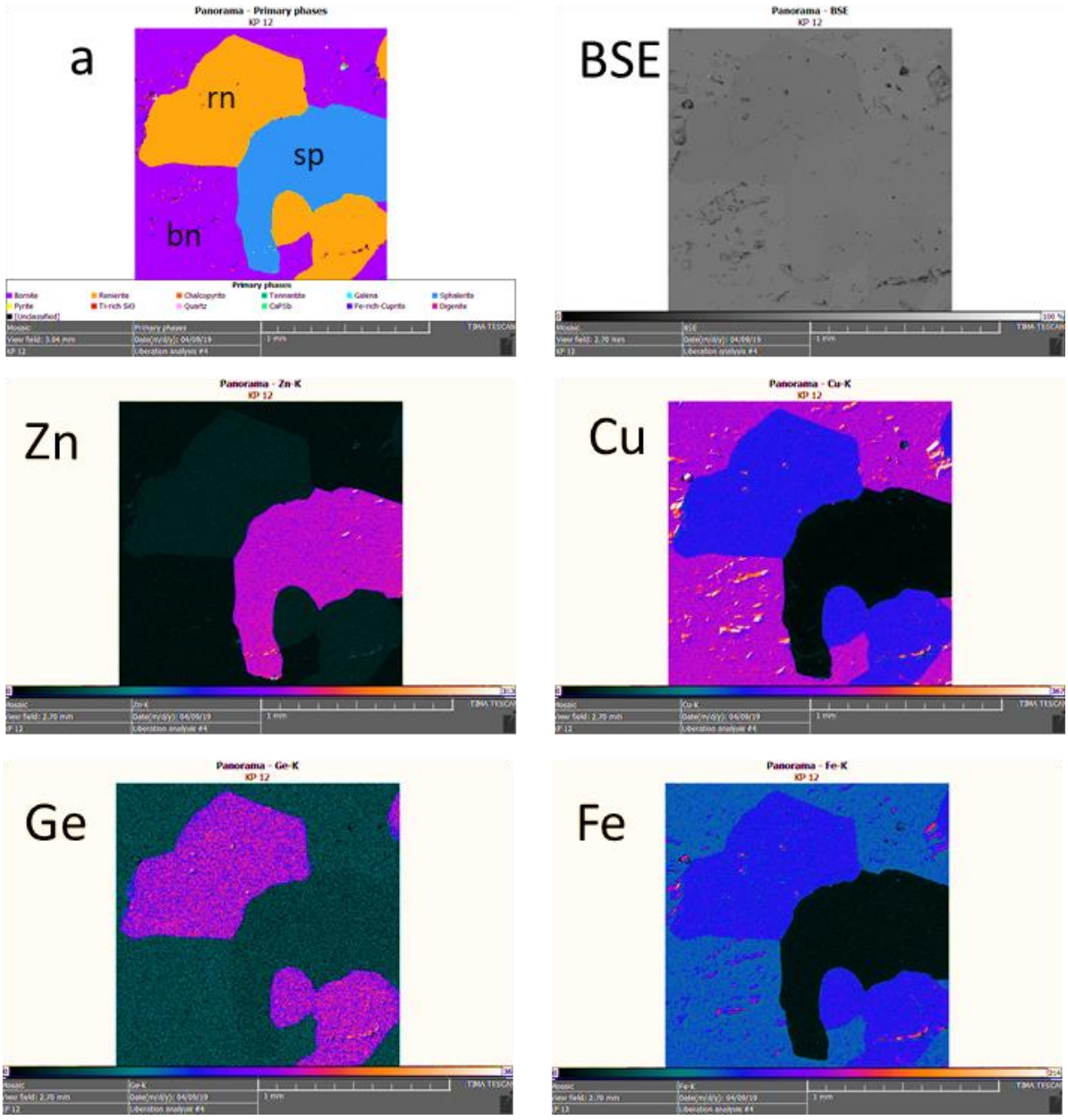

Figure 3.20: False colour primary phase map (a) showing sphalerite, bornite and renierite, backscatter electron image and element maps for Zn, Cu, Ge and Fe from sample KP12. These images were all obtained using the TIMA. Ge is concentrated into renierite.

An area of sphalerite and bornite, with no renierite in the assemblage was selected from a bornite-chalcopyrite-dominant sample 1216 (Figure 3.21). The element maps of Cu, Zn, Ge and Fe for this area show that there is no detectable concentration of Ge in either of these minerals (Figure 3.22).

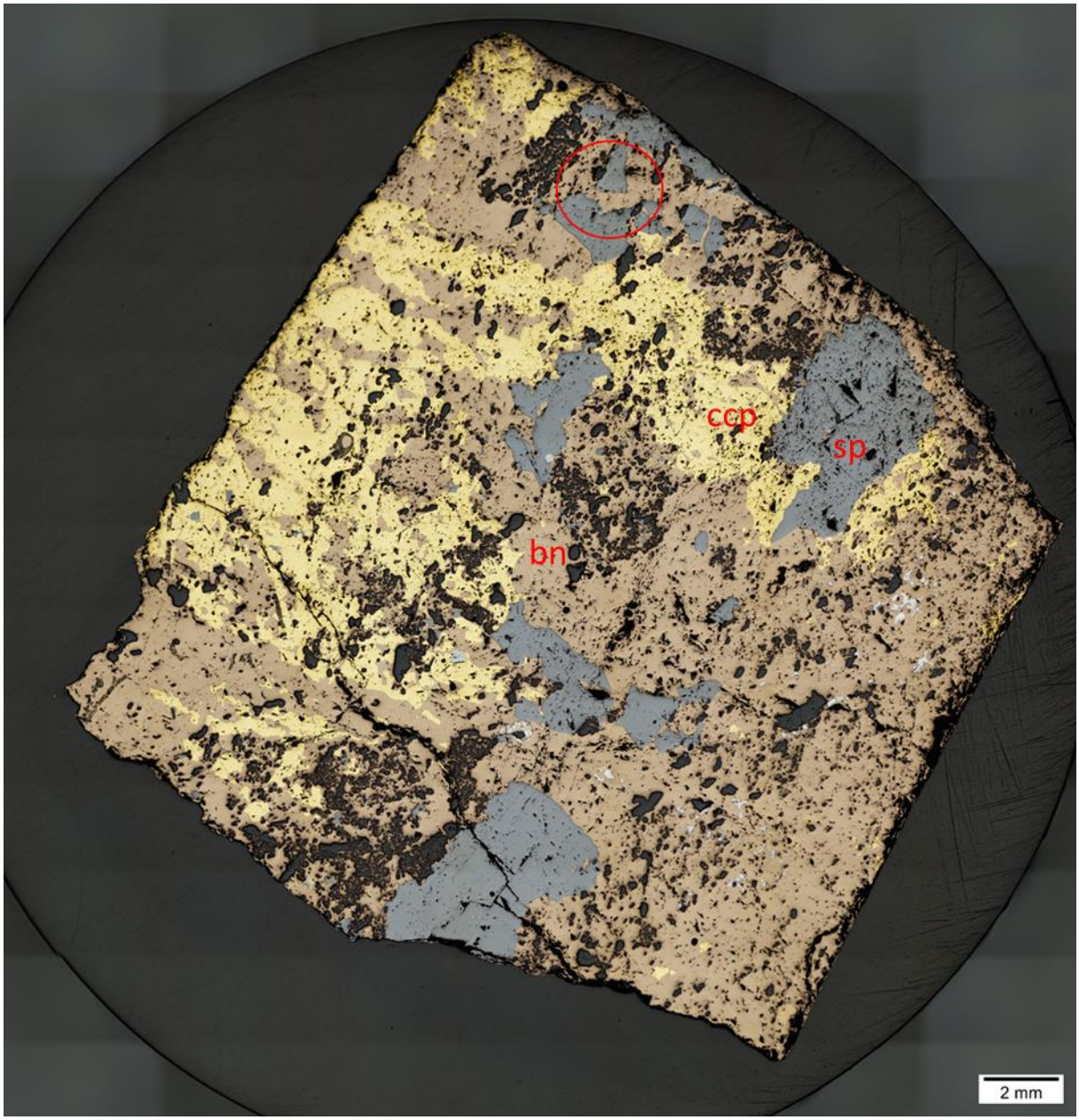

Figure 3.21: Full ore block image in reflected light showing bornite-chalcopyrite sample 1216 and the area selected for TIMA analysis (red circle).

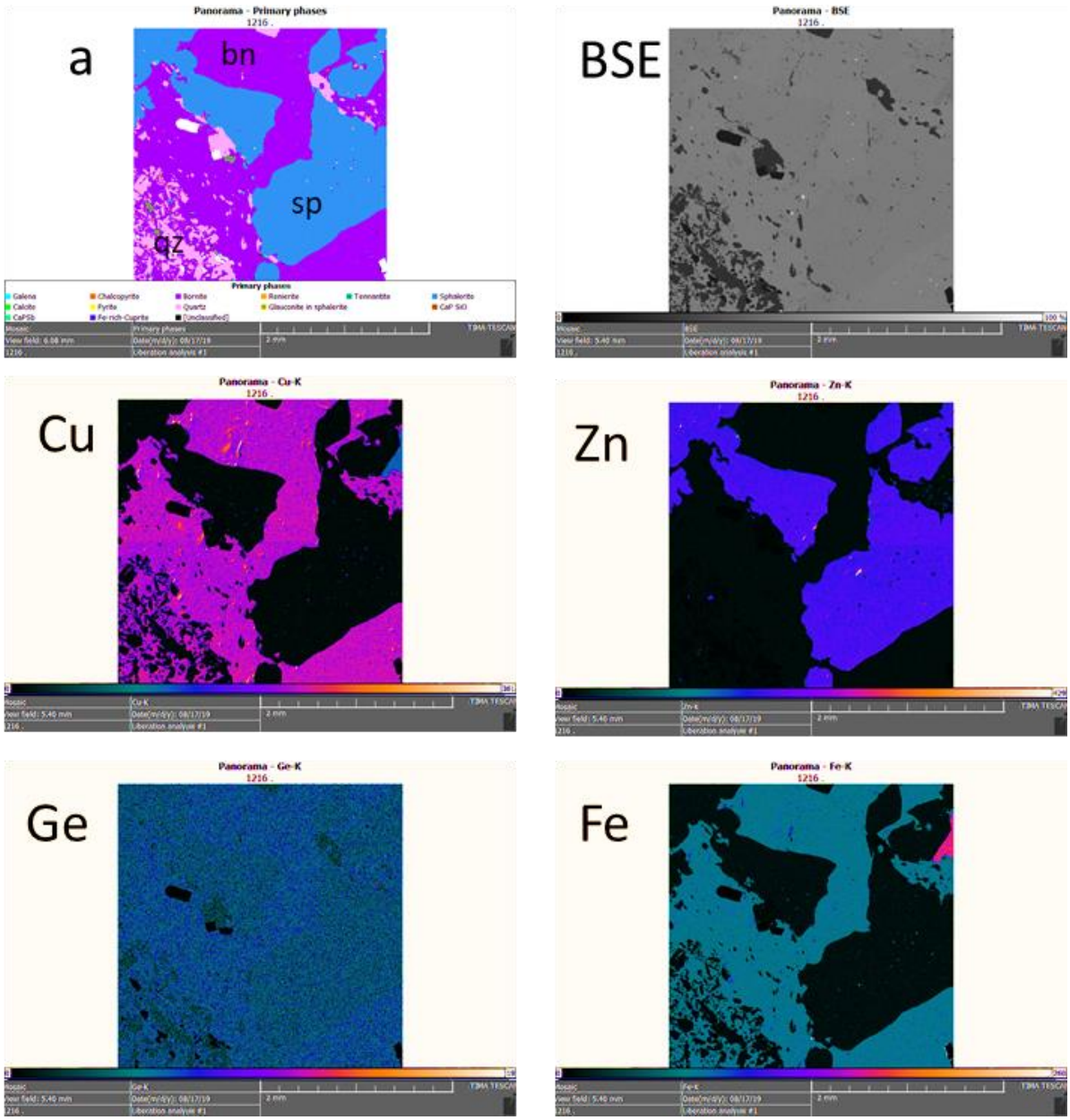

Figure 3.22: False colour primary phase map (a) showing sphalerite, bornite and quartz (qz), backscatter electron image and element maps for Cu, Zn, Ge and Fe from sample 1216. These images were all obtained using the TIMA. No Ge concentration in any of these phases.

An area of massive sphalerite with minor galena, chalcopyrite, renierite and tennantite was selected from sphalerite-chalcopyrite-dominant sample 1058 (Figure 3.23). The element maps of Pb, Zn, Fe, As, Ge and Ga for this area show Ge concentrating into both renierite and galena (Figure 3.24). Unsurprisingly there is more Ge in renierite than galena, however galena also contains noticeable Ge, Ga and As. This is evident throughout the Kipushi sample suite.

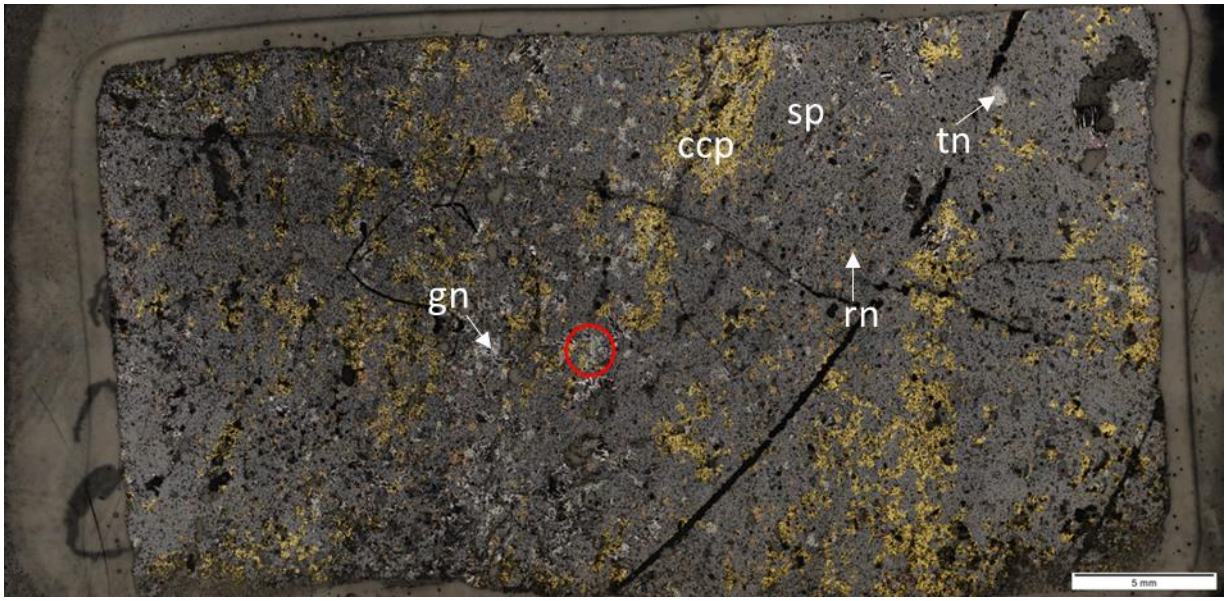

Figure 3.23: Full polished thin section image in reflected light showing sphalerite-chalcopyrite-dominant sample 1058 and the area selected for TIMA analysis (red circle).

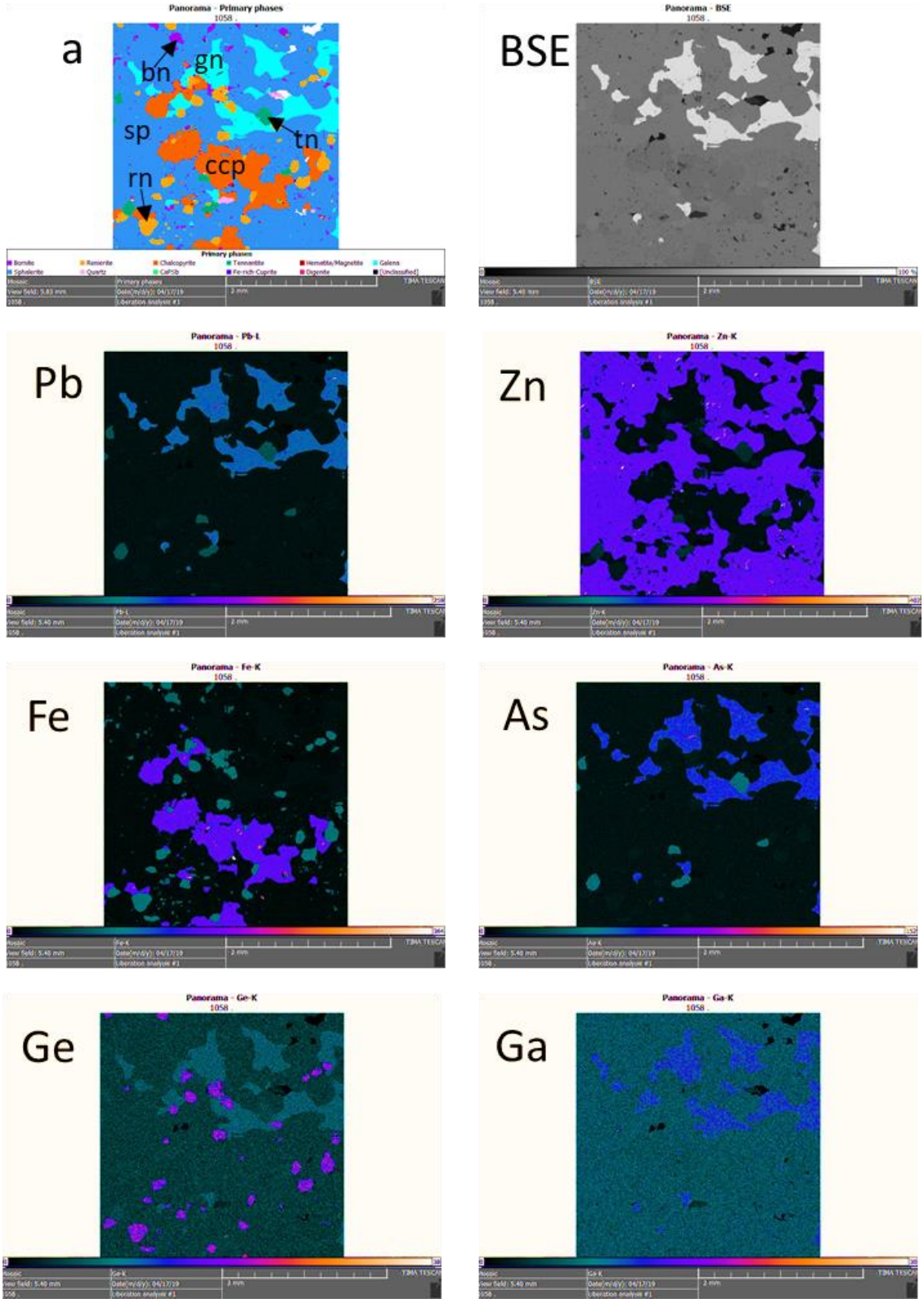

Figure 3.24: False colour primary phase map (a) showing sphalerite, galena, chalcopyrite, bornite, tennantite and renierite, backscatter electron image and element maps for Pb, Cu, Fe, As, Ge and Ga from sample 1058. These iages were all obtained using the TIMA. Ge concentrates into renierite and galena. There is more Ge in renierite than in galena. Galena contains As and Ga, and tennantite contains Pb.

An area of sphalerite, chalcopyrite and tennantite was selected as area 1 from a sphalerite-chalcopyrite-dominant sample 6548 (Figure 3.25). This area does not contain renierite or galena. Element maps of Zn, Cu, Ge, As and Fe were obtained for this area (Figure 3.26). In this case it was noted that Ge partitions into tennantite, although to a lesser extent than into renierite or galena. Galena is also found to have a high concentration of As and Ga, and tennantite also contains Pb.

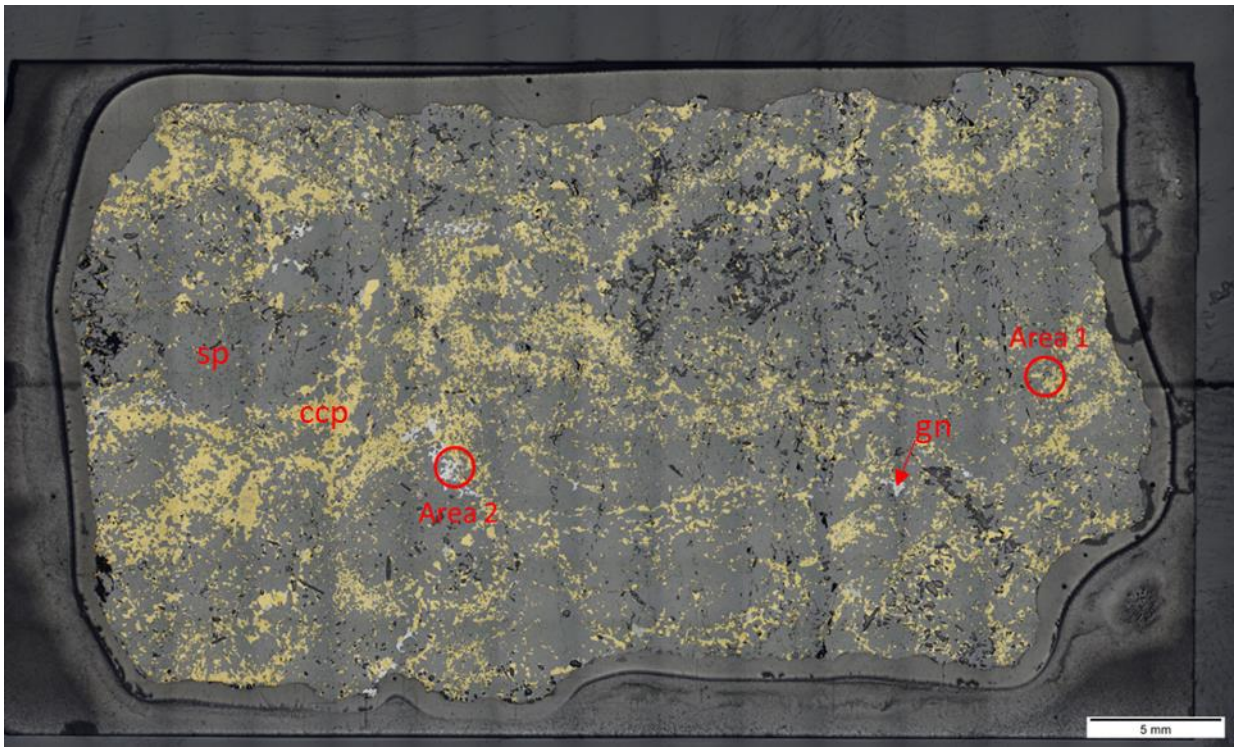

Figure 3.25: Full polished thin section image in reflected light showing sphalerite-chalcopyrite-dominant sample 6548 and the areas selected for SEM analysis (red circles).

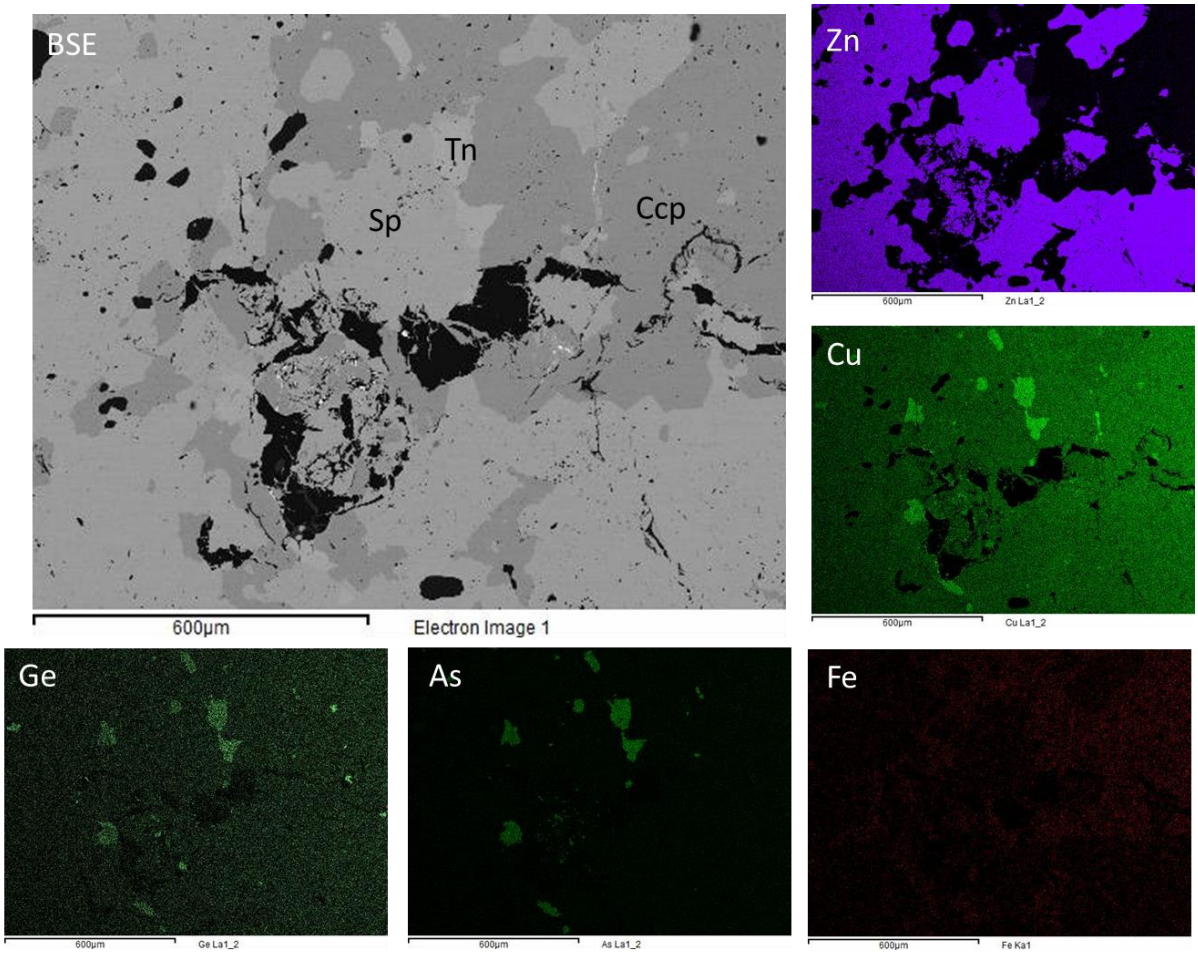

Figure 3.26: Backscatter electron image showing sphalerite, chalcopyrite and tennantite and element maps of Zn, Cu, Fe, Ge and As from sample 6548. These images were all obtained using the SEM. Ge is concentrated into tennantite.

A second area consisting of sphalerite, galena and chalcopyrite was chosen as area 2 from the sphalerite-chalcopyrite-dominant sample 6548 (Figure 3.25). Once again, the element maps of Zn, Cu, Ag, Ge and Pb show Ge concentrating into galena together with Ag (Figure 3.27). Further evidence of this can be found in Appendix C.1.1 in samples KP 12, 15452b.

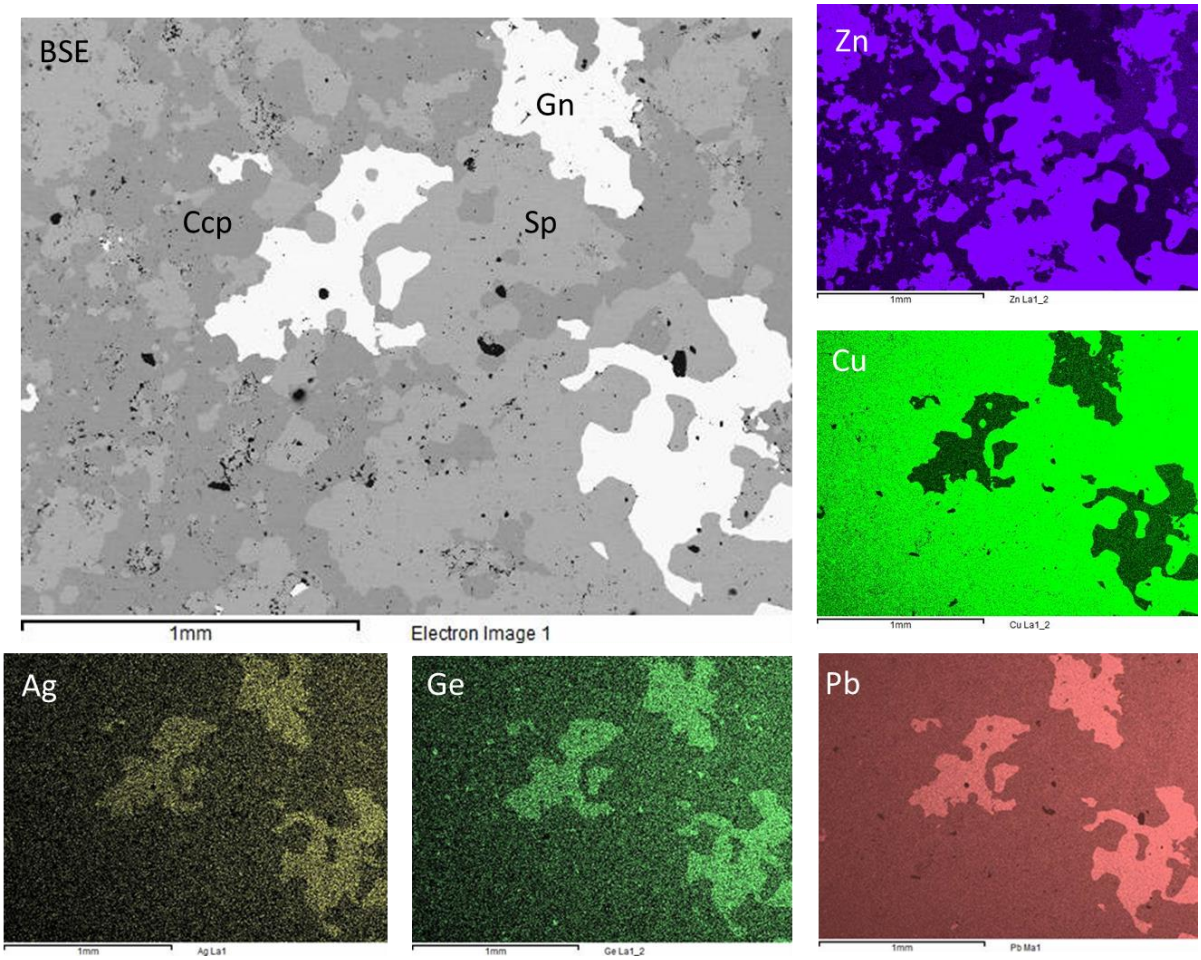

Figure 3.27: Backscatter electron image showing sphalerite, galena and chalcopyrite and element maps of Zn, Cu, Fe, Ge and As from sample 6548. These images were all obtained using the SEM. Ge and Ag concentrate into galena.

A vein containing galena, tennantite, chalcopyrite, pyrite and arsenopyrite between quartz and sphalerite was selected from the sphalerite-dominant sample KP11c (Figure 3.28). The element maps of Ge, As, Co and Fe show Ge concentrating into galena (Figure 3.29). Interestingly, there is a high concentration of Co within the Fe-rich phases, in this case, chalcopyrite, arsenopyrite and pyrite. Further examples of this Co distribution can be seen in Appendix C.1.2, C2.1 and C.2.4.

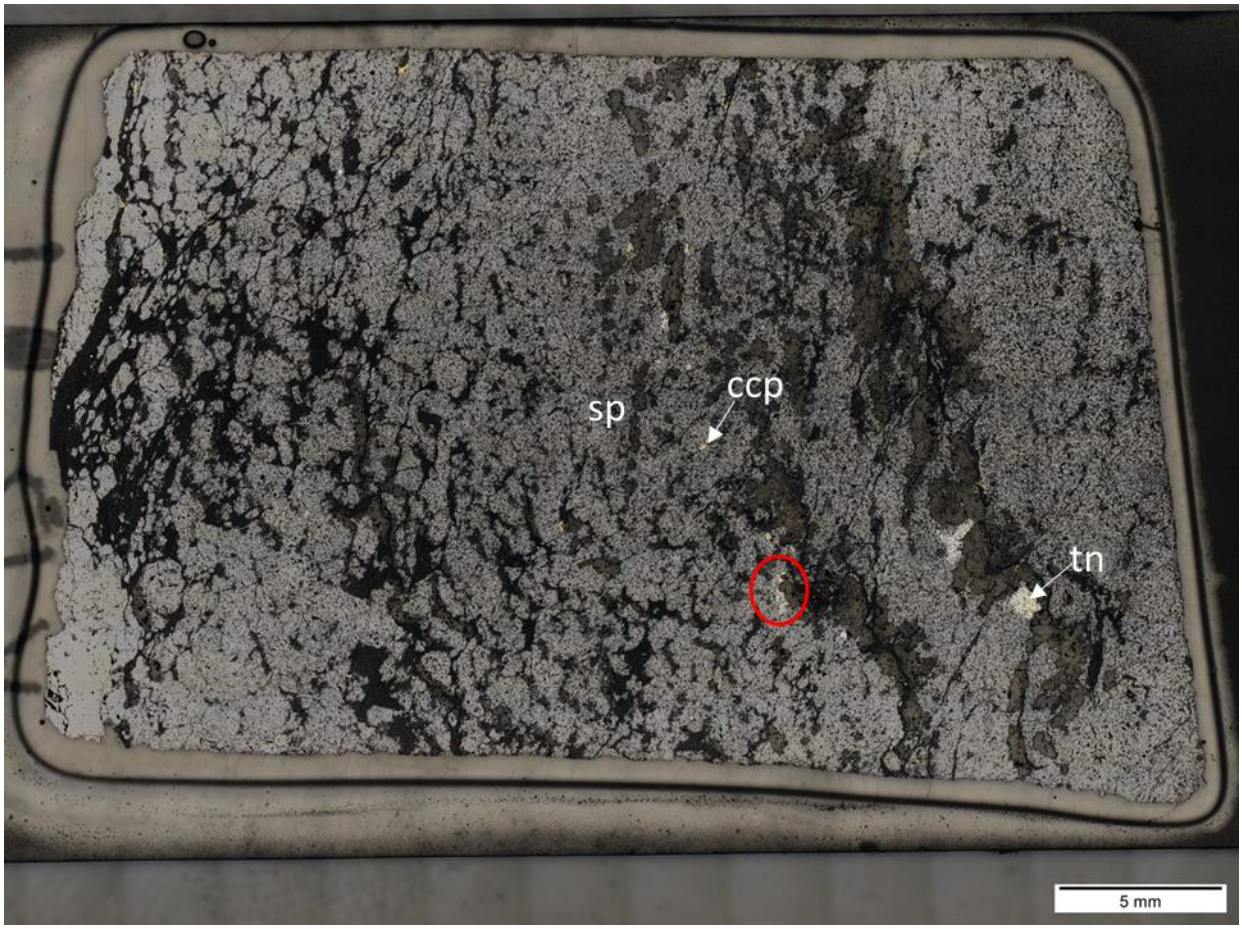

Figure 3.28: Full polished thin section image in reflected light showing sphalerite-dominant sample KP11c and the area selected for TIMA analysis (red circle).

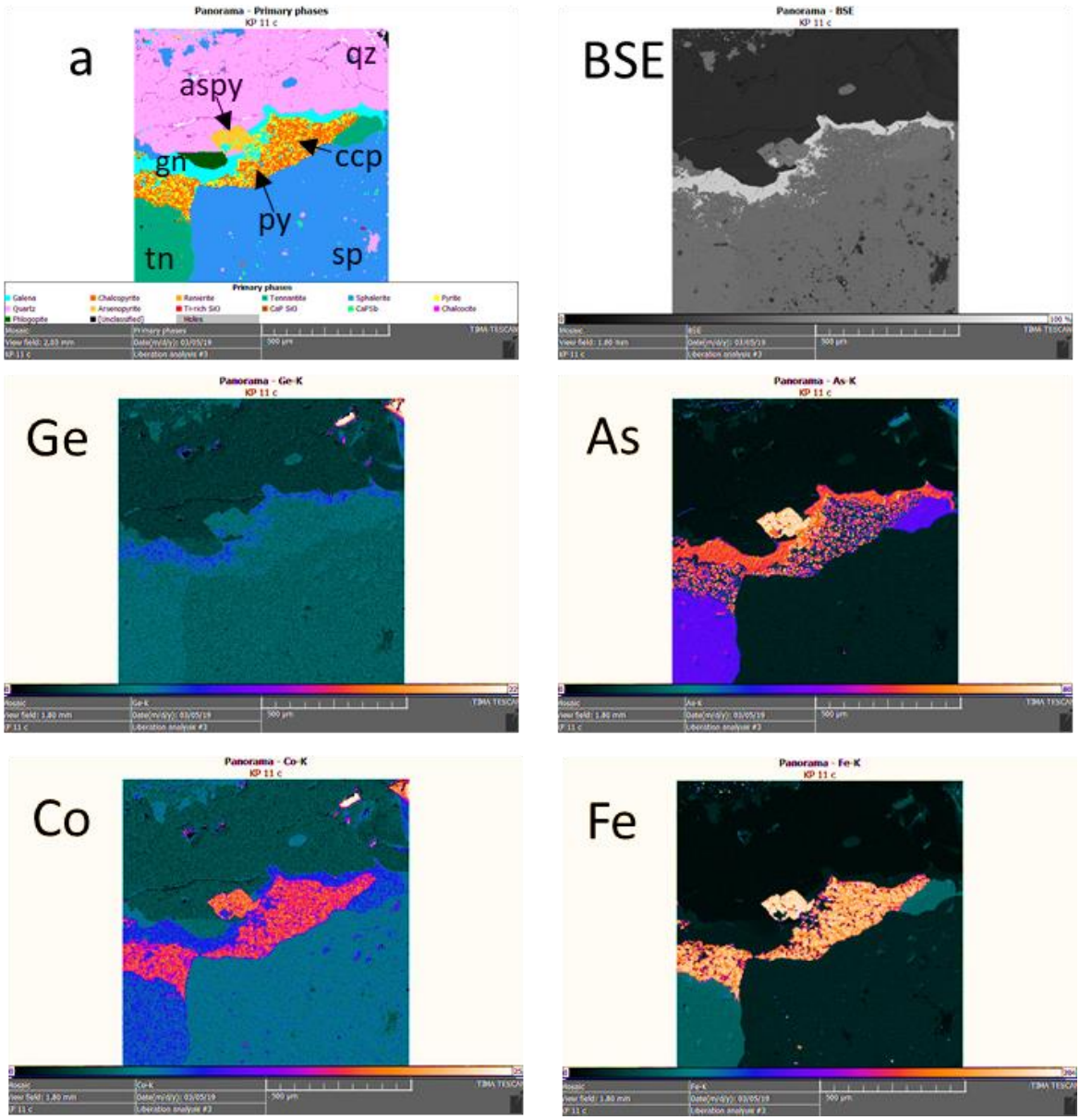

Figure 3.29: False colour primary phase map (a) showing quartz (qz), sphalerite, tennantite, galena, chalcopyrite, pyrite and arsenopyrite, backscatter electron image and element maps for Pb, S, Cu, Fe, Ge and As from sample KP11c. These images were all obtained using the TIMA. Ge is concentrated into galena, as is As. The Fe-rich phases, chalcopyrite, pyrite and arsenopyrite all contain Co.

The unknown dusty brown-grey mineral was analysed by the TIMA, but unfortunately it had a BSE level % to be below 15, and so no data was gathered for this mineral.

This data and all other element maps present in Appendix C shows that most Ge is found in renierite, where present. Where renierite is not present in the assemblage, Ge partitions into galena and to a lesser extent into tennantite. Ge also occurs in galena and tennantite when renierite is present in the assemblage, although to a lesser extent.

Galena generally contains As and less commonly hosts Ga. Tennantite contains As and no Sb, confirming it is in fact tennantite, and not tetrahedrite. Tennantite also contains Pb. Co typically concentrates into the Fe-rich phases; chalcopyrite, pyrite and arsenopyrite. Ag minerals allargentum and stromeyerite were found within samples KP 13 and 587 (Appendix C.2.2). There is also an unidentified Sb and Ca-rich gangue present throughout the ore suite.

TIMA Semi-Quantitative Analysis

The TIMA software is able to calculate a mineral composition for any mineral when a full element scan is undertaken on an area. It will calculate this mineral composition using the elements that represent the highest peaks in a mineral spectrum. However, care needs to be taken as this is only a semi-quantitative instrument, and no background corrections were done for this section due to limited knowledge on the instrument. Normalised mineral compositions have been gathered for bornite, chalcopyrite, sphalerite and renierite (Table 3.5) from samples KP13, a bornite-chalcopyrite-dominant sample, and KP2, a sphalerite-bornite-dominant sample. Three points were selected for each mineral phase for a composition; this was then used to obtain an average composition for each mineral. Bornite, chalcopyrite and sphalerite were used to assess the data produced by the TIMA and to give some indication of the reliability of the analysis.

These average compositions have been compared to published compositions for each mineral (Table 3.6). The bornite published composition was taken from Pessic and Olson (1984), who used a microprobe on a bornite sample from Pinal, Arizona, a Cu, Ag, Au deposit. The sphalerite composition was taken from Mondillo *et al.* (2018), who analysed sphalerite from a Mississippi Valley-type (MVT) deposit. The chalcopyrite published composition was taken from Lundstrom *et al.* (2005) who used chalcopyrite from Pyhasalmi Pb-Zn-Cu mine in Finland. The renierite composition was taken from Sclar and Geier (1957), who used samples from Tsumeb.

Table 3.5: Mineral compositions extracted from the TIMA for bornite, sphalerite and chalcopyrite from sample KP 13, and for renierite from sample KP 2.

Sample	Mineral	S	Fe	Cu	Zn	Ge	Total
KP13	Bornite	24.49	14.93	60.58			100.00
		23.71	7.46	68.83			100.00
		23.08	11.21	65.71			100.00
	Average	23.76	11.20	65.04			100.00
KP 13	Sphalerite	31.87	0.01		68.12		100.00
		31.92	0.01		68.06		99.99
		31.88	0.01		68.11		100.00
	Average	31.89	0.01		68.10		100.00
KP 13	Chalcopyrite	30.59	28.27	41.14			100.00
		31.21	29.06	39.72			99.99
		31.01	29.97	39.02			100.00
	Average	30.94	29.10	39.96			100.00
KP 2	Renierite	31.12	13.74	47.34		7.79	99.99
		30.36	13.59	48.36		7.69	100.00
		29.97	13.70	48.05		8.28	100.00
	Average	30.48	13.68	47.92		7.92	100.00

The bornite compositions are similar, however there is less S and more Cu in the average TIMA composition than there is in the published composition. Sphalerite has almost no Fe, less S and a lot more Zn in the Kipushi sample compared to the published composition, probably due to a temperature difference during the formation of each deposit. Chalcopyrite has a similar Fe composition to the published data, less S and more Cu. The renierite composition obtained from the TIMA is somewhat different to the published composition. There is no As or Zn in the TIMA composition, and about 7 weight % more Cu. This shows that the Kipushi renierite is very poor in As and Zn, but rich in Ge and Cu.

Table 3.6: Published mineral compositions for bornite, sphalerite, chalcopyrite and renierite compared to the average mineral compositions for the same minerals from the TIMA. (Bornite: Pessic and Olson, 1984; sphalerite: Mondillo et al., 2018; chalcopyrite: Lundstrom et al., 2005; renierite: Sclar and Geier, 1957).

Mineral	Published composition							TIMA composition						
	S	Fe	As	Cu	Zn	Ge	Total	S	Fe	As	Cu	Zn	Ge	Total
Bornite	25.55	11.12		63.33			100.00	23.76	11.20		65.04			100.00
Sphalerite	33.30	8.19			58.20		99.69	31.89	0.01			68.10		100.00
Chalcopyrite	34.90	30.40		34.60			99.90	30.94	29.10		39.96			100.00
Renierite	31.83	13.73	0.95	41.63	3.53	7.75	99.42	30.48	13.68		47.92		7.92	100.00

Mineral formulae for each mineral can be calculated using the composition given by the TIMA (Table 3.7).

Table 3.7: Mineral formula for bornite, sphalerite, chalcopyrite and renierite using the chemical composition obtained from the TIMA

Sample	Mineral	Formula
KP13	Bornite	Cu_5FeS_4
KP13	Sphalerite	ZnS
KP13	Chalcopyrite	$CuFeS_2$
KP2	Renierite	$Cu_{11}Fe_4Ge_2S_{16}$

Quantitative Analysis by Electron Microprobe

EPMA

Four representative samples were selected from the Kipushi suite for analysis by electron microprobe. Renierite, galena, tennantite and sphalerite were chosen for multiple point analyses of Ni, Fe, Co, Cu, Zn, Ga, Ge, Ag, In, Pb, As and S. Unfortunately, many of these results did not provide good totals and are only provided in Appendix E, as are the standards used for the analyses. The following data are the useable quantitative results.

Renierite ($(Cu,Zn)_{11}Fe_4(Ge,As)_2S_{16}$)

Six successful renierite analyses were achieved from samples KP12 (bornite-dominant) and KP2 (sphalerite-bornite-dominant) (Table 3.8). The analyses from sample KP12 add up to 100 %, while the analyses from sample KP2 are either 1 weight % above or below 100. The average analysis is similar to the published data for renierite (Table 3.9). There is more Cu in the average renierite composition from the EPMA than there is the published composition (Sclar and Geier, 1957). There is more Pb in the average EPMA composition. The amount of Ge in both compositions is similar, only 0.30 weight % more Ge in the Kipushi samples than the published composition (Sclar and Geier, 1957).

Table 3.8: Weight percentage of Ni, Fe, Co, Cu, Zn, Ga, Ge, Ag, In, Zn, Pb and S analysed for 2 points on a renierite phase in sample KP12, and 3 points on a renierite phase in sample KP2. The average of all these analyses is shown in the last row of the table.

Sample		Ni	Fe	Co	Cu	Zn	Ga	Ge	Ag	In	Pb	As	S	Total
KP 12	Point 1	0.00	13.43	0.00	43.11	2.81	0.00	7.06	0.08	0.00	0.96	0.36	32.94	100.74
	Point 2	0.00	13.58	0.00	43.69	2.42	0.01	6.73	0.22	0.07	0.66	0.34	32.78	100.51
KP 2	Point 1	0.03	13.55	0.00	42.33	3.04	0.00	8.91	0.06	0.00	0.73	0.76	29.99	99.40
	Point 2	0.02	13.53	0.00	42.21	3.16	0.00	8.71	0.09	0.00	1.30	0.70	29.56	99.28
	Point 3	0.00	13.38	0.00	44.29	2.78	0.00	8.64	0.16	0.00	0.36	0.68	31.43	101.72
	Point 4	0.00	13.27	0.00	44.35	3.04	0.01	8.31	0.11	0.00	0.00	0.73	31.23	101.05
	Average	0.01	13.46	0.00	43.33	2.88	0.00	8.06	0.12	0.01	0.67	0.60	31.32	100.45

Table 3.9: Weight percent of S, Fe, As, Cu, Zn, Pb and Ge in a published renierite composition (from Sclar and Geier, 1957) and the average composition obtained from the EPMA from samples KP2 and KP12.

Published composition								EPMA composition							
S	Fe	As	Cu	Zn	Pb	Ge	Total	S	Fe	As	Cu	Zn	Pb	Ge	Total
31.83	13.73	0.95	41.63	3.53		7.75	99.42	31.32	13.50	0.59	43.33	2.87	0.66	8.05	100.32

Calculated mineral formula for each renierite analysis from Kipushi is found in Table 3.10.

Table 3.10: Calculated formula from weight percent for each renierite analysis from the EPMA.

Sample		Formula
KP 12	Point 1	$Cu_{10.33}Zn_{0.67}Fe_4Ge_{1.90}As_{0.10}S_{16}$
	Point 2	$Cu_{10.42}Zn_{0.58}Fe_4Ge_{1.90}As_{0.10}S_{16}$
KP 2	Point 1	$Cu_{10.26}Zn_{0.74}Fe_4Ge_{1.84}As_{0.16}S_{16}$
	Point 2	$Cu_{10.25}Zn_{0.75}Fe_4Ge_{1.85}As_{0.15}S_{16}$
	Point 3	$Cu_{10.33}Zn_{0.67}Fe_4Ge_{1.85}As_{0.15}S_{16}$
	Point 4	$Cu_{10.29}Zn_{0.71}Fe_4Ge_{1.86}As_{0.14}S_{16}$
	Average	$Cu_{10.23}Zn_{0.67}Fe_4As_{0.13}Ge_{1.86}S_{16}$

Galena (PbS)

Three successful galena analyses were obtained from sample KP2 (Table 3.11). All of these analyses add up to 100 weight %. There is little Ge content in these analyses. The average analysis from the EPMA is very similar to that of the published data for galena (Table 3.12). There is slightly more S and slightly less Pb in the average galena

composition obtained from the EPMA than there is the published composition (Peng *et al.*, 2003). Overall, the compositions are almost the same.

Table 3.11: Weight percentage of Ni, Fe, Co, Cu, Zn, Ga, Ge, Ag, In, Zn, Pb and S analysed for 3 points on a galena phase in sample KP2. The average of all these analyses is shown in the last row of the table.

KP 2	Ni	Fe	Co	Cu	Zn	Ga	Ge	Ag	In	Pb	As	S	Total
Point 1	0.00	0.00	0.00	0.06	0.05	0.00	0.05	0.04	0.03	86.77	0.00	13.27	100.28
Point 2	0.02	0.00	0.03	0.02	0.11	0.07	0.07	0.12	0.00	85.96	0.02	13.69	100.09
Point 3	0.00	0.01	0.00	0.12	0.06	0.00	0.00	0.06	0.00	86.84	0.00	13.32	100.40
Average	0.01	0.00	0.01	0.07	0.07	0.02	0.04	0.07	0.01	86.52	0.01	13.42	100.26

Table 3.12: Weight percent of S, Fe, As, Cu, Zn, Pb and Ge in a published galena composition (from Peng et al., 2003) and the average composition obtained from the EPMA from sample KP2.

Published composition								EPMA composition							
S	Fe	As	Cu	Zn	Pb	Ge	Total	S	Fe	As	Cu	Zn	Pb	Ge	Total
13.20					86.10		99.30	13.42					86.52		99.94

Sphalerite ((Zn,Fe)S)

Three successful analyses of sphalerite were obtained from sample KP2 (Table 3.13). Two of these analyses add up to 100 weight %, while one is just over 100 weight %. The Ge content in these analyses is negligible. The average analysis is somewhat different to the published data for sphalerite (Table 3.14). There is 4 weight % less S in the analysed data than there is in the published data (Mondillo *et al.,* 2018). There is significantly more Zn in the Kipushi samples, and no Fe.

Table 3.13: Weight percentage of Ni, Fe, Co, Cu, Zn, Ga, Ge, Ag, In, Zn, Pb and S analysed for 3 points on a sphalerite phase in sample KP2. The average of all these analyses is shown in the last row of the table.

KP 2	Ni	Fe	Co	Cu	Zn	Ga	Ge	Ag	In	Pb	As	S	Total
Point 1	0.00	0.02	0.00	0.10	70.35	0.00	0.00	0.00	0.00	0.00	0.01	30.21	100.70
Point 2	0.01	0.00	0.00	0.04	71.61	0.02	0.00	0.00	0.00	0.70	0.00	28.99	101.37
Point 3	0.00	0.03	0.01	0.00	72.17	0.00	0.00	0.10	0.01	0.00	0.00	28.49	100.81
Average	0.00	0.02	0.00	0.05	71.38	0.01	0.00	0.03	0.00	0.23	0.00	29.23	100.96

Table 3.14: Weight percent of S, Fe, As, Cu, Zn, Pb and Ge in a published sphalerite composition (Mondillo et al., 2018) and the average composition obtained from the EPMA from sample KP2.

Published composition								EPMA composition							
S	Fe	As	Cu	Zn	Pb	Ge	Total	S	Fe	As	Cu	Zn	Pb	Ge	Total
33.30	8.19			58.20			99.69	29.29				71.38			100.67

The mineral formula for sphalerite from Kipushi can be calculated from the weight % of each point to be ZnS.

Synthesis

Sulphide assemblages from the Kipushi samples analysed were divided into two main assemblage-types: Cu-dominant and Zn-dominant. These assemblages were defined by looking at the most abundant minerals for each sample. SEM analyses determined that there is more Ge in the Cu-dominant samples than in the Zn-dominant samples. This can be attributed to more renierite being present in the Cu-dominant assemblages. Ge preferentially partitioned into the renierite, galena and then tennantite. Trace amounts of Ge were found within the galena by the microprobe, supporting the findings from the SEM analyses.

Chapter 4

Germanium in the Tsumeb Deposit

The Tsumeb deposit is an epigenetic, hydrothermal massive sulphide 'pipe-like' system in Namibia. The most abundant minerals are bornite, galena, sphalerite and tennantite, with many more less-abundant sulphides (Melcher, 2006). Two of these less abundant sulphide minerals are renierite and germanite, which are both Ge minerals. As Tsumeb is the second known locality for the occurrence of Ge-rich minerals, data from this deposit can be used as a comparison for the Kipushi deposit. This chapter presents the results of petrology, whole-rock geochemistry and SEM studies investigating the presence of Ge in sulphide minerals of the Tsumeb deposit.

Petrography

The samples from Tsumeb have been divided into three main assemblage-types: Cu-dominant, Zn-dominant and Pb-dominant, which can be broken down into various assemblages (Table 4.1). The Cu assemblages include bornite-dominant and tennantite-dominant while Zn assemblages are divided into sphalerite-dominant and sphalerite-pyrite dominant. The Pb assemblage is galena-dominant. All samples were examined under reflected light using a petrographic microscope and images of complete polished ore blocks were acquired using an Olympus BX53 microscope (Appendix A.2.2).

*Table 4.1: Table detailing samples and sample assemblages examined for the Tsumeb ore suite. Sample numbers in **bold** were examined using microbeam techniques.*

Assemblage type	Dominant Sulphide	Sample #
Copper	Bornite	107, **263**, **333**, 337, 434, 477, 523, 256 C, 99A a, **717**,**125**, **253 b**, **TS 3**, TS 6, TS 8, TS 9, TS 10
	Tennantite	470, TS 1, **TS 7**, **99A b**
Lead		**253 a**, TS 4, **TS 5**, **TS 11**, 8, **259**, 560, 91, 340, **423**, 90
Zinc	Sphalerite	**110**, 149, **735**, **272 A**, 519, 268, 395
	Sphalerite-pyrite	519, 268, 395

Cu Assemblages

Bornite-dominant

Most of the Tsumeb samples are from this assemblage which is dominated by massive bornite. A photomicrograph of the entire ore block of bornite-dominant sample 263 shows the bornite-dominant assemblage (Figure 4.1). This comprises massive bornite with chalcocite veins and minor tennantite, renierite, galena and pyrite. Chalcocite veins which occur between more massive areas of chalcocite are noted to have replaced bornite (Figure 4.2a). Tennantite (Figure 4.2a) and renierite (Figure 4.2b) occur as blebs within the bornite. Galena and sphalerite can be found as small blebs or larger networks. Large blebs of betekhtinite occur in this assemblage (Figure 4.2c). Chalcopyrite and digenite are present. Euhedral pyrite and carrollite grains up to 2 mm in size occur in some of these samples, as well as minor renierite and germanite (Figure 4.2d).

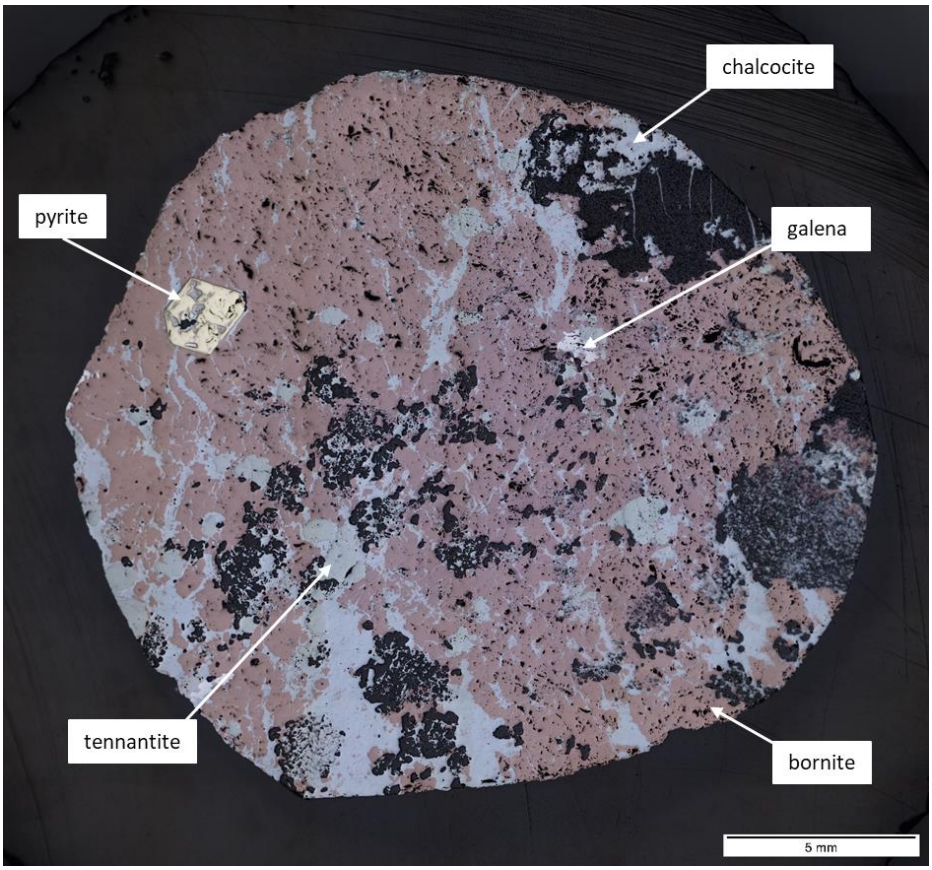

Figure 4.1: Photomicrograph of the entire ore block of sample 263 in reflected light, showing massive bornite with chalcocite veins and minor tennantite and galena, and one euhedral pyrite grain with gangue (black).

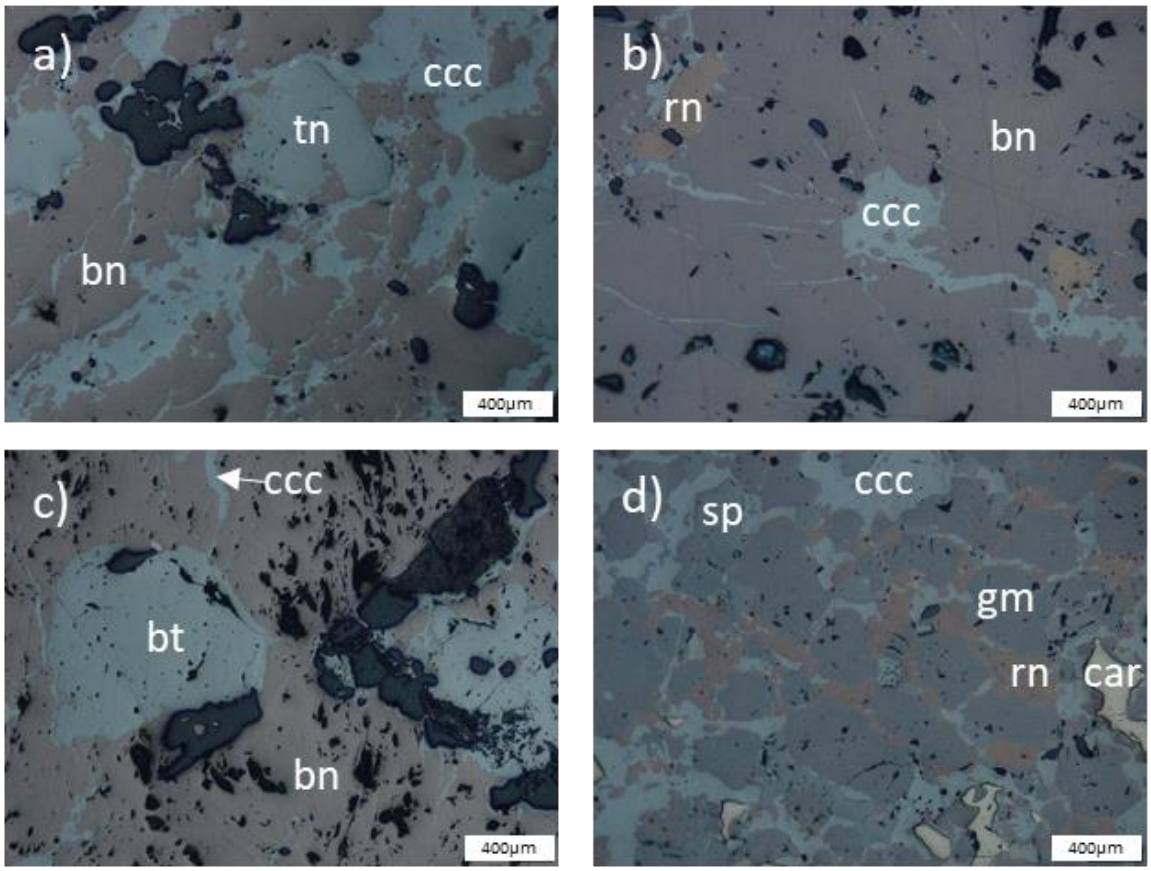

Figure 4.2: Mineral textures from the bornite-dominant assemblage in reflected light. (a) shows small chalcocite (ccc) veins and larger masses of chalcocite all surrounding a tennantite (tn) bleb from sample 263. (b) shows chalcocite veins and two blebs of renierite (rn) from sample 263. (c) shows a large bleb of betekhtinite (bt) in sample 477. (d) shows many blebs of germanite (gm) interspersed with renierite, chalcocite and sphalerite (sp) from sample TS 8

Tennantite-dominant

In this assemblage, an underlying bornite-dominant assemblage has been replaced by massive tennantite. This is noted in remnant blebs of bornite with chalcocite veins within the tennantite. Sphalerite veins (Figure 4.3a) cross-cut, and are therefore younger than the tennantite. Renierite and germanite occur as disseminations in this assemblage and are associated with each other (Figure 4.3b). Galena and digenite are found to be replacing germanite (Figure 4.3b).

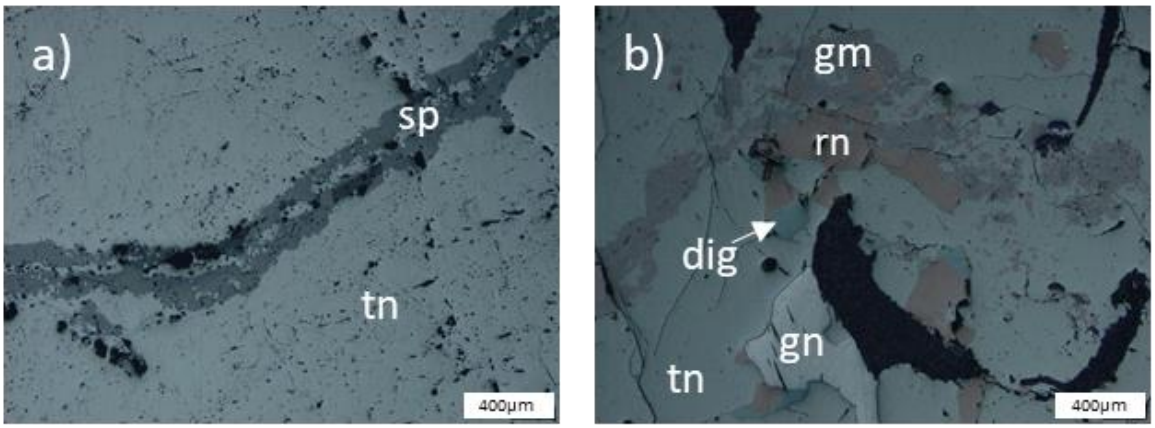

Figure 4.3: Mineral textures from the tennantite-dominant assemblage in reflected light. (a) shows a vein of sphalerite (sp) cross-cutting massive tennantite (tn) from sample 470. (b) shows renierite (rn), germanite (gm), digenite (dig) and galena (gn) within the massive tennantite from sample TS7.

Pb Assemblage

Galena-dominant

This assemblage is made up of massive galena with lesser bornite, sphalerite, tennantite, betekhtinite, digenite and pyrite. A photomicrograph of the entire ore block of sample 8 is shown in Figure 4.4. This assemblage is interspersed with euhedral to subhedral pyrite of approximately 1 mm in size and sphalerite blebs (Figure 4.5a). Blebby tennantite occurs throughout this assemblage (Figure 4.5b). Blebs and disseminated bornite as well as chalcocite are present. Irregular digenite that is often associated with gangue is found (Figure 4.5c). Small areas of chalcopyrite or irregular arsenopyrite (Figure 4.5d) occur in some of the samples.

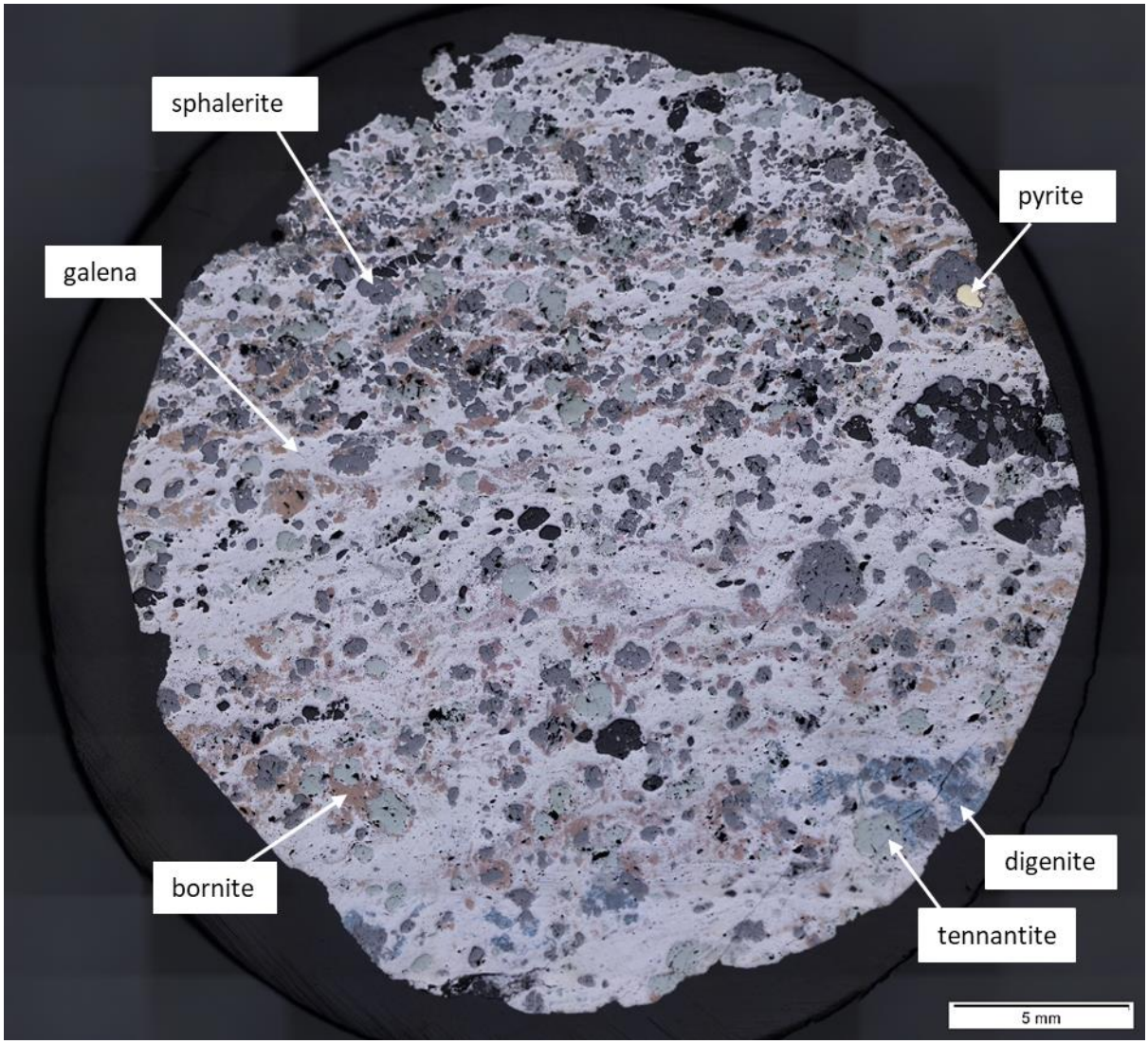

Figure 4.4: Photomicrograph of entire ore block of sample 8 in reflected light, showing sphalerite, tennantite, bornite and digenite in massive galena, with a single pyrite grain and with gangue (black).

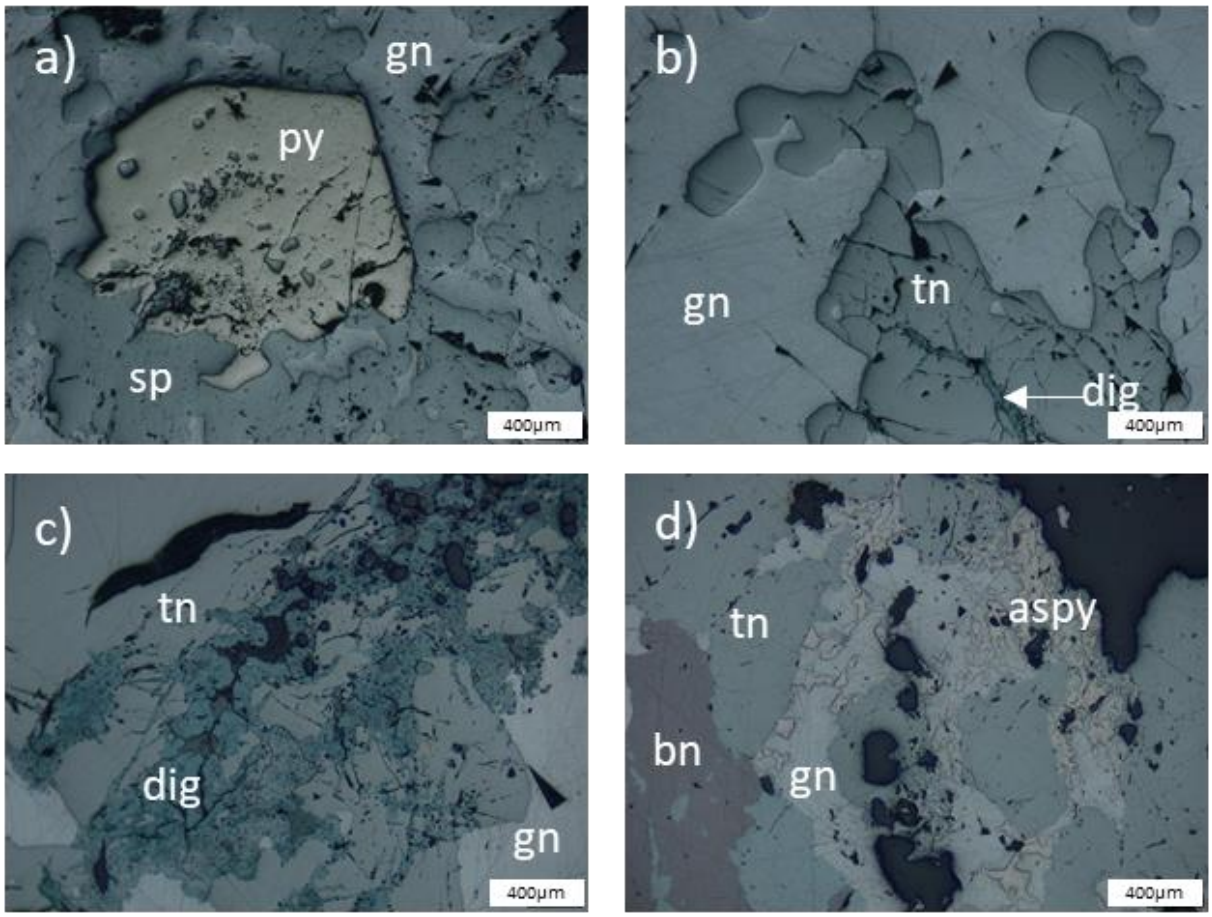

Figure 4.5: Mineral textures from the galena-dominant assemblage in reflected light. (a) shows sphalerite (sp) and pyrite (py) from sample 91. (b) shows blebby tennantite (tn) within the massive galena (gn) from sample 253a. (c) shows digentite (dig) within the tennantite from sample 253a. (d) shows small sections of arsenopyrite (aspy) next to tennantite blebs and bornite (bn) TS11.

Zn Assemblages

Sphalerite-dominant

Massive sphalerite dominates this assemblage. A photomicrograph of the entire ore block of sample 110 shows an irregular network of galena in a sphalerite groundmass, with minor blebs of tennantite, bornite, chalcocite, digenite, and disseminated pyrite (Figure 4.6). Galena can also occur as blebs. In some samples tennantite creates a network. Irregular renierite and bornite are found, with digenite and chalcocite replacing the bornite. A few pyrite grains that are usually disseminated are seen and native copper has been found in this assemblage. Minor chalcopyrite can also occur within this assemblage.

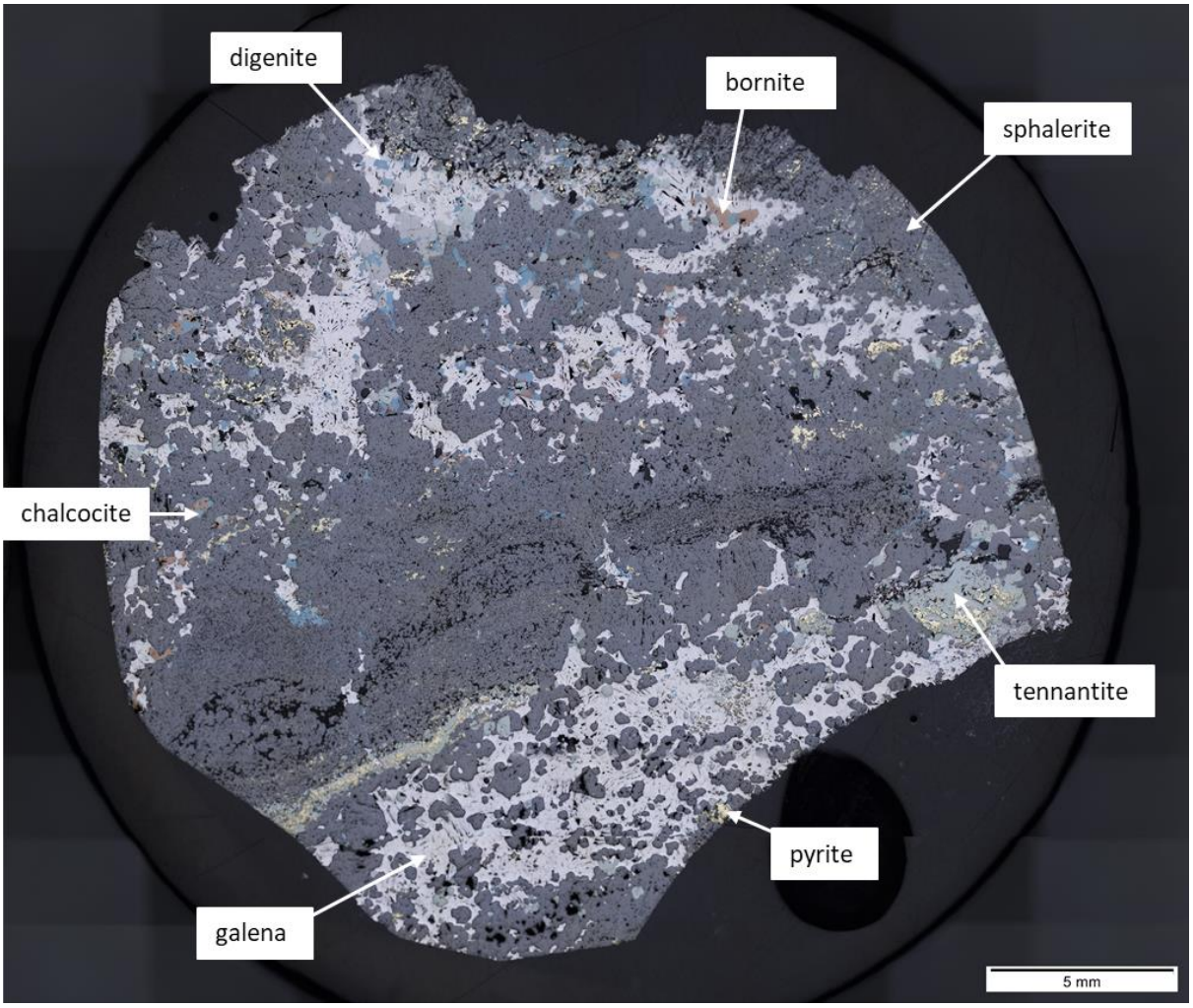

Figure 4.6: Photomicrograph of sample 110 in reflected light, showing massive sphalerite, a galena network and minor digenite, tennantite, bornite, chalcocite and pyrite, with gangue (black).

Sphalerite-pyrite-dominant

This assemblage consists of massive sphalerite that is interspersed with large areas of massive and disseminated anhedral pyrite. In sample 395 (Figure 4.7) the percentage of gangue is very minor.



Figure 4.7: Blebby pyrite (pale yellow) throughout the massive sphalerite (dark grey), with gangue (black) of sample 395 in reflected light.

Petrological summary

Only two samples contained germanite, while seven samples contained renierite. Seven of these samples are from the Cu-dominant assemblage-type (Table 4.2) while one sample was from the Zn-dominant assemblage-type and none from the Pb-dominant assemblage-type. Chalcocite, digenite and carrollite are also more prevalent within the Cu-dominant assemblage-type. Chalcopyrite is not abundant within any of these samples, while pyrite, galena and tennantite are equally abundant throughout the different assemblage-types.

Paragenesis

Bornite formed first, as it is being replaced by all subsequent phases. Chalcocite formed second, as it can be seen as small veins within the bornite, and it has remnant

globules of bornite within it. The next phases to form were renierite, germanite, tennantite, betekhtinite then sphalerite, creating blebs and disseminations that replaced the bornite and chalcocite. Galena was the next phase to form, as it replaces all the previously mentioned minerals and their textures, along with the galena was digenite, which also replaces the other minerals. Last to form was pyrite, arsenopyrite and carrollite. These phases coat the previous phases, in some cases leaving remnant blebs of the earlier phases within the pyrite or carrollite.

Sclar and Geier (1957) suggest that pyrite was the first phase to form, followed by germanite, bornite and enargite. Sphalerite formed next, then tennantite. After those phases, an unknown mineral and chalcopyrite formed, followed by renierite. Finally, digenite and galena formed.

Samples were selected for further study based on the complexity of the mineral assemblages and their textures. Areas that contained sphalerite, and areas with galena, as well as areas with renierite and germanite were given preference for further analyses. Some areas contained silicates; however silicates were not given preference as this study focused on the polymetallic sulphide minerals. The chosen areas were thoroughly polished.

Table 4.2: A comprehensive table showing the mineral assemblages for each sample. The purple background represents the Cu-dominant assemblage-type, blue represents the Pb-dominant assemblage-type and grey represents the Zn-dominant assemblage-type.

Sample Number	Bn	Sp	Ccp	Tn-Td	Ren	Gn	Py	Aspy	Ccc	Dig	Bt	Car	Gm
107	✓			✓		✓	✓		✓				
263	✓			✓	✓	✓	✓		✓				
333	✓					✓			✓		✓		
337	✓				✓	✓			✓				
434 a	✓			✓		✓	✓		✓		✓	✓	
434 b	✓					✓	✓		✓			✓	
477 a	✓			✓		✓			✓		✓	✓	
523	✓				✓		✓		✓		✓	✓	
99 A a	✓				✓	✓	✓		✓				
717	✓								✓		✓	✓	
125	✓								✓		✓		
253 b		✓	✓			✓			✓	✓			
TS 3	✓		✓			✓	✓		✓			✓	✓
TS 6	✓					✓			✓				
TS 8	✓		✓		✓	✓	✓		✓				
TS 9						✓	✓		✓			✓	
TS 10	✓		✓						✓			✓	
470		✓		✓									
TS 7	✓		✓	✓	✓	✓			✓			✓	✓
TS 1				✓									
99 A b	✓		✓	✓		✓							
TS 11	✓	✓				✓	✓	✓	✓				
8	✓	✓		✓		✓	✓			✓	✓		
259		✓	✓			✓	✓						
560						✓							
91	✓	✓				✓	✓	✓	✓				
340		✓		✓		✓	✓						
423						✓					✓		
253 a				✓		✓				✓			
TS 4	✓		✓			✓	✓					✓	
TS 5		✓		✓		✓	✓					✓	
90	✓	✓				✓	✓		✓				
110	✓	✓		✓		✓			✓				
149		✓		✓									
268	✓	✓	✓				✓						
395		✓				✓	✓						
735		✓		✓	✓	✓	✓			✓		✓	
272 A		✓	✓			✓	✓						
519		✓					✓						

X-Ray Diffraction

Mineral phases identified using petrographical methods were confirmed using XRD. XRD results include the weight % of the identified mineral phases (Table 4.3). The weight % of the phases confirms most of the assemblages that were identified using petrography. Sample 99A does not fit the bornite-dominant assemblage that was identified by petrography. The XRD results claim this sample as a galena-dominant sample also rich in tennantite. Sample 125 has a high weight % of quartz as it is a mineralised country rock. Once again, there are two bornite phases identified by XRD. 'Bornite high' refers to bornite that formed at high temperatures, while 'bornite' refers to bornite that formed at lower temperatures. This suggests that there were two phases of bornite. However, petrographical methods suggest only one.

Table 4.3 Results of XRD analysis showing the various mineral phases identified, including weight % of each phase by Rietveld method.

Tsumeb	Dolomite	Bornite	Tennantite	Quartz	Renierite	Chalcopyrite	Galena	Sphalerite	Bornite high	Pyrite	Total
110	0	4.2	5.8	0.4	3.3	0	21.4	57.5	1.1	6.3	100
125	0.6	18.8	0.2	76.9	0.4	0	0.1	0	2.8	0	99.8
340	0	0	0	15.6	0	1.9	72.4	1.8	0	8.2	99.9
477	0	3.7	2.6	13.9	0.1	0.1	9.3	6.4	63.9	0	100
99A	0	1	24.7	12.7	0	0.1	31.8	17.1	4.8	7.8	100

Whole Rock Geochemical Analysis

Specific samples were selected for whole rock geochemical analysis at Intertek Genalysis laboratories using ICP-MS and ICP-OES. Samples from each assemblage-type were selected to determine the variation of Ge concentration within the different assemblage-types. Similar samples to that of the Kipushi whole rock geochemical analyses samples were chosen to be able to compare the Ge concentration of the two deposits. One mineralised country rock with bornite veining was selected to determine whether the gangue contains concentrations of Ge. Four samples were selected from the Zn-dominant assemblage-type as well as four samples from the Cu-dominant assemblage-type. One sample from the Pb-dominant assemblage-type was chosen for trace element analysis. Details of analytical methods and element accuracies and precisions are contained in Appendix B. Samples were analysed for Ag, As, Be, Bi, Cd, Co, Cr, Cs, Cu, Ga, Ge, In, Li, Mn, Mo, Na, Ni, Pb, Rb, Re, Sb, Sc, Se, Tl and Zn (Table 4.4). Although this is a limited data set, due to restricted number of samples, it

can prove indicative of trace element relationships within the assemblages and the different minerals.

All samples were plotted in a ternary diagram of Pb, Zn and Cu (Figure 4.8), which shows that the mineralised country rock is relatively rich in Cu, as are three of the Cu-dominant samples. This suggests the presence of abundant bornite or tennantite within these samples. While the fourth Cu-dominant sample is enriched in Cu, it has a lower normalised Cu concentration than the rest of the Cu-dominant samples. It also has a significant concentration of Pb. One Zn-dominant sample is rich in Cu, while the rest of the Zn-dominant samples have a lower normalised Cu concentration, but more Pb. These Zn-rich samples have a high sphalerite content. The Pb-dominant sample is rich in Pb, suggesting a high galena content.

Table 4.4: Results from whole rock analysis. The amount of each trace element is measured in ppm. Samples are colour-coded to the basic assemblage-types. Brown represents the mineralised country rock, grey represents the Zn-dominant assemblage-type, purple represents the Cu-dominant assemblage-type and blue represents the Pb-dominant assemblage-type.

	Country	Zn				Cu				Pb
Sample # / Element	125	91	340	519	110	477	470	99A	TS 1	259
Ag	551	199.48	24.84	399.3	144.56	1325	658	171.11	323.85	37.48
As	13200	49000	3706.2	38300	9412.3	9967	134400	56600	138200	2985
Be	0	0	0	0	0.1	0	0	0	0	0
Bi	0.1	1.21	0.06	0.11	0.09	0.18	0.18	0.23	0.25	0.07
Cd	279.34	696.12	3895	320.86	9046	162.29	672.08	471.15	2355	4302
Co	34.3	209.5	56.6	28	63.4	462.2	30.4	275.9	5.8	36.2
Cr	8	0	0	0	6	0	0	5	0	0
Cs	0	0.11	0	0.05	0.18	0.13	0	0.08	0.05	0.05
Cu	382800	208300	10900	87600	59700	531900	501500	156400	322400	8329
Ga	125.19	153.91	718.67	91.67	10.82	211.08	142.74	292.53	339.18	39.62
Ge	76.9	152.7	10	91.7	26.9	100.4	33.6	14444.8	175.2	128.3
In	0.57	0.64	4.52	1.05	0.02	1.22	3.97	2.67	6.68	0.21
Li	1.2	1.6	0.4	2.3	4.2	2.1	1	1.9	1.6	0.8
Mn	122	234	979	586	1043	52	207	166	1364	519
Mo	2244.6	2551.1	3080.9	275.3	3670.8	26800	132.5	4328.9	2.3	1784.1
Na	0	62	36	0	73	0	156	0	0	33
Ni	18	50	19	22	43	171	8	139	3	10
Pb	13600	508900	448700	4903.2	276400	121000	68500	189700	107.1	516300
Rb	0.9	2.66	0.35	1.31	9.16	3.46	0.1	2.24	0.88	0.99
Re	12.15	2.795	0.106	1.281	0.957	120.943	0.019	7.486	0.019	0.438
Sb	309.77	383.57	473.72	448.65	172.39	408.7	1869.67	1018.12	5720.88	162
Sc	0	0	0	0	0.8	0.2	0	0.1	0.3	0
Se	29.5	8.6	11.7	56.8	7.2	31.2	51.3	341.1	39.6	50
Te	0.4	0.3	0.6	1.9	0	1.7	12.5	5	47.9	0.4
Tl	0.63	0.98	0.41	0.14	2.49	8.78	0.17	0.87	0.5	1.57
Zn	6286	15100	319000	32500	375000	3892	55400	18600	55800	212100

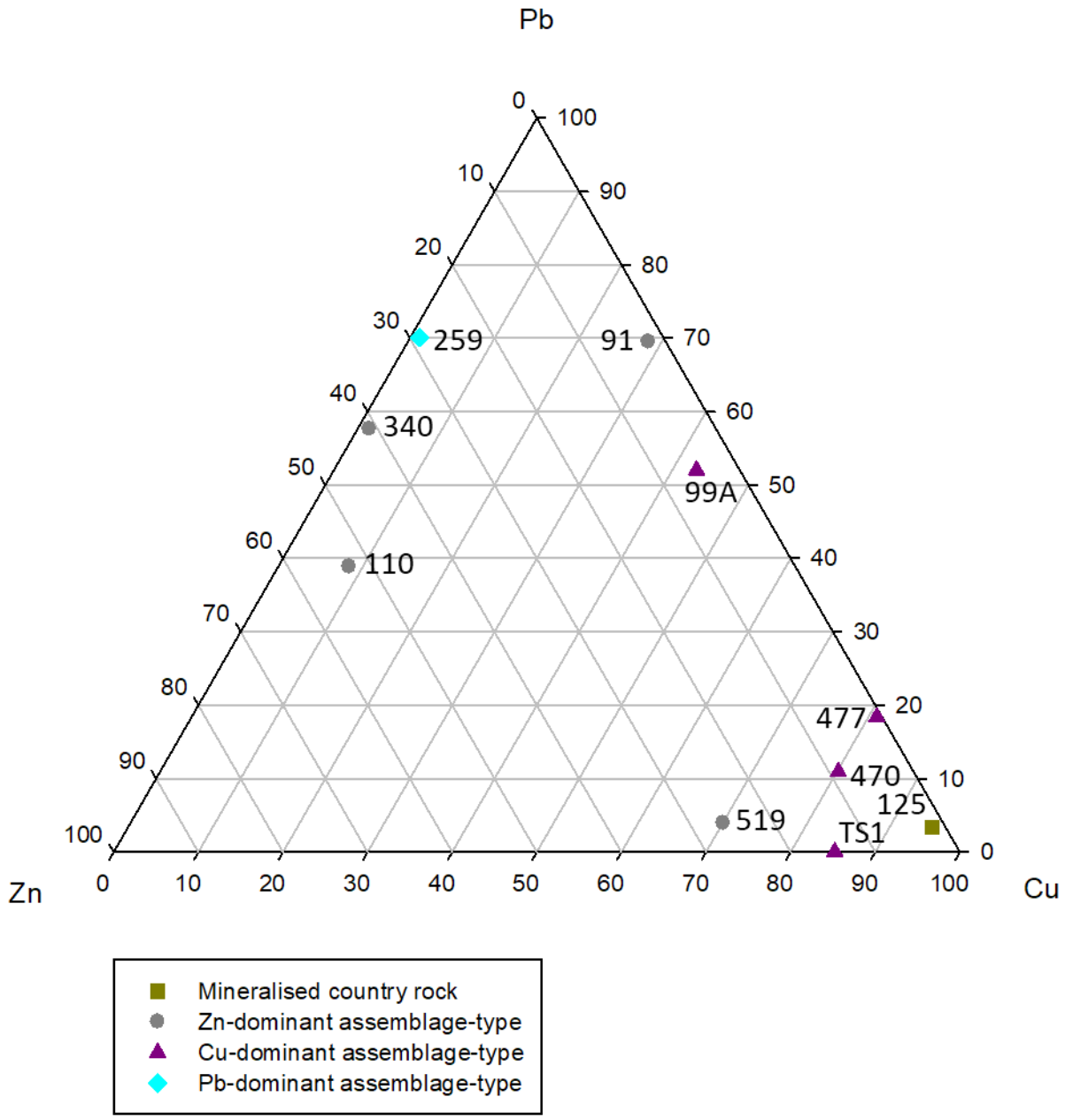

Figure 4.8: Ternary diagram showing where the analysed samples fall with respect to Pb, Zn and Cu. Grey represents the Zn-dominant assemblage-type, purple the Cu-dominant assemblage-type, blue is the Pb-dominant assmeblage-type and the brown is the mineralised country rock with bornite veining.

None of the samples contained detectable Be, and they all contained very little Bi, Cs, Cr, In, Li, Rb, Re, Sc, Te and Tl. There are extremely high concentrations of Cu, Pb and Zn in all the samples with greater Pb in the samples that contain galena. Most samples contained moderately high quantities of Ag, As, Cd, Ga, Ge and Mo (Table 4.3 and Figure 4.9). Cu, Zn and Pb are considered essential elements within these samples due to the high content of galena, sphalerite and bornite. Trace elements within these samples, excluding the essential elements, show Ge to be present within

one Cu-dominant sample, sample 99A. The rest of the samples contain low Ge. All samples have very little Ag and the Pb-dominant sample as well as two Zn-dominant samples contain minor Cd. All samples are enriched in As, with one Cu-dominant sample showing higher concentration of Sb, possibly due to tennantite within this sample. All but one sample, TS1 a Cu-dominant massive tennantite sample, have significant Mo. One Cu-dominant sample, 477, contains more Mo than the rest of the samples. One sample, 99A contains a significantly larger amount of Ge compared to all the other samples. This sample was considered an outlier and so removed from further graphs to see any possible correlations between other trace elements more clearly.

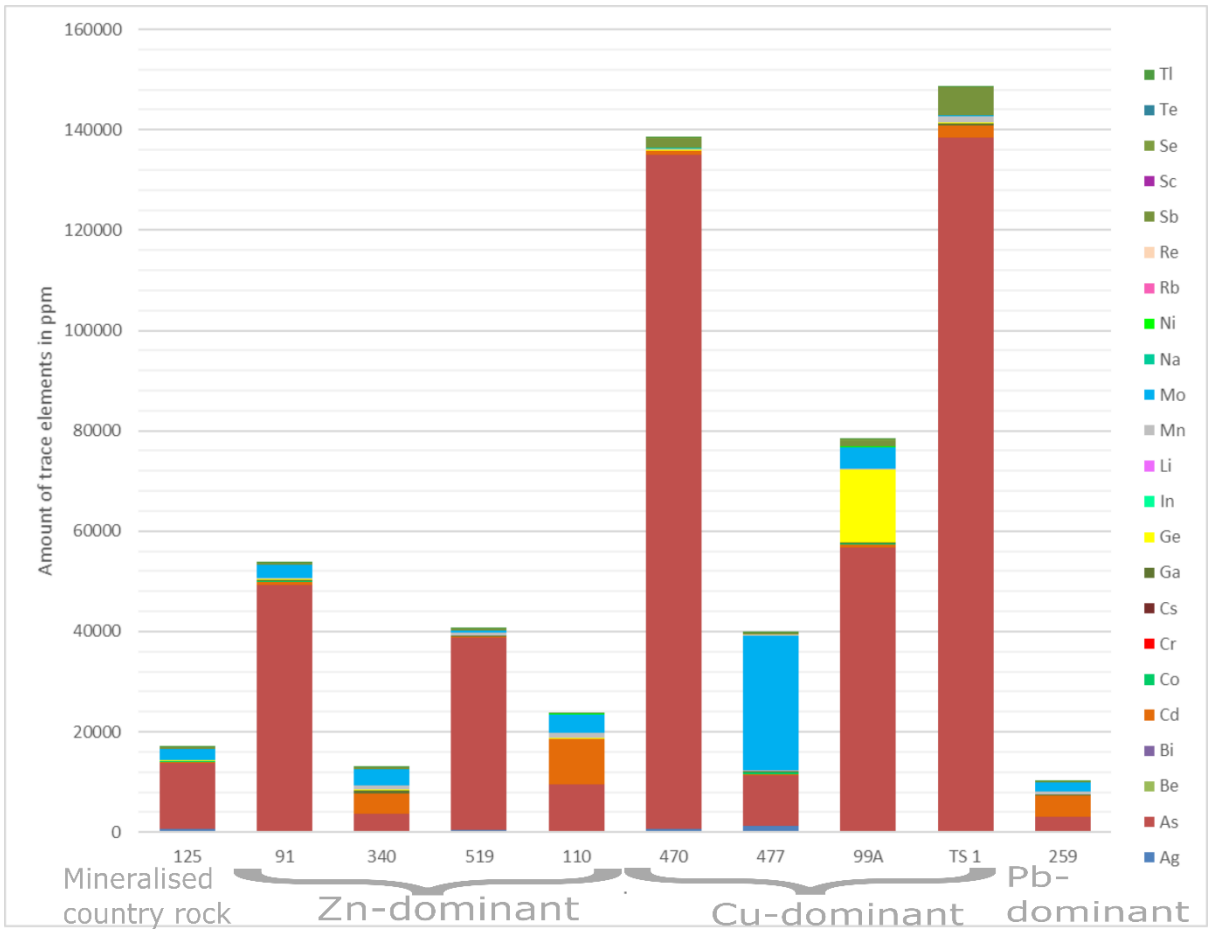

Figure 4.9: Graphical representation of trace elements within 10 samples from the Tsumeb ore suite. All samples are rich in As. Ge is only seen in high concentrations in sample 99A, a Cu-dominant sample. Most samples contain high concentrations of Mo.

The Tsumeb samples show no obvious correlation between Pb and Ge (Figure 4.10). This suggests no relationship between Ge and galena, although there are two isolated samples which contain high Pb and Ge.

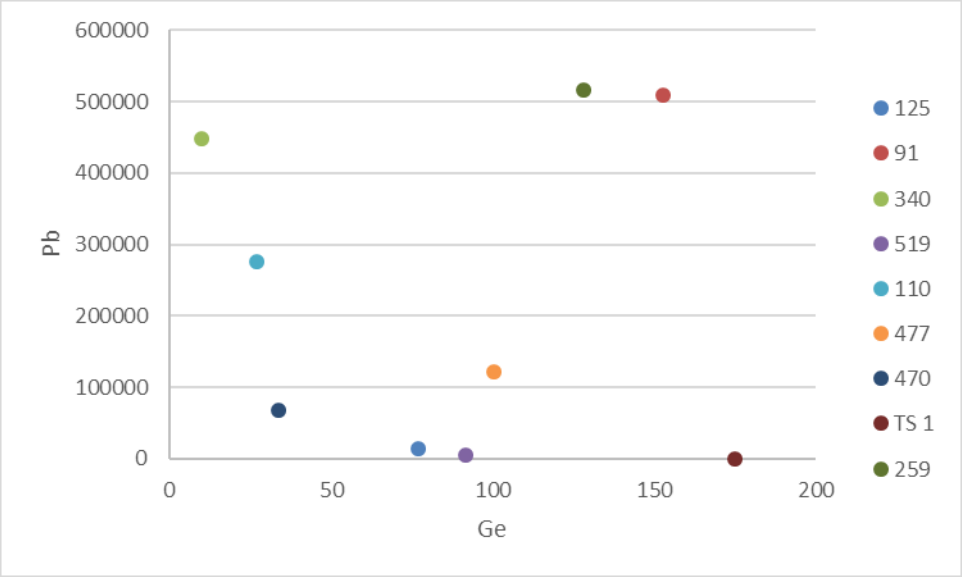

Figure 4.10: Ge, in ppm, plotted against Pb, in ppm, showing no correlation between the two elements.

Similarly, Zn and Ge show no obvious correlation (Figure 4.11), which suggests there is little Ge within the sphalerite.

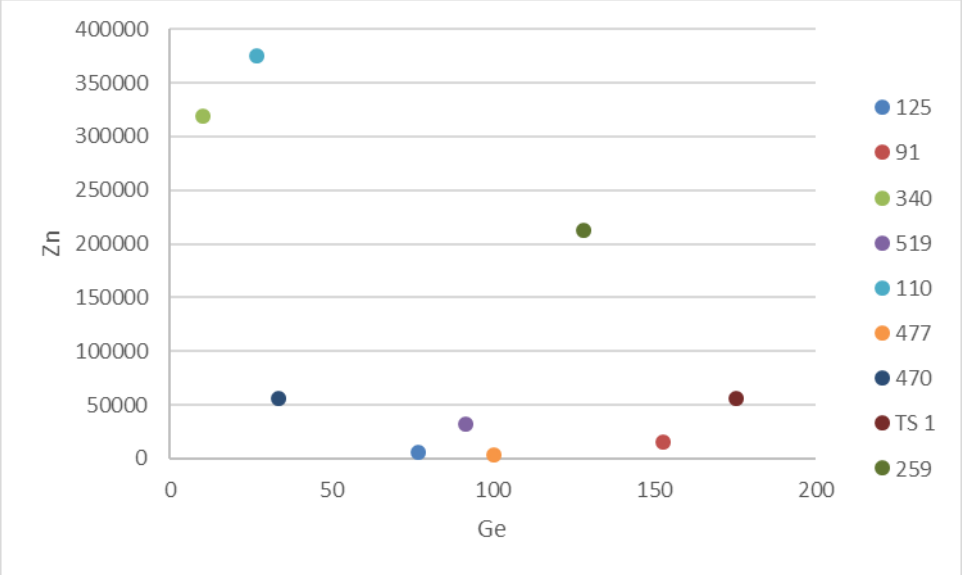

Figure 4.11: Ge, in ppm, plotted against Zn, in ppm, showing no correlation.

With increasing As in a sample, Sb also increases (Figure 4.12), suggesting that these elements may occur within tennantite or arsenopyrite. Sample TS1, which is rich in both As and Sb, is a massive tennantite sample, while sample 259, a galena-dominant sample, contains neither tennantite nor arsenopyrite.

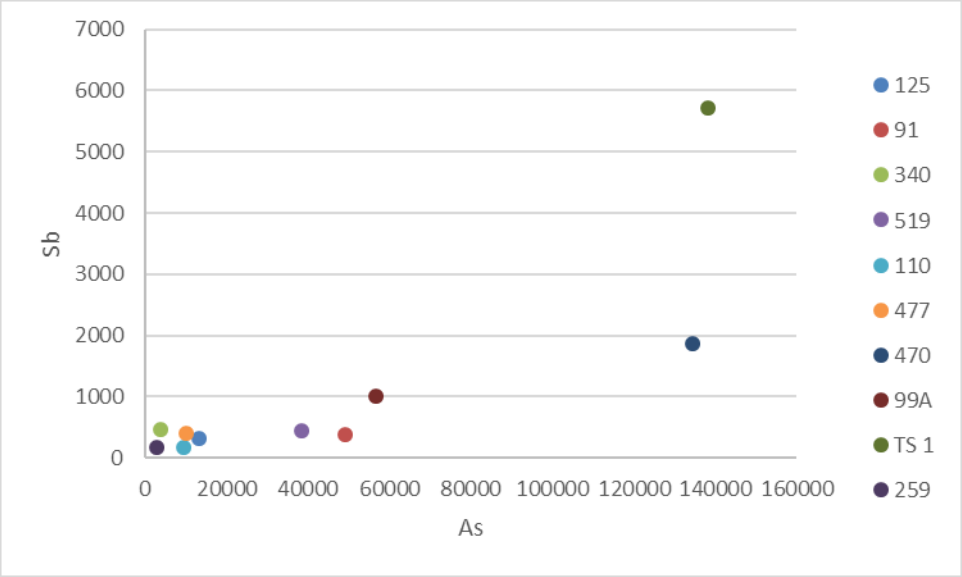

Figure 4.12: As, in ppm, plotted against Sb, in ppm, showing a slight correlation between the two elements.

Zn and Cd show a good correlation (Figure 4.13). This suggests the presence of Cd within sphalerite.

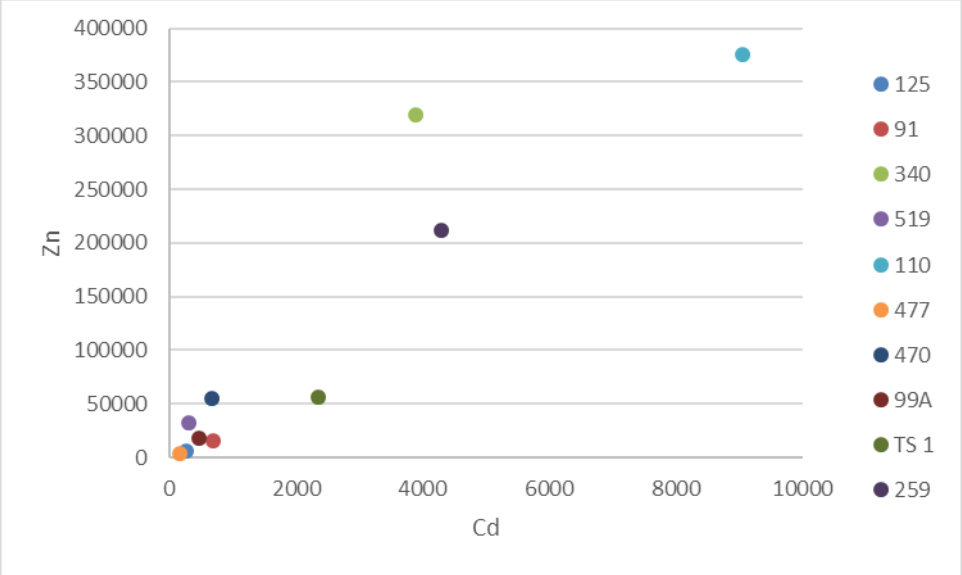

Figure 4.13: Cd, in ppm, plotted against Zn, in ppm, showing a correlation between the two elements.

Scanning Electron Microscopy and Mineral Analysis

Semi-quantitative SEM studies were used to gather mineralogical information, element maps and mineral compositional data for the Tsumeb samples. A Tescan Integrated Mineral Analyser (TIMA) with an EDS detector was used. Numerous areas on each sample were chosen for analysis. These areas were selected based on the

minerals present in the samples, as well as the mineral textures. Areas containing renierite and germanite were selected, as well as areas without these minerals, to see if Ge concentrates exclusively into renierite and germanite when they are present within the assemblage. Areas consisting of both sphalerite and galena were given priority to assess the distribution of Ge between them. A complete set of element maps, BSE images and false colour primary phase maps can be found in Appendix D.

Element Maps

An area containing germanite, renierite, pyrite, tennantite and galena in an unknown gangue was chosen for analysis from the bornite-dominant sample TS3 (Figure 4.14). The element maps of Pb, As, Ge, Sb, Zn and Ga for this area show Ge partitioning into renierite and galena (Figure 4.15). The renierite in the false colour primary phase map is labelled incorrectly, as most of the labelled renierite is actually germanite. Germanite can be distinguished from renierite from the Ge element map as germanite typically contains a higher concentration of Ge than renierite. Galena contains less Ge than both germanite and renierite. Galena also contains As and Ga and tennantite contains Pb.

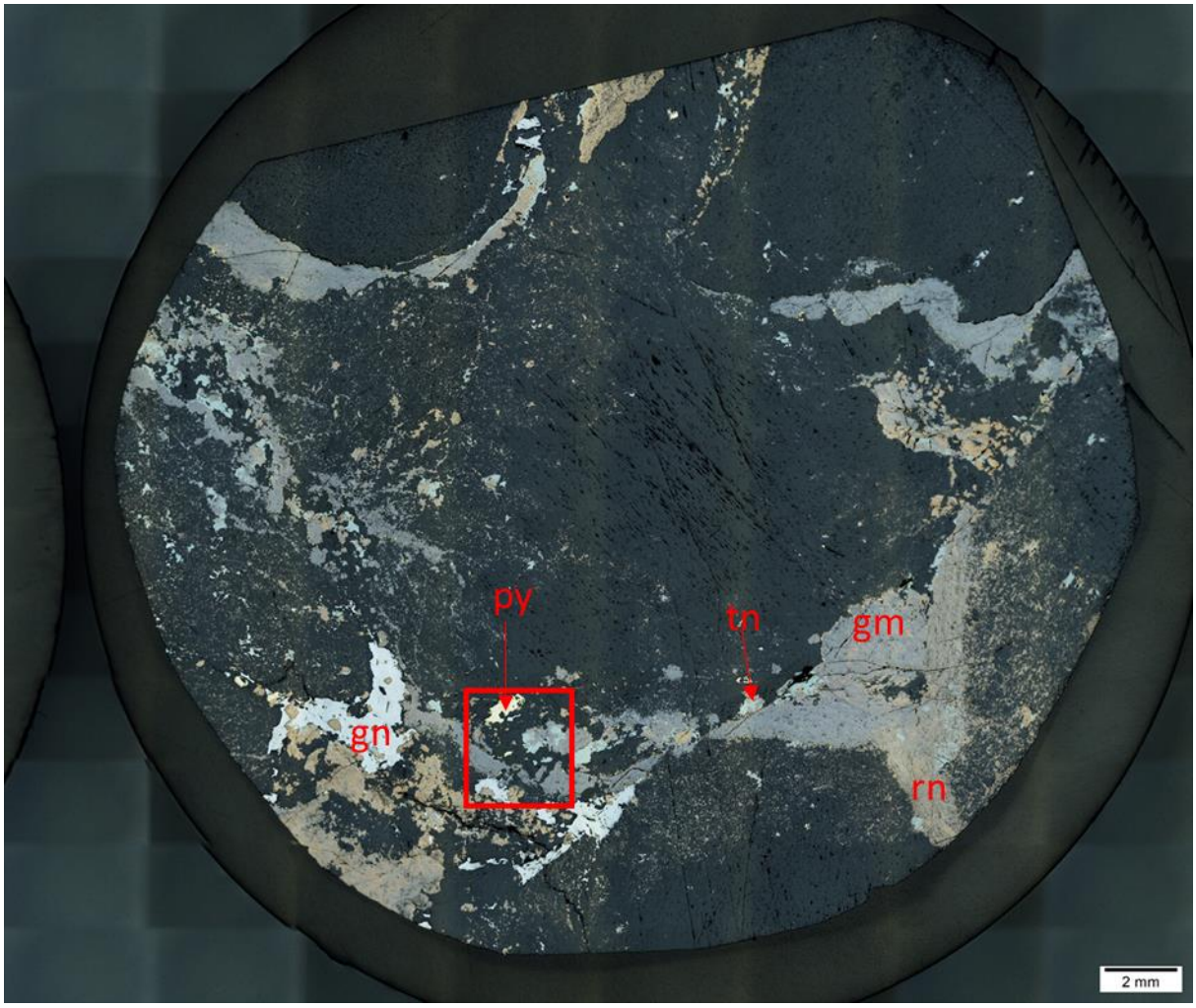

Figure 4.14: Full polished ore block reflected light image showing sample TS3 and the area selected for TIMA analysis (red rectangle).

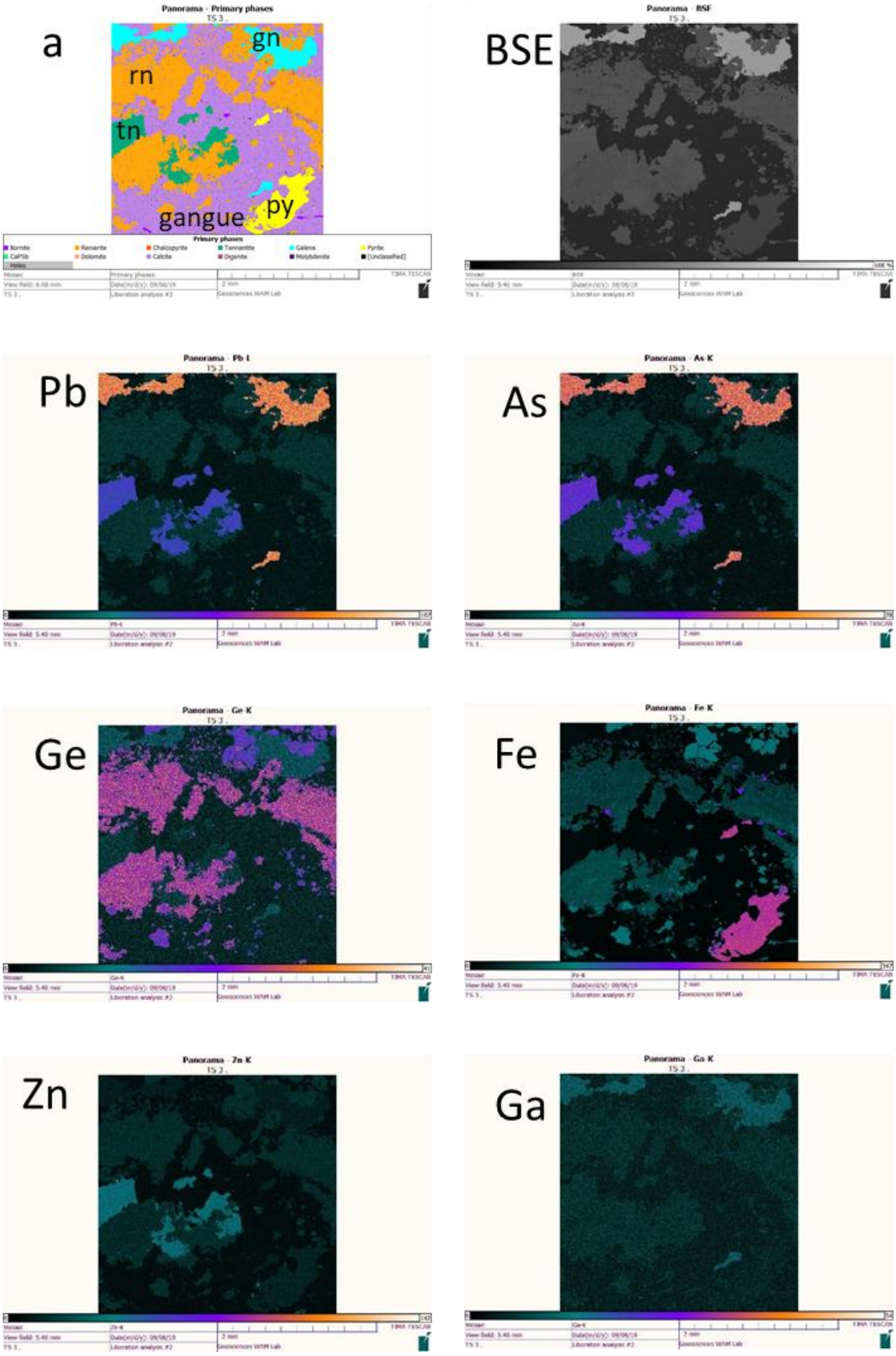

Figure 4.15: False colour primary phase map (a) showing renierite, galena, tennantite, pyrite and gangue, backscatter electron image and element maps for Pb, As, Ge, Sb, Zn and Ga from bornite-dominant sample TS3. These images were all obtained using the TIMA.

An area consisting of galena, sphalerite, digenite, tennantite and pyrite was selected from the sphalerite-dominant sample 110 due to its high diversity of minerals (Figure 4.16). Element maps were obtained for Pb, Zn, Ge, As, Cu, Fe, Co and Ga (Figure 4.17). In this sample Ge concentrates into galena and to a lesser extent tennantite. Galena contains As and tennantite contains Pb, but not as rich as in galena, while pyrite contains Co.

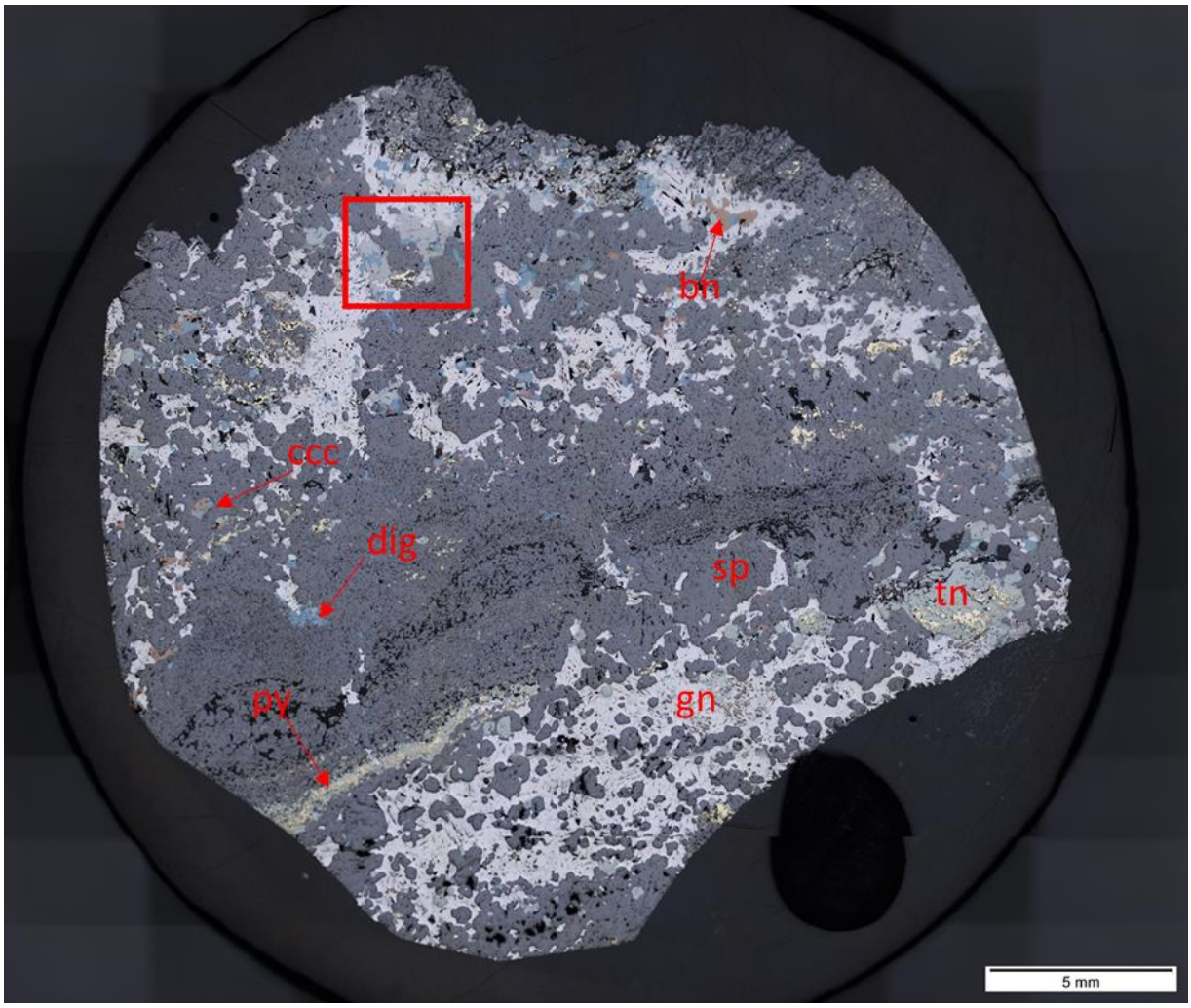

Figure 4.16: Full polished ore block reflected light image showing sample 110 and the area selected for TIMA analysis (red rectangle).

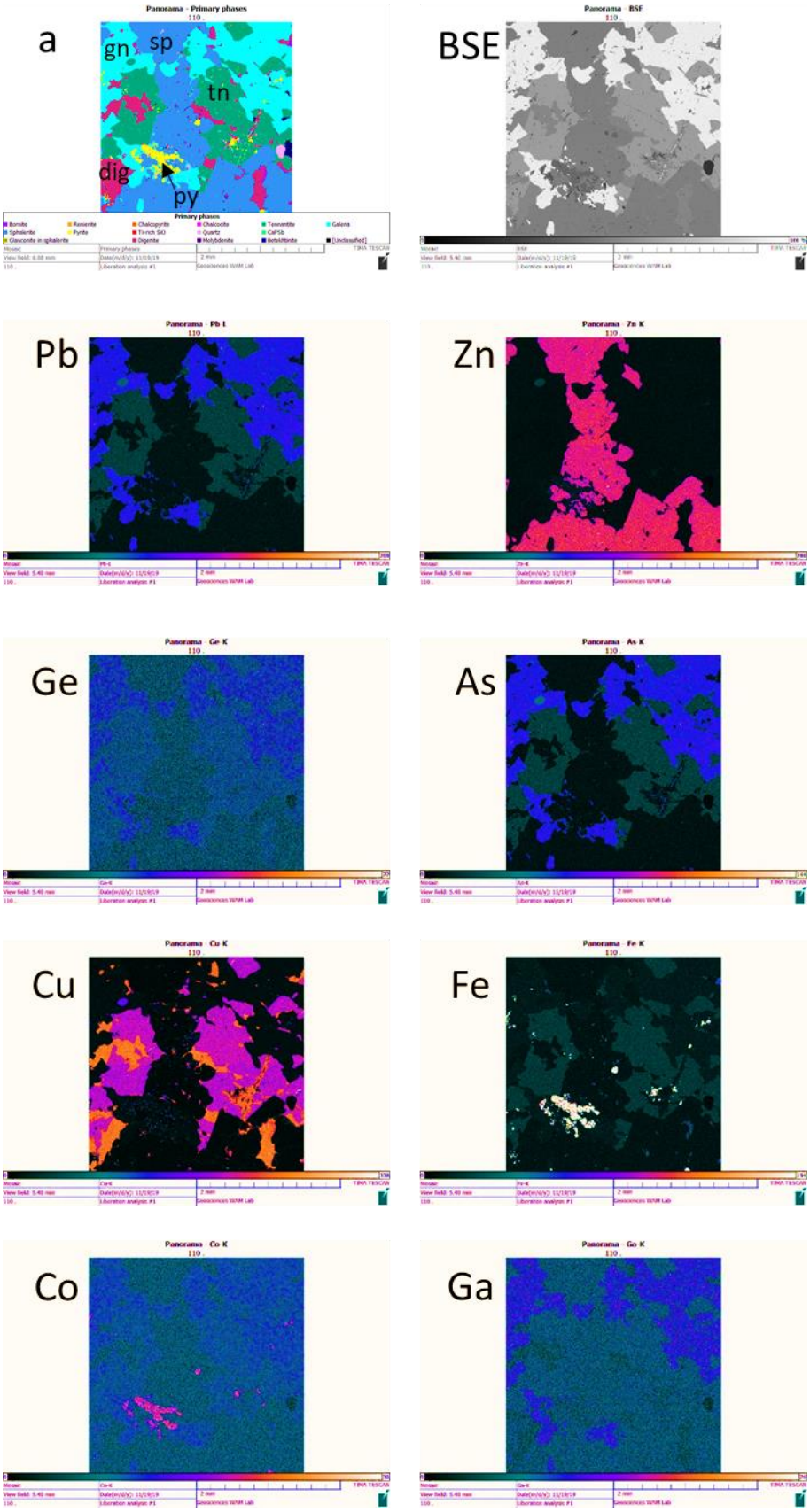

Figure 4.17: False colour primary phase map (a) showing galena, sphalerite, tennantite, digenite and pyrite, backscatter electron image and element maps for Pb, Zn, Ge, As, Cu, Fe, Co and Ga from sphalerite-dominant sample TS 3. These images were all obtained using the TIMA.

For TIMA analysis of the galena-dominant sample TS11, an area that was host to galena, tennantite and betekhtinite with minor chalcocite and quartz was chosen for element mapping (Figure 4.18). Analysed elements are Pb, Cu, Ge, As, Ag and Zn. These elements maps show Ge partitioning into galena (Figure 4.19). Galena also contains As, while tennantite contains Pb and Zn. The potential betekhtinite is enriched in Ag. The spectrum for this mineral shows it is a Fe, Cu sulphide (Figure 4.20), and therefore could be betekhtinite.

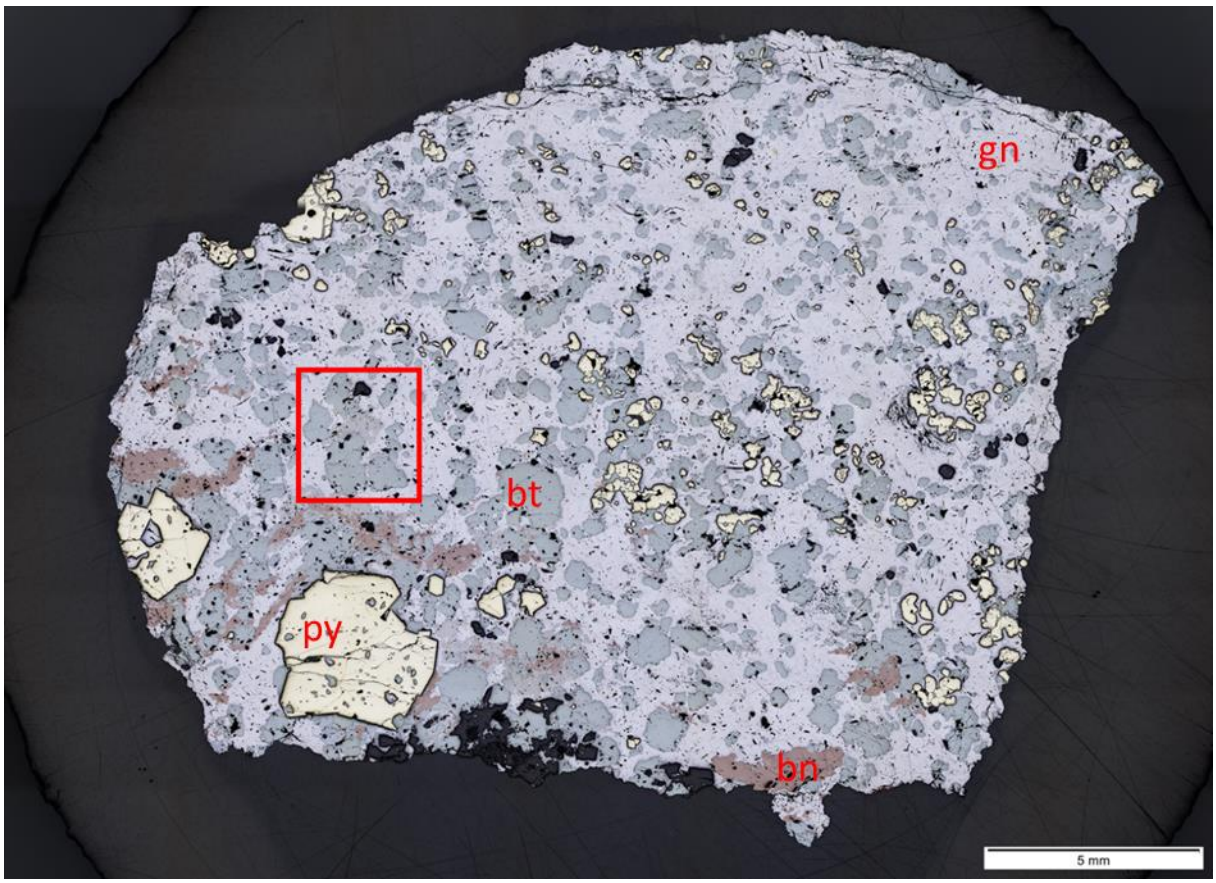

Figure 4.18 Full polished ore block reflected light image showing galena-dominant sample TS11 and the area selected for TIMA analysis (red rectangle).

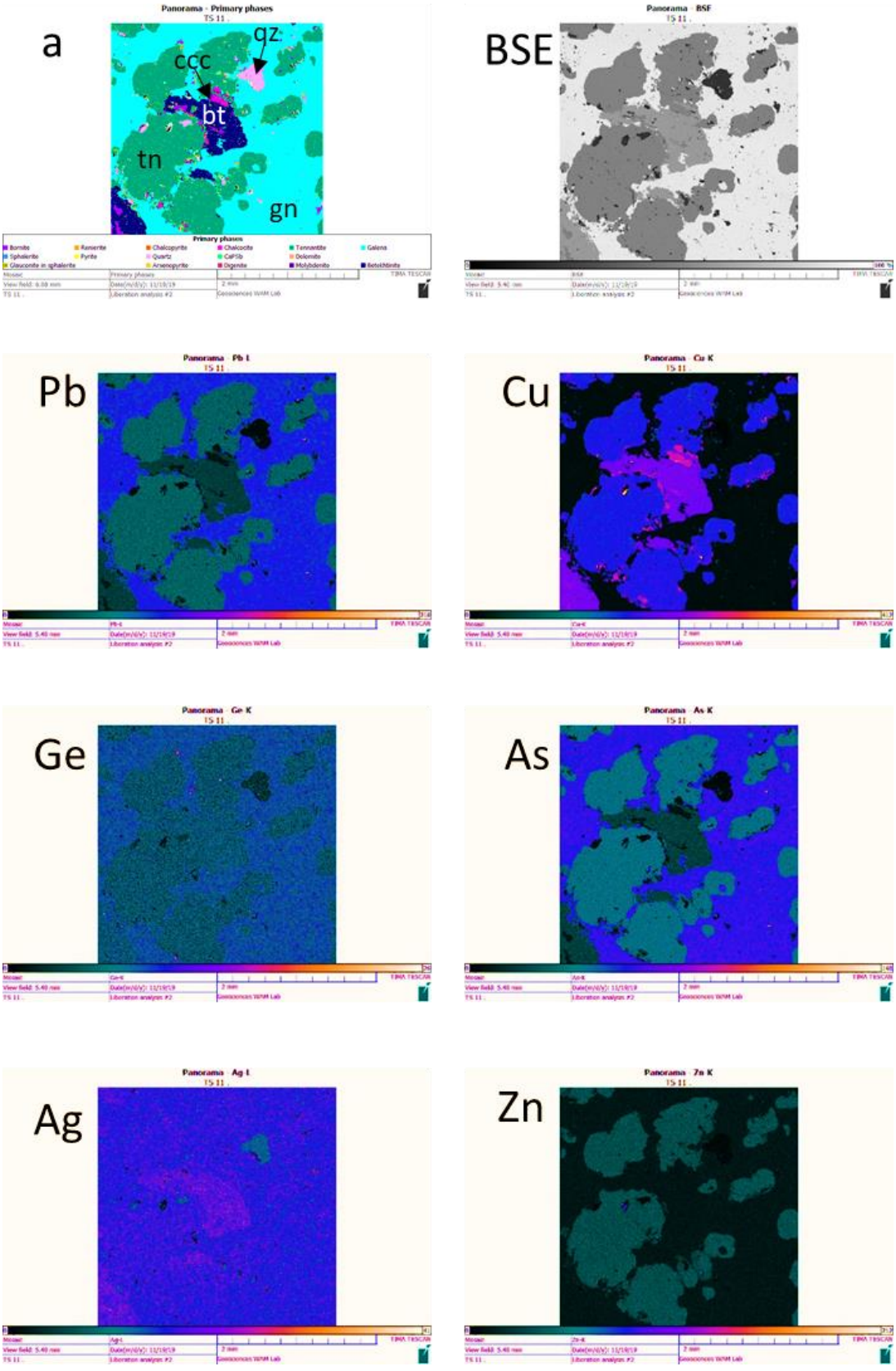

Figure 4.19: False colour primary phase map (a) showing galena, tennantite, betekhtinite chalcocite and quartz, backscatter electron image and element maps for Pb, Cu, Ge, As, Ag and Zn from sample TS11. These images were all obtained using the TIMA.

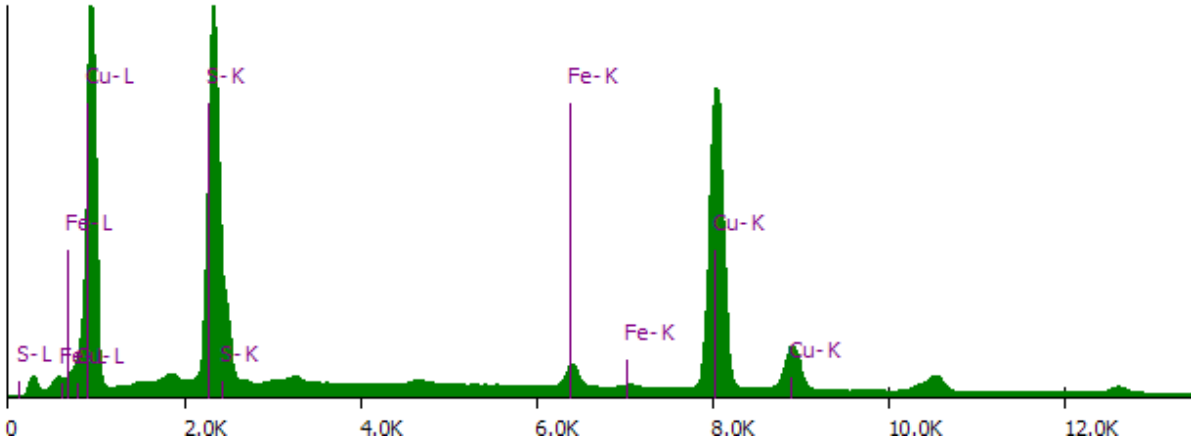

Figure 4.20: Mineral spectrum for unknown grey mineral. Cu, Fe and S suggest it could be betekhtinite, as does this mineral being found within the Tsumeb deposit in the past.

This data and all other element maps presented in Appendix D show that, whilst Ge partitions into renierite and germanite, where they are present, when they are absent from an assemblage, Ge partitions preferentially into galena and then into tennantite. However, it also occurs in galena and tennantite when the Ge-essential minerals are present in the assemblage, although to a lesser extent.

Galena is host to As and occasionally Ga. Tennantite is found to concentrate As, but not Sb, confirming it is tennantite and not tetrahedrite. Tennantite also contains a high concentration of Pb and Zn. Co typically concentrates into pyrite, while minor Ag is found in betekhtinite.

TIMA Semi-Quantitative Analysis

Normalised mineral compositions have been obtained for bornite, sphalerite, galena, renierite and germanite (Table 4.5) from samples 125 and TS3, both of which are bornite-dominant samples. Three points were selected for each mineral phase for a composition; this was then used to obtain an average composition for each mineral. Bornite, sphalerite and galena were used to assess the data produced by the TIMA and to give some indication of the reliability of the analysis.

The average compositions for each mineral that have been extracted from the TIMA were compared to compositions from various published literature (Table 4.6). The published composition for bornite was taken from Pessic and Olson (1984), who

analysed a bornite sample from Pinal, Arizona, a Cu-Ag-Au deposit. The published composition for sphalerite was taken from Mondillo *et al.* (2018), who looked at sphalerite from a Mississippi Valley-type (MVT) deposit. The galena published composition used is from Peng *et al.* (2003), who analysed a galena sample from Willyama Earth History Supplies. The published compositions for renierite and germanite were taken from Sclar and Geier (1957), who looked at samples of each mineral from Tsumeb.

Table 4.5: Mineral compositions extracted from the TIMA for bornite, sphalerite and renierite from sample 125, and for galena, renierite and germanite from sample TS 3.

Sample	Mineral	S	Fe	Cu	Zn	Ge	Pb	Total
125	Bornite	22.20	10.07	67.73				100.00
		22.14	9.94	67.92				100.00
		22.38	9.88	67.75				100.01
	Average	22.24	9.96	67.80				100.00
125	Sphalerite	32.19			67.81			100.00
		32.18			67.82			100.00
		32.53			67.47			100.00
	Average	32.30			67.70			100.00
TS 3	Galena	13.82					86.18	100.00
		13.87					86.13	100.00
		13.34					86.66	100.00
	Average	13.68					86.32	100.00
125	Renierite	30.04	13.58	49.68		6.70		100.00
TS 3		29.30	13.91	50.89		5.91		100.01
		30.21	13.12	49.41		7.27		100.01
	Average	29.85	13.54	49.99		6.63		100.01
TS 3	Germanite	29.07	6.24	54.47		10.23		100.01
		29.47	7.47	52.98		10.07		99.99
		29.24	6.19	54.16		10.41		100.00
	Average	29.26	6.63	53.87		10.24		100.00

The two bornite compositions are somewhat different, the S and Fe is less in the average TIMA composition, than in the composition given by Pessic and Olson (1984). This is balanced by an increase in Cu. The sphalerite is very different. The average sphalerite composition gathered using the TIMA contains no Fe, while the published composition by Mondillo *et al.* (2018) contains Fe. The lack of Fe is made up for by an increased Zn. The galena is similar between the analysis obtained from the TIMA and

published data from Peng *et al.* (2003). The renierite contains no As or Zn, as does the published composition by Sclar and Geier (1957). There is also less Ge and an increased amount of Cu in the TIMA composition. The germanite also contains no As or Zn and has a higher concentration of Cu than for the analysis published by Sclar and Geier (1957).

Table 4.6: Published mineral compositions for bornite, sphalerite, galena, renierite and germanite compared to the average mineral compositions for the same minerals from the TIMA. (Bornite: Pessic and Olson, 1984; sphalerite: Mondillo et al., 2018; galena: Peng et al., 2003; renierite and germanite: Sclar and Geier, 1957)

Mineral	Published composition									TIMA composition						
	S	Fe	As	Cu	Zn	Ge	Pb	Ga	Total	S	Fe	Cu	Zn	Ge	Pb	Total
Bornite	25.55	11.12		63.33					100.00	22.24	9.96	67.8				100.00
Sphalerite	33.30	8.19			58.20				99.69	32.3			67.70			100.00
Galena	13.20						86.10		99.30	13.68					86.32	100.00
Renierite	31.83	13.73	0.95	41.63	3.53	7.75			99.42	29.85	13.54	49.99		6.63		100.01
Germanite	31.27	7.80	1.37	42.12	3.93	10.19	0.96	1.85	99.49	29.26	6.63	53.87		10.24		100.00

Quantitative Analysis by Electron Microprobe

Three representative samples were selected from the Tsumeb suite for multiple point analyses on a CAMECA SX 5 FE electron microprobe. The equipment was configured to analyse Ni, Fe, Co, Cu, Zn, Ga, Ge, Ag, In, Pb, As and S; however, the electron beam failed or was unreliable for multiple attempts. In many cases, the instrument took over an hour to pump to the correct vacuum level, when it should have taken 10 minutes at most. This is most likely due to the nature of the ore blocks. The possibility of air bubbles in the resin could have been the reason for the instrument taking so long to reach the correct vacuum. None of the results summed to 100 % in weight percentage for this deposit. The results came to approximately 1 % on many of the attempts, with a beam that was stable at the incorrect current (normal beam current: 20nA; incorrect beam current for multiple runs: 0.02nA). When the beam was at the correct current for a run, the results ranged from 64 % to 97 %. The weight percentages may have increased if different elements were included on the scan, but this would not explain the much lower weight percentages. This would most likely be due to a fault of the instrument. This data has been included in Appendix F for reference, however it was not used in this study.

Synthesis

The samples analysed in this chapter were divided into three assemblage-types, Cu-dominant, Pb-dominant and Zn-dominant, by using the most abundant minerals in each sample to characterise the assemblages. The TIMA helped to determine that more Ge was found to concentrate in the Cu-dominant assemblages, than in the other assemblages. This is mostly probably because there is a larger concentration of germanite and renierite in the Cu-dominant assemblages. Ge was found to preferentially partition into germanite and renierite, as well as into galena and then into tennantite. Germanite was found to have larger concentrates of Ge than renierite did.

Chapter 5

Discussion

Results from the Kipushi and Tsumeb samples have been collated and interpreted. This interpretation covers the petrography and mineral assemblages, whole rock trace element geochemical analyses, the electron microscopy analyses and a brief synthesis covering the findings of the two deposits.

Petrography and Mineral Assemblages

Kipushi

Samples from the Kipushi suite have been divided into various Cu-dominant and Zn-dominant assemblages based on their most abundant minerals (Table 5.1). The assemblages proposed in this study are based on those developed by De Vos *et al.* (1974) and further developed by Stewart (2015).

Table 5.1: Sulphide mineral assemblages found within the Kipushi sample suite from this study.

Type	Assemblage/Dominant Mineral	Accessory Minerals	Trace Minerals
Cu	Bornite	Chalcocite, chalcopyrite, renierite, galena, tennantite, sphalerite, betekhtinite	Carrollite
	Bornite, chalcopyrite	Renierite, tennantite, sphalerite, galena	Pyrite, arsenopyrite, chalcocite
	Bornite, renierite	Chalcocite, betekhtinite	
	Chalcopyrite	Pyrite, sphalerite	
	Chalcopyrite, pyrite	Aresenopyrite, sphalerite	
Zn	Sphalerite	Chalcopyrite, tenanntite, galena, pyrite	Arsenopyrite
	Sphalerite, chalcopyrite	Galena, bornite, renierite, tennantite	Pyrite, arsenopyrite
	Sphalerite, bornite	Chalcocite, chalcopyrite, teannantite, renierite, galena, betekhtinite	

The bornite-chalcopyrite assemblage and bornite-renierite assemblage have been created due to the abundance of chalcopyrite and renierite within the samples. The other assemblages are very similar to those defined by De Vos *et al.* (1974).

The paragenesis obtained from petrological studies differs from that provided by Heijlen *et al.* (2008). This study suggests that bornite formed first, followed by chalcocite, based on the fact that chalcocite forms veins within bornite, as well as forming remnant blebs of bornite within the chalcocite, while Heijlen (2008) suggests bornite and chalcocite formed together after sphalerite, chalcopyrite, tennantite and renierite. Both this study and Heijlen *et al.* (2008) suggest the sphalerite and chalcopyrite formed together, although at different stages. In addition, both suggest that tennantite and renierite formed at the same time. The textures observed are a consequence of annealing of the mineral assemblages at various temperatures governed by the thermodynamic equilibrium of an assemblage of phases.

Tsumeb

Samples from the Tsumeb suite were also divided into assemblages. These assemblages were created using the same method as that used for Kipushi; having the dominant mineral/s define the assemblages. Here, assemblages were divided into Cu-dominant, Pb-dominant and Zn-dominant assemblage types (Table 5.2).

Table 5.2: Sulphide mineral assemblages found in the Tsumeb deposit of this study. Purple represents the Cu-dominant assemblage-type, blue the Pb-dominant assemblage-type and grey represents the Zn-dominant assemblage-type.

Type	Assemblage/Dominant Mineral	Accessory Minerals	Trace Minerals
Cu	Bornite	Chalcocite, renierite, galena, sphalerite, betechtinite, chalcopyrite, digenite	Pyrite, carrollite
	Tennantite	Spahlerite, galena, digenite, renierite, germanite	
Pb	Galena	Pyrite, sphalerite, tennantite, bornite, chalcocite, digenite	Arsenopyrite, chalcopyrite
Zn	Sphalerite	Galena, tennantite, digenite, renierite, bornite, chalcopyrite	Pyrite, native Cu
	Sphalerite, pyrite		

The paragenesis obtained from petrological studies in this work differs from that interpreted by Sclar and Geier (1957). This study suggests pyrite is a late-stage mineral from observations of remnant blebs of bornite and chalcocite within the pyrite, whereas Sclar and Geier (1957) suggest it was the first mineral to form. Both this study and Sclar and Geier (1957) suggest that bornite is an early stage mineral phase, followed by sphalerite and tennantite. This study suggests that germanite and renierite formed together, while Sclar and Geier (1957) suggests they formed separately.

Whole Rock Trace Element Geochemical Analysis

Kipushi

The results from the ICP-MS and ICP-OES trace element analysis for the Kipushi samples showed that, generally, there is more Ge in the Cu-dominant assemblage type. This could be attributed to the occurrence of more renierite in the Cu-dominant assemblages, and less renierite in the Zn-dominant assemblages. There is also a positive correlation between Pb and Ge, which suggests that Ge is likely to occur within galena. This is confirmed by high Ge and Pb contents in galena-bearing samples. Ge also positively correlates with As, which could suggest the presence of Ge in tennantite and/or arsenopyrite. In addition, there is also a correlation between Ge and Ga. This suggests these two elements are associated with the same mineral. This becomes evident where Ge and Ga within galena is noted from the element maps from SEM and TIMA anaylses. There is no correlation between Ge and Zn, suggesting a lack of Ge within sphalerite.

Tsumeb

The whole rock trace element analysis from the Tsumeb samples showed that only one sample contained significant amounts of Ge, a tennantite-dominant sample. This sample contained renierite, which may explain the high Ge content. Ge does not correlate with Pb or Zn, suggesting it does not occur in either galena or sphalerite within these samples.

Electron Microscopy

SEM and EPMA were used to determine the distribution of Ge within the sulphide assemblages, and therefore to confirm into which minerals Ge would preferentially

partition. This was aimed at helping to develop a better understanding of where Ge would substitute in the different minerals.

Substitution occurs when one or more ions substitute with another ion in the crystal lattice of a mineral. Types of substitution include simple ionic substitution and coupled substitution (George *et al.,* 2016). In a simple ionic substitution two elements of a similar ionic radius and ionic charge will swap with each other e.g. $Fe^{2+} \leftrightarrow Zn^{2+}$. In a coupled substitution two or more ions would substitute for one ion in order to maintain electrical neutrality e.g. $2Na^{+} \leftrightarrow Ca^{2+}$. This then distorts the structure of the crystal lattice (George *et al.,* 2016).

Some sulphides have simple formulae, such as pyrite (FeS) and arsenopyrite (FeAsS), however many sulphides have formulae that allow for the substitution of two ions, such as sphalerite ((Zn,Fe)S) and tennantite ($(Cu,Fe)_{12}As_4S_{13}$). Many sulphides are known to accommodate trace elements within their crystal lattice, substituting for one or other elements in their formula. An example of this is Ge^{2+} substituting for Zn^{2+} within sphalerite (Sinclair, 2014; Mondillo *et al.*, 2018).

Kipushi

SEM and TIMA analyses for the Kipushi samples both yielded similar results; that the Ge is concentrated into the renierite, where renierite is present, and into galena and to a lesser extent into tennantite, when renierite is not present in the assemblages. It was also found that the Ge concentrated in galena and tennantite even when renierite is present. Most of the Ge is concentrated into the renierite as expected as it is a Ge-essential mineral.

Ge is expected to concentrate into sphalerite, substituting for the Zn, as they have the same ionic size and charge (Bernstein, 1985; Holl *et al.*, 2007; Kampunzu *et al.,* 2009; Sinclair, 2014; Mondillo *et al.,* 2018), or into silicates, as Ge and Si also have the same ionic charge (Melcher, 2003; Holl *et al*., 2007); however, SEM and TIMA results show that the Ge does not concentrate into the sphalerite or silicates, but rather into the galena and tennantite. This suggests that the Ge is substituting for various elements within the galena and tennantite. It should be noted that Ge has multiple valencies; Ge^{2+} and Ge^{4+}.

Figure 5.1 shows the ionic radius and ionic charge of various elements found within the sulphide mineral assemblages at Kipushi. Elements with similar ionic radii and charge are more likely to substitute with each other in a crystal lattice. It can be noted that Zn, Cu and Ge have the same ionic radius and ionic charge. This makes them most likely to substitute for each other.

Tennantite has the chemical formula $Cu_{12}FeAs_4S_{13}$. Ge is therefore most likely to substitute for the Cu in the tennantite ($Ge^{2+} \leftrightarrow Cu^{2+}$). Ge also has the same ionic charge as Fe, and a similar radius, meaning that the Ge could also be substituting for Fe within the crystal lattice of tennantite ($Ge^{2+} \leftrightarrow Fe^{2+}$).

Galena has the chemical formula PbS. While Ge has the same ionic charge as Pb, its ionic radius is not similar. Pb has a much larger ionic radius than Ge. Goldschmidt (from George *et al.*, 2016) created some rules for ionic substitution:

- Ions can substitute if their radii differ by less than 15%.
- If a crystal is electrically neutral, ions with a charge that differ by 1 unit can substitute.

The radii of Ge and Pb do not fall into the less than 15% rule, however, George *et al.* (2016), suggests that at higher temperatures ions with more than a 15% difference in ionic radii may still substitute. This could explain how Ge and Pb are substituting with each other ($Ge^{2+} \leftrightarrow Pb^{2+}$; $Ge^{4+} \leftrightarrow Pb^{4+}$) in the crystal lattice of galena. The Ge and Pb may also be forming a coupled substitution ($2Ge^{2+} \leftrightarrow Pb^{4+}$) as these have similar ionic radii.

The large amount of As in the galena can be attributed to peak overlaps from the TIMA software. Extensive observation on each mineral's spectra, shows that there is in fact no As within the galena and no Pb within the tennantite.

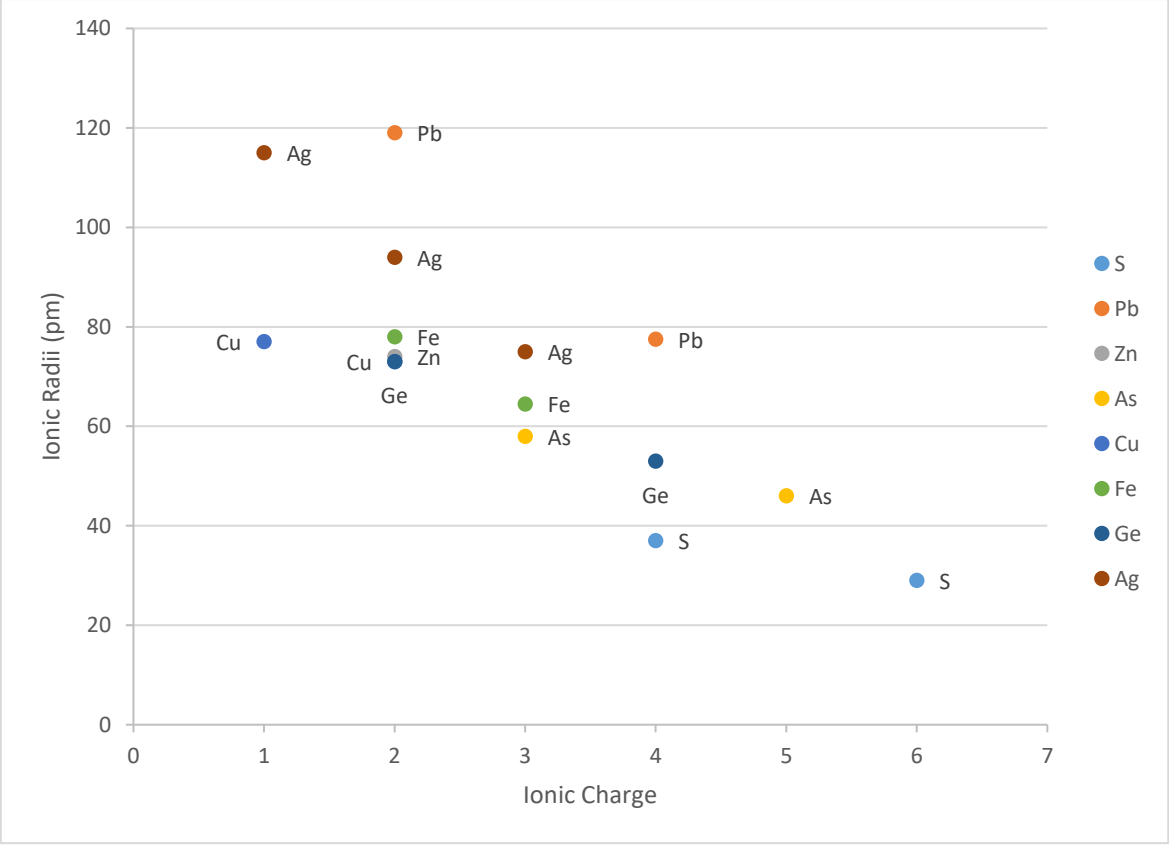

Figure 5.1: Ionic radii plotted against ionic charge for various elements found within the Kipushi sulphide mineral assemblages. Data extracted from Shannon (1976).

The TIMA produced a satisfactory semi-quantitative composition for renierite (Table 5.3). This composition for renierite suggests there is no Zn or As substituting for the Cu and Ge, respectively. The lack of As within this mineral may make the extraction of Ge from renierite simpler or at least more environmentally friendly.

Table 5.3: Average TIMA composition for renierite from the Kipushi suite.

S	Fe	Cu	Ge	Total
30.48	13.68	47.92	7.92	100.00

The majority of the Kipushi samples analysed by EPMA did not return good results as totals did not add up to 100 % by weight. Most of the results were in the high nineties (97/98 %) or above 100 % (102/103 %), while some points gave weight percentages in the eighties or even low sixties. Some of these low percentages could be explained by elements that were not scanned for. For example, Cd showed very high

concentration in the whole rock trace element analysis, yet was not analysed for using the EPMA due to the lack of discussion of the element within literature for the deposit and limitations on the number of elements that the microprobe could analyse. The missing Cd could have made some of the higher weight percentages reach 100 %. This does not, however, explain why some of the weight percentages were as low as 60 %. This is may be due to instrument issues. This is the first-time polymetallic sulphides from geological samples have been analysed on the Wits EPMA.

The sample runs that did yield good results show that the Ge is mostly concentrated in the renierite, as expected. The galena contained trace amounts of Ge. The sphalerite contained no detectable Ge, which is contrary to previous works, such as Bernstein (1985), Holl *et al.* (2007), Kampunzu *et al.* (2009), Sinclair (2014) and Mondillo *et al.* (2018). This once again supports the suggestion that the Ge is substituting for Pb rather than Zn.

The calculated chemical formula for renierite from the EPMA, $Cu_{10.23}Zn_{0.67}Fe_4As_{0.13}Ge_{1.86}S_{16,}$ again shows there to be minimal Zn and As within the renierite.

Tsumeb

The results from the TIMA analysis of the Tsumeb samples show that Ge concentrates into germanite, renierite and galena. A higher concentration in germanite and renierite is expected, as they are both Ge-essential minerals. There is a higher concentration of Ge in the germanite than in renierite. There is less Ge found in galena than either germanite or renierite. When there is no germanite or renierite present in the assemblage, Ge partitions into galena. However, Ge is seen to concentrate into galena even when germanite and renierite are present, once again suggesting the substitution of Ge^{2+} for Pb^{2+} or Ge^{4+} for Pb^{4+} within the crystal lattice of galena. Ge was not found to concentrate into any other phases in the sample suite.

Once again Pb within tennantite and As within galena can be attributed to peak overlaps within the TIMA software.

Tennantite within the Tsumeb suite had traces of Zn partitioning into it, most likely substituting for the Fe.

The TIMA produced adequate semi-quantitative compositions for renierite and germanite (Table 5.4). This composition for renierite suggests there is no Zn or As substituting into the crystal lattice. The composition for germanite also has no As. This lack of As will make extraction of the Ge from these minerals simpler.

Table 5.4: Average TIMA compositions for renierite and germanite from the Tsumeb suite.

	S	Fe	Cu	Ge	Total
Renierite	29.85	13.54	49.99	6.63	100.01
Germanite	29.26	6.63	53.87	10.24	100.00

Synthesis

Samples from Tsumeb were found to contain more galena and tennantite than the samples from Kipushi, defining two new assemblage types. Tsumeb contained considerably less chalcopyrite than Kipushi. Kipushi contained no germanite, but did have significantly more renierite than Tsumeb.

Kipushi and Tsumeb have similar mineral abundances. Bornite and sphalerite are the most abundant minerals in both deposits, with chalcopyrite being the third most abundant mineral in the Kipushi samples, and galena being the third most abundant mineral in the Tsumeb samples. Both deposits have similar chalcocite abundance and textures as it forms veins within the bornite. Renierite, tennantite and betekhtinite form as blebs in both set of samples. Pyrite and carrollite occur in the same level of abundance within each deposit.

The paragenesis of the Kipushi and Tsumeb deposits was based on the petrological studies of the available samples. Both sets of samples showed similar parageneses. Both suites showed bornite was the first to form, followed by chalcocite. The Ge-essential minerals, tennantite, betekhtinite and sphalerite were next to form for Tsumeb, while sphalerite and chalcopyrite formed next for Kipushi, followed by Ge-essential minerals, tennantite and betekhtinite, Galena was the next to form in both deposits, with Tsumeb including digenite in this stage. Finally, carrollite, pyrite and arsenopyrite formed last in both deposits.

ICP-MS and ICP-OES trace element analysis show that there is generally more Ge in the Kipushi samples than in the Tsumeb samples. Ge correlated with many elements in the Kipushi sample set while there was no obvious correlation with Ge within the Tsumeb sample set. This suggests there is less Ge associated with galena and tennantite in the Tsumeb samples compared to the Kipushi samples.

The analysed compositions for renierite show there is no Zn or As within the renierite, making extraction of Ge from renierite simpler without the worry of abundant As.

All sulphide minerals within the samples from the Kipushi and Tsumeb deposits were analysed for Ge by SEM and/or TIMA. The Ge was found to partition into only a few of these sulphides; germanite, renierite, galena and tennantite, in order of abundance of Ge. It is expected there would be Ge within germanite and renierite, as these are Ge-essential minerals. Ge is not expected to be found to concentrate within galena and tennantite. According to the published literature, Ge will prefer to partition into sphalerite, substituting for Zn (Bernstein, 1985; Holl *et al*., 2007; Kampunzu *et al.*, 2009; Sinclair, 2014; Mondillo *et al.*, 2018). Belissont *et al.* (2019) also found Ge concentrating into chalcopyrite. The chalcopyrite analysed in this study was found not to concentrate Ge, but rather Co.

.

Chapter 6

Conclusion

While previous studies have been instrumental in understanding the substitution of elemental Ge within sulphide mineral assemblages, it has become clear from the results for Kipushi and Tsumeb that Ge substituting with Zn is not always the case. In these Kipushi-type deposits, the Ge partitioned into galena and tennantite, substituting with the Pb and Cu respectively, rather than with the Zn. This occurred when Ge sulphides were both present and absent from the assemblage (Figure 6.1).

The results from this study support the SEM data and conclusions of Stewart (2015), using newer instrumentation (TIMA) and a few quantitative analyses (EPMA). These methods could be applied to similar deposits to determine where Ge is concentrated which could assist with future exploitation. Future studies can focus on *why* the Ge substitutes with the Pb and Cu rather than the more suitable Zn. New findings could lead to more Ge being located and mined, making Ge more accessible to the market.

While these two deposits are very similar, there are some fundamental differences between them. Tsumeb contains Mo, while Kipushi does not. Tsumeb has a wider range of Ge-bearing sulphide minerals (germanite and renierite) compared to Kipushi, that only has one (renierite). Kipushi contains significantly higher concentrations of Ge than Tsumeb. It is recommended that further studies are conducted into the term ‘Kipushi-type deposit’ and what defines this deposit type, and if both these deposits are in fact of the same type.

Future studies could focus on the elevated concentrations and economic potential of Cd, Ag and Co within these deposits. Both Kipushi and Tsumeb have high concentrations of Cd that is correlated with Zn, and therefore sphalerite. Cd occurring in sphalerite is common in various types of polymetallic sulphide deposits (Schwartz, 2000). Further research should be conducted on the abundance of this element in sphalerite in order to make extraction of Zn from sphalerite more viable, as Cd can be harmful during Zn processing. Both deposits, but more so Tsumeb, contain significant concentrations of Ag and Co, which are of economic importance. A study focusing on each of these elements would be useful in order to exploit the most economically viable

elements from each deposit. Tsumeb also has a significant amount of economically important Mo within its ore minerals. The knowledge of how much is in the deposit, and where it is primarily hosted would be useful for potential exploitation of the element.

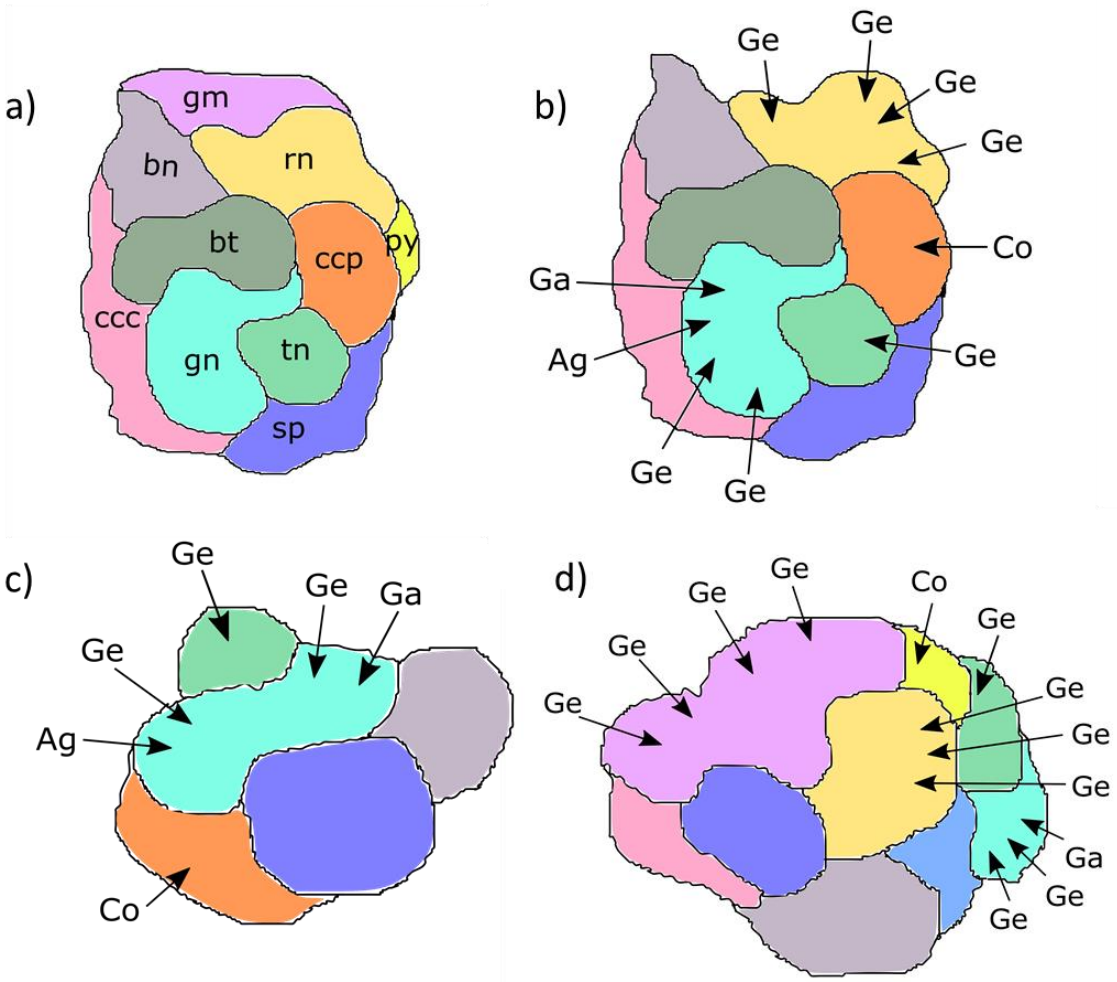

Figure 6.1: Schematic diagrams, not to scale, of various sulphide mineral assemblages from Kipushi and Tsumeb. The key to the mineralogy for all the minerals used in the other diagrams is shown in (a); gm (germanite), bn (bornite), rn (renierite), bt (betekhtinite), ccp (chalcopyrite), py (pyrite), ccc (chalcocite), gn (galena), tn (tennantite) and sp (sphalerite). (b) shows a renierite-present assemblage from the Kipushi deposit with elements partitioning into the relevant minerals; Ge into renierite, galena and tennantite, in order of abundance, Co into chalcopyrite, and Ag and Ga into the galena. (c) shows a renierite absent assemblage from the Kipushi deposit. Here the Ge partitions into the galena and tennantite. Co still partitions into the chalcopyrite and Ga and Ag into the galena. (d) shows a germanite and renierite-present assemblage from the Tsumeb deposit. The Ge partitions into the germanite, renierite, galena and tennantite, in order of abundance. Ga and Ag also partition into the galena, and Co concentrates into the pyrite.

References

Amcoff, O. 1988. Experimental replacement of chalcopyrite by bornite: Textural and chemical changes during a solid state process, *Mineralium Deposita,* 23, 286-292.

Belissont, R., Munoz, M., Boiron, M. C., Luais, B. and Mathon, O. 2019. Germanium crystal chemistry in Cu-bearing sulfides from micro-XRF mapping and micro-XANES spectroscopy, *Minerals*, 9, 227.

Bernstein, L. R. 1985. Germanium Geochemistry and Mineralogy, *Geochimica et Cosmochimica Acta,* 49, 2409-2422.

Craig, J. R. and Vaughn, D. J. 1994. *Ore Microscopy and Ore Petrography* (Second edition) New York, Chichester, Brisbane, Toronto, Singapore, John Wiley and Sons, Inc. 434.

De Vos, W., Viaene, W. and Moreau, J. 1974. Minéralogie du gisement de Kipushi Shaba, Zaire, IN: Bartholome, P. (Ed.) *Gisements Stratiformes et Provinces Cupriféres* Centenaire de la Société Géologique de Belgique, Liége*,* 165-183.

Dimanche, F. 1974. Paragenese des sulfures de cuivre dans les gisements du Shaba (Zaire): I. Kipushi; II. Kamoto, IN: Bartholome, P. (Ed.) *Gisements Stratiformes et Provinces Cupriféres* Centenaire de la Société Géologique de Belgique, Liége*,* 185-201.

Fortier, S.M., Nassar, N.T., Lederer, G.W., Brainard, Jamie, Gambogi, Joseph, and McCullough, E.A. 2018. Draft critical mineral list—Summary of methodology and background information—U.S. Geological Survey technical input document in response to Secretarial Order No. 3359: U.S. Geological Survey Open-File Report 2018–1021, 15 p.

Gait, R. I. 2002. African type-minerals, *Rocks and Minerals*, 77, 25-30.

George, L., Cook, N. J. and Ciobanu, C. L. 2015. Mineral resources in a sustainable world, *13th SGA Biennial Meeting Proceedings*, 2, 737-740.

George, L. L., Cook, N. J. and Ciobanu, C. L. 2016. Partitioning of trace elements in co-crystallized sphalerite-galena-chalcopyrite hydrothermal ores, *Ore Geology Reviews*, 77, 97-116.

Graedel, T.E., Gunn, G. and Espinoza, L.T. 2014. Metal resources, use and criticality in Gunn, G (Ed.) *Critical Metals Handbook*, American Geophysical Union.

Grguric, B. A., Putnis, A. and Harrison, R. J. 1998. An investigation of the phase transitions in bornite (Cu_5FeS_4) using neutron diffraction and differential scanning calorimetry, *American Mineralogist,* 83, 1231-1239.

Heijlen, W., Banks, D. A., Muchez, P., Stensgard, B. M. and Yardley, B. W. D. 2008. The nature of mineralizing fluids of the Kipushi Zn-Cu deposit, Katanga, Democratic Republic of Congo: Quantitative fluid inclusion analysis using laser ablatiob ICP-MS and bulk crush-leach methods, *Economic Geology*, 103, 1459-1482.

Holl, R., Kling M., and Schroll, E. 2007. Metallogenesis of germanium – A review, *Ore Geology Reviews*, 30, 145-180.

Hrstka, T., Gottlieb, P., Skala, R., Breiter, K. and Motl, D. 2018. Automated mineralogy and petrology – applications of Tescan Integrated Mineral Analyser (TIMA), *Journal of Geosciences,* 63, 47-63.

Intiomale, M. M. and Oosterbosch, R. 1974. Geologie et geochimie du gisement du Kipushi, Zaire, IN: Bartholome, P. (Ed.) *Gisements Stratiformes et Provinces Cupriféres* Centenaire de la Société Géologique de Belgique, Liége*,* 123-164.

Ivanhoe Mines 2014. Press Release: Ivanhoe Mines reports exceptionally high-grade silver, zinc and copper assay results from Big Zinc drill holes at the Kipushi Mine in the Democratic Republic of Congo, Lumbumbashi, DRC, 24/11/2014.

Kamona, A.F. and Gunzel, A. 2007. Stratigraphy and base metal mineralisation in the Otavi Mountain Land Northern Namibia – a review and regional interpretation, *Gondwana Research,* 11, 396-413.

Kampunzu, A. B., Cailteux, J. L. H., Kamona, A. F., Intiomale, M. M. and Melcher, F. 2009. Sediment-hosted Zn–Pb–Cu deposits in the Central African Copperbelt, *Ore Geology Reviews*, 35, 263-297.

Lhoest, J. J. 1995. The Kipushi Mine: Zaire, *Mineralogical Record,* 26, 163-187

Li, K., Brugger. J. and Pring, A. 2018. Exsolution of chalcopyrite from bornite-digenite solid solution: an example of a fluid driven back-replacement reaction, *Mineralium Deposita,* 53, 903-908.

Lundstrom, M., Aromaa, J., Forsen, O., Hyvarinen, O. and Barker, M. H. 2005. Leaching of chalcopyrite in cupric chloride solution, *Hydrometallurgy,* 77, 89-95.

Makovicky, E., Tippelt, G., Forcher, K., Lottermoser, W., Karup-Moller, S. and Amthauer, G. 2003. Mossbauer study of Fe-bearing synthetic tennantite, *The Canadian Mineralogist*, 41, 1125-1134.

Melcher, F. 2003. The Otavi Mountain Land in Namibia: Tsumeb, Germanium and Snowball Earth, *Mitteilungen der Osterreichischen Mineralogischen Gesellschaft*, 148, 413-435.

Melcher, F. and Buchholz, P. 2014. Germanium IN: Gunn, G (Ed.) Critical Metals Handbook, *American Geophysical Union.*

Melcher, F., Oberthur, T. and Rammlmair, D. 2006. Geochemical and mineralogical distribution of germanium in the Khusib Springs Cu-Zn-Pb-Ag sulfide deposit, Otavi Mountain Land, Namibia, *Ore Geology Reviews,* 28, 32-56.

Mondillo, N., Arfe, G., Herrington, R., Boni, M., Wilkinson, C. and Mormone, A. 2018. Germanium enrichment in superhene settings: evidence from the Cristal nonsulfide Zn prospect, Bongara district, northern Peru, *Mineralium Deposita,* 53, 155-169.

Olesik, J. W. 1991. Element analysis using an evaluation and assessment of remaining problems, *Analytical Chemistry,* 63, 12-21.

Peng, Y., Grano, S., Fornasiero, D. and Ralston, J. 2003. Control of grinding conditions in the floatation of galena and its separation from pyrite, *International Journal of Mineral Processes,* 70, 67-823.

Pesic, B. and Olson, F. A. 1984. Dissolution of bornite in sulphuric acid using oxygen as oxidant, *Hydrometallurgy*, 12, 195-215.

Pillarisetty, R. 2011. Academic and industry research progress in germanium nanodevices, *Nature,* 479, 324-328.

Post, J. E. and Bish, D. L. 1989. Rietveld refinement of the coronadite structure, *American Mineralogist,*74, 913-917.

Putnis, A. and Grace, J. 1976. The transformation behaviour of bornite, *Contributions to Mineralogy and Petrology,* 55, 311-315.

Rice, S. 2017. Yilgarn Geochemistry Seminar, Super Trace 4-Acid Digestion and ICP-MS/AES Anaysis, Perth.

Rueden, C.T., Schindelin, J., Hiner, M.C., De Zonia, B.E., Walter, A.E., Arena, E.T. & Eliceiri, K.W. 2017. ImageJ2: ImageJ for the next generation of scientific image data. *BMC Bioinformatics*, 18, 529.

Schindelin, J., Arganda-Carreras, I., Frise, E., Kaynig, V., Longair, M., Pietzsch, T., Preibisch, S., Rueden, C., Saalfeld, S., Schmid, B., Tinevez, J-Y., White, D.J., Hartenstein, V., Eliceiri, K., Tomancak, P. & Cardona, A. 2012. Fiji: an open-source platform for biological-image analysis. *Nature methods*, 9, 676-682.

Schneider, J., Melcher, F. and Brauns, M. 2007. Concordant ages for the giant Kipushi base metal deposit (DR Congo) from direct Rb–Sr and Re–Os dating of sulphides, *Mineralium Deposita,* 42, 791-797.

Schulz, K.J., DeYoung, J.H., Jr., Seal, R.R., II, and Bradley, D.C., eds. 2017. Critical mineral resources of the United States—Economic and environmental geology and prospects for future supply: U.S. Geological Survey Professional Paper 1802, 797 p.

Schwartz, M. O. 2000. Cadmium in Zinc Deposits: Economic Geology of a Polluting Element, *International Geology Review*, 42, 445-469.

Sclar, C. B. and Geier, B. H. 1957. The paragenetic relationship of germanite and renierite from Tsumeb, South West Africa, *Economic Geology,* 52, 612-631.

Shannon, R. D. 1976. Revised effective ionic radii and systematic studies of interatomic distances in halides and chalcogenides, *Acta Chrystallographic,* 32, 751-767.

Sinclair, W.D. 2014. Electronic Metals (In, Ge and Ga): Present and Future Resources, *Acta Geologica Sinica* (English Edition) 88, 463-465.

Söhnge, P. G. 1964. The geology of the Tsumeb Mine. *The geology of some ore deposits in southern Africa*, *2*, 367-382.

Stewart, C. 2015. Ore mineral assemblages and the distribution of germanium and silver at the Kipushi Mine (DRC). Unpublished Honours Report, University of the Witwatersrand, South Africa, 93 p.

Turner, E.C., Broughton, D. W. and Brooks, T. 2018. Neoproterozoic carbonate lithofacies and ore distribution at the Kipushi Cu-Zn deposit, Democratic Republic of Congo, and Gayna River Zn camp, northwest territories, Canada, *Economic Geology,* 113, 779-788.

Von Bezing, L., Bode, R. and Jahn, S. 2014. *Namibia: Minerals and Localities I,* Bode Verlag GmbH, Salzhemmendorf, Germany.

Yakushi, D. and Enjoji, M. 2004. Chemical composition or ores from the Takara volcanogenic massive sulphide deposit, central Japan, *Resource Geology,* 54, 437-446.

Appendix A

Petrography

A.1. Hand Specimen Descriptions

Kipushi

Bornite-dominant assemblage

Sample No	Observations	Scan
586	Massive bornite with some sphalerite throughout the polished hand specimen. Networks of chalcopyrite are present. Galena occurs mostly around the sphalerite and within the tennantite. Tennantite is found in blebs of varying sizes. Renierite occurs as small blebs within the bornite and tennantite.	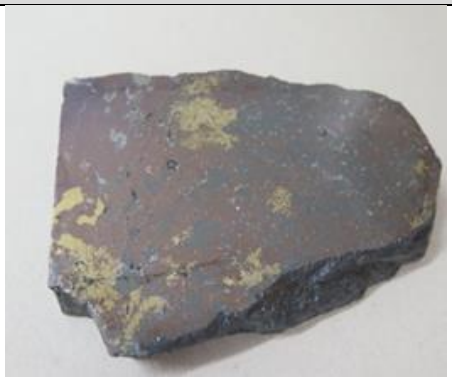
587	Massive bornite interspersed with chalcopyrite flares. Sphalerite looks be replaced by some chalcopyrite. Some renierite blebs are seen within the bornite.	
12492A	Massive bornite with many cross-cutting silvery-blue veins of chalcocite. Patches of networked galena is seen. Chalcopyrite is found in small blebs.	

Sample No	Observations	Scan
15453	Massive bornite with a network of chalcocite. Renierite is found to be replacing the chalcocite.	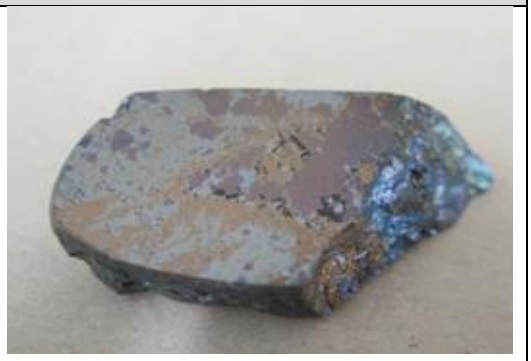
KP 3	Massive bornite with large blebs of galena. Chalcopyrite blebs appear to be mostly disseminated. Small tennantite blebs that appear to be replacing the galena are seen in this hand specimen. Smaller renierite blebs are possibly replacing the tennantite.	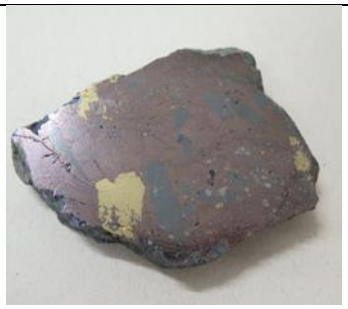
KP 7	Fine, black shale country rock with multiple cross-cutting veins of varying thickness of chalcocite and bornite.	
KP 5	Bornite in this hand specimen appears to be banded with some galena. Few small chalcopyrite blebs.	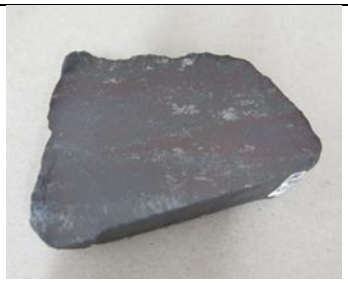

Bornite-chalcopyrite-dominant assemblage

Sample No	Observations	Scan
6547	This hand specimen consists dominantly of bornite with abundant chalcopyrite throughout. Lots of sphalerite can be seen being replaced by the chalcopyrite. Galena is found within the sphalerite. Small tennantite blebs can be seen.	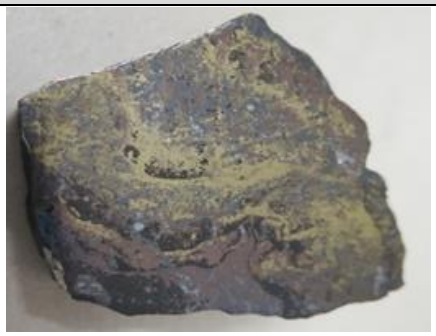

Chalcopyrite-dominant assemblage

Sample No	Observations	Scan
KP 6	Country rock of calcite and black silicates have been partially replaced by chalcopyrite. As has some galena. Minor sphalerite within this sample.	

Chalcopyrite-pyrite-dominant assemblage

Sample No	Observations	Scan
12492	Massive chalcopyrite with many euhedral to subhedral pyrite crystals. The pyrite is clustered around the silicates. A few small sphalerite blebs are seen.	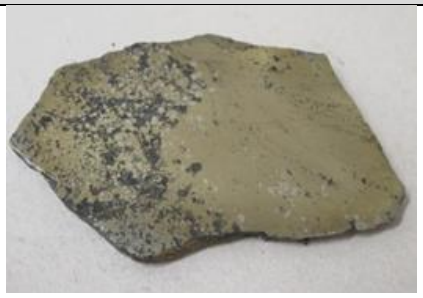

Sphalerite-dominant assemblage

Sample No	Observations	Scan
KP 11	Lots of sphalerite. Some a grey colour, some more red and some more a honey brown colour. Small bleb of galena with some minor chalcopyrite.	

Sphalerite-bornite-dominant assemblage

Sample No	Observations	Scan
1058	Massive sphalerite with a network of galena, chalcopyrite and bornite is seen in this specimen.	

A.2. Ore Microscopy

A.2.1. Kipushi sample suite

Twenty-six polished thin sections and 19 polished ore blocks were examined under reflected light using a petrographical microscope at the University of the Witwatersrand. Below is a comprehensive table of samples descriptions and full-section photomicrographs. Thin section scans were taken using an Olympus BX 63 microscope at the MMU at The University of the Witwatersrand and polished block scans were done using an Olympus BX 53 microscope in the School of Geosciences at the University of the Witwatersrand.

Bornite-dominant assemblage

Sample No	Observations	Scan
586a	Massive bornite from one-half of the section replacing massive sphalerite from the other half of the section. Tennantite is also seen replacing the sphalerite (blebby tennantite), mostly along the bornite/sphalerite boundary areas. Chalcocite replaces the bornite, in some places incomplete replacement is shown by remnant globules of bornite within chalcocite. Chalcopyrite replaces the bornite in a similar network pattern. Renierite is also replacing the sphalerite.	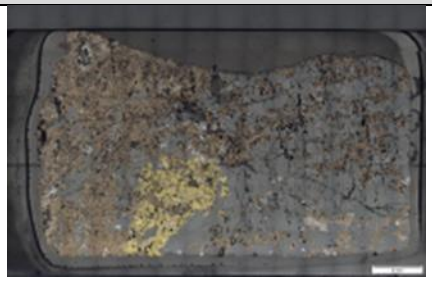
586b	Massive bornite with large and small chalcocite veins, some of which form remnant globules of bornite within chalcocite. Galena, tennantite and renierite are found within the chalcocite veins.	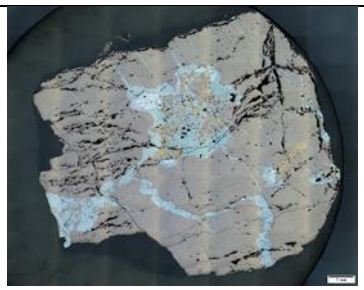
586c	Massive bornite with large and small chalcocite veins, some of which form remnant globules of bornite within chalcocite. Galena, tennantite and renierite are seen within the chalcocite veins. Tennantite appears to be replacing the chalcocite veins.	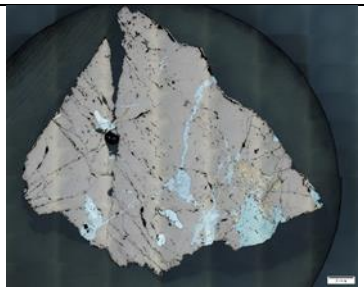

Sample No	Observations	Scan
6547	This sample has a base of bornite that was replaced by sphalerite. In turn, the sphalerite was replaced by chalcopyrite. Galena and tennantite can be seen to have replaced some gangue, sphalerite and chalcopyrite.	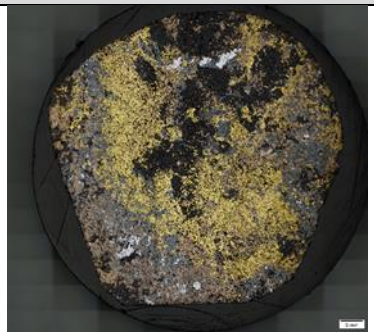
12492Aa	Massive bornite with multiple cross-cutting chalcocite veins are seen in this section. Galena and some tennantite are seen in this sample too.	
12492Ab	Massive bornite with chalcocite veins. The chalcocite veins form along the edges of the gangue. Blebs of renierite and betekhtinite are found within the bornite.	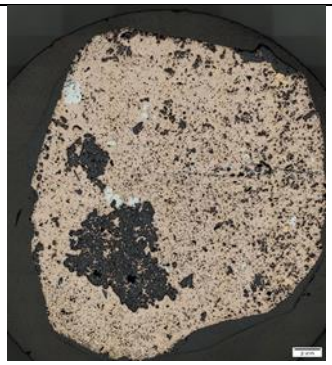
12492Ac	Massive bornite with chalcocite veins. The chalcocite veins form along the edges of the gangue. Blebs of renierite and betekhtinite are found within the bornite.	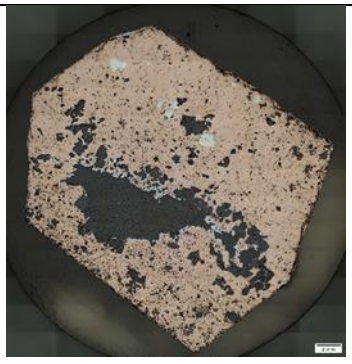

Sample No	Observations	Scan
KP 1	Massive bornite with small chalcocite veins and remnant globules of bornite within chalcocite is noted. Larger veins of betekhtinite containing renierite blebs	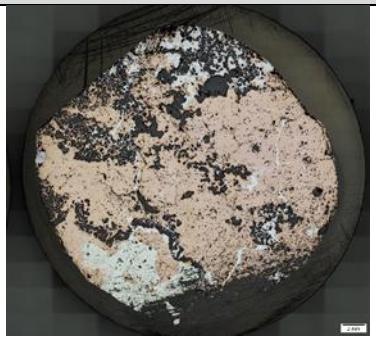
KP 3	Massive bornite with large blebs of sphalerite and small chalcocite veins. The sphalerite has chalcopyrite disease. Small blebs of galena are seen within the bornite. Renierite blebs some of the galena is associated with the gangue. Some chalcopyrite is seen within the bornite.	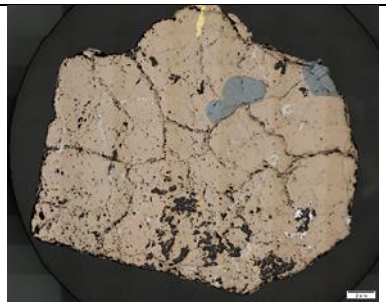
KP 4	Massive bornite with small veins of chalcocite, large renierite blebs and chalcopyrite laths.	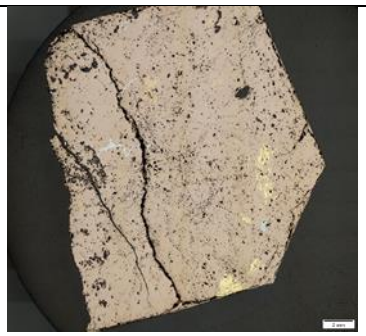
KP 7	This sample consists of country rock with veins of bornite and chalcocite. The chalcocite has remnant globules of bornite within chalcocite. There are a few renierite blebs within these veins. There are speckles of arsenopyrite within the gangue.	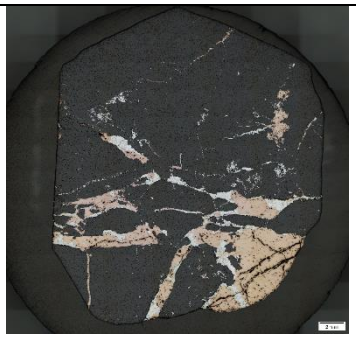

Sample No	Observations	Scan
KP 12	This sample contains mostly bornite, with large sections, and blebs, of sphalerite. Chalcopyrite is seen at the edges of this section replacing the sphalerite. Galena replaces the sphalerite to form a network texture, while tennantite and renierite can also be seen replacing the sphalerite to form blebs.	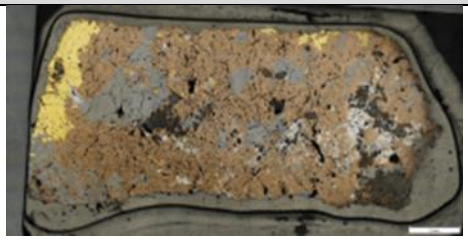
KP 16	Massive bornite with multidirectional laths of chalcopyrite. Pyrite is being consumed by the gangue. Veins of chalcocite are found around the edges of the gangue. Renierite blebs are present.	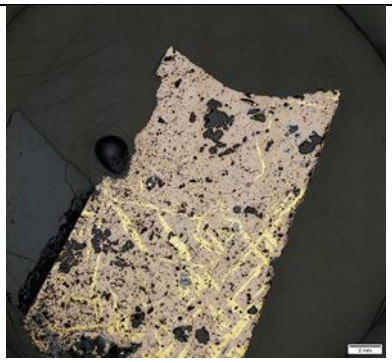

Bornite-chalcopyrite-dominant assemblage

Sample No	Observations	Scan
587	Massive bornite with some elongated sphalerite and chalcopyrite within the bornite. A small section of this polished block has some chalcocite forming remnant globules of bornite within chalcocite. Small galena blebs can be seen within the bornite. There is a large bit of pyrite in this sample. The pyrite has inclusions of chalcopyrite. This pyrite appears to be replacing the bornite and chalcocite.	

Sample No	Observations	Scan
1216	Massive bornite with a network of chalcopyrite. Large blebs of sphalerite are replacing the chalcopyrite. Renierite blebs, tennantite blebs and small blebs of galena are found within the bornite. The dusty brown-grey mineral (anisotropic - black grey – light grey) is found within this sample. One highly broken arsenopyrite grain is found.	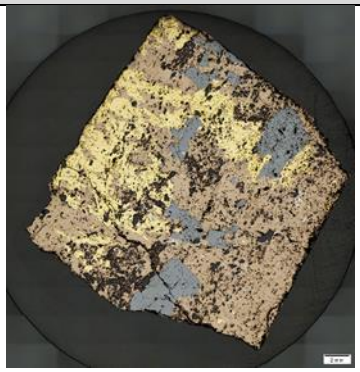
KP 13a	Massive bornite. Large veins of chalcocite that have formed around the gangue. Multidirectional laths of chalcopyrite is found within the bornite. There is a network of sphalerite. Renierite blebs can be seen replacing the chalcopyrite and chalcocite. The dusty brown-grey mineral (anisotropic - black grey – light grey) is found in this sample.	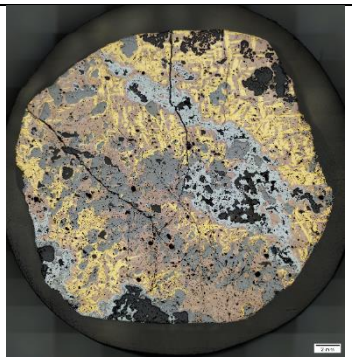
KP 13b	Massive bornite with multidirectional chalcopyrite laths. Chalcocite veins have formed around the gangue. There is a network of sphalerite present. Pyrite is being consumed by the gangue. Few renierite and tennantite blebs.	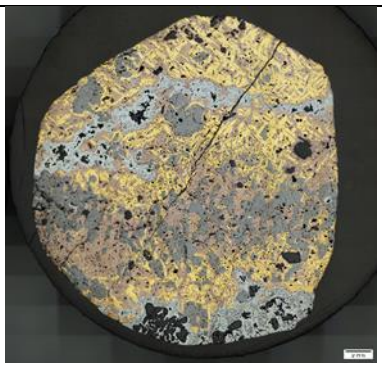

Bornite-renierite-dominant assemblage

Sample No	Observations	Scan
15453a	Bornite with huge chalcocite veins. Large veins of renierite occur within these chalcocite veins. Some of the chalcocite forms remnant globules of bornite within chalcocite.	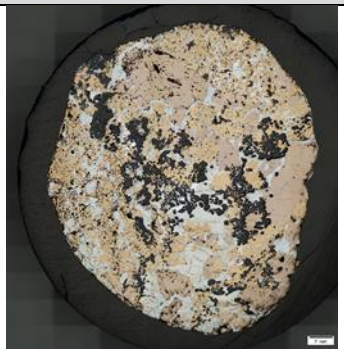
15453b	Bornite with huge chalcocite veins. Large veins of renierite occur within these chalcocite veins. Some of the chalcocite forms remnant globules of bornite within chalcocite. Betekhtinite is also seen.	

Chalcopyrite-pyrite-dominant assemblage

Sample No	Observations	Scan
12492a	This section contains mostly chalcopyrite with large anhedral pyrite grains throughout. There is some disseminated sphalerite. An unknown dusty brown-grey mineral (anisotropic - black grey – light grey), is seen associated with the gangue.	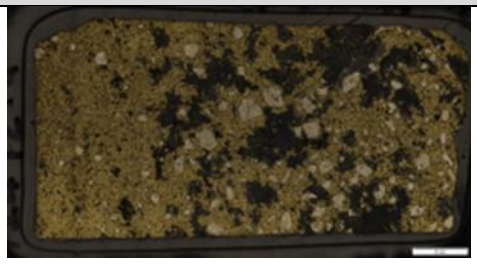

Sample No	Observations	Scan
S2801c	Massive chalcopyrite with large, mostly euhedral pyrite grains is seen in this section. There is a dusty brown-grey mineral (anisotropic - black grey – light grey) replacing some of the gangue. Some sphalerite, as well as small blebs of arsenopyrite are also replacing the gangue. The pyrite could be replacing the gangue.	

Chalcopyrite-dominant assemblage

Sample No	Observations	Scan
KP 6	This sample consists of country rock with chalcopyrite and sphalerite. It appears that the sphalerite is replacing the chalcopyrite.	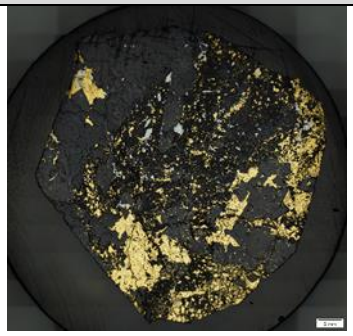
KP 8	This sample consists of country rock with chalcopyrite that is replacing it.	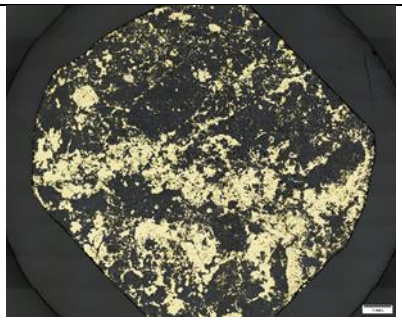

Sample No	Observations	Scan
12492b	Massive chalcopyrite with some gangue veins running across the section. One subhedral pyrite can be seen. Disseminated sphalerite can be seen associated with the gangue.	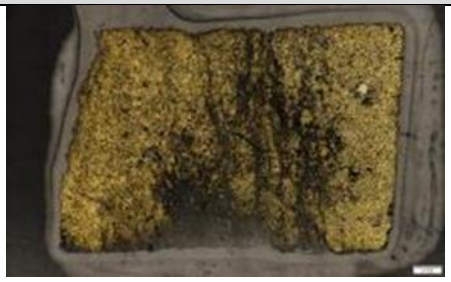

Sphalerite-dominant assemblage

Sample No	Observations	Scan
KP 11a	Massive sphalerite with large veins of the brown mineral. Small disseminations of chalcopyrite and tennantite are associated with the dusty brown-grey mineral (anisotropic - black grey – light grey).	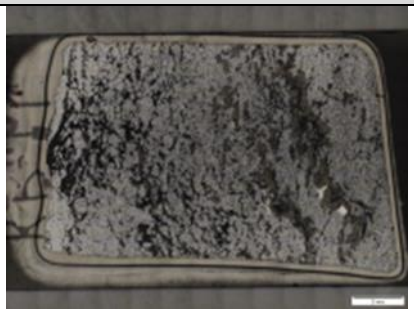
KP 11b	Massive sphalerite with veins of the brown mineral running through the sphalerite. Chalcopyrite is associated with the dusty brown-grey mineral (anisotropic - black grey – light grey).	
KP 11c	Massive sphalerite with a large vein of tennantite, galena and chalcopyrite. This vein occurs alongside a vein of host rock. Galena appears to be replacing the tennantite, and the chalcopyrite has many small blebs of arsenopyrite in it. There is one large euhedral pyrite grain, and many smaller ones. There are many specs of	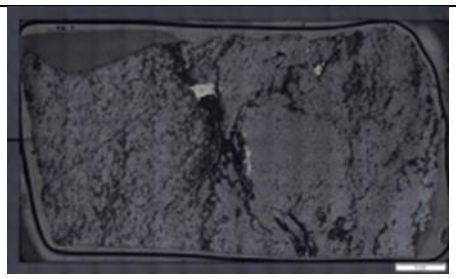

Sample No	Observations	Scan
	chalcopyrite replacing the gangue throughout the section.	
KP18	Massive sphalerite, with a bit of chalcopyrite disease. Chalcopyrite is replacing some of the host minerals. Blebs of tennantite can be seen within the sphalerite.	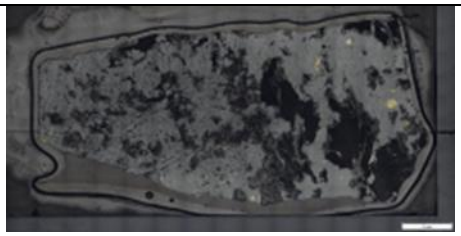

Sphalerite-chalcopyrite-dominant assemblage

Sample No	Observations	Scan
1058a	Massive sphalerite with chalcopyrite replacing the gangue. Disseminated galena, bornite and tennantite occur within the sphalerite and chalcopyrite.	
1058b	Massive sphalerite with a network of chalcopyrite and galena. The galena appears to be replacing the chalcopyrite. Disseminated bornite and tennantite blebs can be seen. The bornite also seems to be replacing the chalcopyrite. It looks as if the tennantite is replacing the bornite.	
6548	Massive sphalerite with a network of chalcopyrite. Some of the chalcopyrite is disseminated. Tennantite and galena both appear to replace some of the chalcopyrite. There are a few small pieces of renierite that are also replacing the chalcopyrite. A few veins of a dusty brown-	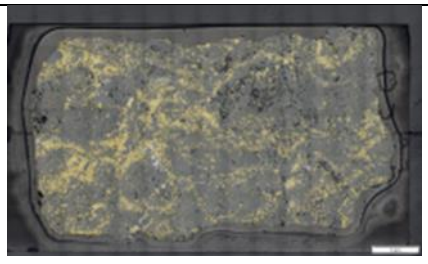

Sample No	Observations	Scan
	grey mineral appear through the section (anisotropic - black grey – light grey), mostly associated with the chalcopyrite and tennantite. Minor arsenopyrite is disseminated as tiny blebs within the sphalerite.	
12492c	Massive sphalerite with a network of chalcopyrite is seen in this section. A dusty brown-grey mineral (anisotropic - black grey – light grey) is replacing the chalcopyrite.	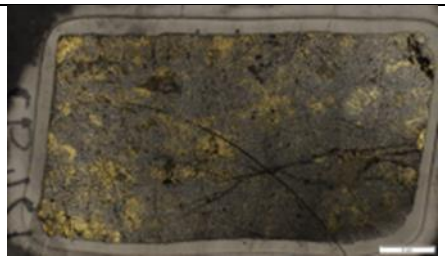
12492d	Massive sphalerite with an equilibrium network of chalcopyrite. There are a few small blebs of pyrite replacing the sphalerite, and in a few instances replacing the chalcopyrite too. It appears chalcopyrite is more likely to be replacing the gangue left over after the infill of sphalerite. The dusty brown-grey mineral (anisotropic - black grey – light grey) is seen replacing the chalcopyrite in the section.	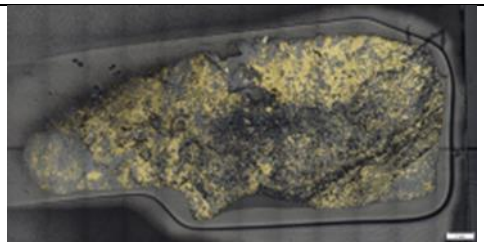
12492e	Massive sphalerite with both a network and dissemination of chalcopyrite makes up this section. Chalcopyrite looks to be replacing the gangue. The dusty brown-grey mineral (anisotropic - black grey – light grey) is found to be replacing the gangue and/or chalcopyrite. One small euhedral pyrite grain is seen in this section.	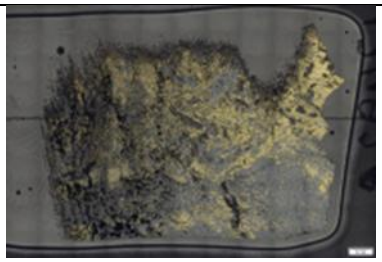

Sample No	Observations	Scan
12492f	Massive sphalerite with mostly disseminated chalcopyrite makes up this polished thin section. Some of the chalcopyrite is networked, while there are sections of massive chalcopyrite. The chalcopyrite seems to be mostly associated with the gangue. The same dusty brown-grey mineral (anisotropic - black grey – light grey) looks to be replacing the chalcopyrite.	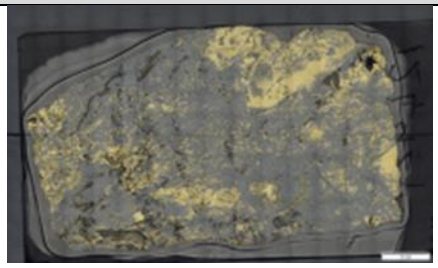
S2801a	This section was badly scratched during polishing. It consists of sphalerite and chalcopyrite in equilibrium. Some pyrite and the dusty brown-grey mineral (anisotropic - black grey – light grey) can be found.	
S2801b	Massive sphalerite with a networked chalcopyrite. The brown mineral is replacing the chalcopyrite. Euhedral pyrites can be found mostly associated with the gangue.	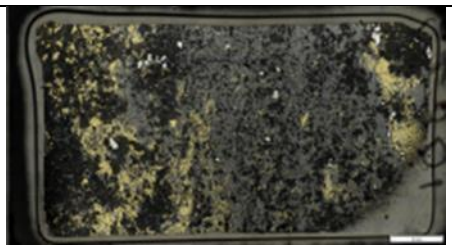

Sphalerite-bornite-dominant assemblage

Sample No	Observations	Scan
KP 2	Massive sphalerite is replaced by a bornite network. Bornite appears to be replaced by galena, tennantite and renierite. Renierite and tennantite look blobbier in some sections of the	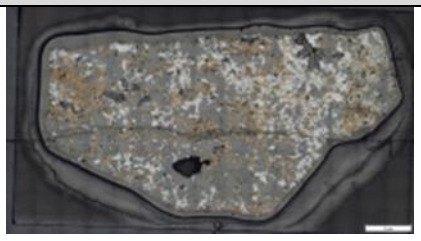

Sample No	Observations	Scan
	bornite, while the galena appears to be more networked.	
KP 5a	Massive sphalerite with a network of bornite that is replacing the sphalerite. Galena and chalcopyrite both appear to be replacing the bornite. Tennantite is seen to be replacing the sphalerite and the galena. Betekhtinite is replacing the bornite.	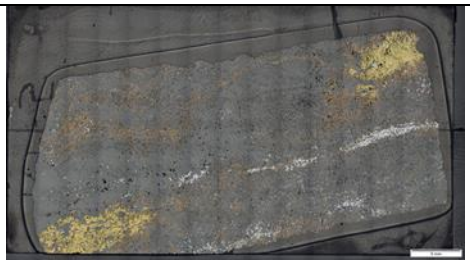
KP 5b	Base of bornite that was replaced by sphalerite. Galena, chalcopyrite, renierite and tennantite are then replacing the sphalerite. Betekhtinite is found to be replacing galena.	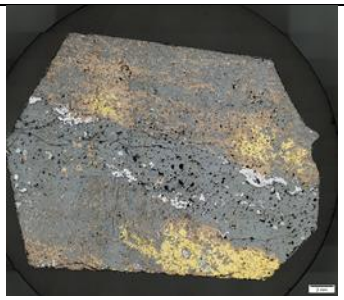
KP 17a	Massive sphalerite is replaced by bornite to create a network texture. Chalcocite replaces the bornite within the sphalerite, leaving remnant globules of bornite within chalcocite. Blebs of tennantite are also replacing the sphalerite.	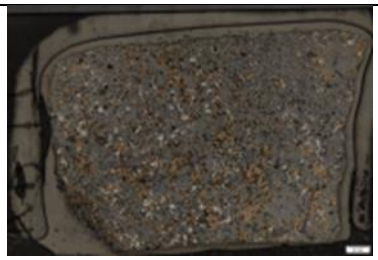
KP 17b	Another badly scratched section shows sphalerite with a network of bornite. This bornite is being replaced by tennantite and galena. Disseminated blebs of chalcopyrite are seen replacing the bornite too.	

Sample No	Observations	Scan
KP 17c	Massive sphalerite being replaced by a network of bornite (so that the sphalerite appears as large grains surrounded by the bornite when viewed with the naked eye). Chalcocite is replacing the bornite, incomplete replacement is shown by remnant globules of bornite within chalcocite. Arsenopyrite is seen replacing the sphalerite, and is sometimes surrounded by tennantite. Tiny blebs of chalcopyrite are found in the sphalerite. There are a few large blebs of tennantite. Renierite occurs as blebs that have formed predominately around the boundaries of the bornite and sphalerite, and are also surrounded by tennantite.	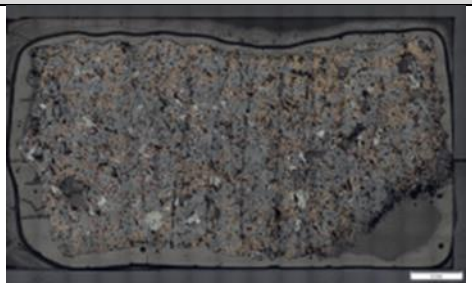
15452a	Massive bornite with large sections of sphalerite. Chalcopyrite appears to be replacing the sphalerite. Galena is found to be replacing the chalcopyrite. Renierite blebs are found mostly on the bornite-sphalerite boundaries. Large tennantite blebs are found throughout the section.	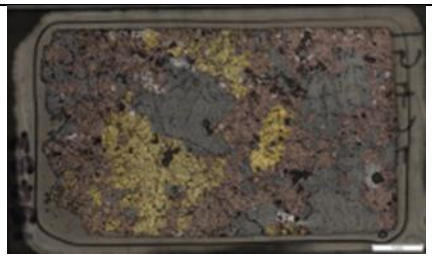
15452b	Massive sphalerite replaced by a network of bornite. Lots of tennantite and renierite replacing the bornite that is included in the sphalerite. Some chalcocite is replacing bornite, leaving remnant globules of bornite within chalcocite. Lots of galena is also replacing the sphalerite.	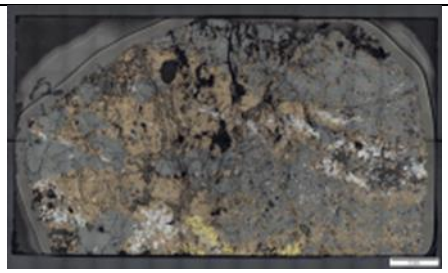

Sample No	Observations	Scan
	Tennantite and renierite are also replacing the galena, along with arsenopyrite. Chalcopyrite appears to be replacing either the bornite or sphalerite, and the galena is replacing chalcopyrite. Some chalcocite is seen to replace tennantite at its boundary.	

A.2.2. Tsumeb sample suite

Thirty-nine polished ore blocks were examined under reflected light using a petrographical microscope at the University of the Witwatersrand. Below is a comprehensive table of samples descriptions and full-section photomicrographs. Each polished block was scanned using an Olympus BX 53 microscope in the School of Geosciences at the University of the Witwatersrand.

Bornite-dominant assemblage

Sample No	Observations	Scan
107	Massive bornite with veins of chalcocite running through and networks of sphalerite and galena. Blebs of tennantite and pyrite.	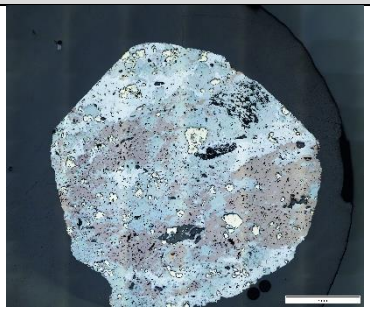
263	Massive bornite. Chalcocite veins join up areas of more massive chalcocite within the bornite. Small blebs of renierite and larger blebs of tennantite. Small networks of galena. 1 large broken up pyrite with bornite, chalcocite and gangue inside.	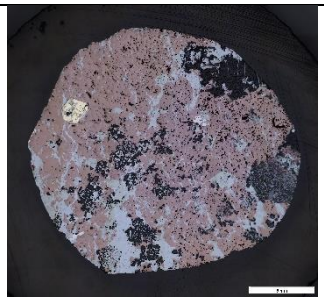

Sample No	Observations	Scan
333	Massive gangue with veins of bornite, chalcocite, galena and betekhtinite.	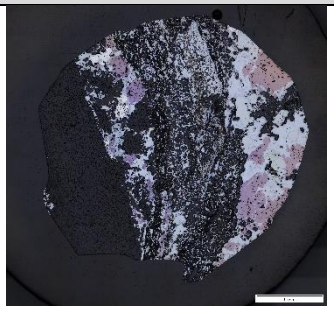
337	Massive bornite with chalcocite veins. Galena occurs as veins and disseminations. Few renierite blebs.	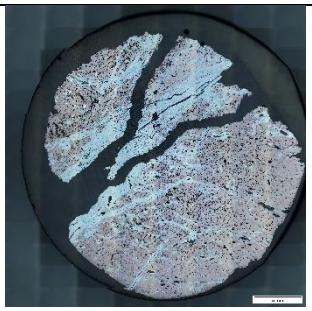
434 a	Massive bornite with chalcocite veins. Soma galena is present in these chalcocite veins. Betekhtinite can be seen replacing the chalcocite veins. Some small grains of carrollite are present. Tennantite is also present in the sample.	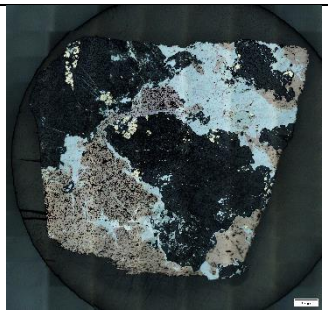
434 b	Bornite veins are found within the gangue of this sample. Smaller chalcocite veins are found within the bornite veins. Carrollite is found within the chalcocite and galena is found within the bornite.	

Sample No	Observations	Scan
477	Massive bornite with chalcocite veins. Large blebs of tennantite and betekhtinite. Galena is found to replace the chalcocite. 1 carrollite grain is found.	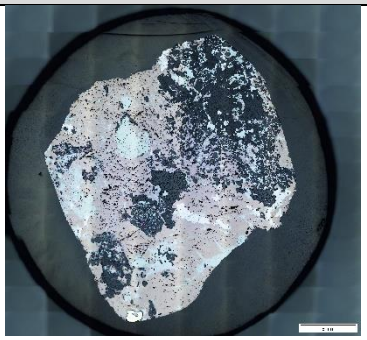
523	Chalcocite is seen to be replacing bornite. Large subhedral grains of carrollite. Renierite and betekhtinite blebs are found within the chalcocite.	
99A a	Massive bornite with disseminated gangue. Small chalcocite veins occur within the bornite. Blebs of galena and tennantite. 1 large pyrite grain.	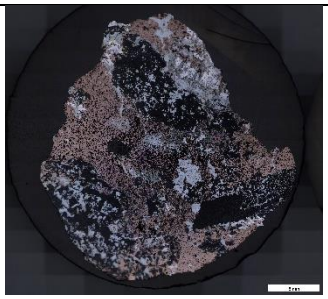
717	Bornite is replaced by chalcocite so that the bornite is left as small globules within the chalcocite. Large blebs of betekhtinite are found replacing the chalcocite. Subhedral grains of carrollite with galena in between the pieces is seen.	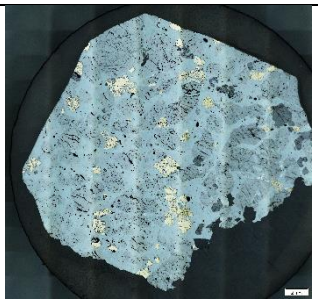

Sample No	Observations	Scan
125	Country rocks with bornite veins. A network of chalcocite is replacing a lot of the bornite. Betekhtinite as well as an unknown brown phase is present.	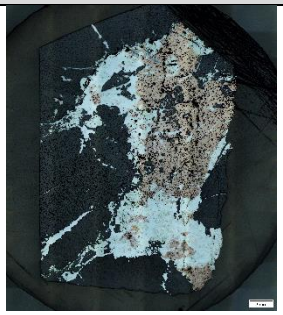
253 b	Massive chalcocite with tiny flecks of chalcopyrite, galena and digenite associated with the gangue. There is some sphalerite around the digenite. Some larger blebs of chalcopyrite are also associated with the gangue.	
TS 3	Disseminated bornite, chalcopyrite, chalcocite, renierite, germanite and galena in the gangue. Bornite vein is being replaced by many smaller chalcocite veins. There is some galena and chalcopyrite are around the edge of the ore block. Some carrollite has formed within the gangue.	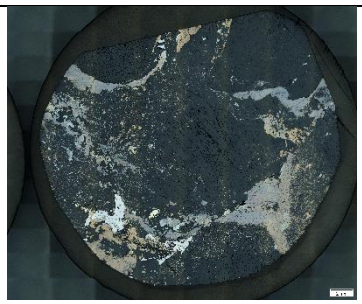
TS 6	Massive gangue with grainy bornite and chalcocite. Small galena blebs are seen within the bornite.	

Sample No	Observations	Scan
TS 8	Massive bornite with many chalcocite veins. Pyrite and renierite associated with the bornite. Exsolution of chalcopyrite within the renierite. There is lots of galena within the bornite and chalcocite.	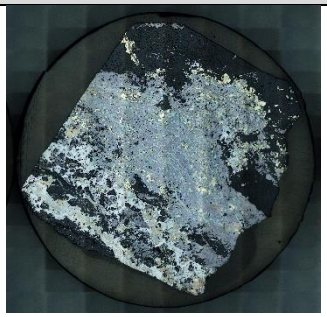
TS 9	Large chalcocite veins within the host gangue. The chalcocite disseminates into the gangue. Irregular blebs of galena, and carrollite within the chalcocite.	
TS 10	Massive gangue with streaks of disseminated chalcocite. Broken up carrollite grains with bornite and chalcopyrite inside.	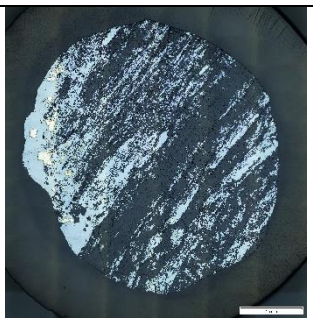

Tennantite-dominant assemblage

Sample No	Observations	Scan
TS 1	Disseminated tennantite around the country rock gangue.	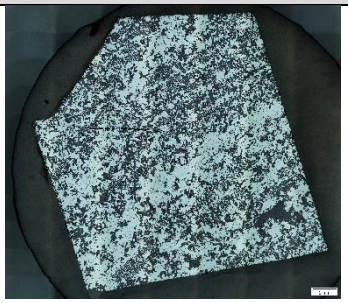

Sample No	Observations	Scan
TS 7	Massive tennantite that appears to be replacing the underlying bornite and chalcocite. Galena is also seen to be replacing the bornite and chalcocite. Specks of chalcocite are seen within the underlying bornite. Blebs of germanite and renierite are seen. One large broken up carrollite crystal with gangue within it is noted.	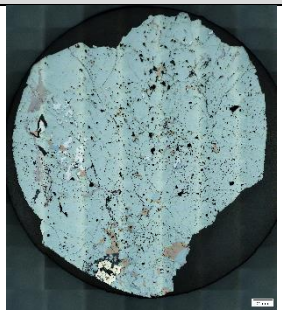
470	Massive tennantite with some sphalerite veins associated with the gangue.	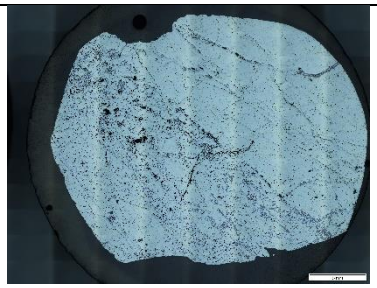
99A b	Massive tennantite with disseminated bornite, chalcopyrite and galena. These phases are being replaced by the tennantite.	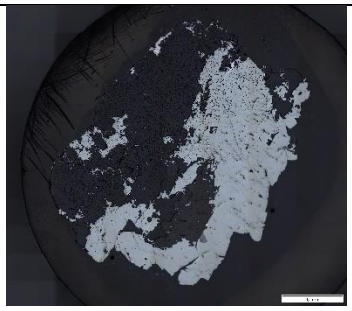

Galena-dominant assemblage

Sample No	Observations	Scan
8	Massive galena with blebs of sphalerite, betekhtinite and tennantite. Bornite occurs as both blebs and disseminations. Disseminated digenite is found.	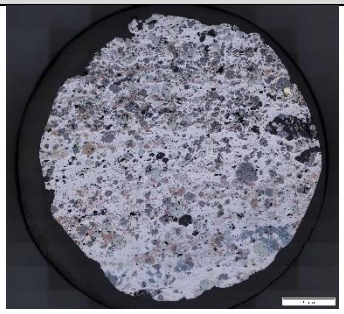

Sample No	Observations	Scan
90	Massive galena with disseminated pyrite and sphalerite. The pyrite looks to be replacing the sphalerite. Bornite and chalcocite also appear as disseminations that are being replaced by the sphalerite.	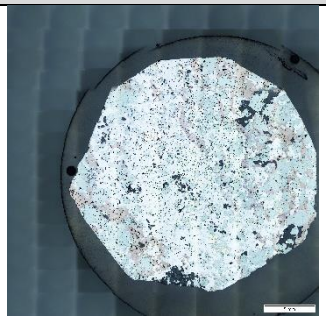
91	Massive galena with disseminated pyrite and sphalerite. The pyrite looks to be replacing the sphalerite. Bornite and chalcocite with small blebs of chalcopyrite also appear as disseminations that are being replaced by the sphalerite.	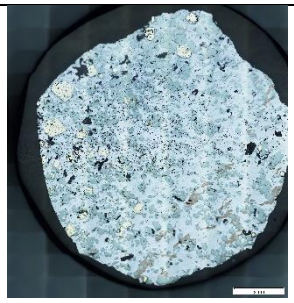
253 a	This sample is massive galena with digenite associated with tennantite.	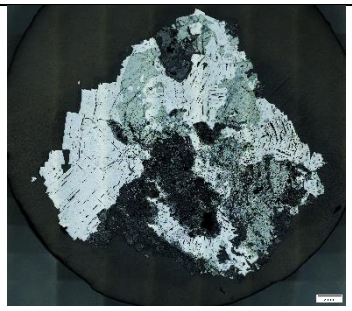
259	Massive galena and sphalerite in a network with minor blebby tennantite, chalcopyrite and pyrite.	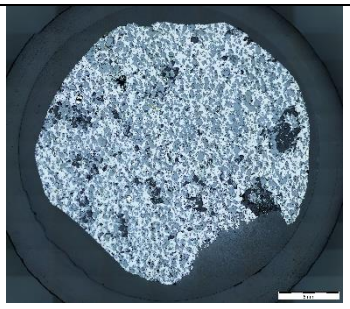
340	Massive galena with a network of pyrite that is replacing the gangue. Sphalerite and tennantite occur as blebs.	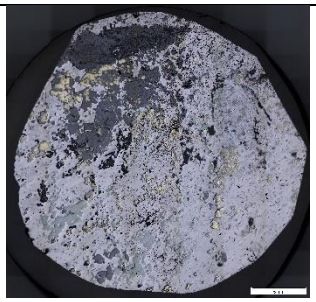

Sample No	Observations	Scan
423	Massive galena with many small and large blebs of betekhtinite.	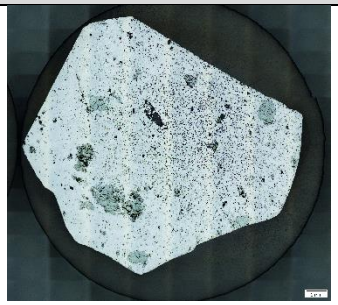
560	Large galena veins are seen in this country rock.	
TS 4	Massive galena with broken euhedral carrollite. This broken up carrollite has bornite with a chalcopyrite network within it.	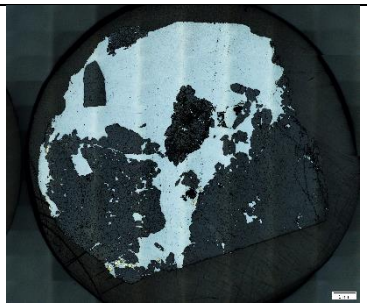
TS 5	Galena creates a network within the sphalerite. Large blebs of tennantite are seen, as well as some carrollite.	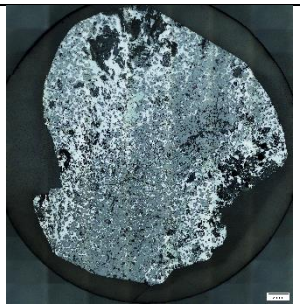
TS 11	Massive galena with disseminated pyrite and sphalerite. The pyrite looks to be replacing the sphalerite. Bornite and chalcocite also appear as disseminations that are being replaced by the sphalerite.1 large pyrite grain is seen, as well	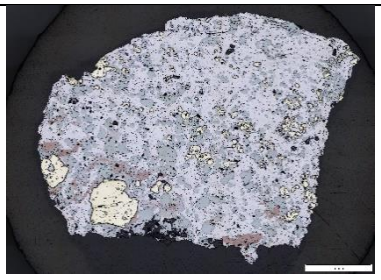

Sample No	Observations	Scan
	as a very small network of arsenopyrite.	

Sphalerite-dominant assemblage

Sample No	Observations	Scan
110	Massive sphalerite. Galena occurs as both a network and disseminations. Blebs of tennantite, bornite, chalcocite, digenite and betekhtinite are found within the galena. Small pyrites are found within the galena and tennantite.	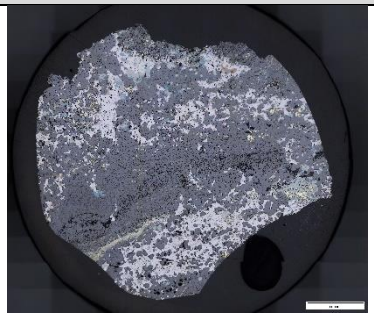
149	Lots of disseminated sphalerite hosting a network of tennantite and large flecks of native copper.	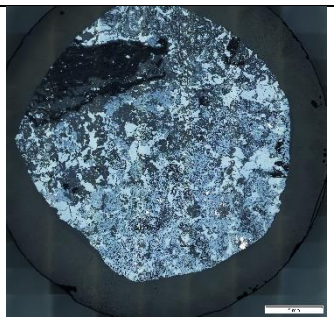
272A	Massive gangue with a large network of sphalerite. There are sections of galena that are replacing the sphalerite. Chalcopyrite is also seen replacing the sphalerite. There are some pyrite grains.	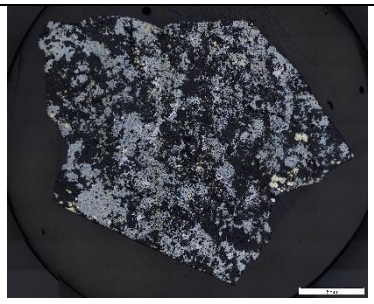

Sample No	Observations	Scan
735	Sphalerite veins within the host rock gangue. Galena, tennantite, carrollite, unknown brown mineral and digenite are found within the sphalerite.	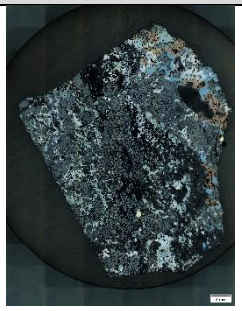

Sphalerite-pyrite-dominant assemblage

Sample No	Observations	Scan
268	Massive sphalerite with a network of blebby pyrite in sections. Bornite and chalcopyrite occur as small flecks throughout the sphalerite.	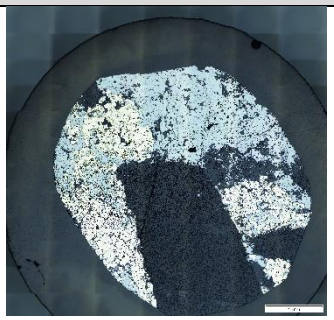
395	Massive sphalerite with disseminated blebby pyrite. Parts of the ore block have a network of the blebby pyrite.	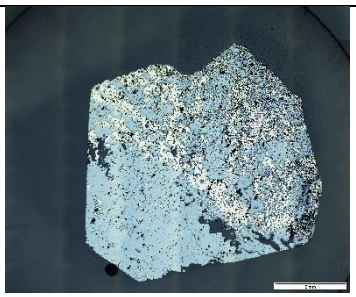
519	Disseminated sphalerite and pyrite, where the pyrite is observed to have replaced the sphalerite.	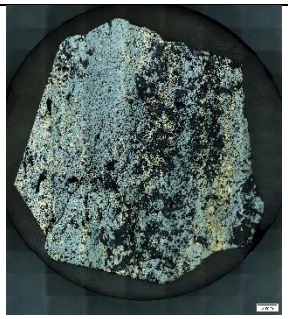

Appendix B

Whole rock trace element geochemistry

B.1. Geochemical analysis

Samples were sent to Intertek Genalysis for trace element analysis. Samples could not be analysed at the Wits Earth Lab due to the nature of massive sulphides; a specialised method was needed. Samples were crushed and milled to a grain size of <75 µm. A specialised four-acid digest method was used in conjunction with inductively coupled plasma-optical emission spectroscopy (ICP-OES) and inductively coupled plasma-mass spectrometry (ICP-MS) to obtain the whole rock composition for 26 different trace elements.

In the four-acid digest method, nitric, hydrofluoric, perchloric and hydrochloric acids are used to digest the crushed sample. The hydrofluoric acid is used to dissolve any silicates in the powder, this method is thus referred to as ‘near total’ digestion (Rice, 2017). In most cases, the nitric and perchloric acids are added first. The sample is heated to over 150 ^{0}C. The other two acids are added, and the solution is dried.

The ICP-MS method was used to detect Ag, As, Be, Bi, Cd, Co, Ga, Ge, In, Li, Mo, Pb, Rb, Re, Sb, Sc, Se, Te, and Tl. The ICP-OES method was used for Cr, Cu, Mn, Na, Ni, and Zn. Ag, Cd, Cu, Pb and Zn, which were all measured above detection limits. Cu and Zn were above detection limits and were therefore measured again using ICP-MS. Ag, Cd, and Pb were also above detection limits and as a result were repeated using the ICP-OES method.

B.2. Kipushi whole rock trace element geochemical results

ELEMENTS	Ag	Ag-Rp1	As	Be	Bi	Cd	Cd-Rp1	Co	Cr	Cs	Cu	Cu-Rpt1	Ga	Ge
UNITS	ppm	ppm	ppm	ppm	ppm	ppm	ppm	ppm	ppm	ppm	ppm	ppm	ppm	ppm
DETECTION	0.05	5	0.5	0.05	0.01	0.02	10	0.1	5	0.05	1	0.05	0.05	0.1
METHOD	4A/MS	4AH/OE	4A/MS	4A/MS	4A/MS	4A/MS	4AH/OE	4A/MS	4A/OE	4A/MS	4A/OE	4A/OE	4A/MS	4A/MS
COMMENTS: 1268.0/1812700 (25/09/2018) CLIENT O/N: Caitlin Stewart 1/1														
SAMPLE NUMBERS	Ag	Ag-Rp1	As	Be	Bi	Cd	Cd-Rpt1	Co	Cr	Cs	Cu	Cu-Rpt1	Ga	Ge
KP 7	>500.00	2942	23.6	X	0.08	8.43		0.6	X	X	>20000	192900	2.12	49
KP 11	9.99		688.5	0.22	0.1	>2000.00	4694	2.3	17	0.41	1326		3.35	39.6
1058	198.8		3780.6	X	0.67	>2000.00	3347	91.4	X	X	>20000	196900	621.36	1845
S2801	18.51		2665.7	X	8.85	>2000.00	2060	19.4	X	X	>20000	116700	3.27	25
586	>500.00		2341.1	X	1.59	>2000.00	2386	55.7	X	0.16	>20000	298400	186.97	387.8
12492 A	>500.00		69.1	X	39.25	9.59		28	6	X	>20000	495500	2.99	21.5
12492	78.1		1546.9	X	7.87	22.2		6.8	X	X	>20000	311900	1.77	7.1
15453	>500.00		7188.9	X	0.28	156.67		29.5	6	X	>20000	460700	92.08	>2000.0
15452	>500.00		1628.6	X	0.24	950.61		39.8	X	X	>20000	431500	118.5	474.9
1213	>500.00	839	892.8	X	2.37	29.79		9	X	X	>20000	467800	51.02	137.9
CHECKS														
1058	193.91		3710.7	X	0.58	>2000.00		89.5	7	0.06	>20000		610.72	>2000.0
STANDARDS														
OREAS 351		106					1068					10200		
OREAS 624	44.41		107.2	0.78	21.69	127.77		251.7	29	1.23	>20000		22.97	1.9
OREAS 630	11.03		657.3	1.18	7.47	13.13		5.8	18	6.09	462		21.89	4.1
OREAS 622	103.17		114.4	0.96	5.33	460.32		36.9	41	1.85	4946		26.64	5.6
MP-1b	50.62		>10000.0	0.38	1042.97	571.42		3.9	5	0.95	>20000		113.53	2.8
OREAS 932	20.96		16.4	1.56	370.33	3.1		60.5	57	6.98	>20000		17.52	9.2
OREAS 935	44.87		10.8	1.1	763.83	2.24		79.2	42	7.17	>20000		13.28	9
BLANKS														
Control Blank	0.42		1.6	X	X	0.03		X	X	X	107		X	7.7

ELEMENTS	In	Li	Mn	Mo	Na	Ni	Pb	Pb-Rpt1	Rb	Re	Sb	Sc	Se	Te	Tl	Zn	Zn-Rpt1
UNITS	ppm	ppm	ppm	ppm	ppm	ppm	ppm	ppm	ppm	ppm	ppm	ppm	ppm	ppm	ppm	ppm	ppm
DETECTION	0.01	0.1	1	0.1	20	1	0.5	50	0.05	0.002	0.05	0.1	0.5	0.2	0.02	1	10
METHOD	4A/MS	4A/MS	4A/OE	4A/MS	4A/OE	4A/OE	4A/MS	4AH/OE	4A/MS	4A/MS	4A/MS	4A/MS	4A/MS	4A/MS	4A/MS	4A/OE	4AH/OE
COMMENTS: 1268.0/1812700 (25/09/2018) CLIENT O/N: Caitlin Stewart 1/1																	
SAMPLE NUMBERS	In	Li	Mn	Mo	Na	Ni	Pb	Pb-Rpt1	Rb	Re	Sb	Sc	Se	Te	Tl	Zn	Zn-Rpt1
KP 7	0.28	3.9	467	0.7	265	3	3083.4		0.8	0.007	0.52	0.2	5.7	X	0.02	1046	
KP 11	X	26.7	125	9.4	149	4	3042.5		16.02	0.006	7.72	2.9	X	X	0.32	>20000	525200
1058	3.16	5.7	136	1.9	579	20	>10000.0	112500	0.47	0.017	66.59	X	63.7	X	0.17	>20000	420500
S2801	4.77	4	75	0.8	27	14	319.9		2.42	0.003	3.88	0.3	5.4	X	0.16	>20000	336500
586	3.64	5.5	102	1.2	430	3	>10000.0	32700	0.43	0.002	33.85	X	92.1	X	0.05	>20000	305200
12492 A	0.18	0.9	26	8.3	X	8	>10000.0	126600	1.09	0.628	2.28	X	47.1	X	0.25	1147	
12492	2.44	5	913	1.3	X	15	722.8		2.92	0.006	3.54	0.3	2.2	X	0.09	2823	
15453	0.81	1	34	2.7	124	13	3324.1		0.39	0.022	50.73	X	45.4	X	0.07	14499	
15452	1.55	1.6	45	0.3	164	6	>10000.0	53000	0.18	0.006	22.32	X	105.2	X	0.08	>20000	108500
1213	0.3	0.7	24	17.2	X	9	4551.5		0.46	0.004	30.22	X	5.4	X	0.08	1843	
CHECKS																	
1058	3.12	5.3	127	1.8	564	21	>10000.0		0.42	0.018	68.75	X	60.4	X	0.11	>20000	
STANDARDS																	
OREAS 351								37600									456600
OREAS 624	3.94	9	626	16.2	4720	20	6258.9		32.77	0.002	69.3	7.6	28.4	0.8	1.03	>20000	
OREAS 630	0.43	20.7	22271	10.9	5606	12	2767.8		197.77	0.003	43.82	9.9	X	X	52.33	5692	
OREAS 622	4.62	7.6	592	17.4	7262	29	>10000.0		58.31	0.002	202.98	6.7	4.6	X	3.92	>20000	
MP-1b	635.07	23.7	521	288.9	140	3	>10000.0		32.82	0.006	52.2	1.9	5.2	2.7	1.02	>20000	
OREAS 932	5.5	20.3	926	1.4	1952	33	255.5		135.62	X	2.28	8.8	64.5	X	0.67	856	
OREAS 935	15.18	12	700	1.7	1527	33	260.8		91.42	X	3.34	6.2	92.2	0.4	0.52	824	
BLANKS																	
Control Blank	X	0.2	X	X	X	X	1.1		0.08	X	X	X	X	X	X	6	

B.3. Tsumeb whole rock trace element geochemical results

ELEMENTS	Ag	Ag-Rp1	As	As-Rp1	Be	Bi	Cd	Cd-Rp1	Co	Cr	Cs	Cu	Cu-Rp1	Ga	Ge
UNITS	ppm	ppm	ppm	ppm	ppm	ppm	ppm	ppm	ppm	ppm	ppm	ppm	ppm	ppm	ppm
DETECTION	0.05	5	0.5	50	0.05	0.01	0.02	10	0.1	5	0.05	1	10	0.05	0.1
METHOD	4A/MS	4AH/OE	4A/MS	4AH/OE	4A/MS	4A/MS	4A/MS	4AH/OE	4A/MS	4A/OE	4A/MS	4A/OE	4AH/OE	4A/MS	4A/MS
COMMENTS:	1268.0/1912573 (23/08/2019) CLIENT O/N: Caitlin Stewart 1/														
SAMPLE NUMBERS															
TS1	323.85		>10000.0	138229	X	0.25	>2000.00	2355	5.8	X	0.05	>20000	322404	339.18	175.2
91	199.48		>10000.0	49037	X	1.21	696.12		209.5	X	0.11	>20000	208303	153.91	152.7
99A	171.11		>10000.0	56564	X	0.23	471.15		275.9	5	0.08	>20000	156420	292.53	1444.8
110	144.56		9412.3		0.10	0.09	>2000.00	9046	63.4	6	0.18	>20000	59659	10.82	26.9
125	>500.00	551	>10000.0	13182	X	0.10	279.34		34.3	8	X	>20000	382773	125.19	76.9
259	37.48		2985.0		X	0.07	>2000.00	4302	36.2	X	0.05	8329		39.62	128.3
340	24.84		3706.2		X	0.06	>2000.00	3895	56.6	X	X	10932		718.67	10.0
470	>500.00	658	>10000.0	134376	X	0.18	672.08		30.4	X	X	>20000	501527	142.74	33.6
477	>500.00	1325	>10000.0	9967	X	0.18	162.29		462.2	X	0.13	>20000	531864	211.08	100.4
519	399.30		>10000.0	38297	X	0.11	320.86		28.0	X	0.05	>20000	87606	91.67	91.7
CHECKS															
259	37.46		2973.0		X	0.07	>2000.00		36.2	X	0.06	8115		39.36	127.6
STANDARDS															
OREAS 46	1.53		337.2		0.97	0.06	4.27		10.6	57	0.63	1155		14.61	1.1
OREAS 47	0.82		62.1		0.99	0.18	8.54		54.3	107	2.22	402		14.41	1.5
AMIS0167	1.14		185.8		0.47	1.03	1.37		40.2	372	1.19	147		3.67	0.9
OREAS 13b	0.91		63.0		1.64	1.59	0.63		71.1	10629	6.33	2414		18.63	1.4
BLANKS															
Control Blank	X		0.5		X	X	X		X	X	X	3		X	X

ELEMENTS	In	Li	Mn	Mo	Mo-Rp1	Na	Ni	Pb	Pb-Rp1	Rb	Re	Sb	Sc	Se		ELEMENTS	Te	Tl	Zn	Zn-Rp1
UNITS	ppm	ppm	ppm	ppm	ppm	ppm	ppm	ppm	ppm	ppm	ppm	ppm	ppm	ppm		UNITS	ppm	ppm	ppm	ppm
DETECTION	0.01	0.1	1	0.1	20	20	1	0.5	50	0.05	0.002	0.05	0.1	0.5		DETECTION	0.2	0.02	1	10
METHOD	4A/MS	4A/MS	4A/OE	4A/MS	4AH/OE	4A/OE	4A/OE	4A/MS	4AH/OE	4A/MS	4A/MS	4A/MS	4A/MS	4A/MS		METHOD	4A/MS	4A/MS	4A/OE	4AH/OE
COMMENTS:	1268.0/1912573 (23/08/2019) CLIENT O/N: Caitlin Stewa															COMMENTS:				
SAMPLE NUMBERS																SAMPLE NUMBERS				
TS1	6.68	1.6	1364	2.3		X	3	107.1		0.88	0.019	5720.88	0.3	39.6		TS1	47.9	0.50	>20000	55843
91	0.64	1.6	234	2551.1		62	50	>10000.0	508941	2.66	2.795	383.57	X	8.6		91	0.3	0.98	15082	
99A	2.67	1.9	166	4328.9		X	139	>10000.0	189675	2.24	7.486	1018.12	0.1	341.1		99A	5.0	0.87	18609	
110	0.02	4.2	1043	3670.8		73	43	>10000.0	276360	9.16	0.957	172.39	0.8	7.2		110	X	2.49	>20000	374957
125	0.57	1.2	122	2244.6		X	18	>10000.0	13647	0.90	12.150	309.77	X	29.5		125	0.4	0.63	6286	
259	0.21	0.8	519	1784.1		33	10	>10000.0	516289	0.99	0.438	162.00	X	50.0		259	0.4	1.57	>20000	212051
340	4.52	0.4	979	3080.9		36	19	>10000.0	448732	0.35	0.106	473.72	X	11.7		340	0.6	0.41	>20000	319046
470	3.97	1.0	207	132.5		156	8	>10000.0	68519	0.10	0.019	1869.67	X	51.3		470	12.5	0.17	>20000	55397
477	1.22	2.1	52	>10000.0	26839	X	171	>10000.0	120989	3.46	120.943	408.70	0.2	31.2		477	1.7	8.78	3892	
519	1.05	2.3	586	275.3		X	22	4903.2		1.31	1.281	448.65	X	56.8		519	1.9	0.14	>20000	32455
CHECKS																CHECKS				
259	0.22	0.9	524	1764.2		40	9	>10000.0		1.00	0.436	154.55	X	48.4		259	0.4	1.55	>20000	
STANDARDS																STANDARDS				
OREAS 46	0.04	10.9	492	4.4		26112	27	457.6		34.52	X	6.00	9.2	X		OREAS 46	X	0.20	388	
OREAS 47	0.06	42.3	514	28.9		26324	91	1298.2		38.83	0.048	2.15	9.5	0.6		OREAS 47	X	0.27	645	
AMIS0167	0.02	4.7	190	8.7		644	100	388.7		17.64	0.015	7.36	2.7	0.7		AMIS0167	X	0.19	247	
OREAS 13b	0.24	16.7	1263	11.7		16891	2214	97.5		117.12	0.005	2.33	24.1	3.0		OREAS 13b	0.3	1.04	158	
BLANKS																BLANKS				
Control Blank	X	X	X	X		X	X	X		X	X	X	X	X		Control Blank	X	X	X	

Appendix C

Scanning electron microscopy and mineral analysis for the Kipushi sample suite

C.1. Zeiss Gemini SEM

C.1.1. Bornite-dominant assemblage

KP 12

Two areas were selected to gather BSE images and element maps from this polished thin section. The BSE image and element maps of the first area selected can be seen in Figure 1. This area shows that the Ge is concentrated into the renierite. The renierite also has a higher than expected concentration of Zn, as does the tennantite. The chalcopyrite has a high Co concentration. The tennantite is rich in Pb.

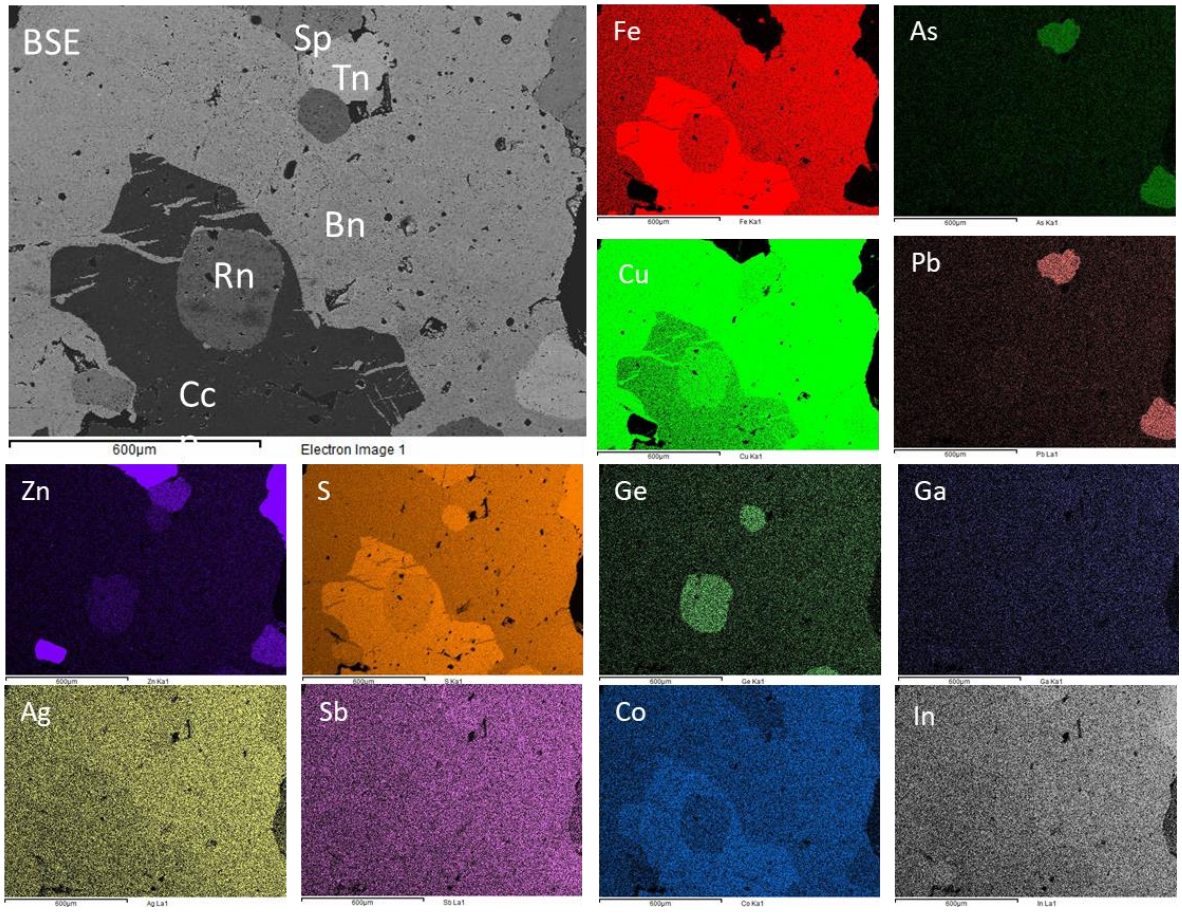

Figure 1: BSE image with labelled minerals of sphalerite (sp), tennantite (tn), bornite (bn), renierite (rn) and chalcopyrite (ccp) along with element maps of Fe, As, Cu, Pb, Zn, S, Ge, Ga, Ag, Sb, Co and In of area one from sample KP 12. Ge is found to concentr

The BSE image and element maps of the second area selected is shown in Figure 2. In this assemblage, Ge is seen to concentrate into the galena. Co, Ag, As, Sb and Ga are also present within the galena.

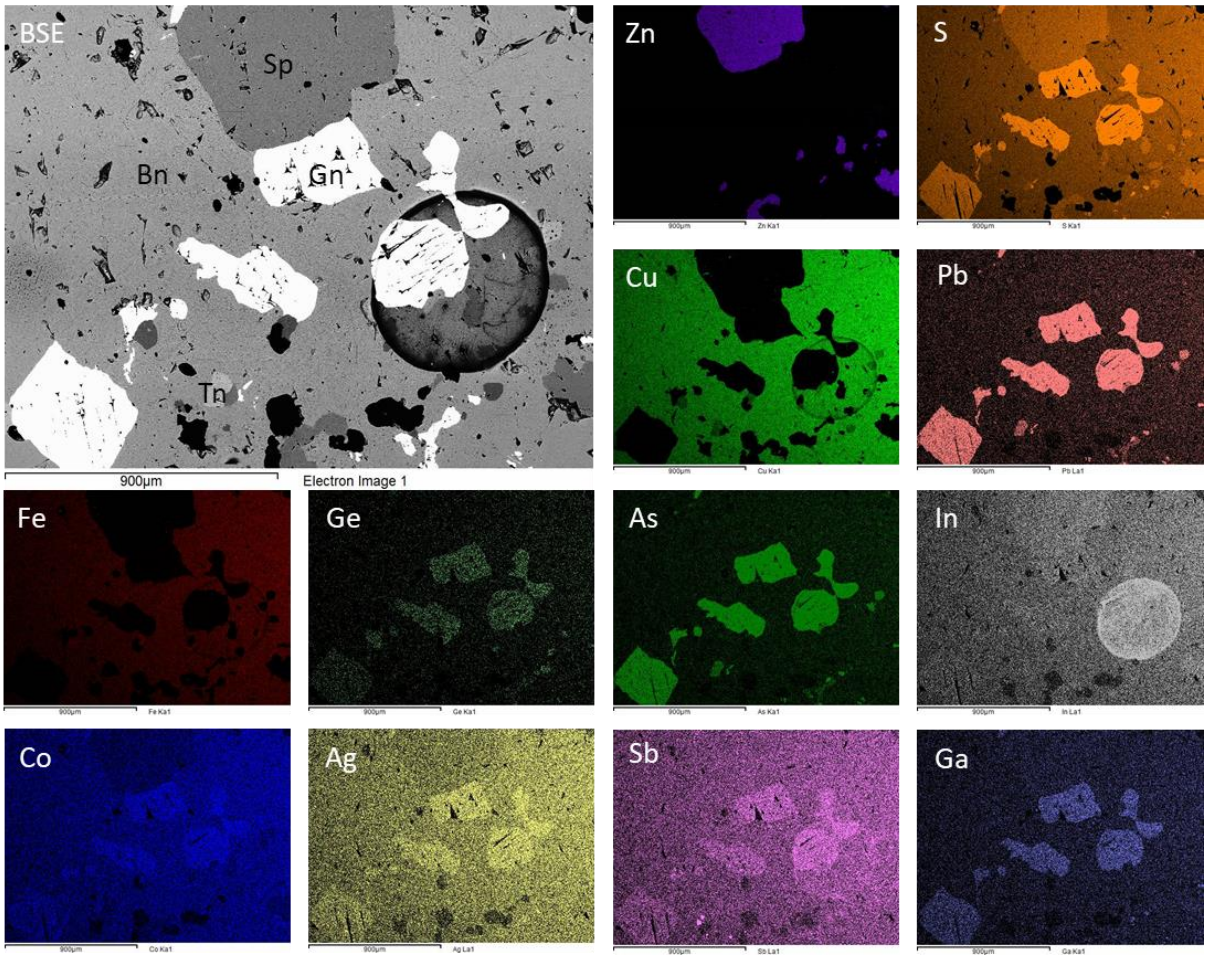

Figure 2: BSE image with labelled minerals of sphalerite (sp), tennantite (tn), bornite (bn), renierite (rn) and chalcopyrite (ccp) along with element maps of Fe, As, Cu, Pb, Zn, S, Ge, Ga, Ag, Sb, Co and In of area one from sample KP 12. Ge is found to concentr

15452 b

Polished thin section b from sample 15452 was selected for SEM analysis. Three areas from this polished thin section were selected for element maps. Figure 3 shows the BSE image and element maps of the first area. This area shows the Ge once again concentrating into the galena, as are the As, Sb, Ga and Ag. A new phase that has a high concentration of Co and Cu is seen in this assemblage. Figure 4 shows the spectrum for this mineral phase. The Cu, Co and Ni in this spectrum identifies this mineral as carrollite.

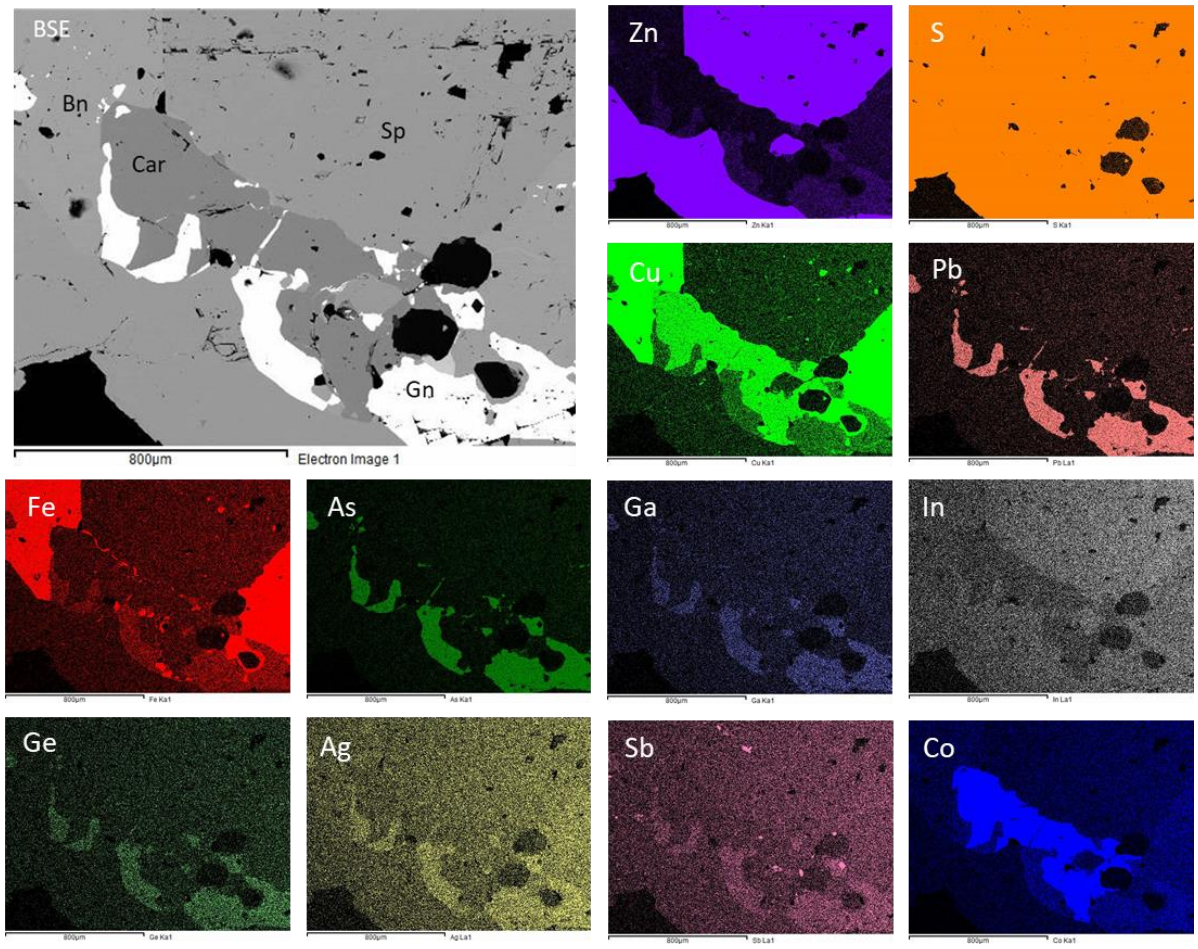

Figure 3: BSE image with labelled minerals of sphalerite (sp), bornite (bn), and carrollite (car), along with element maps of Zn, S, Cu, Pb, Fe, As, Ga, In, Ge, Ag, Sb and Co of area one from sample 15452 b. Ge is found to concentrate into the galena.

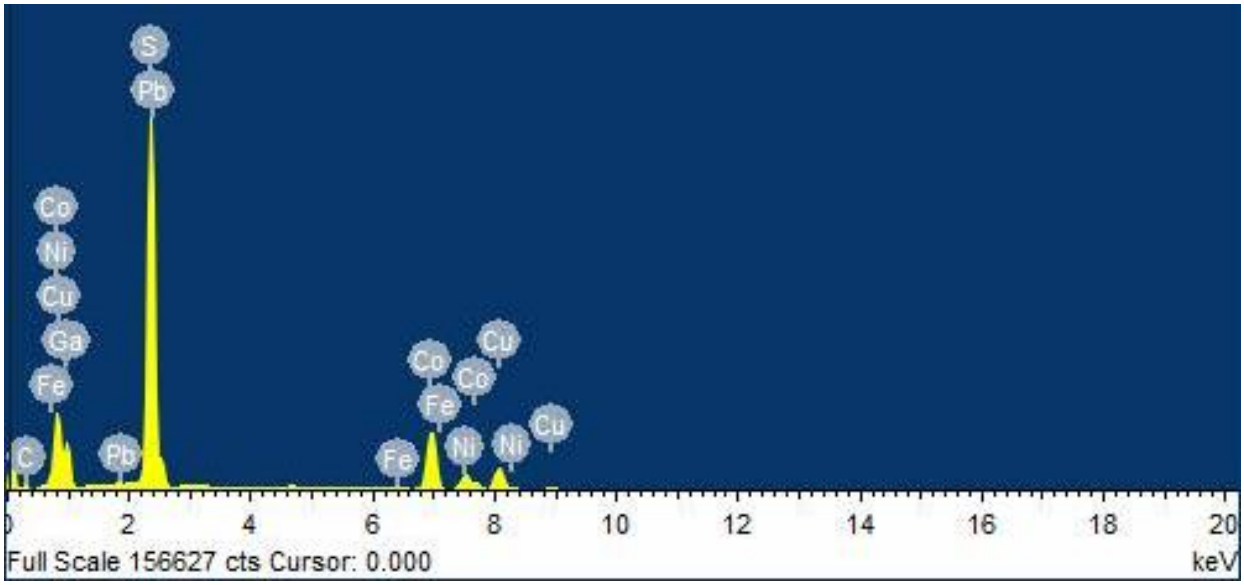

Figure 4 Spectrum for phase identified as carrollite. High in S with lots of Co, Ni and Cu.

Figure 5 shows the BSE image and element maps of the second area for this sample. In this area the Ge also concentrates into the galena, as do Ag, As, Sb, Co and Ga.

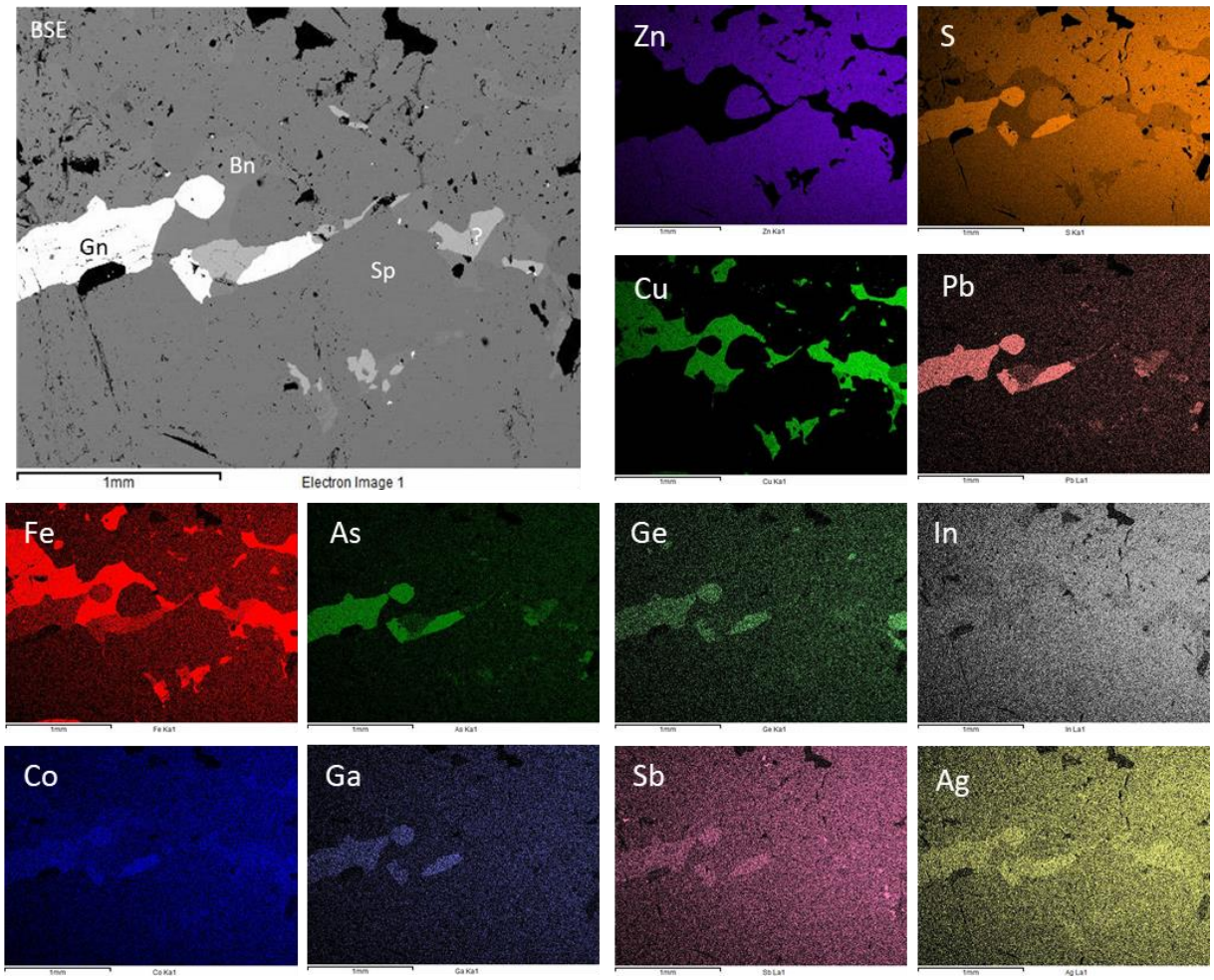

Figure 5: BSE image with labelled minerals of sphalerite (sp), bornite (bn) galena (gn) and an unknown mineral, along with element maps of Zn, S, Cu, Pb, Fe, As, Ge, In, Co, Ga, Sb and Ag of area two from sample 15452 b. Ge is found to concentrate into the galena.

Figure 6 shows the BSE image and element maps of the third and final area for sample 15452. This assemblage shows small Ge rich renierite blebs. The Ge does not concentrate into any other phases, including the very small bit of galena present in this area. The tennantite in this area is rich in Pb.

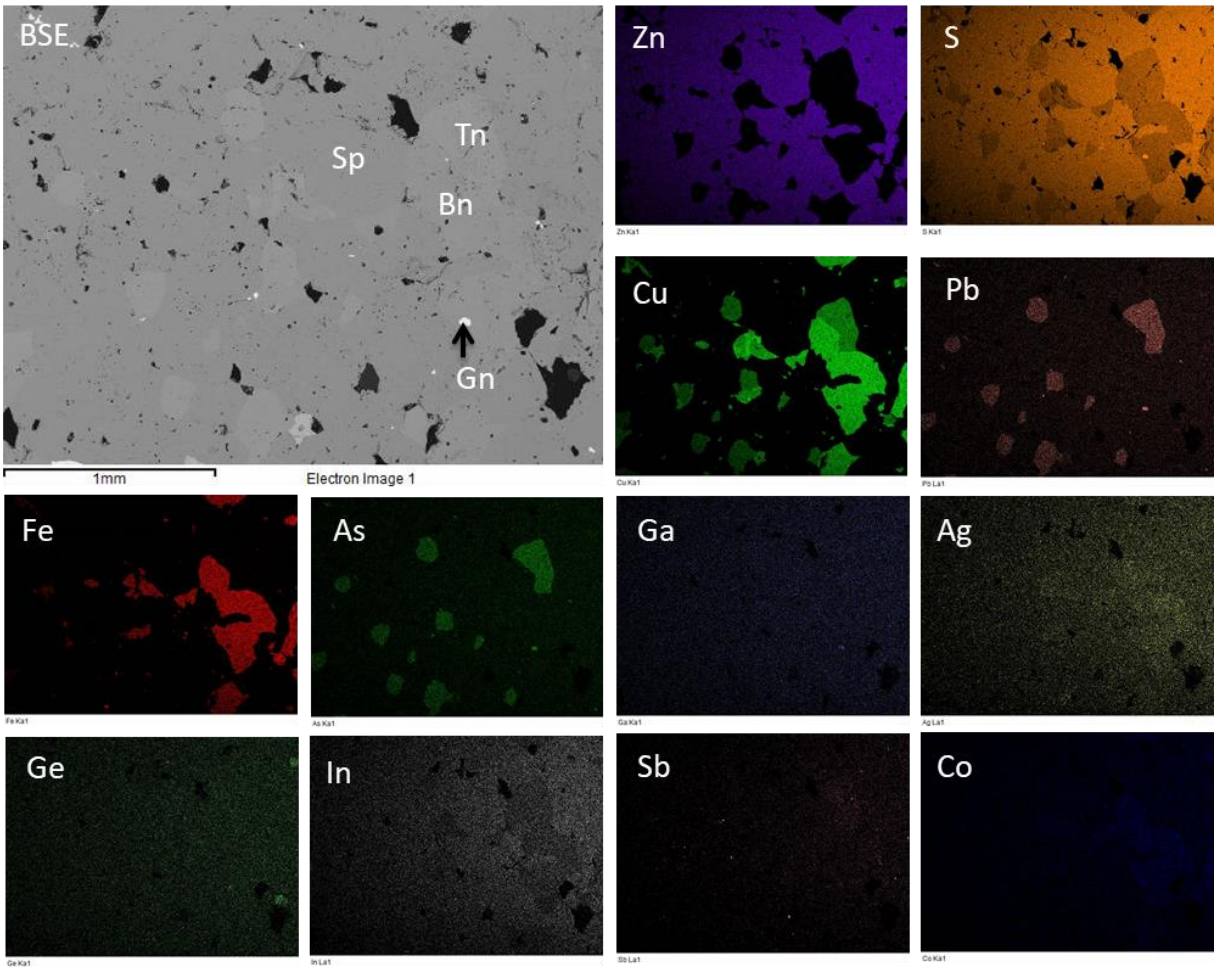

Figure 6: BSE image with labelled minerals of sphalerite (sp), tennantite (tn), bornite (bn) galena (gn) and renierite (rn), along with element maps of Zn, S, Cu, Pb, Fe, As, Ga, Ag, Ge, In, Sb and Co of area three from sample 15452 b. Ge is found to concentrate into the renierite and to a lesser extent, the galena.

C.1.2. Chalcopyrite-pyrite-dominant assemblage

S2801 c

Polished thin section c from sample S2801 was selected for analysis under the SEM. Two areas were identified for element maps. Figure 7 shows the BSE image and element maps of the first area. Little to no Ge concentration is seen in this assemblage. The sphalerite has a higher than expected concentration of In. Pb concentrates into the arsenopyrite. The chalcopyrite has a high Co concentration. There is an iron cobalt rich mineral phase present. This area shows an extremely rich Sb phase, identified as calcite. Further investigation into this mineral's spectrum revealed there is no Sb within this phase, the element map picks up a peak overlap with the Ca. Figure 8 shows the point spectrum for this phase.

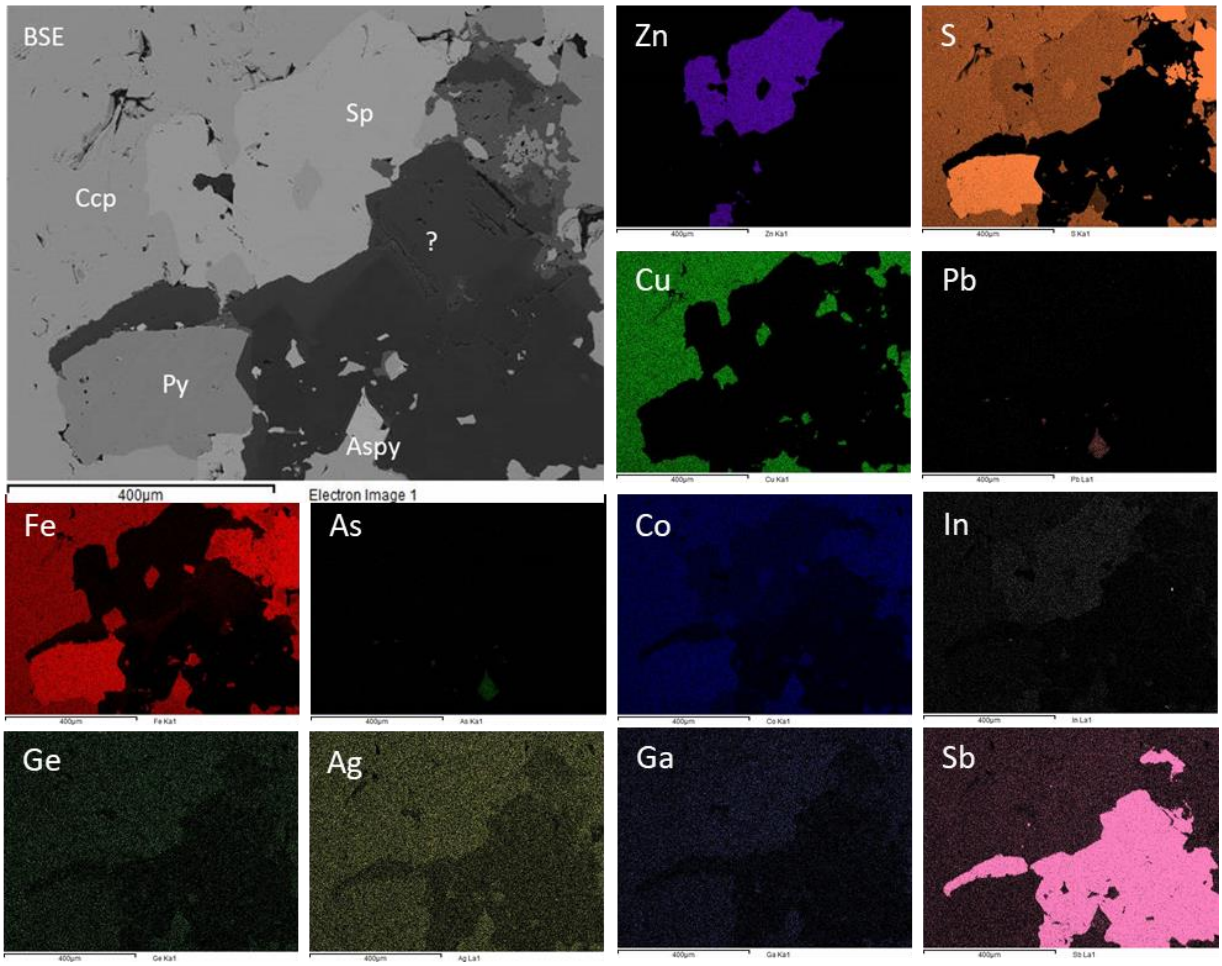

Figure 7: BSE image with labelled minerals of sphalerite (sp), chalcopyrite (ccp), pyrite (py), arsenopyrite (aspy) and an unknown mineral, along with element maps of Zn, S, Cu, Pb, Fe, As, Co, In, Ge, Ag, Ga and Sb of area one from sample S2801. Ge does not concentrate into any of these minerals. The unknown mineral is extremely rich in Sb.

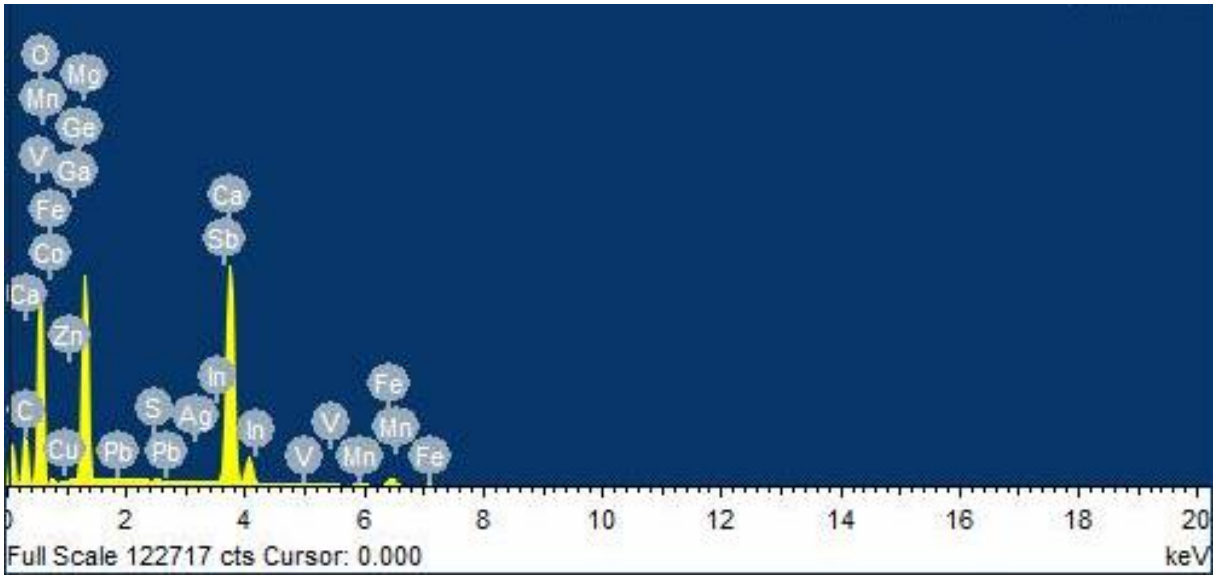

Figure 8: Spectrum for the Sb rich unidentified phase. This phase is shown to be a Ca, Sb phase.

Figure 9 shows the BSE image and element maps of the second area. Area two once again shows little to no Ge concentration. Co and Pb concentration are both present in the arsenopyrite. Co also concentrates into the chalcopyrite and pyrite. The sphalerite has a high concentration of In.

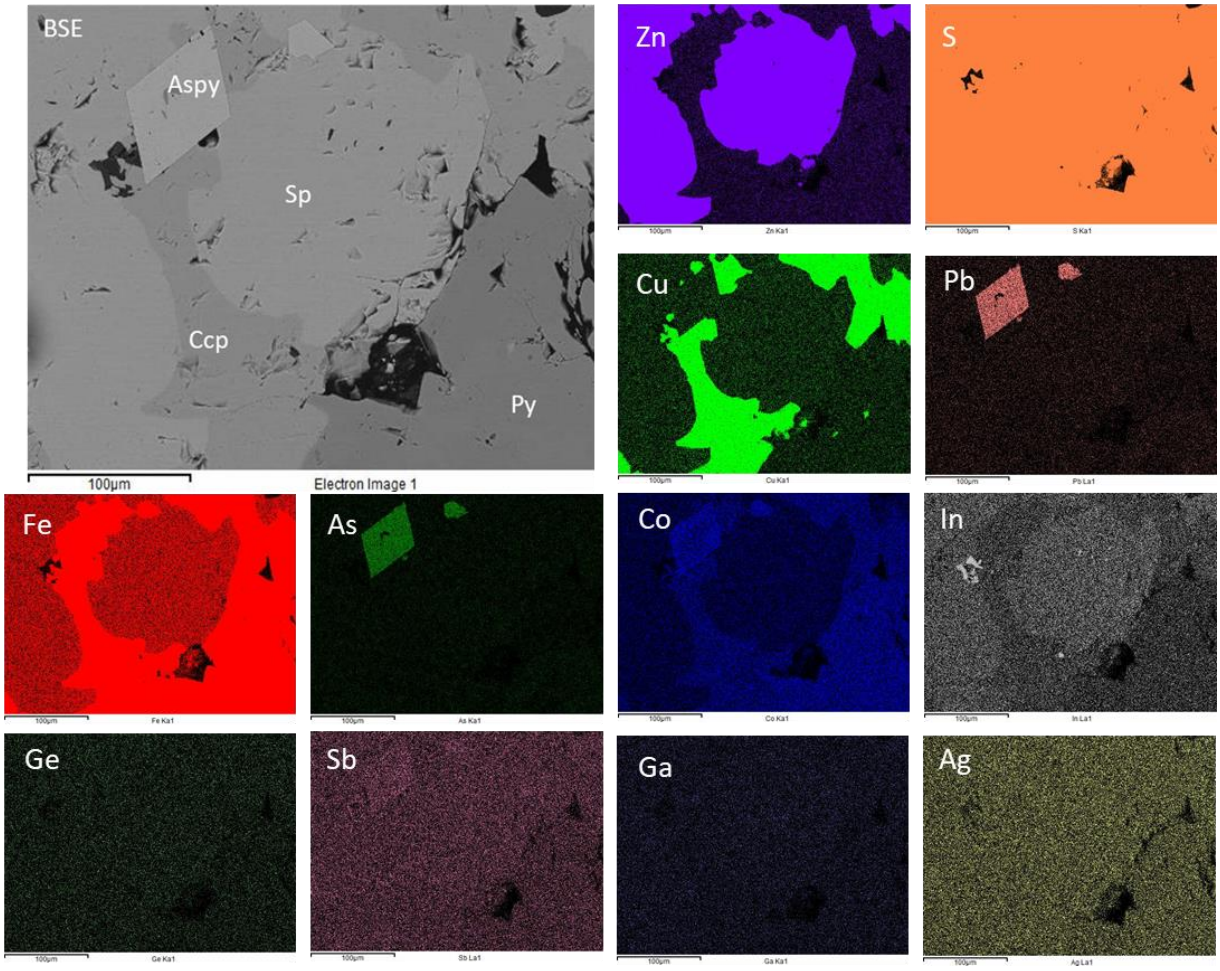

Figure 9: BSE image with labelled minerals of sphalerite (sp), chalcopyrite (ccp), pyrite (py), arsenopyrite (aspy) and an unknown mineral, along with element maps of Zn, S, Cu, Pb, Fe, As, Co, In, Ge, Sb, Ga and Ag of area two from sample S2801.No Ge is found to concentrate into any of the minerals in this area.

C.1.3. Sphalerite-chalcopyrite-dominant assemblage

6548

One polished thin section had three areas scanned using the SEM. Figure 10 shows the BSE image and element maps for the first area. Area one shows that the Ge concentrated into the galena. As does As, Ga and Ag. The tennantite is rich in Pb. An unidentified phase that is not rich in any of the elements scanned can be seen in this area. Figure 11 shows the point spectrum for this phase. The spectrum shows a C rich phase. This could be attributed to an error of the machine as it may be reading the carbon coating instead of the mineral.

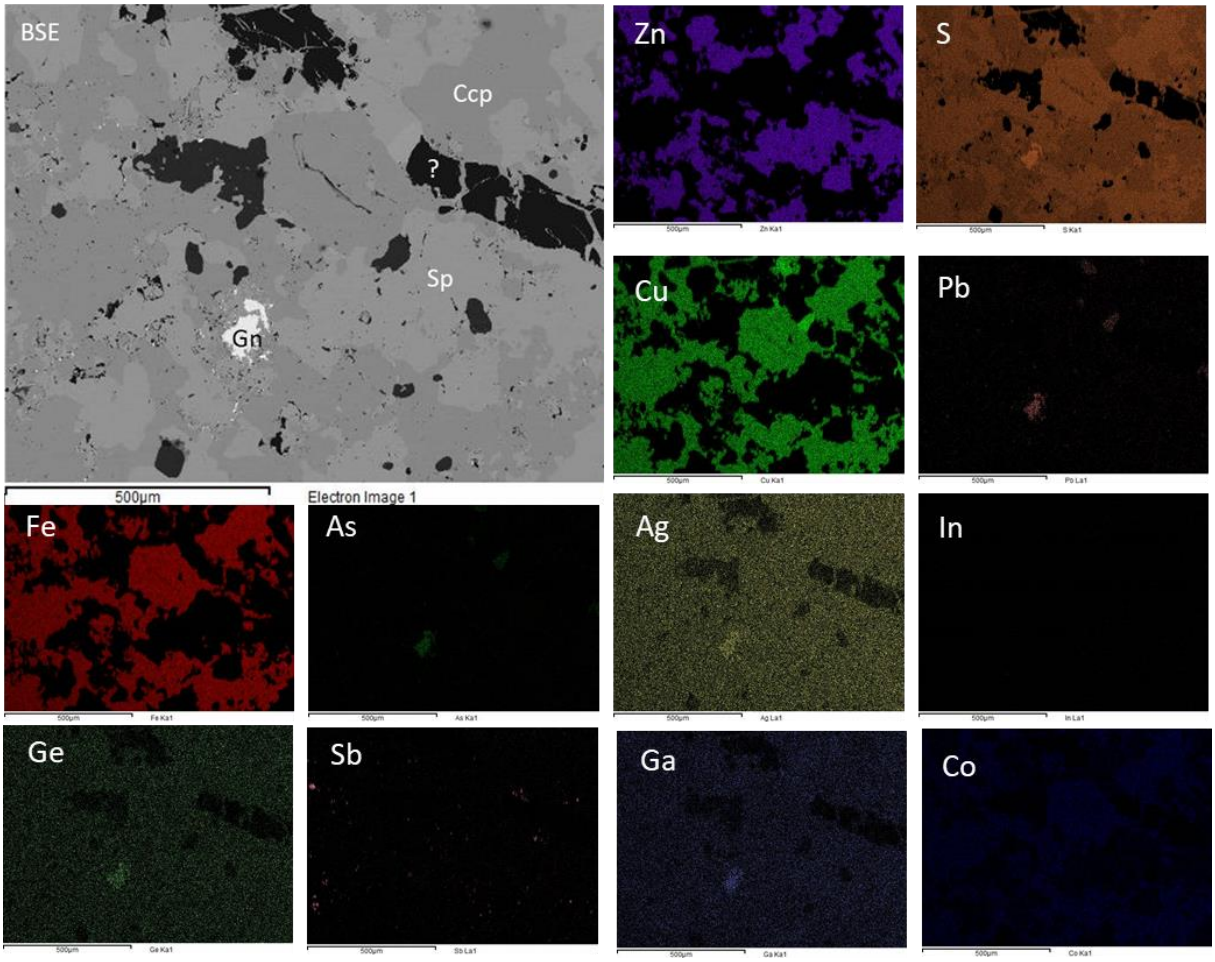

Figure 10: BSE image with labelled minerals of sphalerite (sp), chalcopyrite (ccp), galena (gn) and an unknown mineral, along with element maps of Zn, S, Cu, Pb, Fe, As, Ag, In, Ge, Sb, Ga and Co of area one from sample 6548. Ge is found to concentrate into the galena.

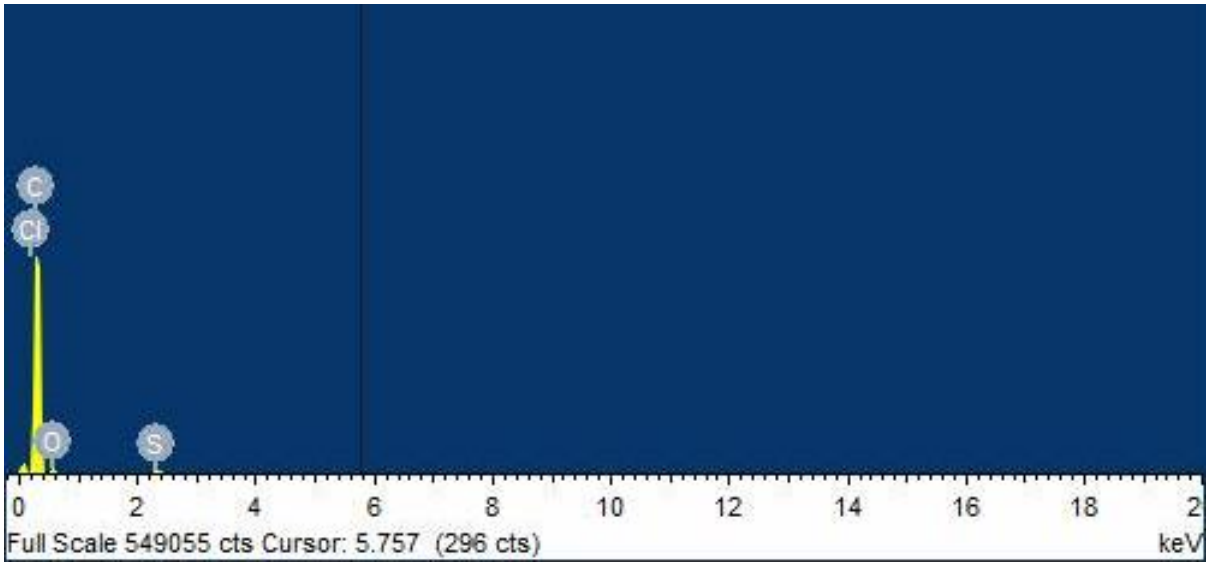

Figure 11: Spectrum for an unidentified phase. This phase is shown to be rich in C. It could be attributed to the carbon coating oh the sample.

Figure 12 shows the BSE image and element maps of the second area. This area shows that in a chalcopyrite, galena, sphalerite assemblage the Ge, as well as Ag, concentrated into the galena. This galena is also rich in In and Sb.

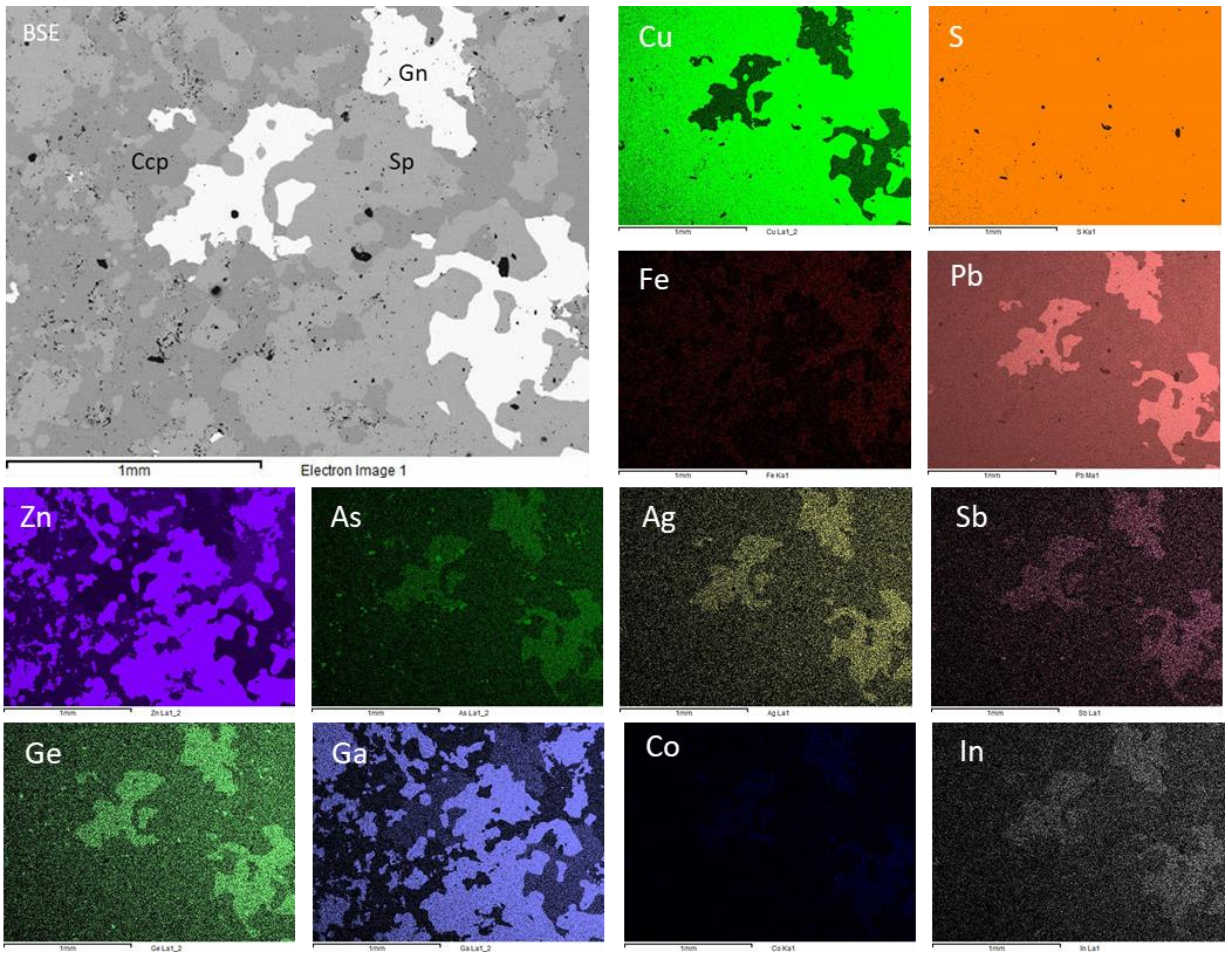

Figure 12: BSE image with labelled minerals of sphalerite (sp), chalcopyrite (ccp), and galena (gn), along with element maps of Cu, S, Fe, Pb, Zn, As, Ag, Sb, Ge, Ga, Co and In of area two from sample 6548. Ge is found to concentrate into the galena, as does Ag.

Figure 13 shows the BSE image ad element maps of the third area for this sample. In this galena-absent assemblage, Ge is found to concentrate into the tennantite. A similar phase to that seen in area one for this same sample, is seen in this area. It has no concentration of any of the elements scanned.

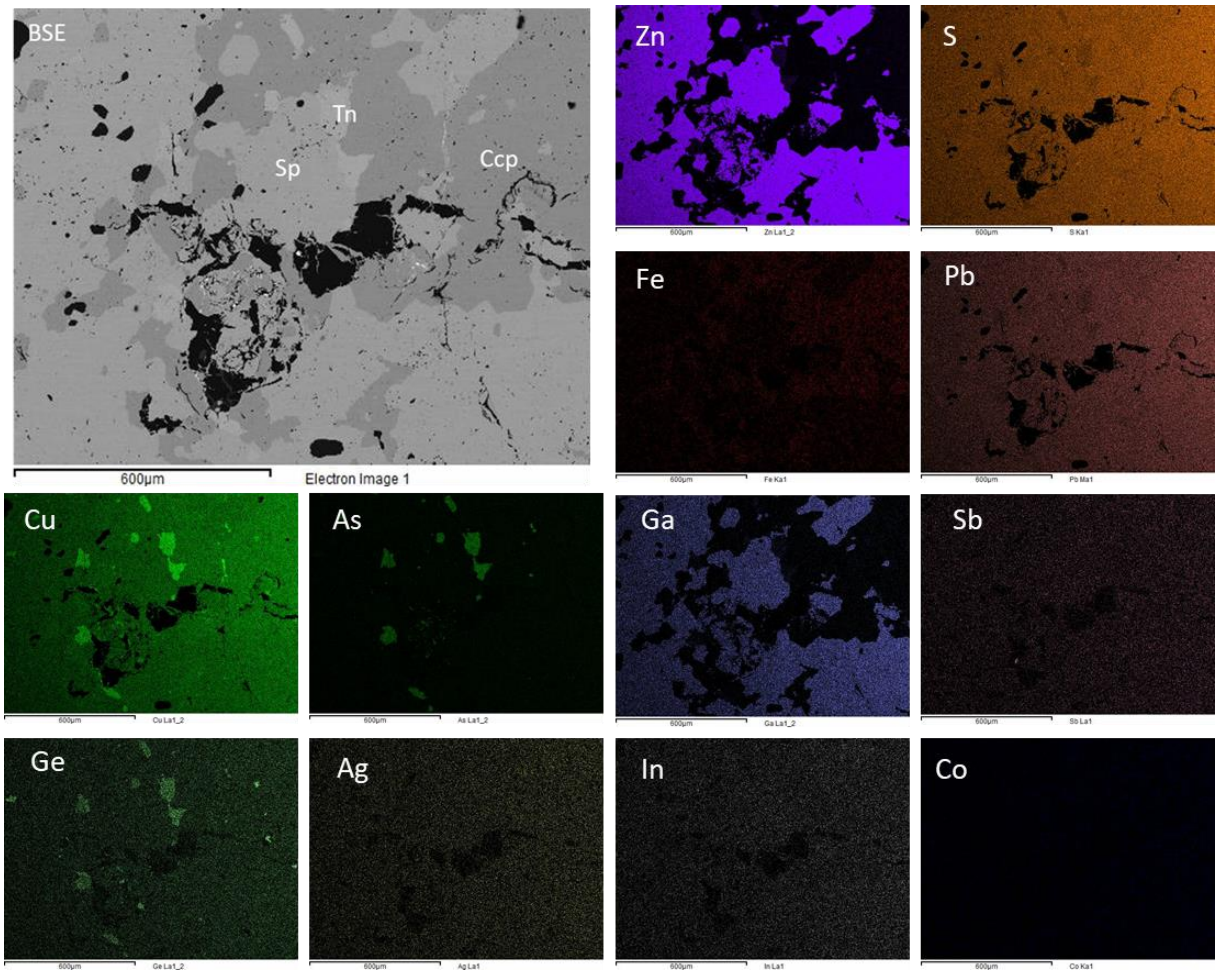

Figure 13: BSE image with labelled minerals of sphalerite (sp), chalcopyrite (ccp), and tennantite (tn), along with element maps of Zn, S, Fe, Pb, Cu, As, Ga, Sb, Ge, Ag, In and Co of area three from sample 6548. Ge is found to concentrate into the tennantite.

These SEM images show that when renierite is present in an assemblage, the bulk of the Ge will always concentrate into the renierite. Where renierite is not present, the Ge will concentrate into the galena. And when galena is not present in the assemblage, the Ge will concentrate into the tennantite. When none of the mentioned mineral phases are present Ge will not concentrate into any other phase, and that assemblage will be Ge poor. Other notable peculiarities include the high concentration of Pb into tennantite, Co rich chalcopyrite, and high concentration of As, and lower concentrations of Ag, Ga and Sb in the galena.

C.2. Tescan Integrated Mineral Analyser

The TIMA is capable of performing particle scans, field scans, line scans, and bright phase searching. It can create phase maps as well as element maps and do point analysis. A TIMA can have multiple detectors, namely a backscatter electron, a secondary electron and an energy-dispersive x-ray spectrometry detector (Hrstka *et al, 2018*). The TIMA in the School of Geosciences has a backscatter electron detector and a cathode luminesce detector. Another way the TIMA differs from an SEM is that it scans the selected area for all minerals and elements, as opposed to selected elements on the SEM. This allows element maps to be created, and spectra and mineral phases to be identified offline.

Polished thin sections were used in the TIMA before a proper thin section holder had been purchased. These polished thin sections had to be carefully mounted onto the ore block sample holder using carbon tape.

The following table is a legend with each colour used to represent each mineral phase in the false colour primary phase maps.

Table 1: Legend for the false colour primary phase maps.

Name
Bornite
Renierite
Tennantite
Digenite
Gallite
Cu Oxide
Chalcopyrite
Chalcocite
Betekhtinite
Silver-bearing phase
Hematite/Magnetite
Baryte
Germanite
Galena
Apatite
Quartz
Sphalerite
Pyrite
Microcline
Ti-rich SiO
Dolomite
CaPSb
Monazite
Phlogopite
Glauconite in sphalerite
Arsenopyrite
Calcite
Carrollite
Fe-rich-Cuprite
Molybdenite

C.2.1. Bornite-dominant assemblage

Sample 586

Two polished ore blocks were scanned by the TIMA for this sample. Both polished ore blocks were scanned in entirety by Louis Coetzee, as well as one smaller area for each polished block. Comparing the primary phase map and element map for Ge from polished ore block A (Figure 14) shows the highest concentration of Ge within the renierite. Other interesting things to note are a high concentration of As and Ga within the galena and a relatively high concentration of Zn and Pb within the tennantite.

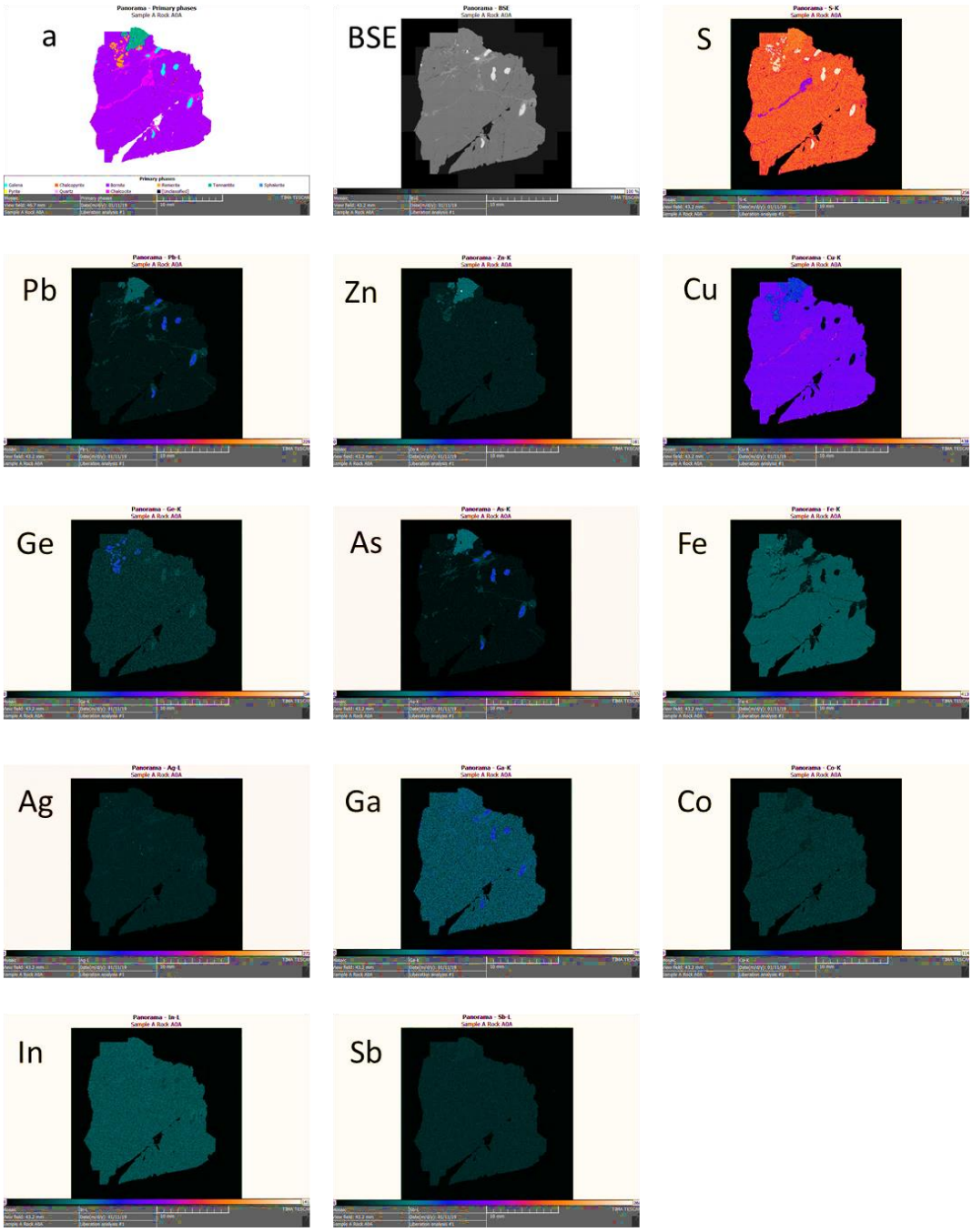

Figure 14: False colour phase map (a), backscatter image, and element maps of S, Pb, Zn, Cu, Ge, As, Fe, Ag, Ga, Co, In and Sb for the entire polished ore block of ore block A from sample 586.

In Figure 15, where the primary phase map shows no renierite, Ge is seen to concentrate within the galena. As and Ga are again found to concentrate within the galena.

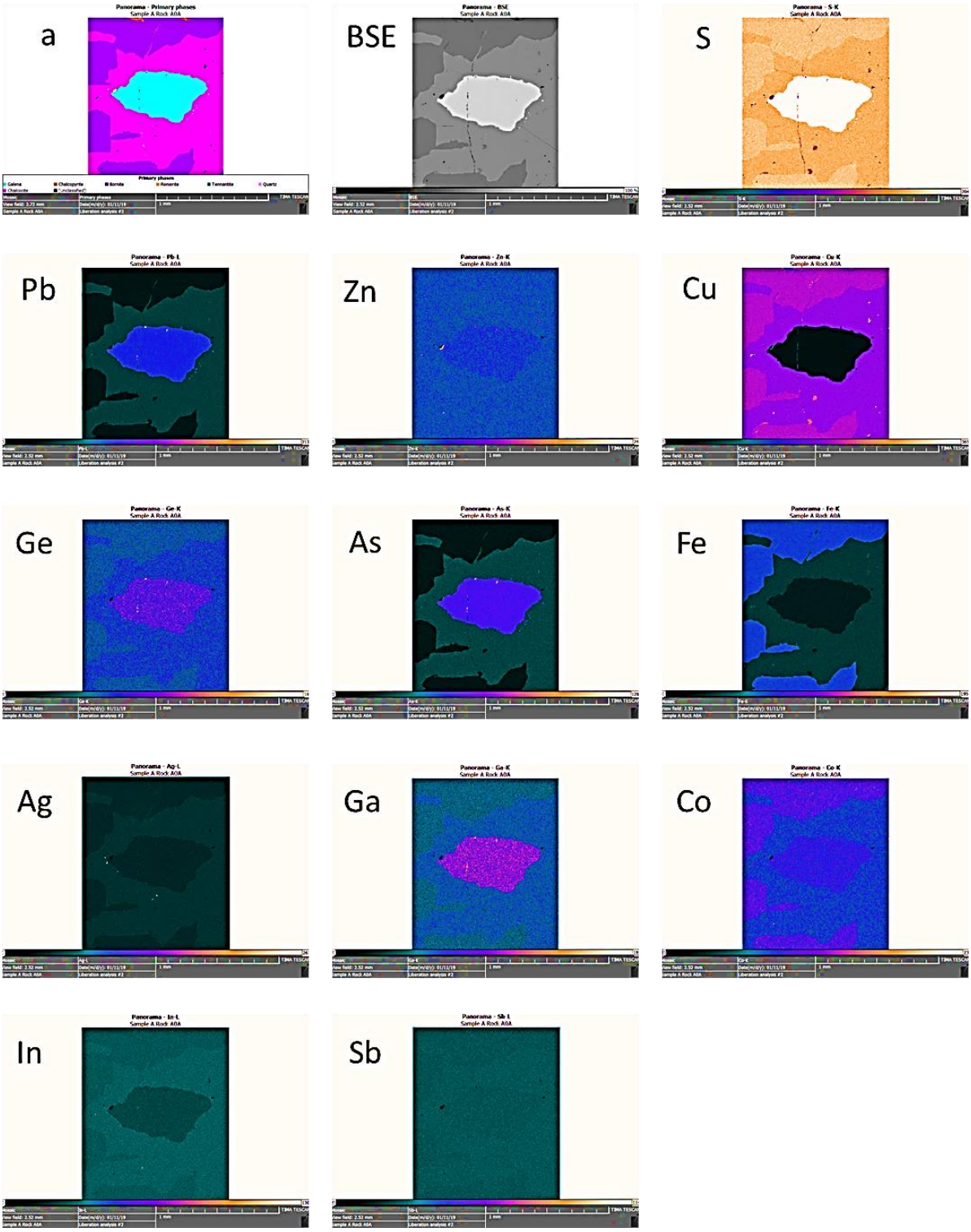

Figure 15: False colour phase map (a), backscatter image, and element maps of S, Pb, Zn, Cu, Ge, As, Fe, Ag, Ga, Co, In and Sb for a section of the polished ore block of ore block A from sample 586.

Figure 3.16 shows similar results to Figure 14, where the Ge concentrates within the renierite. The galena also shows slight concentrations of As and Ga. Zn and Pb can be seen to concentrate within the tennantite.

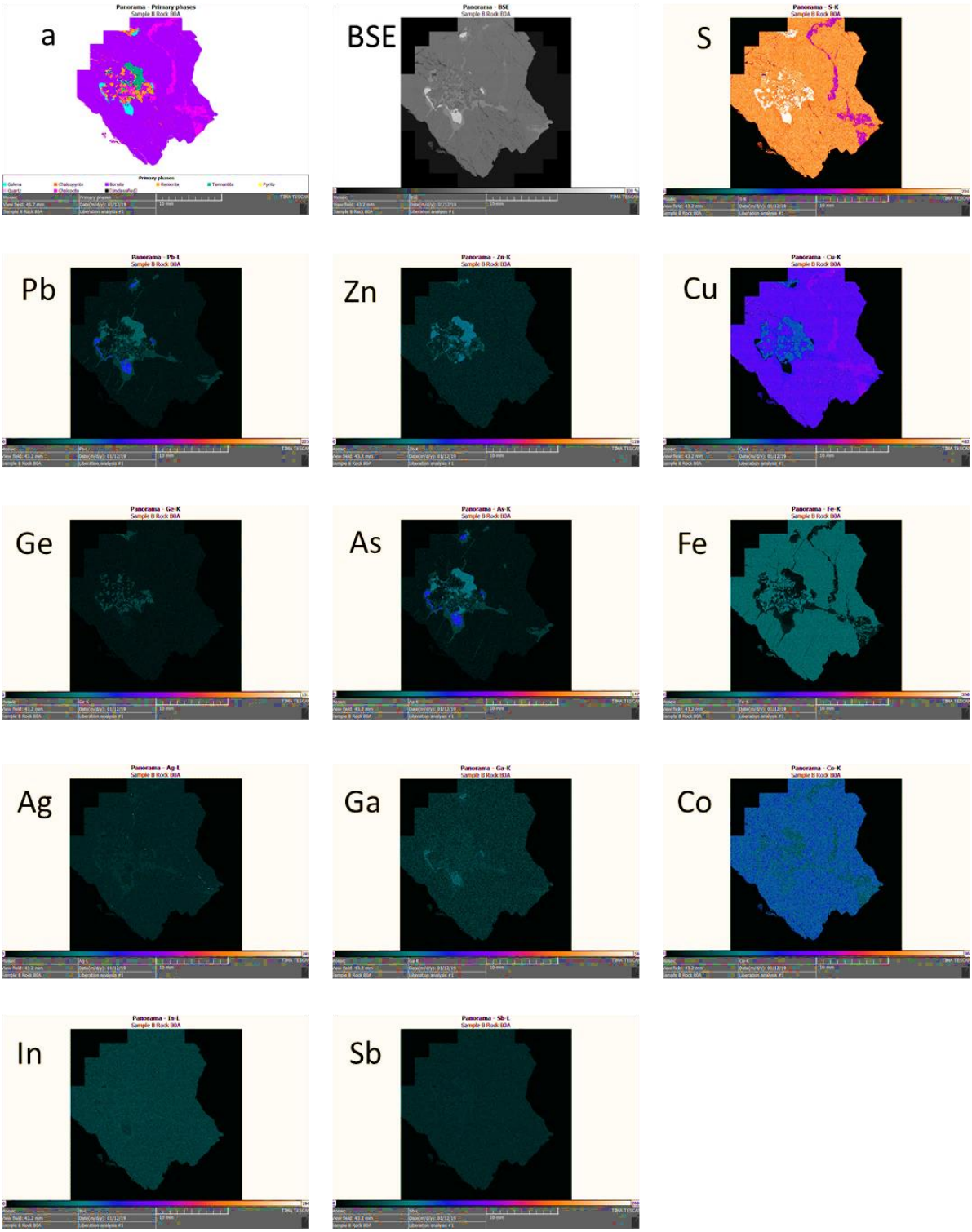

Figure 16: False colour phase map (a), backscatter image, and element maps of S, Pb, Zn, Cu, Ge, As, Fe, Ag, Ga, Co, In and Sb for the entire polished ore block of ore block B from sample 586.

Figure 17 also shows the Ge concentrating into the renierite. A lower concentration of Ge can be seen within the galena. Once again, As and Ga are found to be concentrating into the galena, and Zn and lesser Pb are seen within the tennantite.

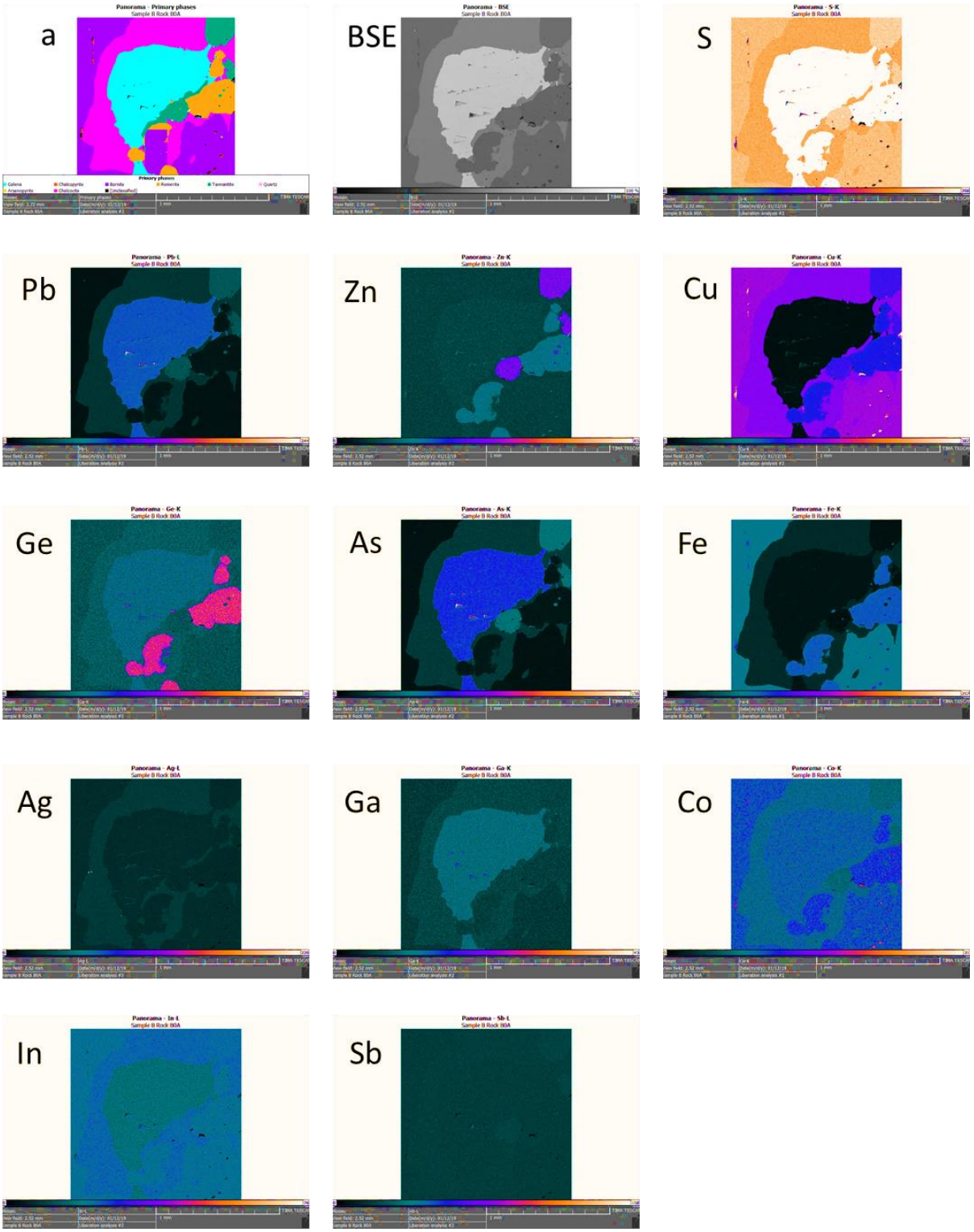

Figure 17: False colour phase map (a), backscatter image, and element maps of S, Pb, Zn, Cu, Ge, As, Fe, Ag, Ga, Co, In and Sb for a section of the polished ore block of ore block B from sample 586.

Sample 12492A

Polished thin section 12492A had two areas chosen for analyses. Figure 18 shows minimal Ge concentrations in the small blebs of galena. The small galena blebs have As and Ga concentrated within them. The chalcopyrite is rich in Co. Quartz and an unknown phase show high concentrations of In.

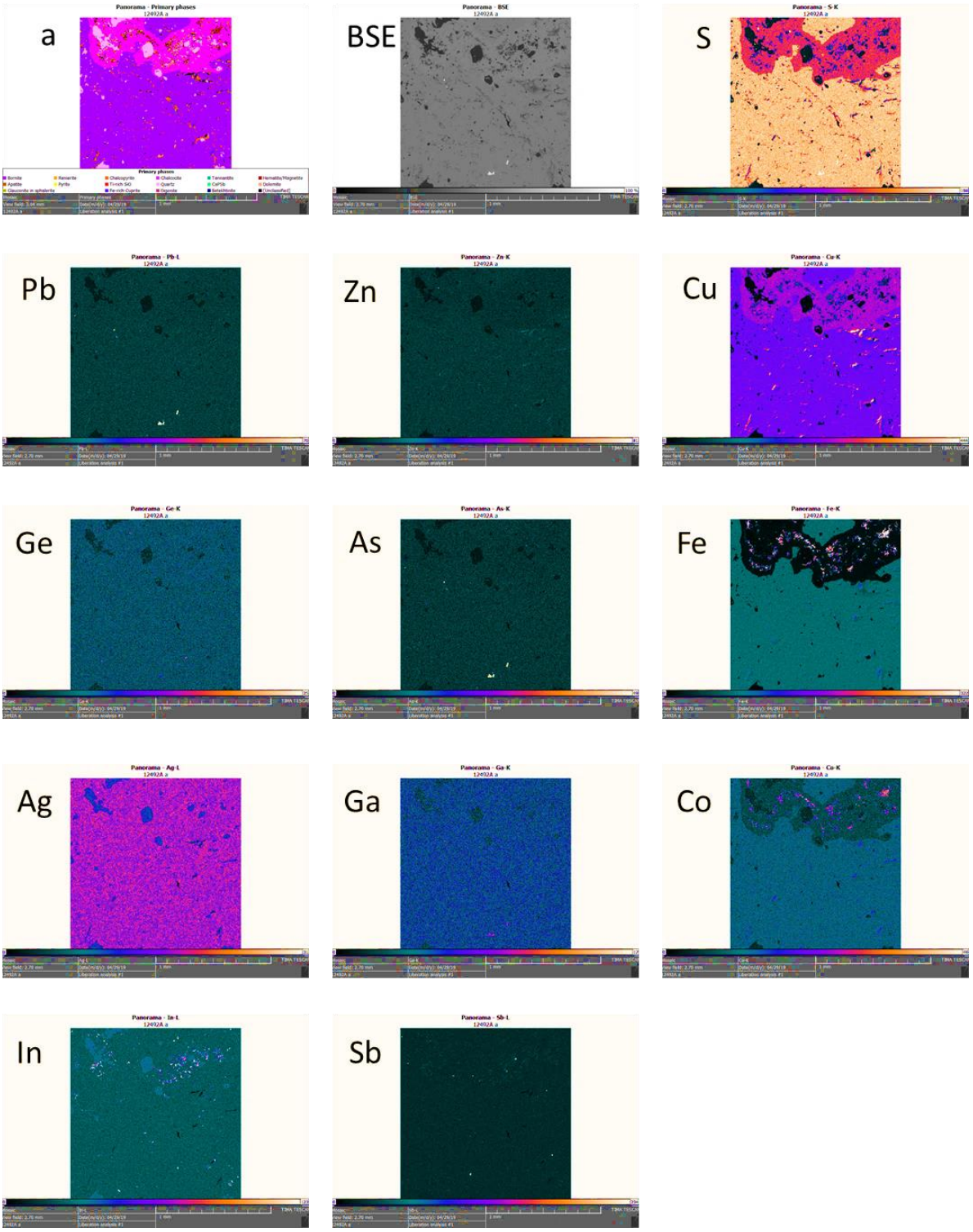

Figure 18: False colour phase map (a), backscatter image, and element maps of S, Pb, Zn, Cu, Ge, As, Fe, Ag, Ga, Co, In and Sb for a section of the polished thin section from thin section a from sample 12492A.

Minimal Ge can be found within the galena, along with As and Ga in Figure 19. An iron oxide mineral phase, possibly hematite or magnetite, with a high concentration of Co can be found in this area.

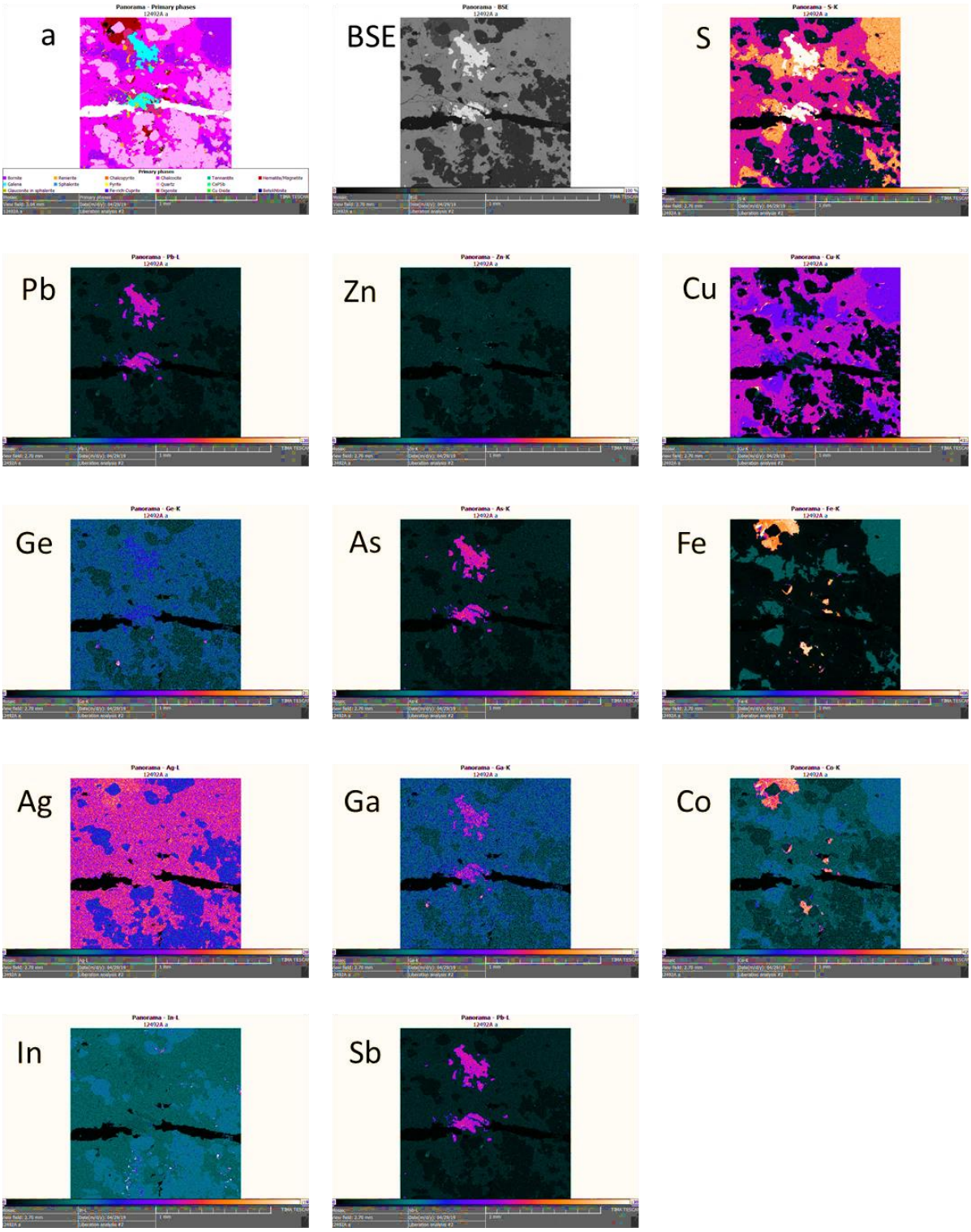

Figure 19: False colour phase map (a), backscatter image, and element maps of S, Pb, Zn, Cu, Ge, As, Fe, Ag, Ga, Co, In and Sb for a section of the polished thin section from thin section a from sample 12492A.

Sample KP 12

Five areas were chosen on the polished thin section to be scanned for this sample. Figure 20 shows a very high concentration of Ge in the renierite. The galena also contains a significant amount of Ge, as well as some As and Ga.

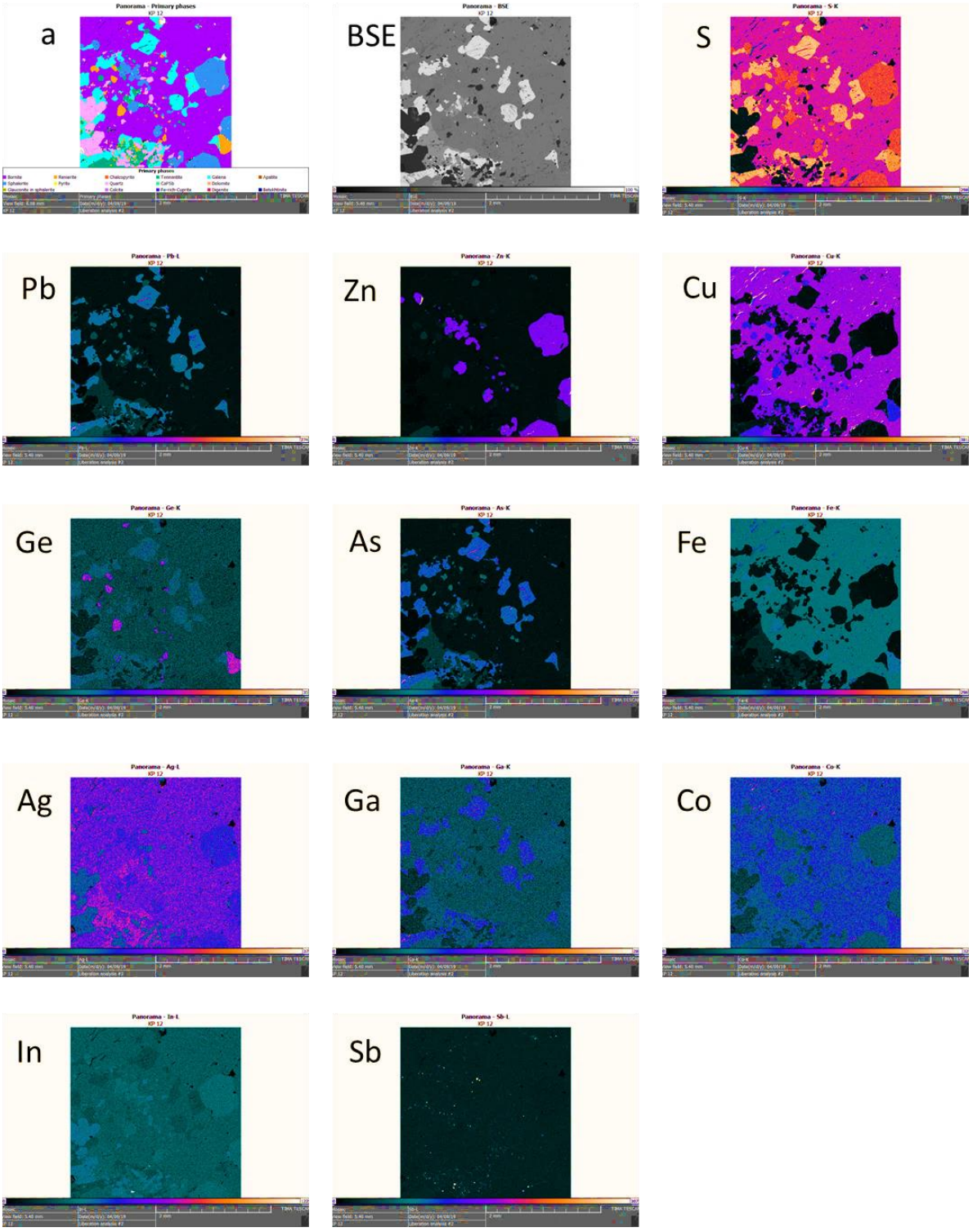

Figure 20: False colour phase map (a), backscatter image, and element maps of S, Pb, Zn, Cu, Ge, As, Fe, Ag, Ga, Co, In and Sb for a section of the polished thin section from sample KP 12.

Figure 21 shows Ge concentrating into the renierite. The chalcopyrite is rich in Co.

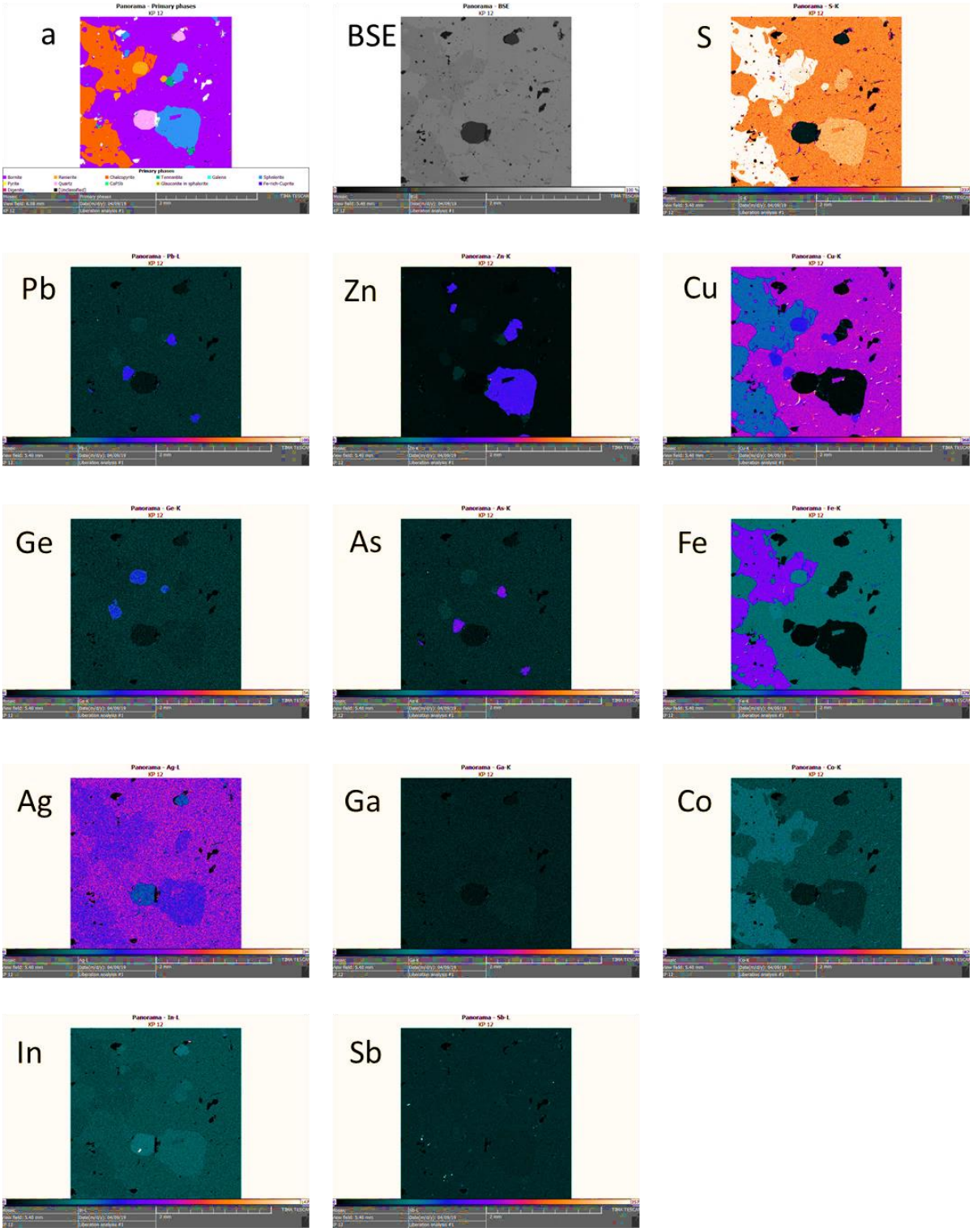

Figure 21: False colour phase map (a), backscatter image, and element maps of S, Pb, Zn, Cu, Ge, As, Fe, Ag, Ga, Co, In and Sb for a section of the polished thin section from sample KP 12.

Figure 22 shows that the Ge, whilst mostly concentrating in renierite, also concentrates into galena and tennantite, respectively. Once again, the galena is As and Ga rich, and the tennantite is Pb rich.

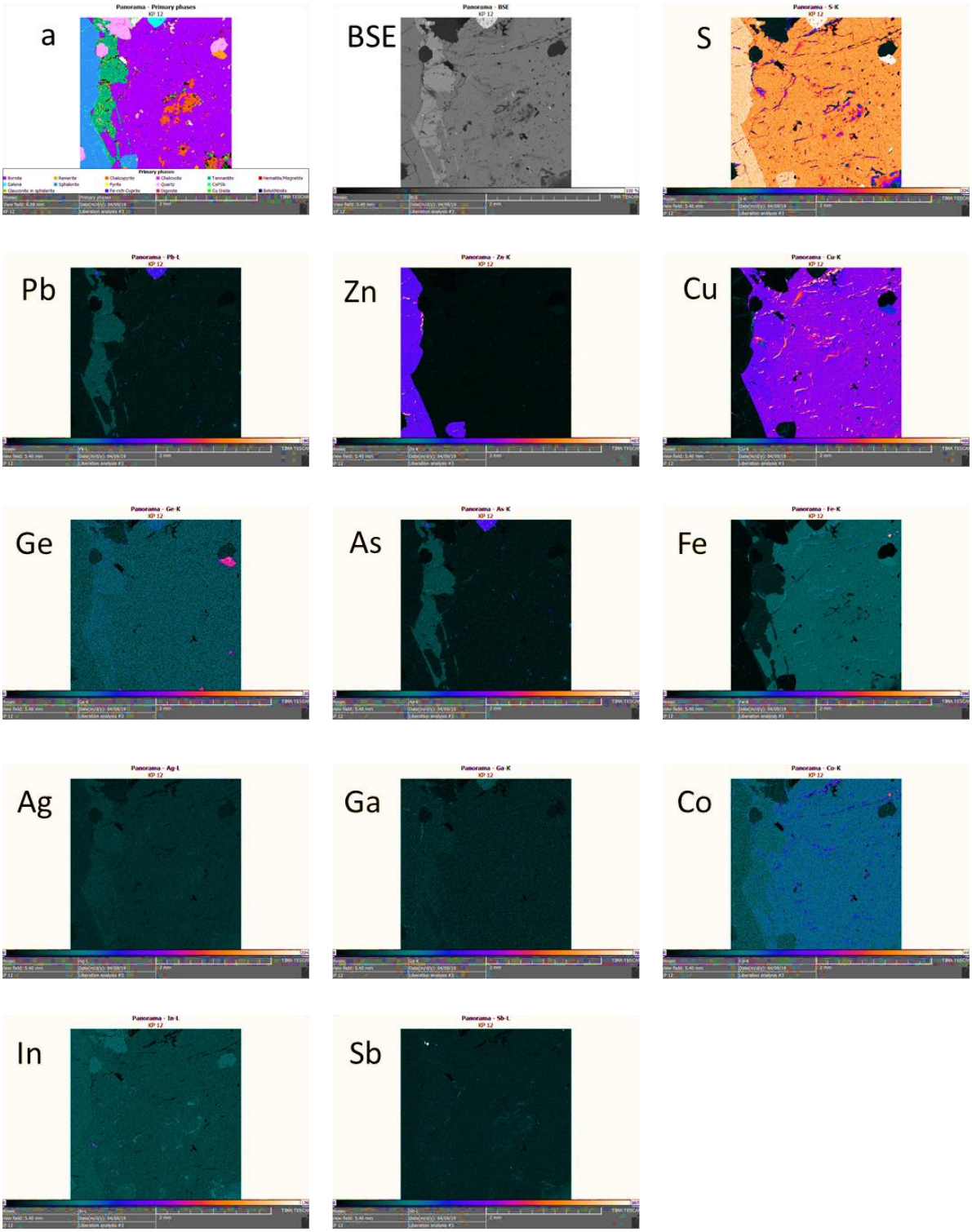

Figure 22: False colour phase map (a), backscatter image, and element maps of S, Pb, Zn, Cu, Ge, As, Fe, Ag, Ga, Co, In and Sb for a section of the polished thin section from sample KP 12.

Figure 23 shows a Ge and Pb rich renierite.

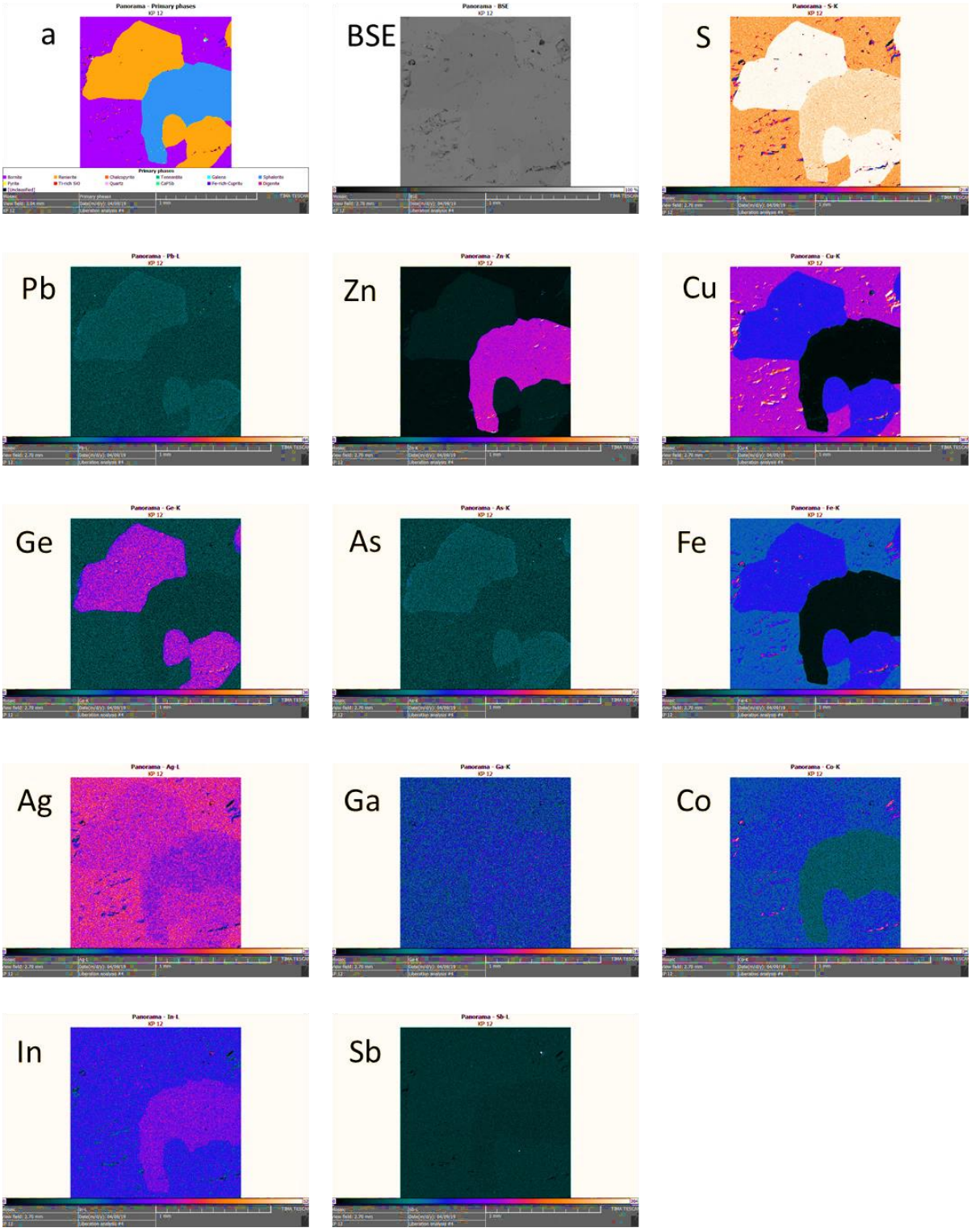

Figure 23: False colour phase map (a), backscatter image, and element maps of S, Pb, Zn, Cu, Ge, As, Fe, Ag, Ga, Co, In and Sb for a section of the polished thin section from sample KP 12.

The last area scanned for this sample is shown in Figure 24. Ge in this area is dominant in the galena. The galena contains some As and Ga. The sphalerite is noted to contain small amounts of In.

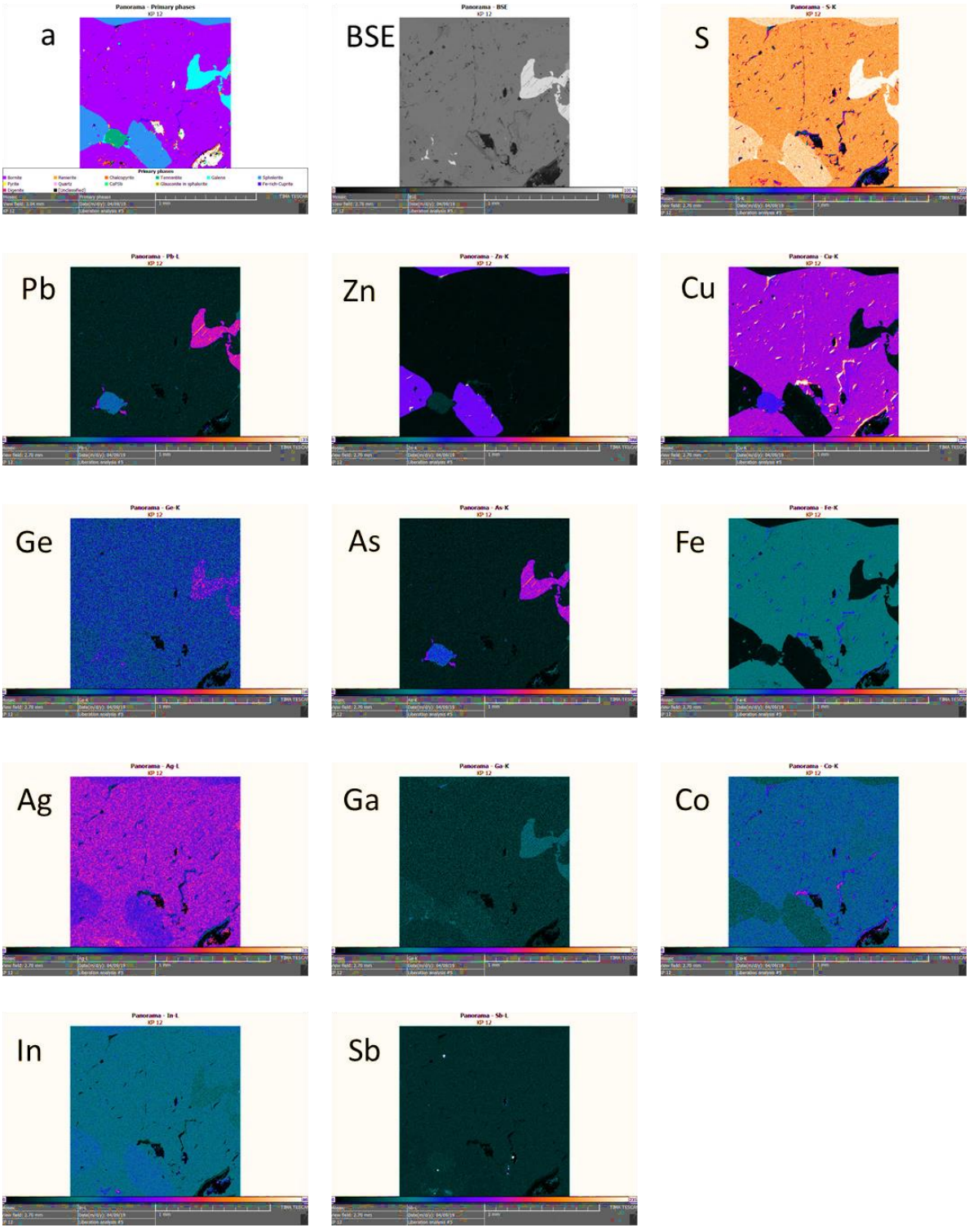

Figure 24: False colour phase map (a), backscatter image, and element maps of S, Pb, Zn, Cu, Ge, As, Fe, Ag, Ga, Co, In and Sb for a section of the polished thin section from sample KP 12.

6547

Three areas were chosen for ore block 6547. The first area, Figure 25, shows the Ge concentrating into the galena, as is minor As and Ga. There is minor Co within the chalcopyrite, In within some of the quartz and significant amounts of Sb within some calcite.

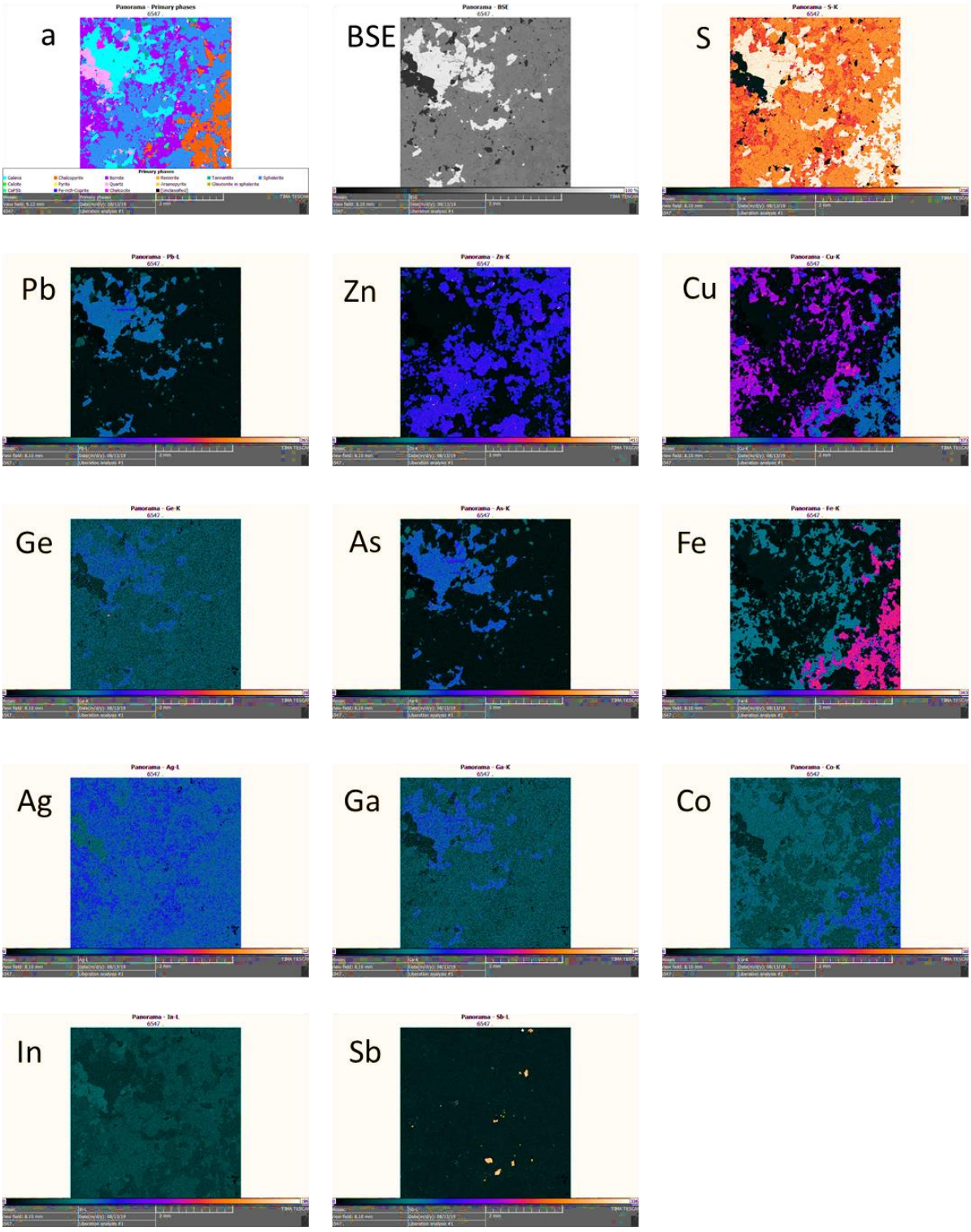

Figure 25: False colour phase map (a), backscatter image, and element maps of S, Pb, Zn, Cu, Ge, As, Fe, Ag, Ga, Co, In and Sb for one area of the ore block from sample 6547.

Figure 26, area two, shows the Ge concentrating into the galena, along with some As and Ga. There is a minor amount of Co within the chalcopyrite. There is also a Sb rich calcite phase.

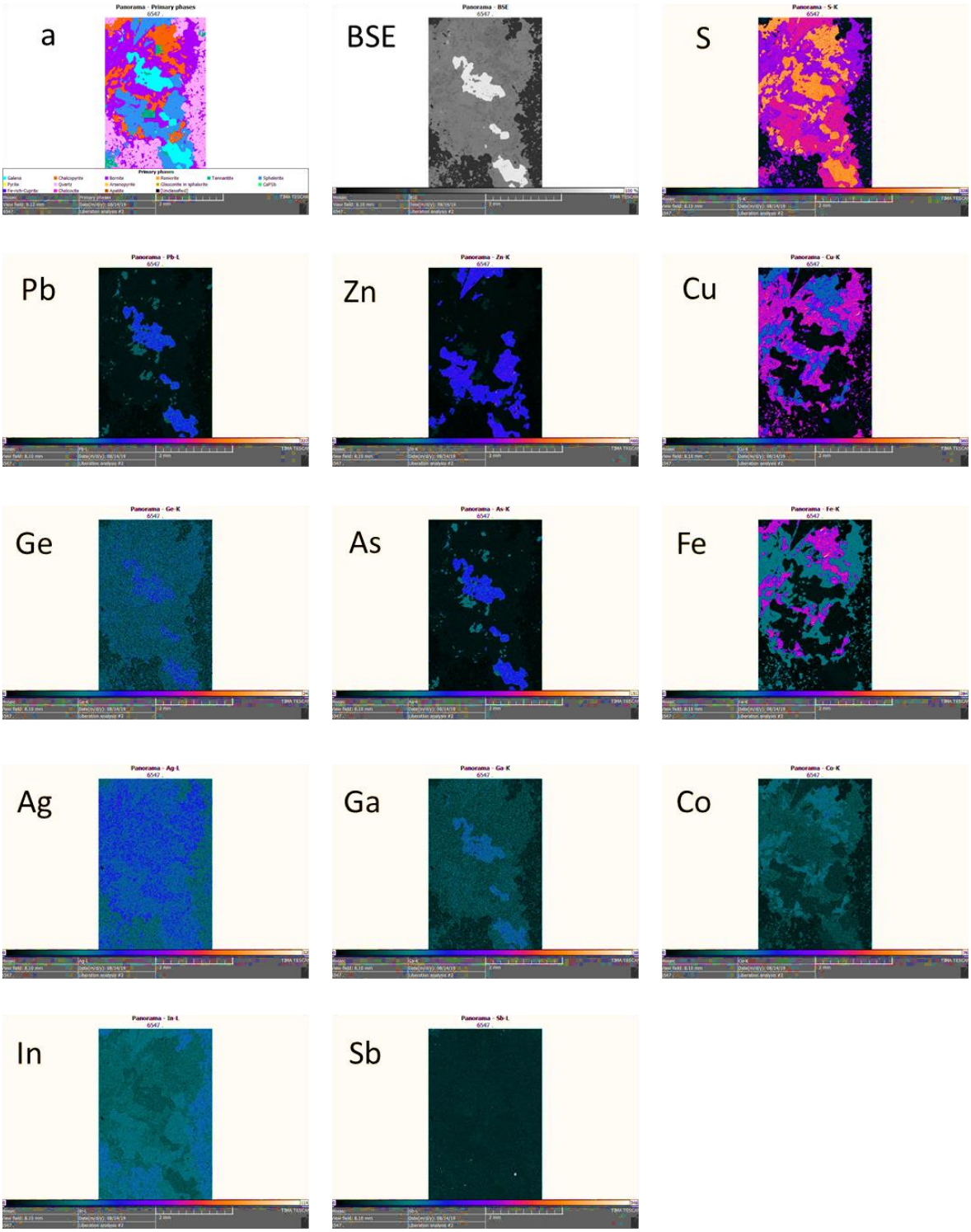

Figure 26: False colour phase map (a), backscatter image, and element maps of S, Pb, Zn, Cu, Ge, As, Fe, Ag, Ga, Co, In and Sb for one area of the ore block from sample 6547.

The last area for this sample, shown in Figure 27, shows concentrations of Ge within the galena, as well as some As and Ga. Chalcopyrite contains notable amounts of Co. Once again there is Sb rich calcite.

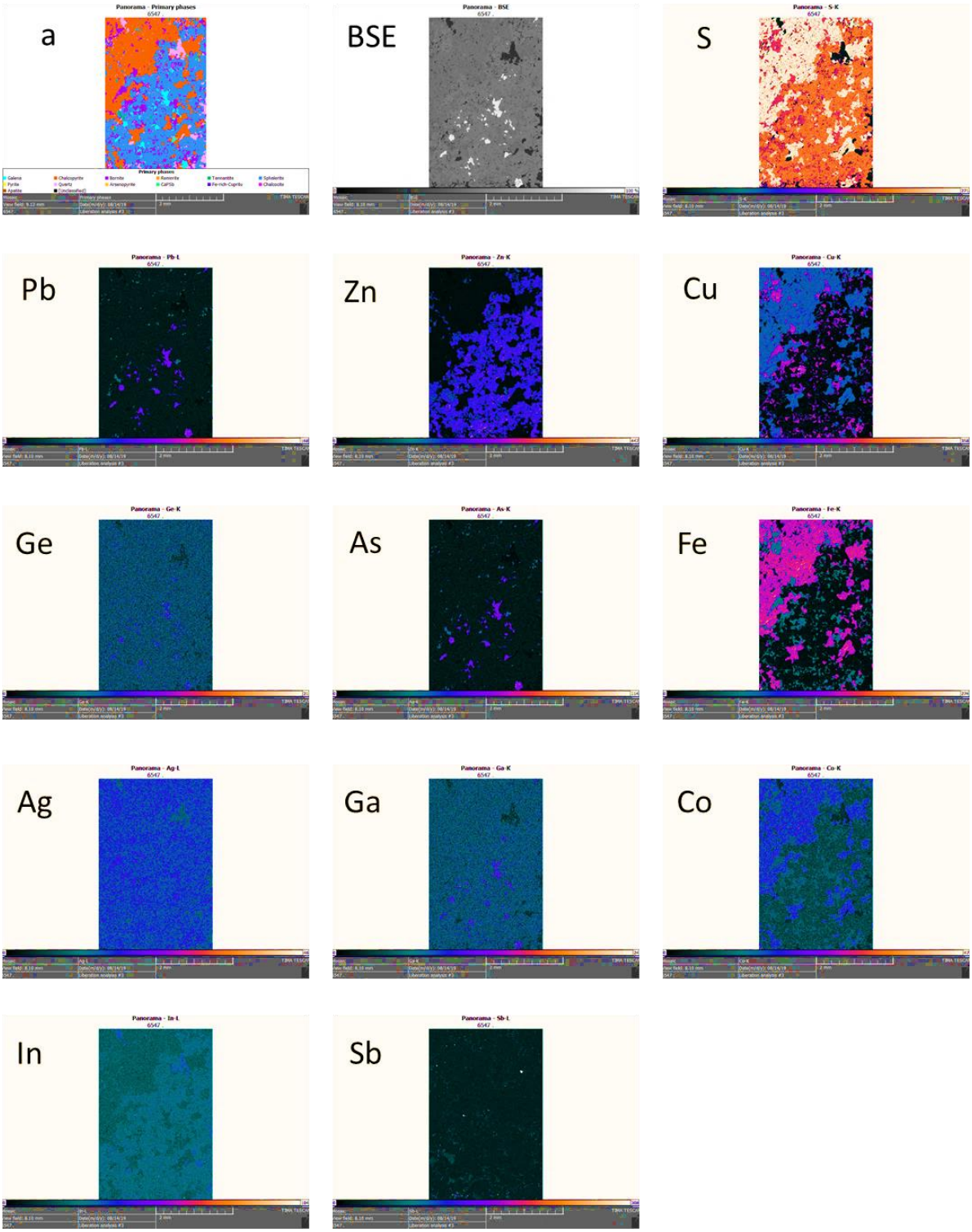

Figure 27: False colour phase map (a), backscatter image, and element maps of S, Pb, Zn, Cu, Ge, As, Fe, Ag, Ga, Co, In and Sb for one area of the ore block from sample 6547.

KP 3

Three areas were selected for scanning from the ore block from sample KP 3. In the first area, Figure 28, Ge is found to concentrate into renierite, as well as galena. As and, Ga and In can also be found concentrating within the galena. There is also an unidentified CaPSb rich phase in this area.

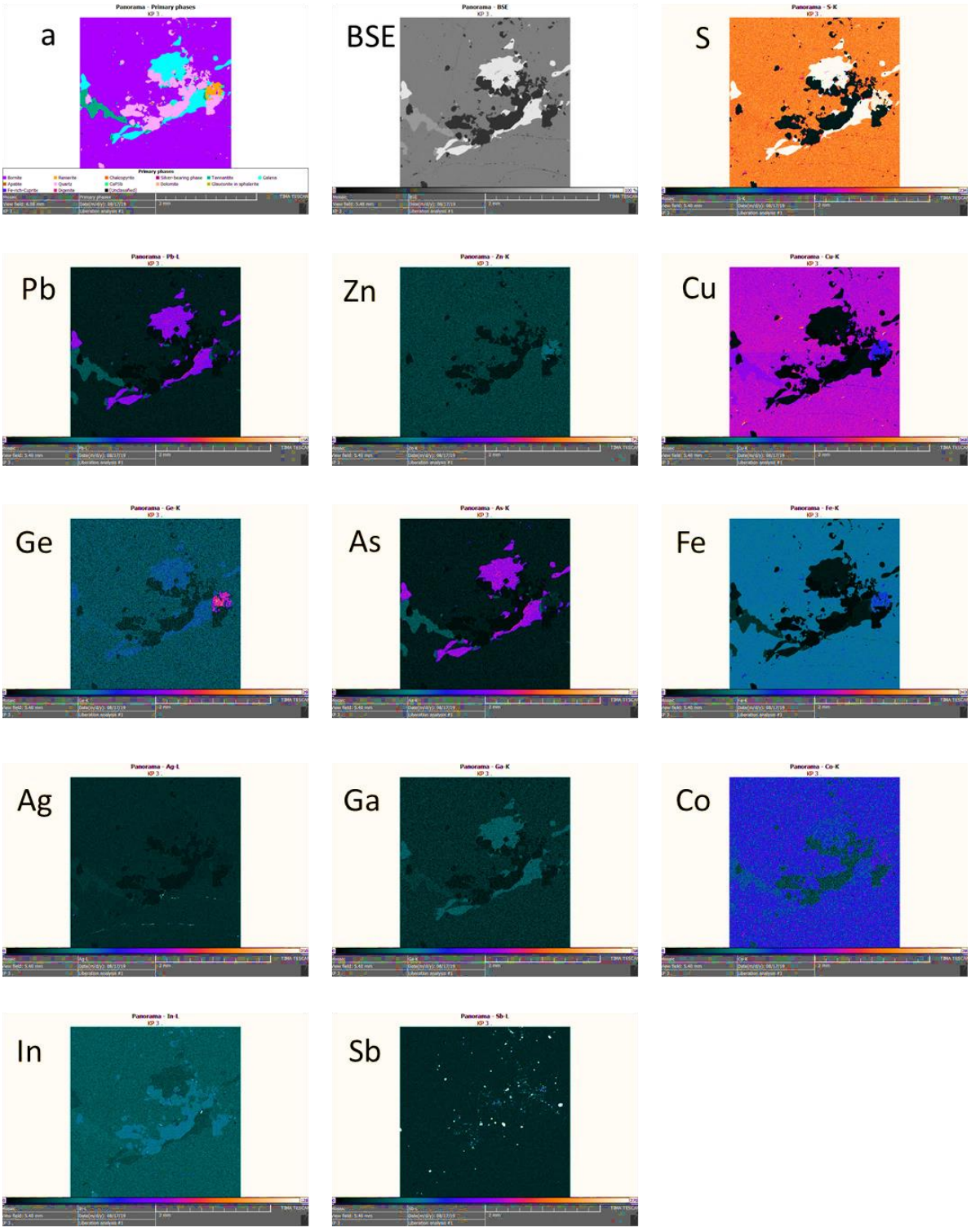

Figure 28: False colour phase map (a), backscatter image, and element maps of S, Pb, Zn, Cu, Ge, As, Fe, Ag, Ga, Co, In and Sb for one area of the ore block from sample KP 3.

In Figure 29, in the second area, finds the Ge concentrates into the renierite. There is some In present within the quartz. The same CaPSb rich phase is present.

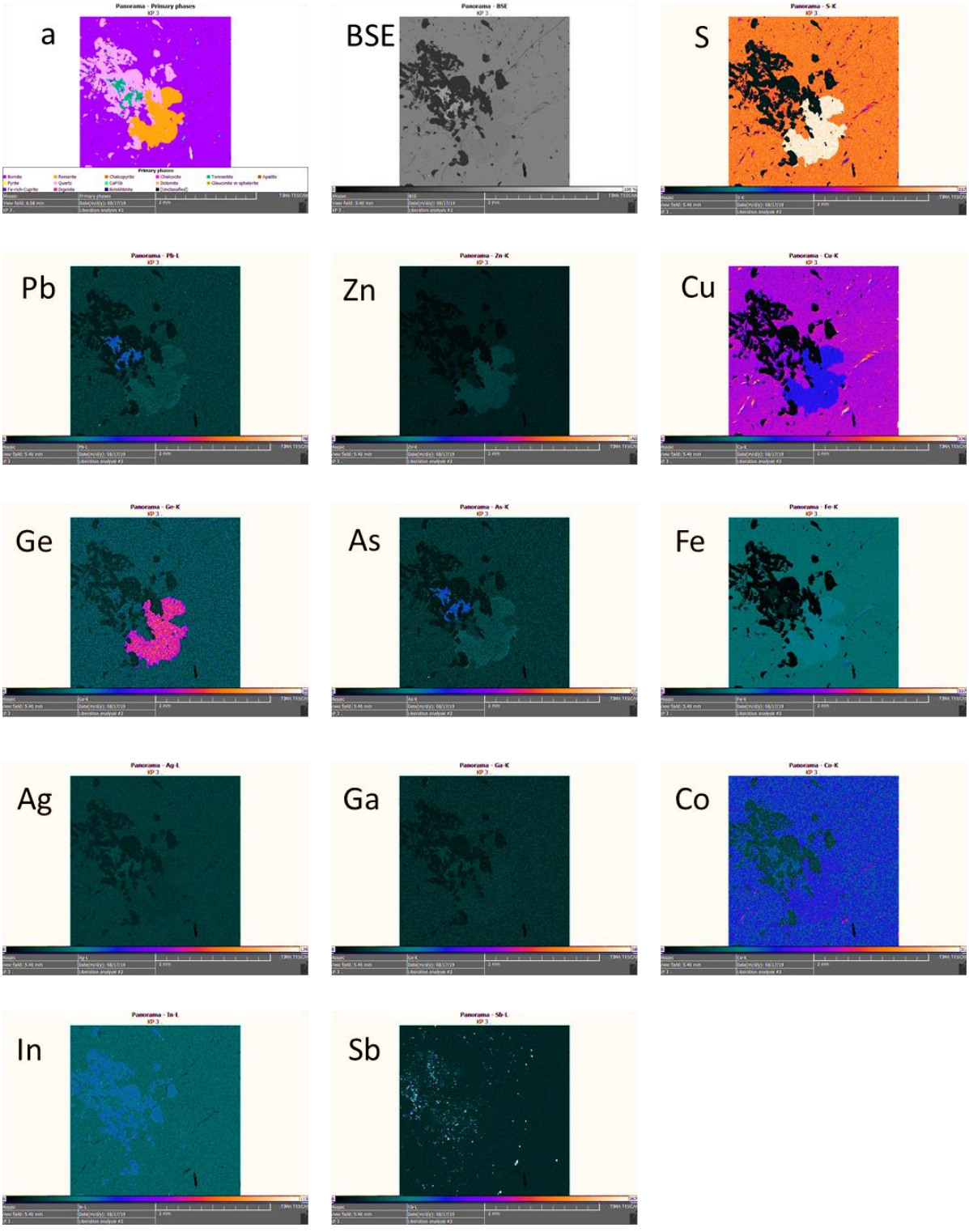

Figure 29: False colour phase map (a), backscatter image, and element maps of S, Pb, Zn, Cu, Ge, As, Fe, Ag, Ga, Co, In and Sb for one area of the ore block from sample KP 3.

The third area for this ore block, seen in Figure 30, contains negligible amounts of Ge, however, it can be noted that the Ge prefers the Cu rich bornite as opposed to the sphalerite. The sphalerite contains minor amounts of Ga and In. The bornite contains some Co.

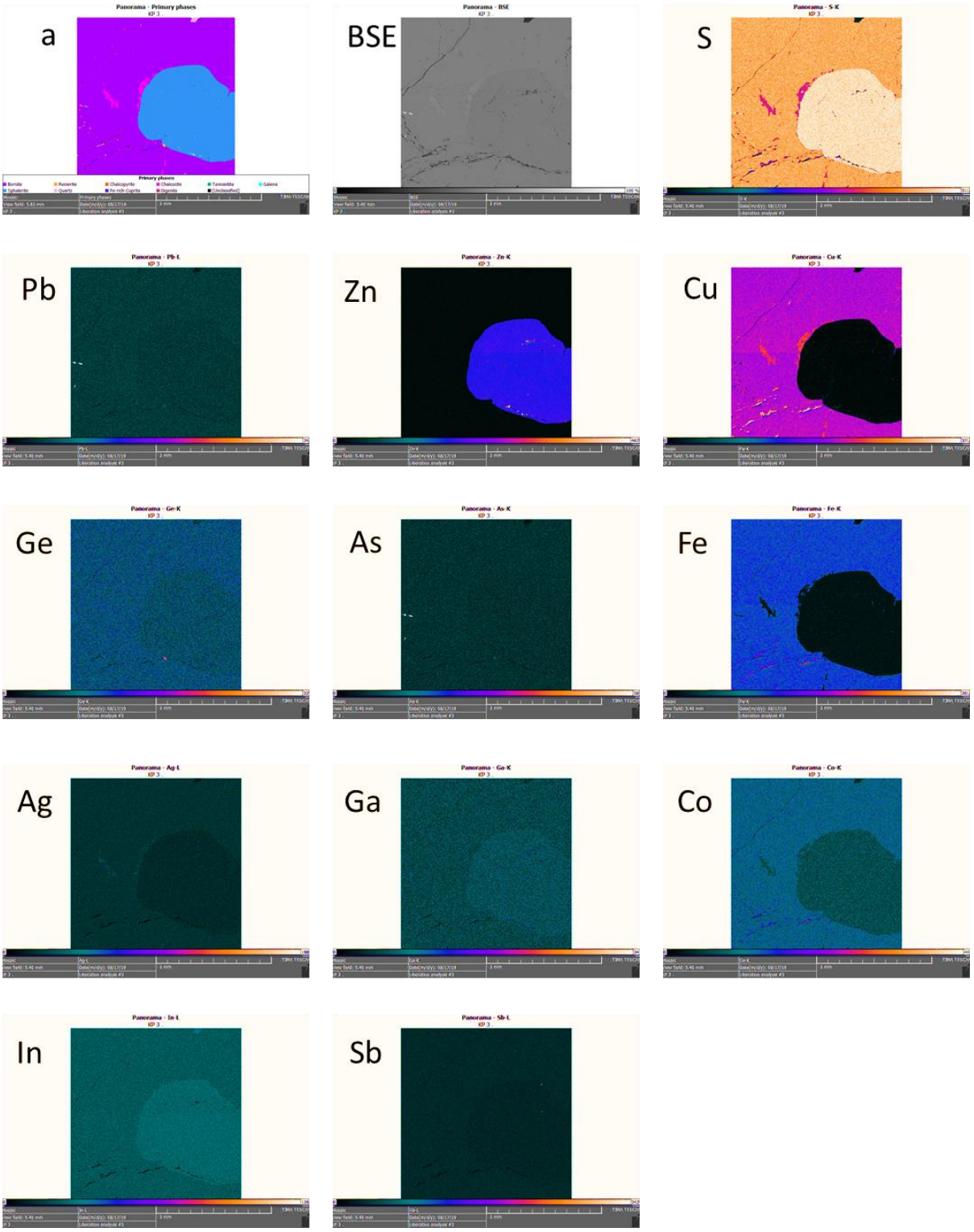

Figure 30: False colour phase map (a), backscatter image, and element maps of S, Pb, Zn, Cu, Ge, As, Fe, Ag, Ga, Co, In and Sb for one area of the ore block from sample KP 3.

KP 7

One area was chosen for this ore block. It is shown in Figure 31. This sample is a country rock with bornite veining. The element maps show that the Sb rich dolomite phase makes up the country rock. The Ge partitions into the renierite, and to a much lesser extent, the bornite, chalcocite and tennantite. The bornite contains some Co, while the CaPSb rich phase contains some In.

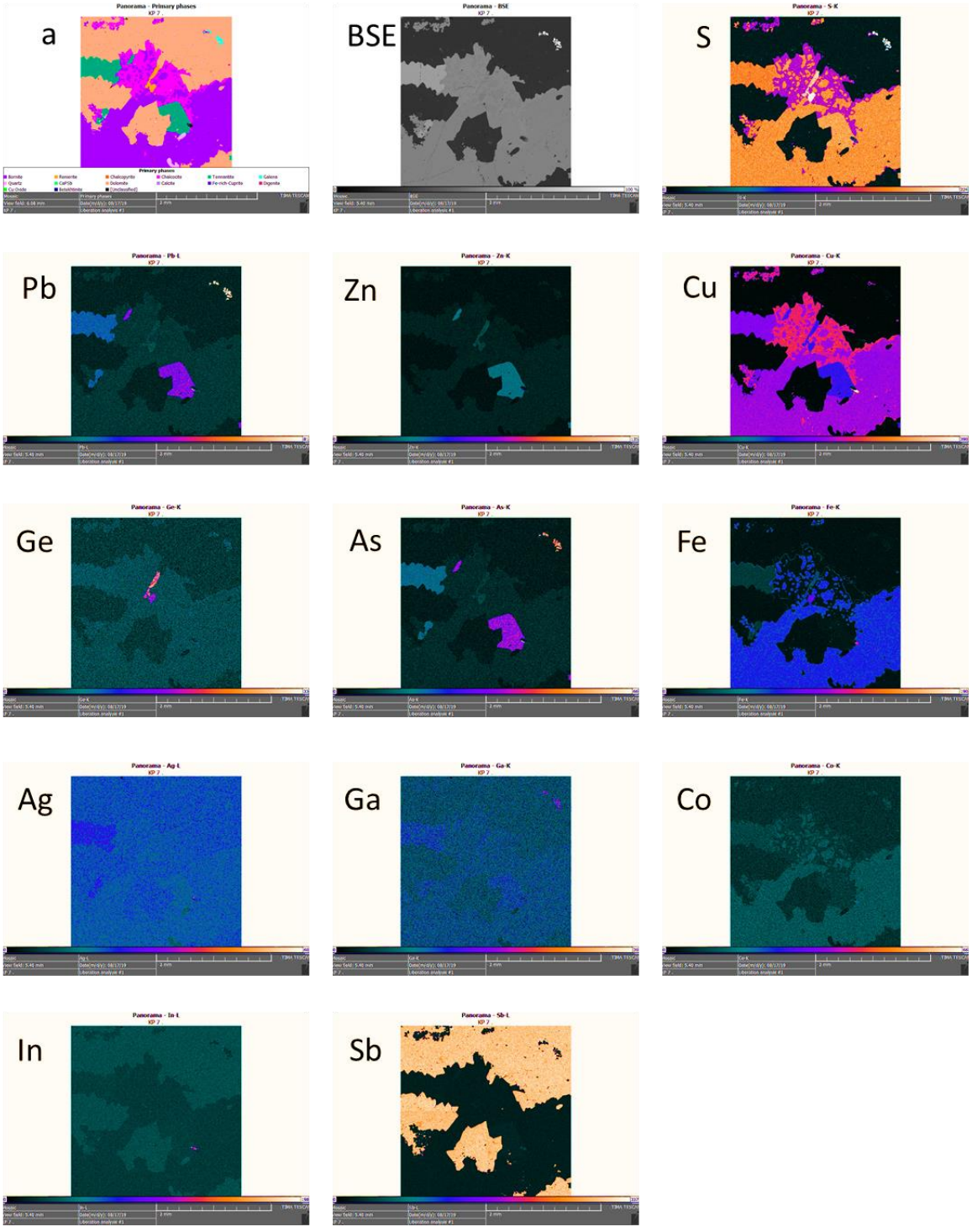

Figure 31: False colour phase map (a), backscatter image, and element maps of S, Pb, Zn, Cu, Ge, As, Fe, Ag, Ga, Co, In and Sb for the area selected for the ore block from sample KP 7.

C.2.2. Bornite-chalcopyrite-dominant assemblage

587

Ore block 587 had two areas selected for scanning by the TIMA. Area one, Figure 32, showed little Ge, however, there is slightly more in the carrollite than in the rest of the sample. The Ag shows the opposite, more in the bornite than in the carrollite. Interestingly, there is some Zn in the bornite, as well as some In. In also appears in the quartz phase.

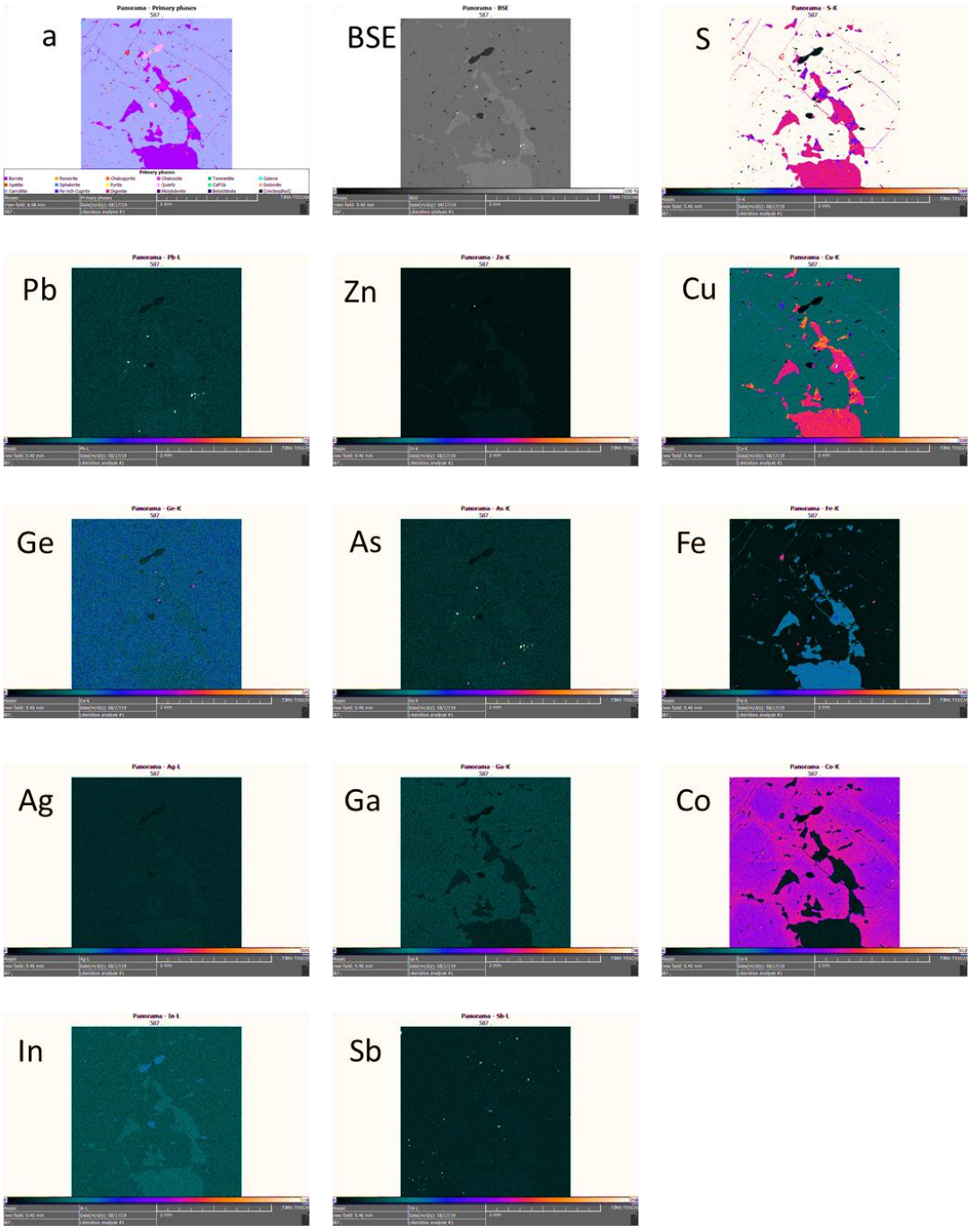

Figure 32: False colour phase map (a), backscatter image, and element maps of S, Pb, Zn, Cu, Ge, As, Fe, Ag, Ga, Co, In and Sb for one area of the ore block from sample 587.

Figure 33, the second area for this sample, shows Ge concentrating into the renierite. Less Ge is found in bornite, sphalerite, and quartz, respectively. There is some In in the quartz and less in the sphalerite. It is also interesting to note that there is an Ag rich phase in this area. This mineral has been identified as stromeyerite. There is also minor Co within the sphalerite.

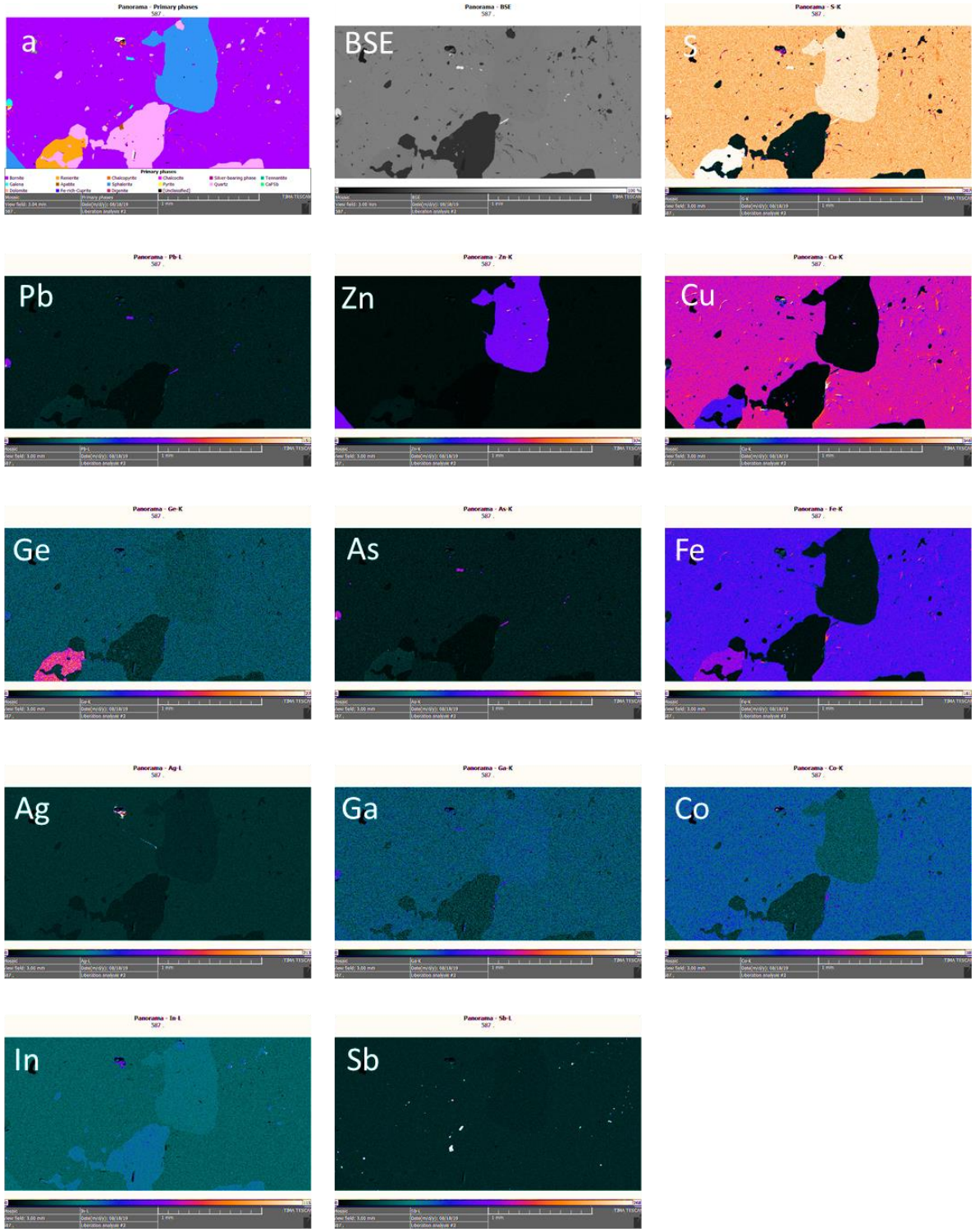

Figure 33: False colour phase map (a), backscatter image, and element maps of S, Pb, Zn, Cu, Ge, As, Fe, Ag, Ga, Co, In and Sb for one area of the ore block from sample 587.

1216

Sample 1216 had one ore block made. Two areas were selected on this ore block for TIMA analysis. Area one, shown in Figure 34, contains negligible Ge. This is unsurprising as this area contains bornite, sphalerite, and quartz. The sphalerite contains minor Ga and In. The bornite has Co concentrating into it.

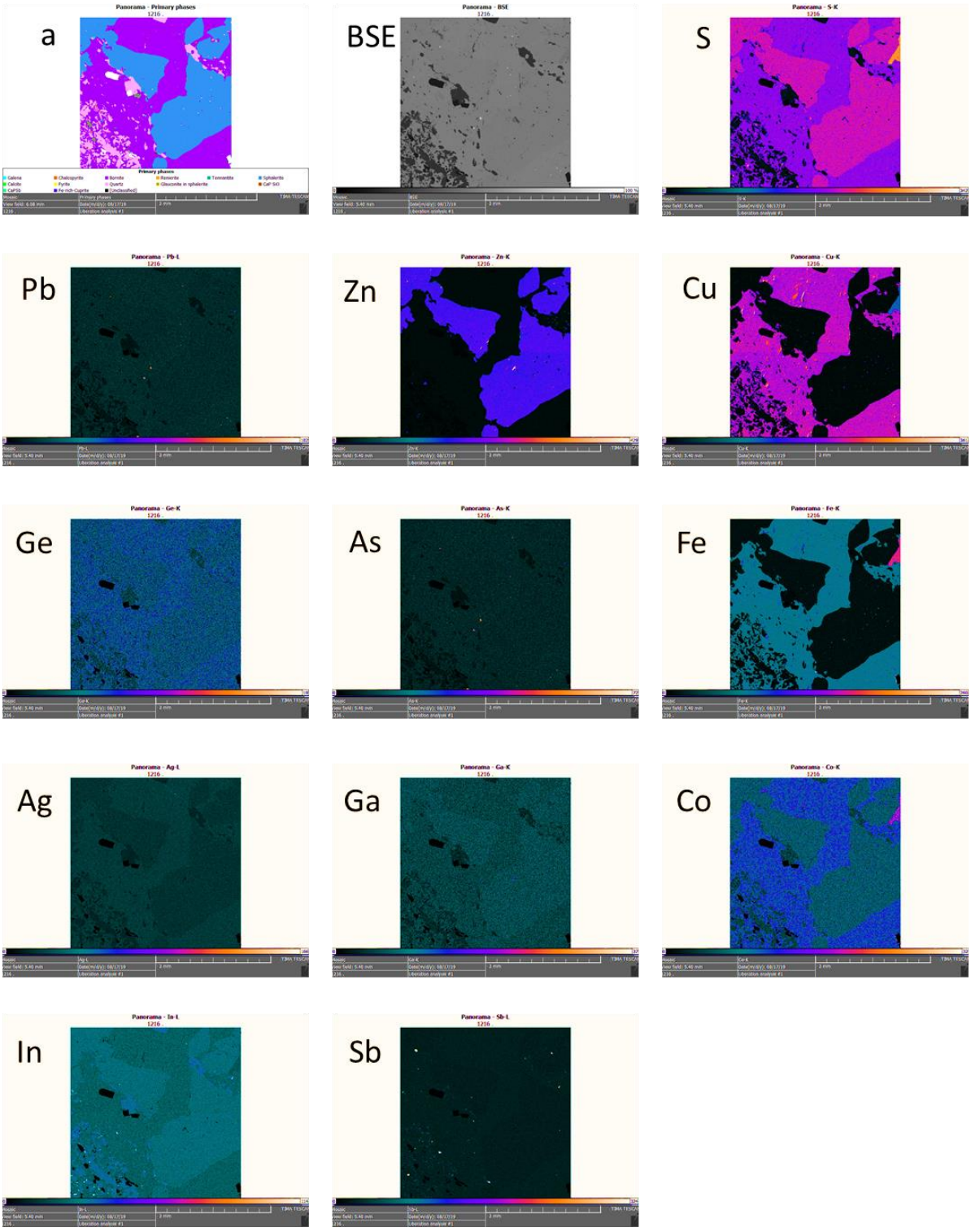

Figure 34: False colour phase map (a), backscatter image, and element maps of S, Pb, Zn, Cu, Ge, As, Fe, Ag, Ga, Co, In and Sb for one area of the ore block from sample 1216.

The second area selected, Figure 35, contains little Ge, with the most being concentrated into the carrollite. The carrollite also contains minor Ga. The sphalerite and quartz contain minor In.

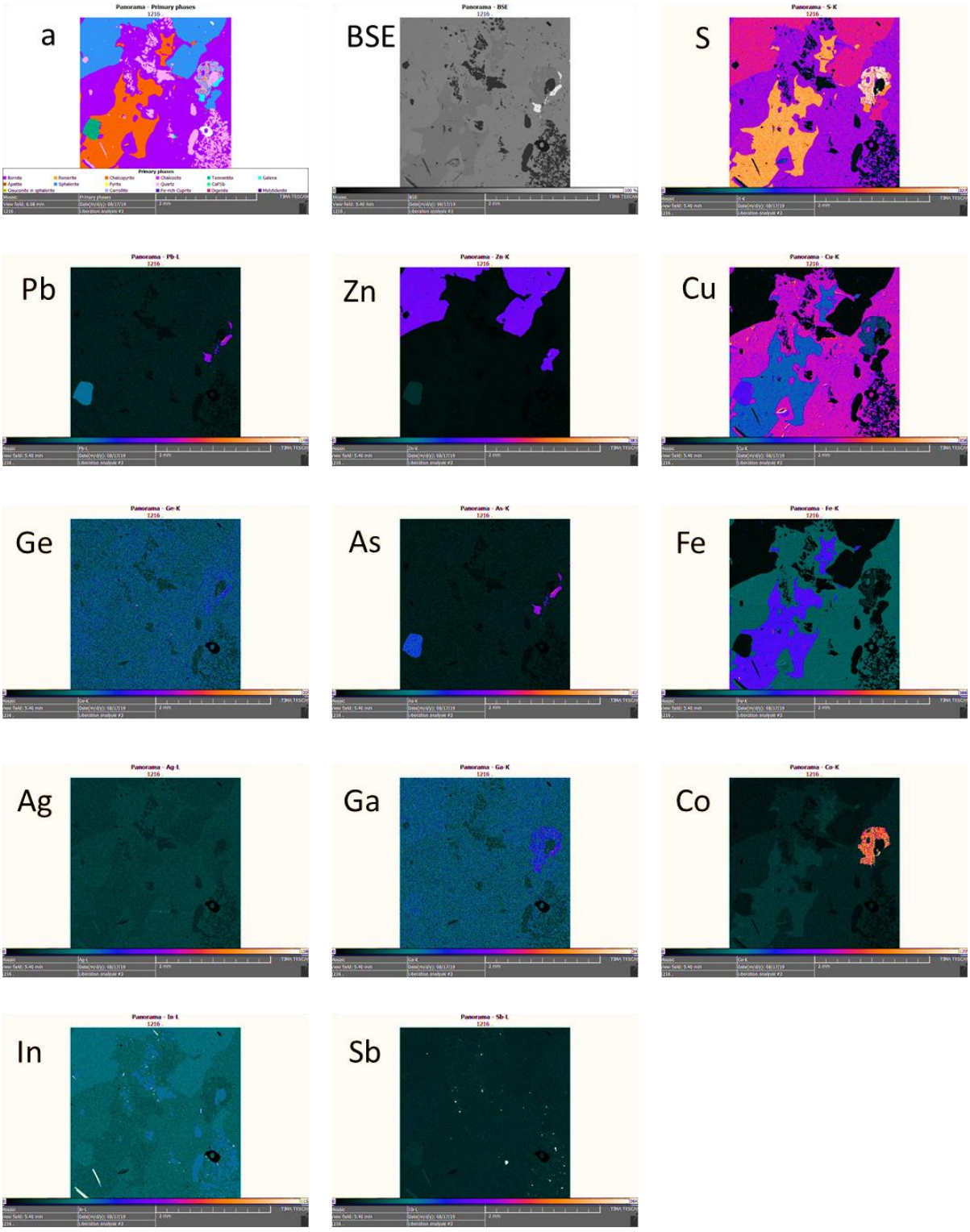

Figure 35: False colour phase map (a), backscatter image, and element maps of S, Pb, Zn, Cu, Ge, As, Fe, Ag, Ga, Co, In and Sb for one area of the ore block from sample 1216.

KP 13

Three areas were selected for the ore block from this sample. Figure 36 shows the maps from the first area. The Ge here is negligible. This sample contains an iron oxide, as well as a second Ag-bearing mineral, allargentum. This Ag-bearing mineral has significant amounts of In. The iron oxide has significant amounts of Co.

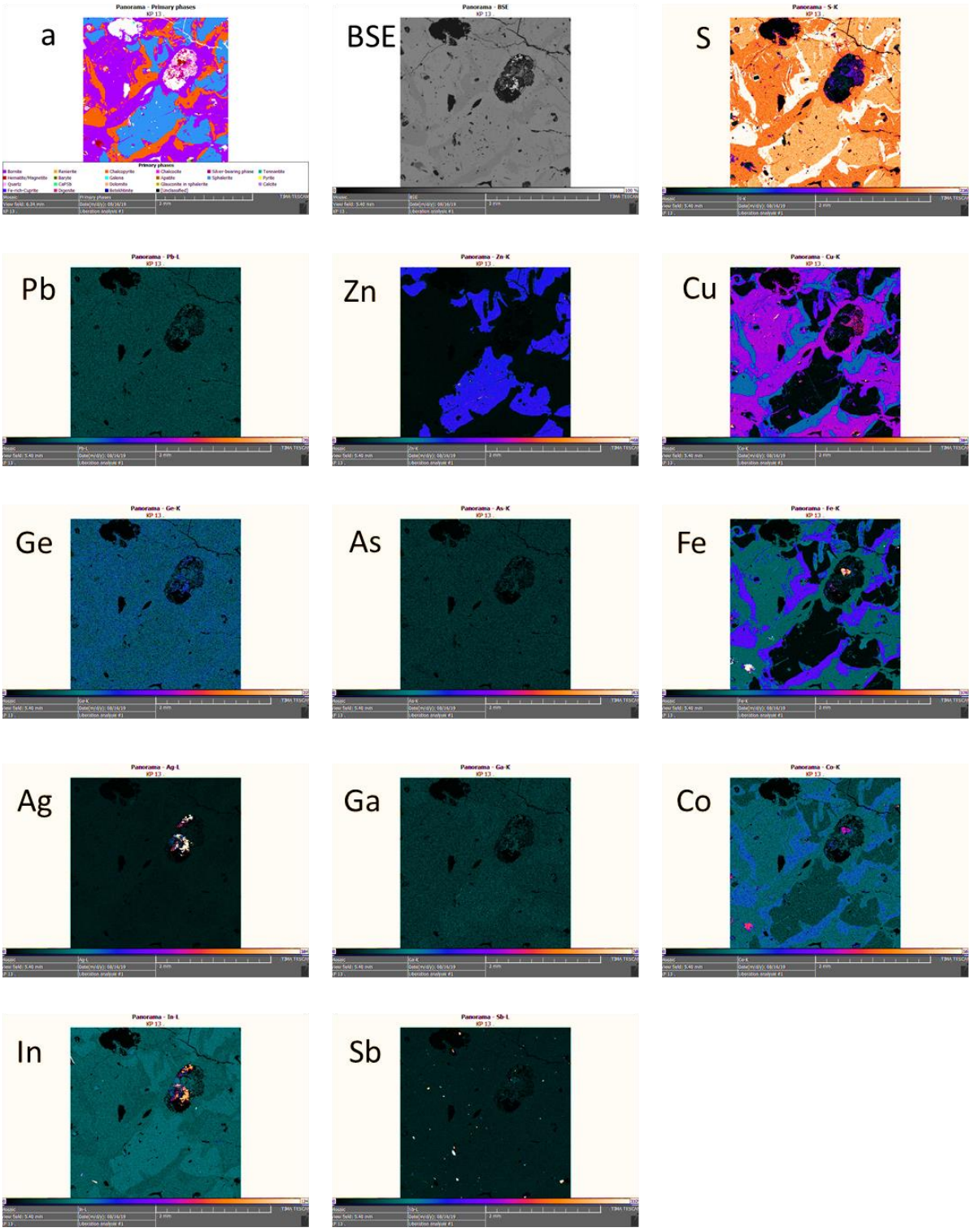

Figure 36: False colour phase map (a), backscatter image, and element maps of S, Pb, Zn, Cu, Ge, As, Fe, Ag, Ga, Co, In and Sb for one area of the ore block from sample KP 13.

Area two is shown in Figure 37. Here the Ge concentrates into the bornite and tennantite. This sample contains an iron oxide. Ag also concentrates into the bornite and tennantite. The sphalerite contains minor Co.

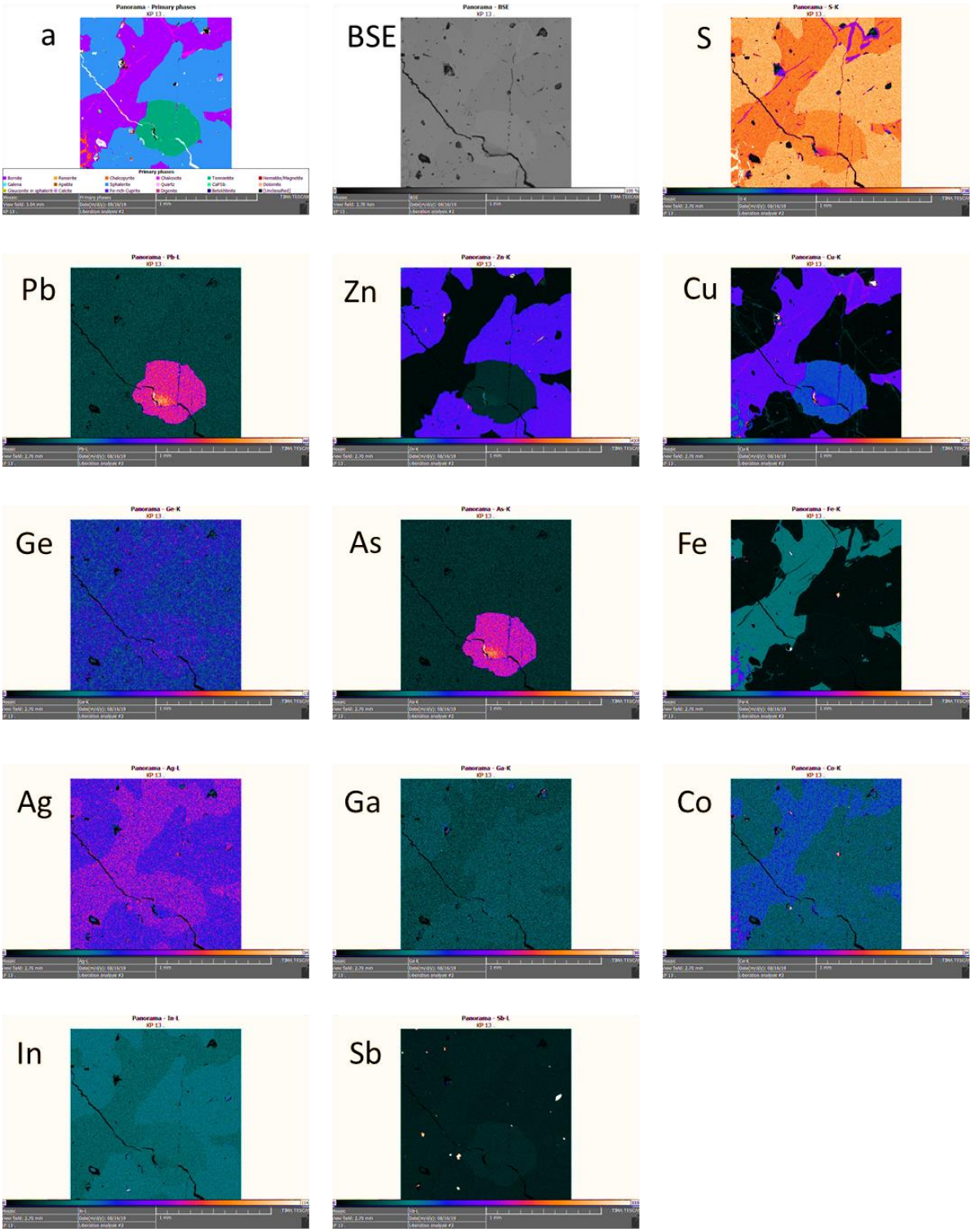

Figure 37: False colour phase map (a), backscatter image, and element maps of S, Pb, Zn, Cu, Ge, As, Fe, Ag, Ga, Co, In and Sb for one area of the ore block from sample KP 13.

Area three, Figure 38, shows the renierite is the only phase the Ge has concentrated into in this area. An iron oxide phase is found throughout this sample. There is an unidentified In rich mineral phase in this area.

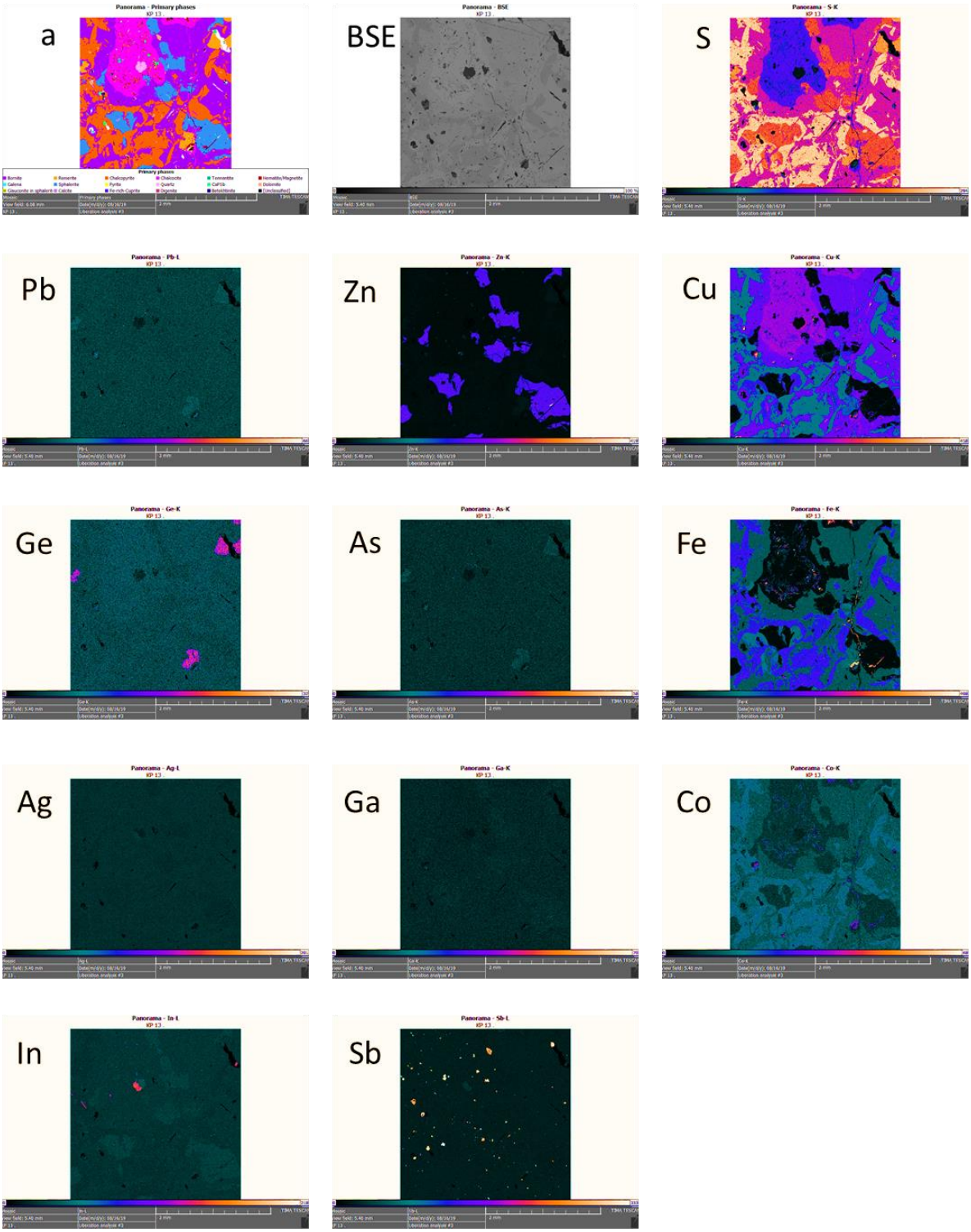

Figure 38: False colour phase map (a), backscatter image, and element maps of S, Pb, Zn, Cu, Ge, As, Fe, Ag, Ga, Co, In and Sb for one area of the ore block from sample KP 13.

C.2.3. Chalcopyrite-pyrite-dominant assemblage

Sample S2801

Polished thin section S2801 c was chosen for analyses. Three key areas were identified for this polished thin section. Figure 39 shows the first area analysed by the TIMA. This area shows chalcopyrite, pyrite, dolomite, sphalerite, quartz and some arsenopyrite, as seen in the false colour primary phase map. The Ge concentration is negligible within this sample area. Some Pb seems to concentrate in the arsenopyrite. In is concentrated within the quartz.

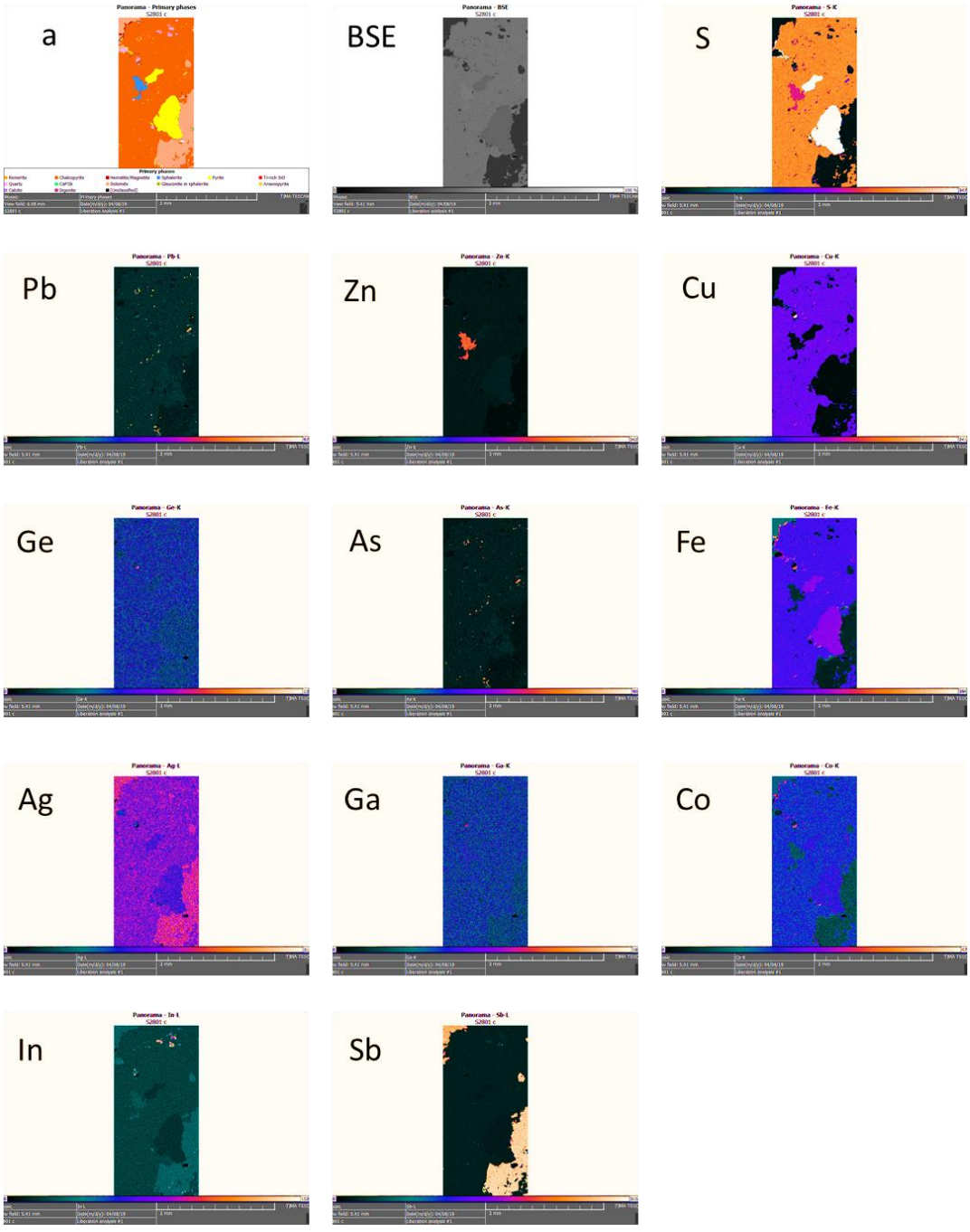

Figure 39: False colour phase map (a), backscatter image, and element maps of S, Pb, Zn, Cu, Ge, As, Fe, Ag, Ga, Co, In and Sb for a section of the polished thin section from thin section c from sample S2801.

Many of the same phases can be seen in Figure 40. The Ge concentration is also negligible within this sample area. The arsenopyrite has Pb concentrated within it. The Co concentrates into an unknown iron rich mineral. In can again be seen to concentrate within the quartz-rich areas.

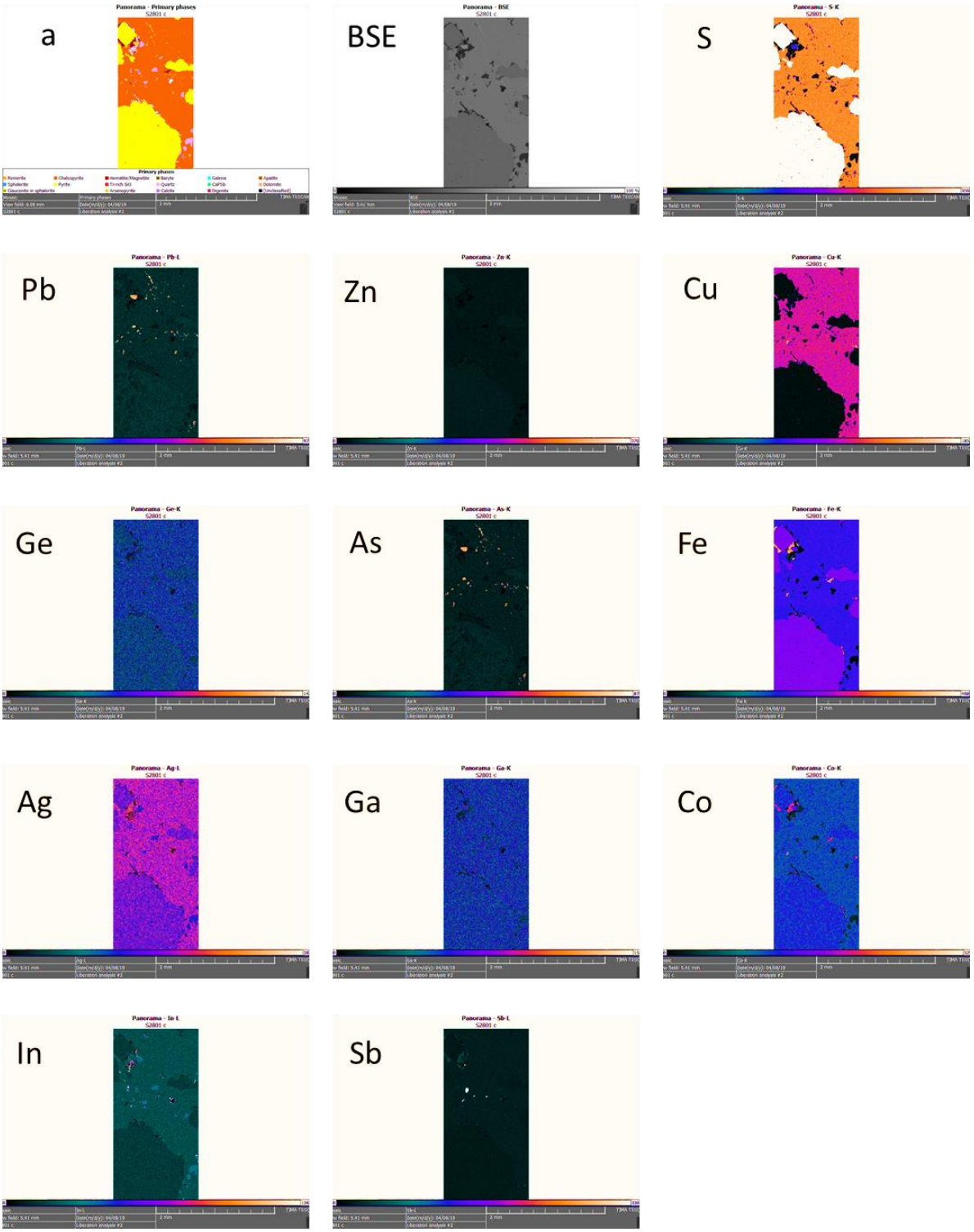

Figure 40: False colour phase map (a), backscatter image, and element maps of S, Pb, Zn, Cu, Ge, As, Fe, Ag, Ga, Co, In and Sb for a section of the polished thin section from thin section c from sample S2801.

The last area for this sample, Figure 41, again shows little to no Ge concentration. The arsenopyrite is rich in Pb. In appears in the dolomite, while Co concentrates into an iron oxide phase.

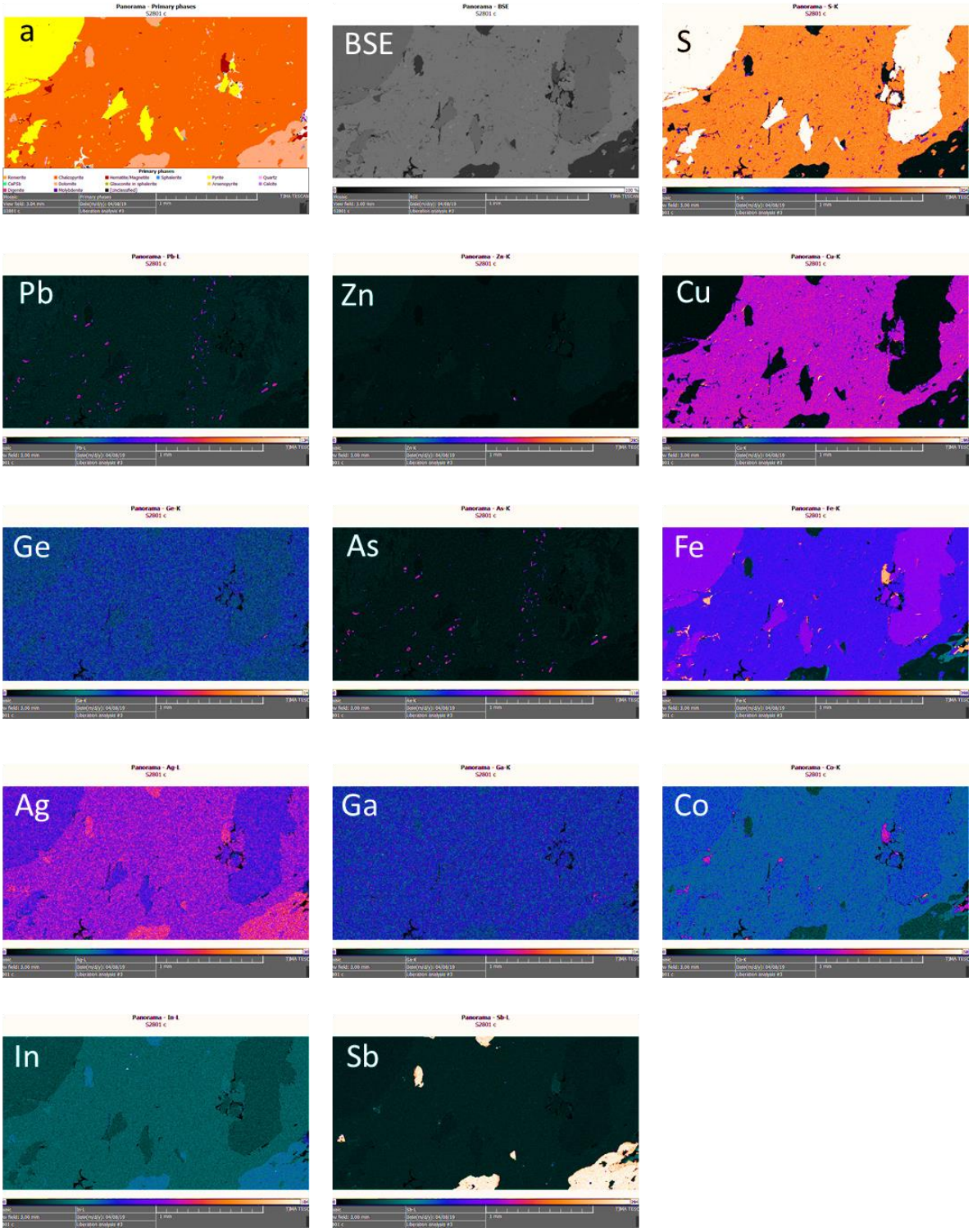

Figure 41: False colour phase map (a), backscatter image, and element maps of S, Pb, Zn, Cu, Ge, As, Fe, Ag, Ga, Co, In and Sb for a section of the polished thin section from thin section c from sample S2801.

C.2.4. Sphalerite-dominant assemblage

Sample KP 11

Two polished thin sections were chosen for this sample, KP 11 a and KP 11 c. Figure 42 shows the first of three areas for KP 11 a. Ge, as well as Ga and As can be found concentrating within the galena. The tennantite has a rather high Pb content. The chalcopyrite, and to a lesser extent, the tennantite have some Co within them. There appears to be some In within the disseminated quartz, and a high concentration of In in the phlogopite.

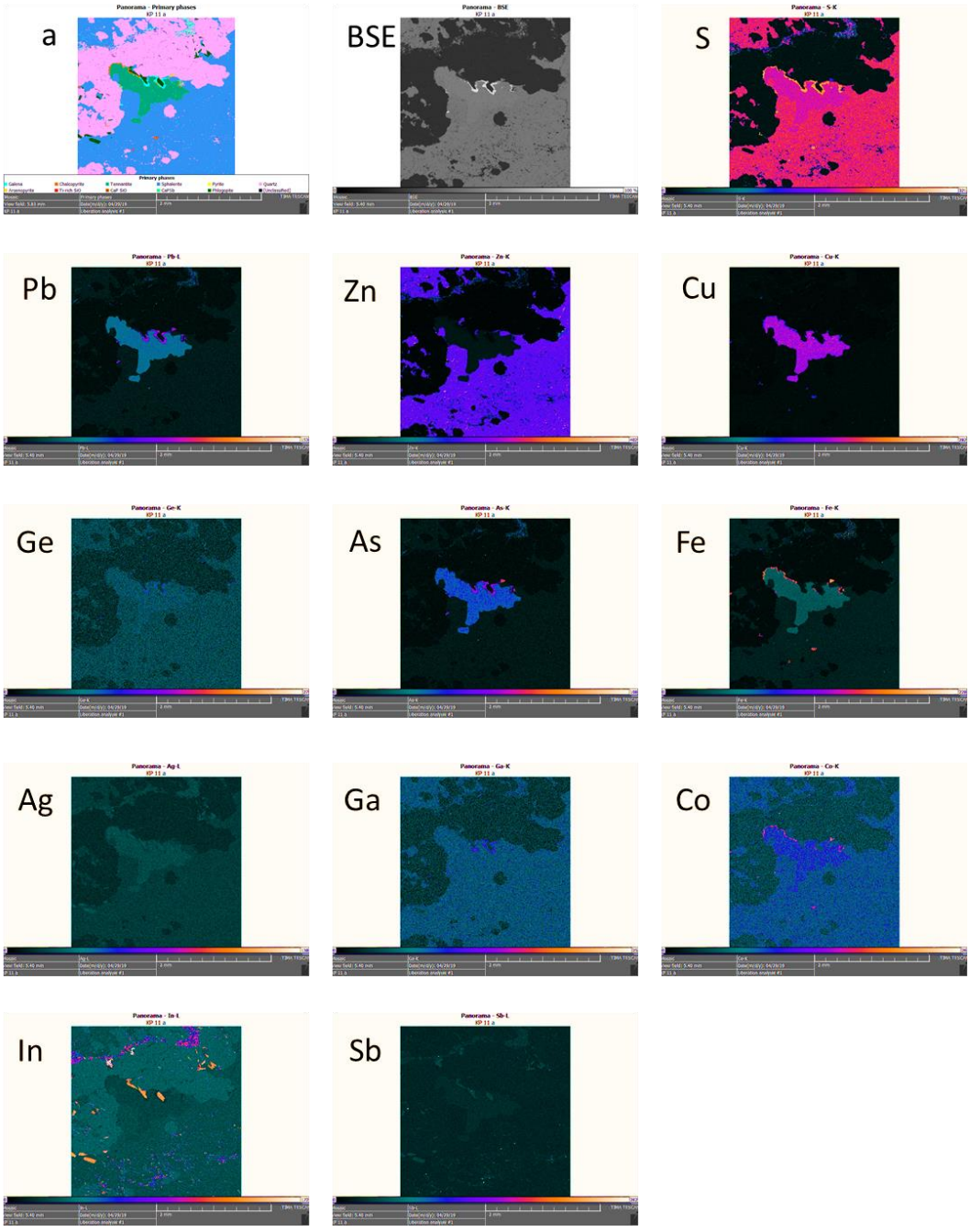

Figure 42: False colour phase map (a), backscatter image, and element maps of S, Pb, Zn, Cu, Ge, As, Fe, Ag, Ga, Co, In and Sb for a section of the polished thin section from thin section a from sample KP 11.

In Figure 43, the second area of polished thin section KP 11 a, shows almost negligible Ge within the galena. The galena contains higher concentrations of As and Ga. The tennantite contains a notable amount of Pb, and much less Co. The chalcopyrite is richer in Co. The disseminated quartz and phlogopite are extremely rich in In.

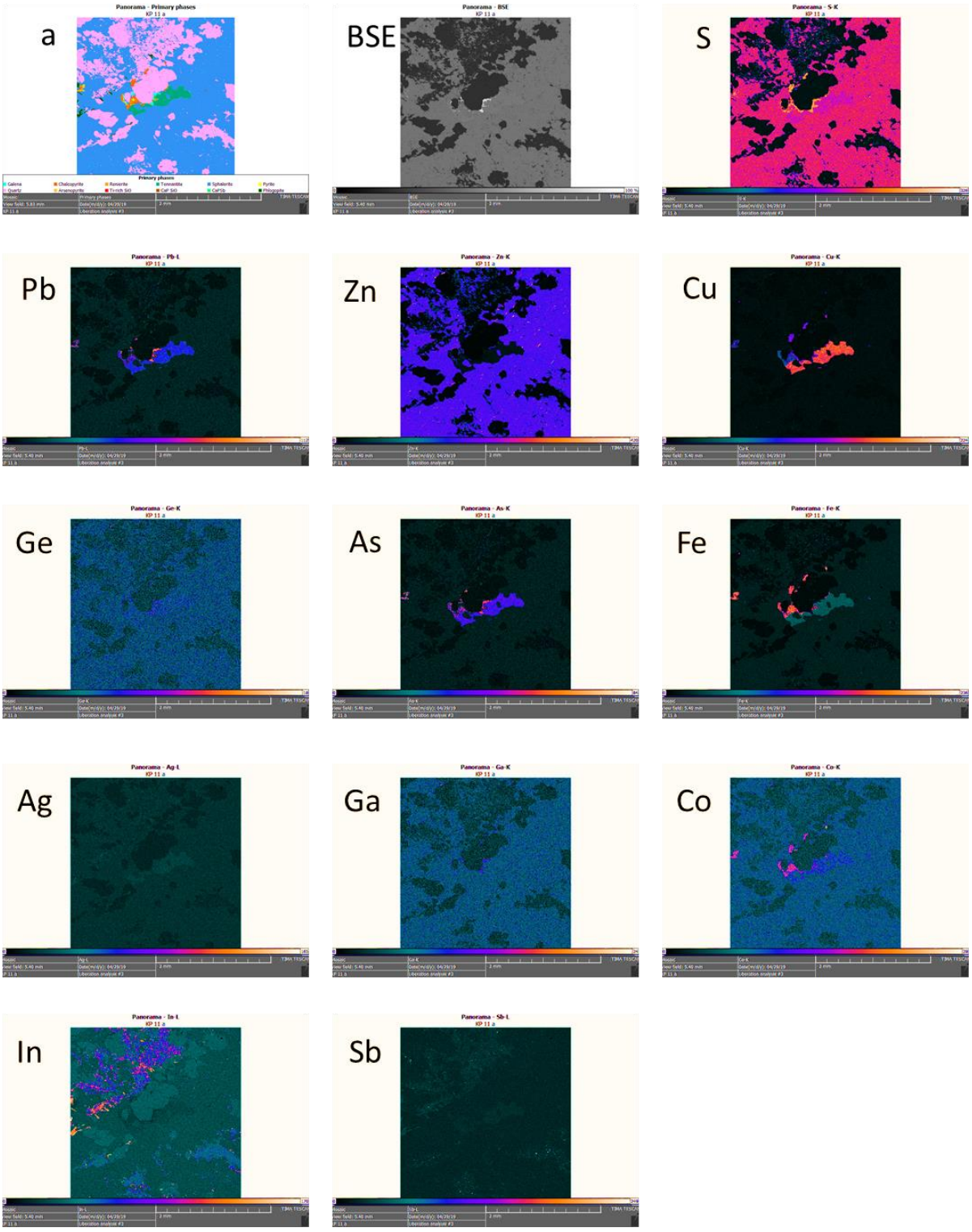

Figure 43: False colour phase map (a), backscatter image, and element maps of S, Pb, Zn, Cu, Ge, As, Fe, Ag, Ga, Co, In and Sb for a section of the polished thin section from thin section a from sample KP 11.

The last area for polished thin section KP 11 a, Figure 44, shows an insignificant concentration of Ge. The small galena veinlet is rich in As. Some of the quartz, particularly the disseminated quartz, and the phlogopite have very high concentrations of In.

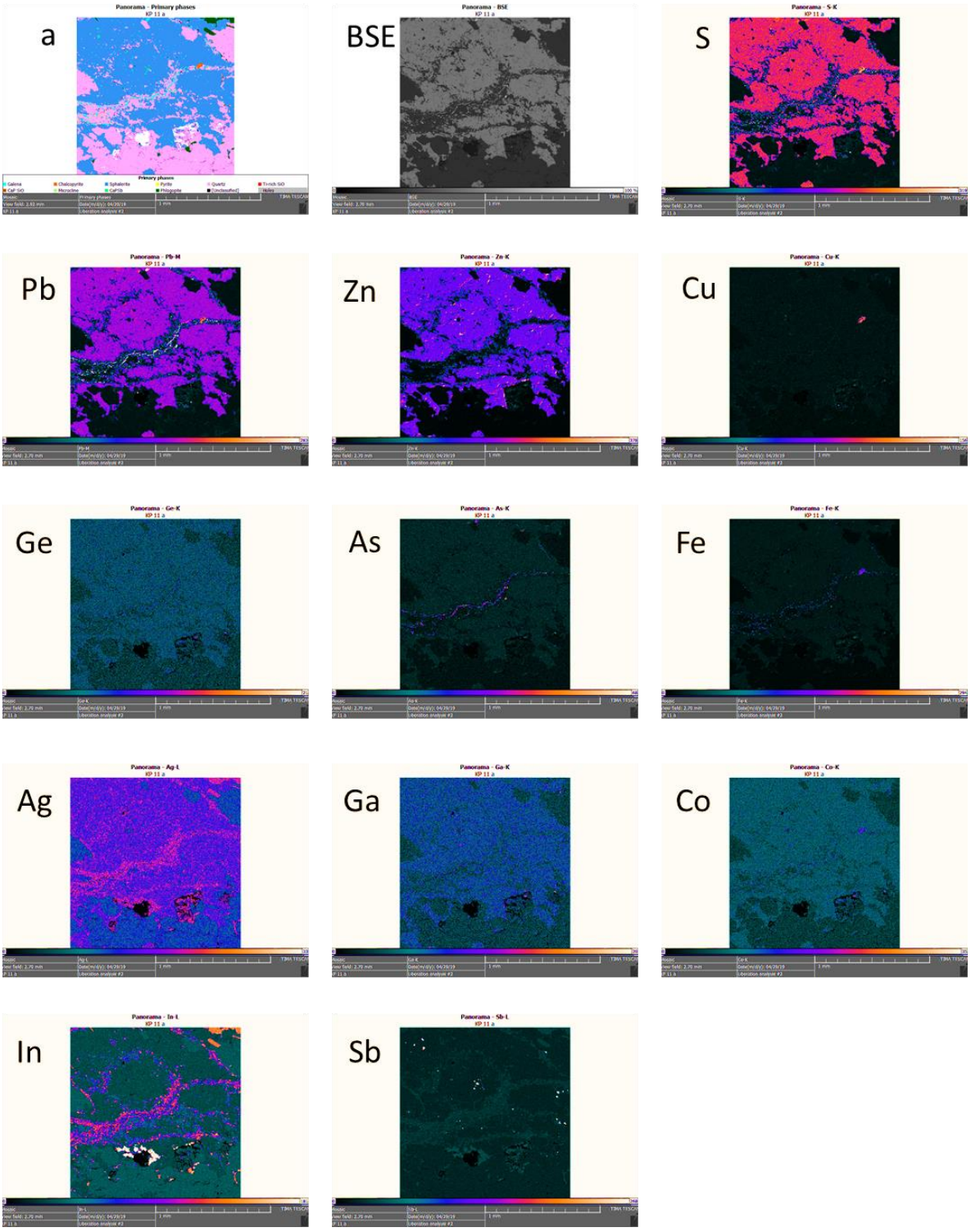

Figure 44: False colour phase map (a), backscatter image, and element maps of S, Pb, Zn, Cu, Ge, As, Fe, Ag, Ga, Co, In and Sb for a section of the polished thin section from thin section a from sample KP 11.

Figure 45 shows the first of three areas selected for polished thin section KP 11 c. The Ge for this area concentrates into the galena, and to a lesser extent, the tennantite. The galena is also rich in As and Ga. The arsenopyrite, interestingly, has a concentration of Pb in it. Co concentrates into both the chalcopyrite and then arsenopyrite. In, again, concentrates into the phlogopite and disseminated quartz.

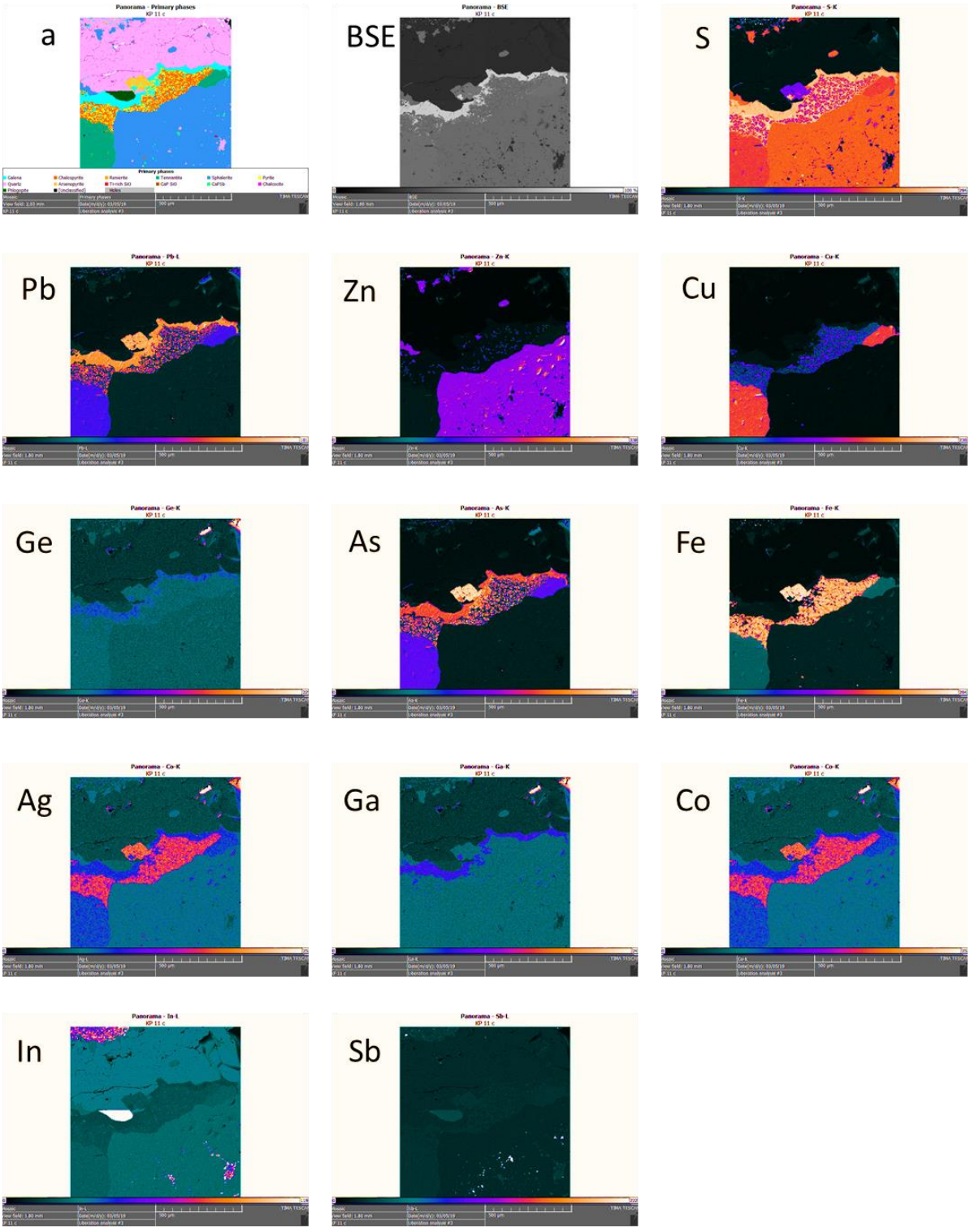

Figure 45: False colour phase map (a), backscatter image, and element maps of S, Pb, Zn, Cu, Ge, As, Fe, Ag, Ga, Co, In and Sb for a section of the polished thin section from thin section c from sample KP 11.

Ge is, once again, negligible in Figure 46. The disseminated galena is rich in As. The chalcopyrite has a relatively high concentration of Co. All the quartz and phlogopite seems to have a high concentration of In.

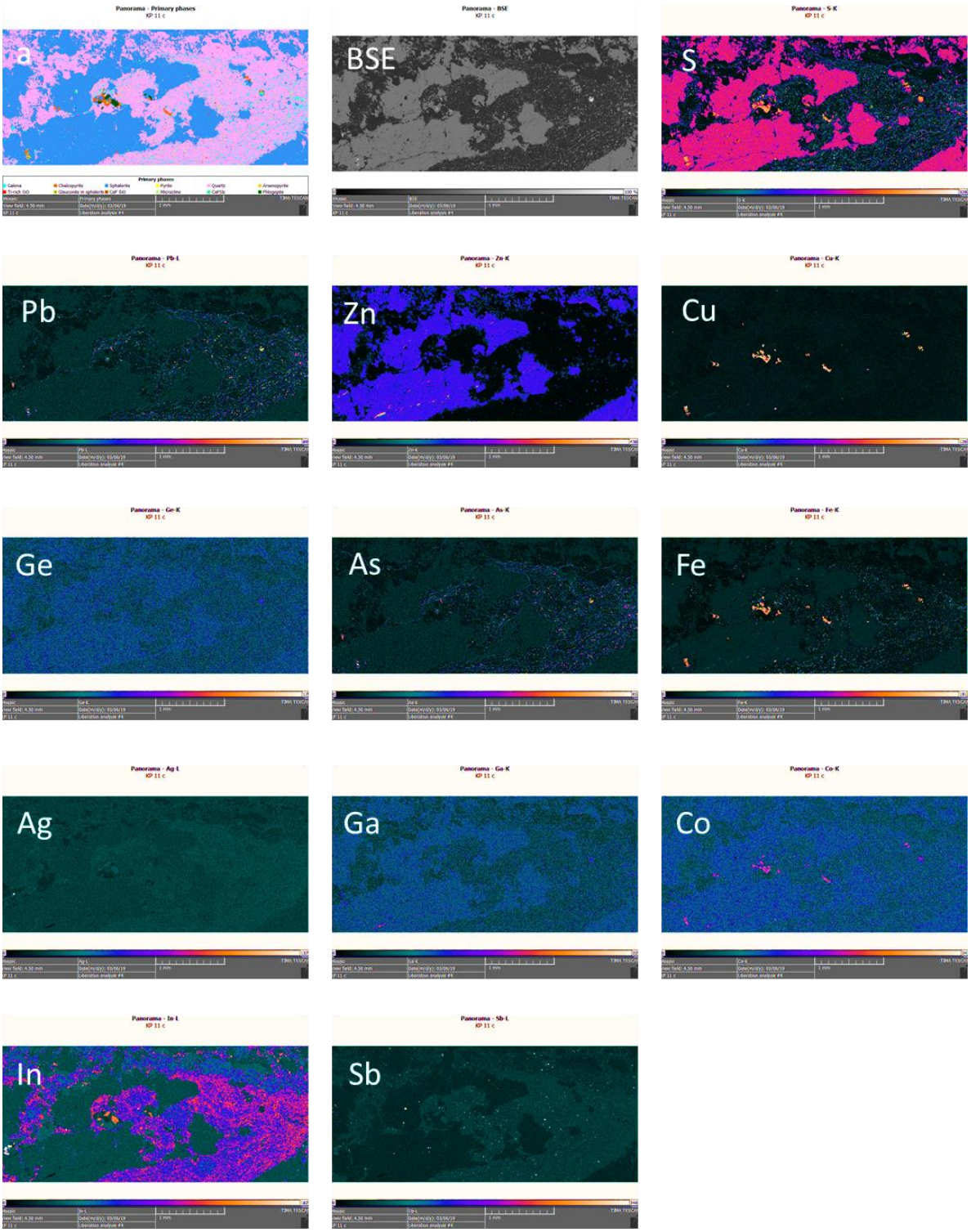

Figure 46: False colour phase map (a), backscatter image, and element maps of S, Pb, Zn, Cu, Ge, As, Fe, Ag, Ga, Co, In and Sb for a section of the polished thin section from thin section c from sample KP 11.

The last area for KP 11 c is seen in Figure 47. The Ge in this area concentrates into the galena, along with some Ga and As. Again, the chalcopyrite has some Co in it. It concentrates into the quartz and phlogopite.

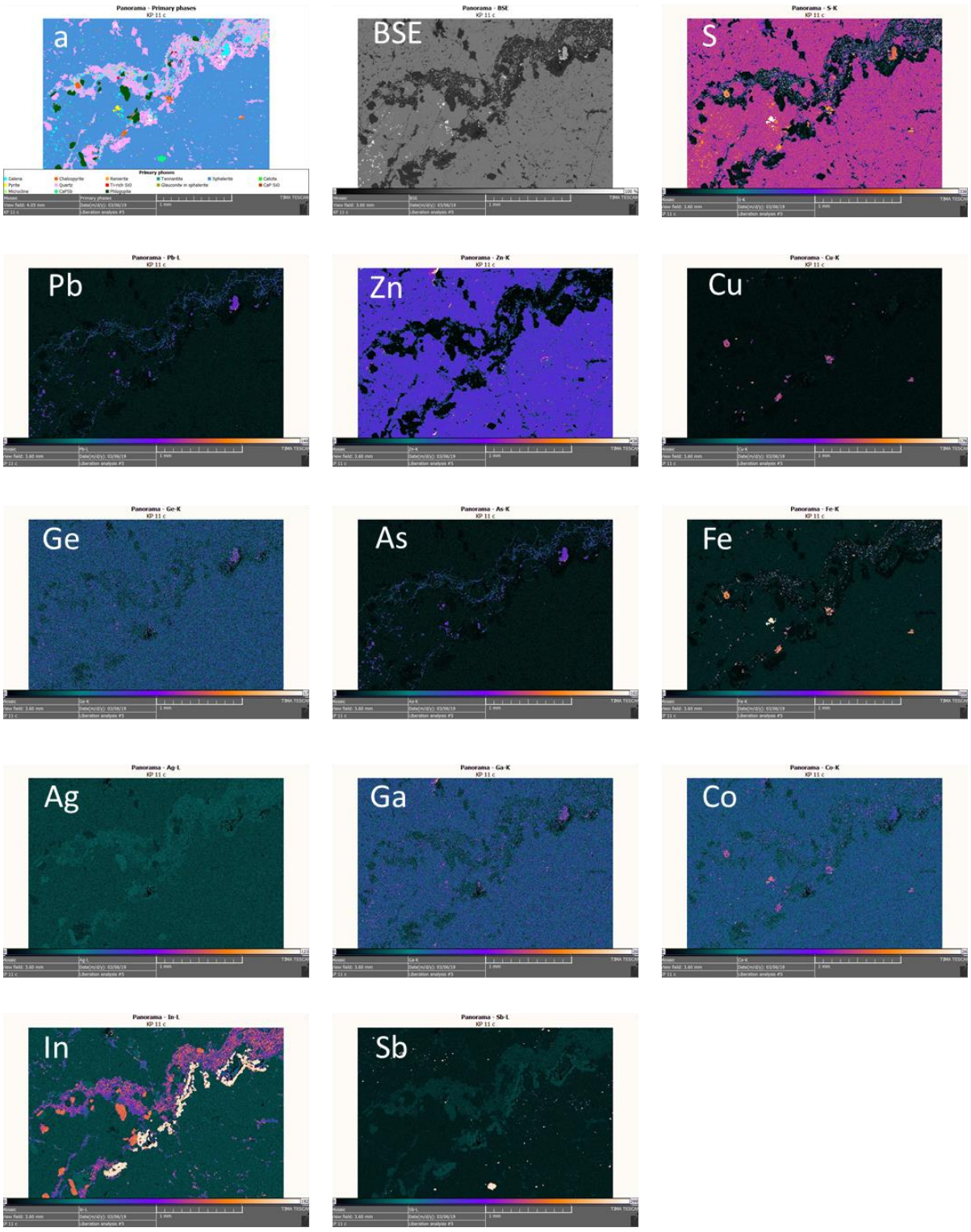

Figure 47: False colour phase map (a), backscatter image, and element maps of S, Pb, Zn, Cu, Ge, As, Fe, Ag, Ga, Co, In and Sb for a section of the polished thin section from thin section c from sample KP 11.

C.2.5. Sphalerite-chalcopyrite-dominant assemblage

Sample 6548

One polished thin section was scanned in 5 different areas for this sample. This polished thin section was labelled 6548 a. This sampled contains little renierite. Figure 48, the first area scanned by the TIMA, shows the highest concentration of Ge in the small blebs of renierite, as seen in the false colour primary phase map. The rest of the Ge concentrates into the galena, along with some As and Ga. A very small concentration of Co can be found within the chalcopyrite.

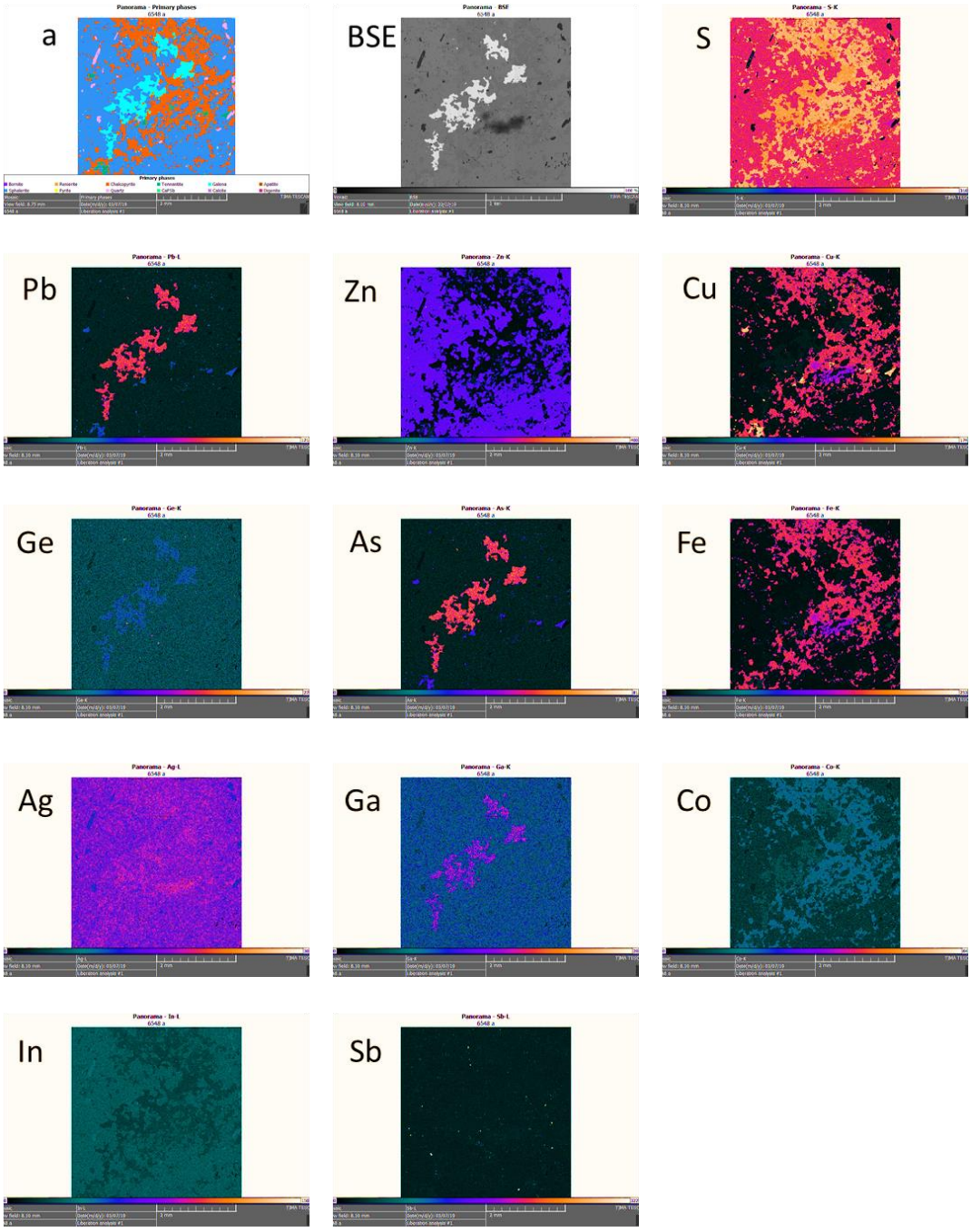

Figure 48: False colour phase map (a), backscatter image, and element maps of S, Pb, Zn, Cu, Ge, As, Fe, Ag, Ga, Co, In and Sb for a section of the polished thin section from thin section a from sample 6548.

Figure 49 shows an area of dominant sphalerite with a network of chalcopyrite, and intermittent quartz, tennantite and renierite. The Ge is concentrated in the small blebs of renierite, and nowhere else within this area. Pb shows quite predominately within the small blebs of tennantite. Co again appears within the chalcopyrite.

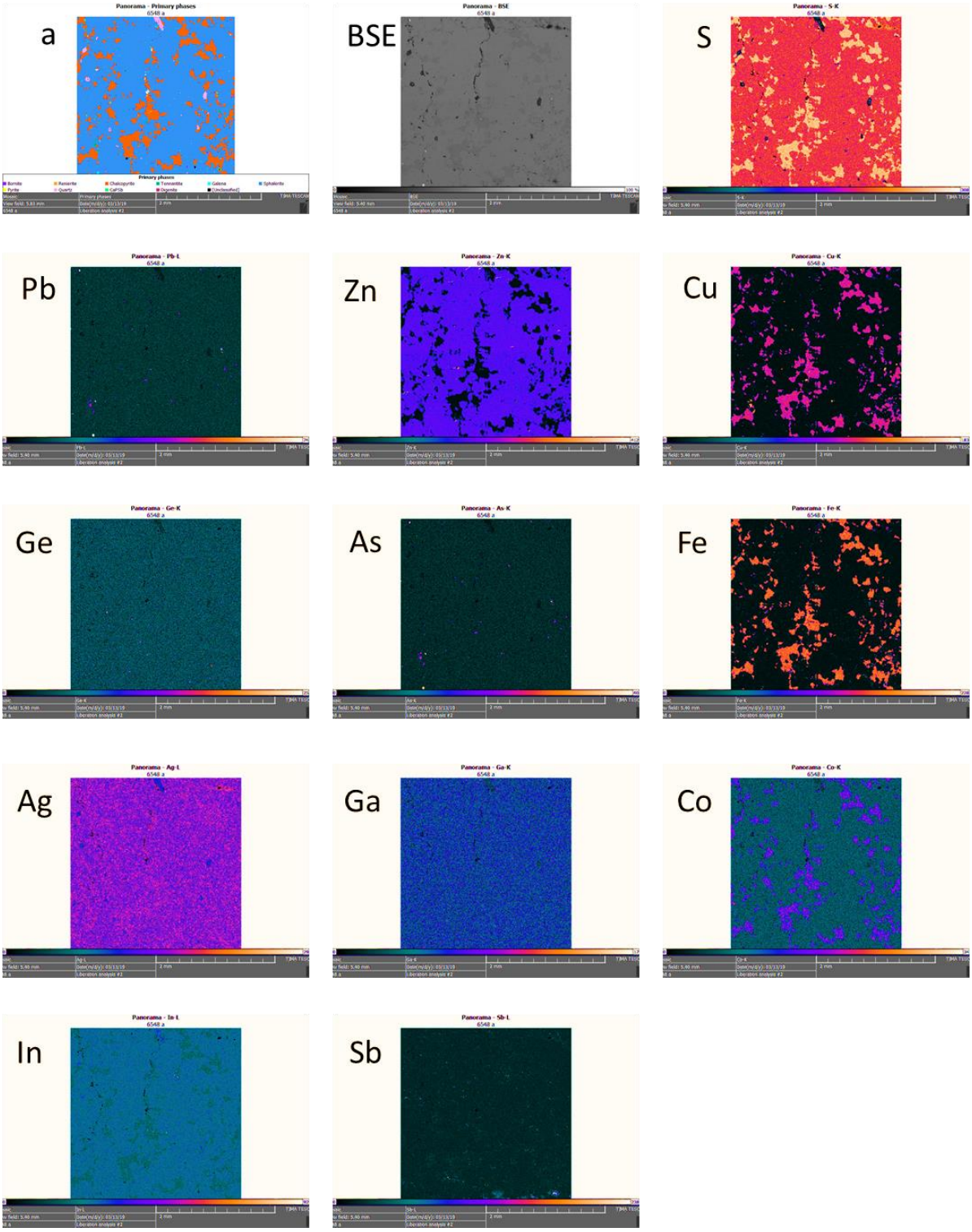

Figure 49: False colour phase map (a), backscatter image, and element maps of S, Pb, Zn, Cu, Ge, As, Fe, Ag, Ga, Co, In and Sb for a section of the polished thin section from thin section a from sample 6548.

The Ge in Figure 50 is once again mostly concentrated within the small renierite blebs. The Ge is also found to be concentrated within the galena, second most to the renierite. And even less so in the tennantite. The galena, once again, has a relatively high concentration of As and Ga. The tennantite shows some Pb within it. Co is found within the chalcopyrite. Interestingly, In can be found concentrating inside the quartz. Sb is seen concentrating within the small flecks of calcite.

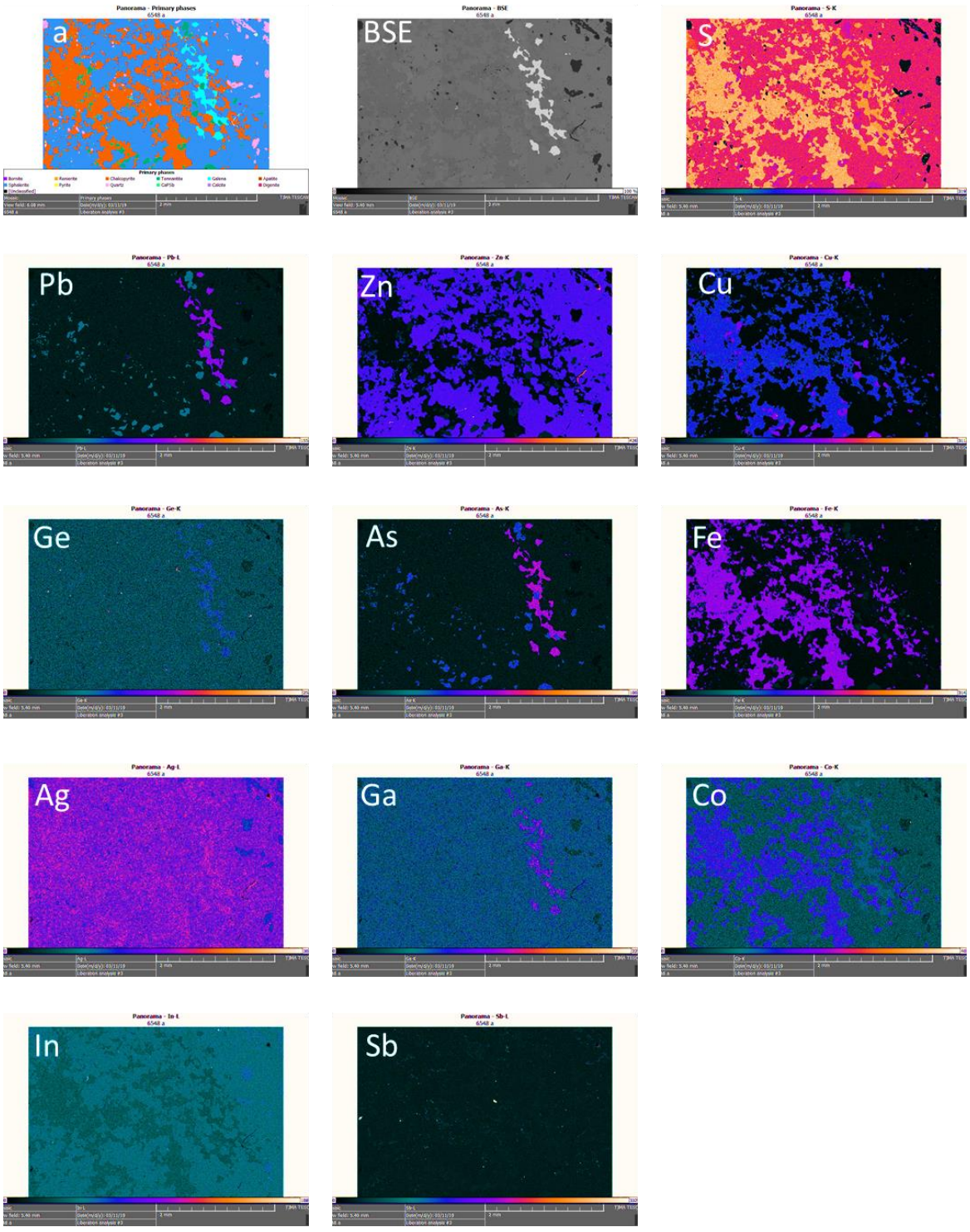

Figure 50: False colour phase map (a), backscatter image, and element maps of S, Pb, Zn, Cu, Ge, As, Fe, Ag, Ga, Co, In and Sb for a section of the polished thin section from thin section a from sample 6548.

Figure 51, the fourth section of sample 6548a to be analysed by the TIMA, shows small flecks of renierite with a high Ge concentration. A lower concentration of Ge can be found within the tennantite, along with some Pb. A relatively high concentration of Co is found within the chalcopyrite. In, once again, concentrates within the quartz.

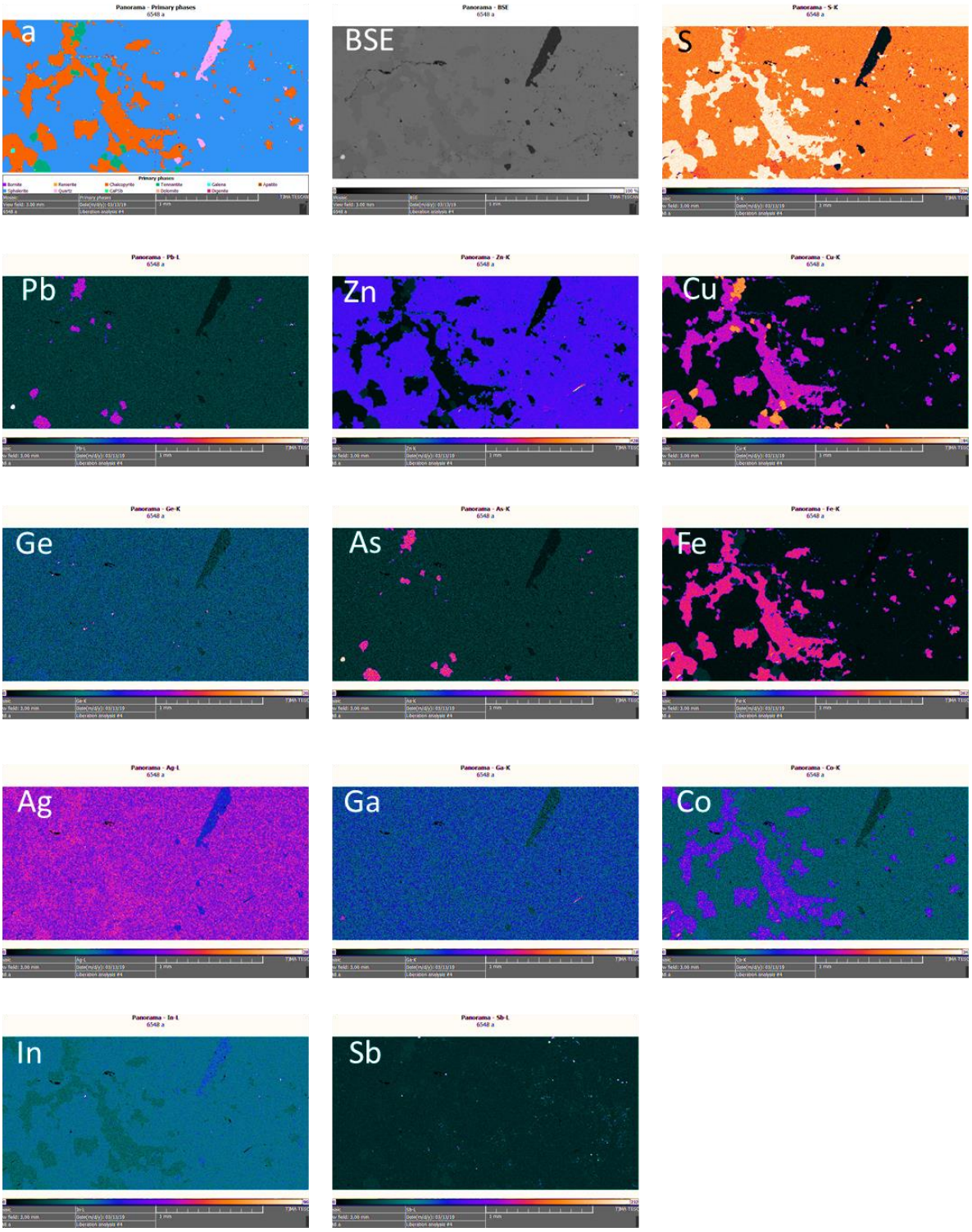

Figure 51: False colour phase map (a), backscatter image, and element maps of S, Pb, Zn, Cu, Ge, As, Fe, Ag, Ga, Co, In and Sb for a section of the polished thin section from thin section a from sample 6548.

Figure 52 shows a few small renierite blebs that have a high concentration of Ge, as well as a few small galena blebs. Ga is also concentrated within the galena. Co, again, has a high concentration within the chalcopyrite. The tennantite also shows high concentration of Pb.

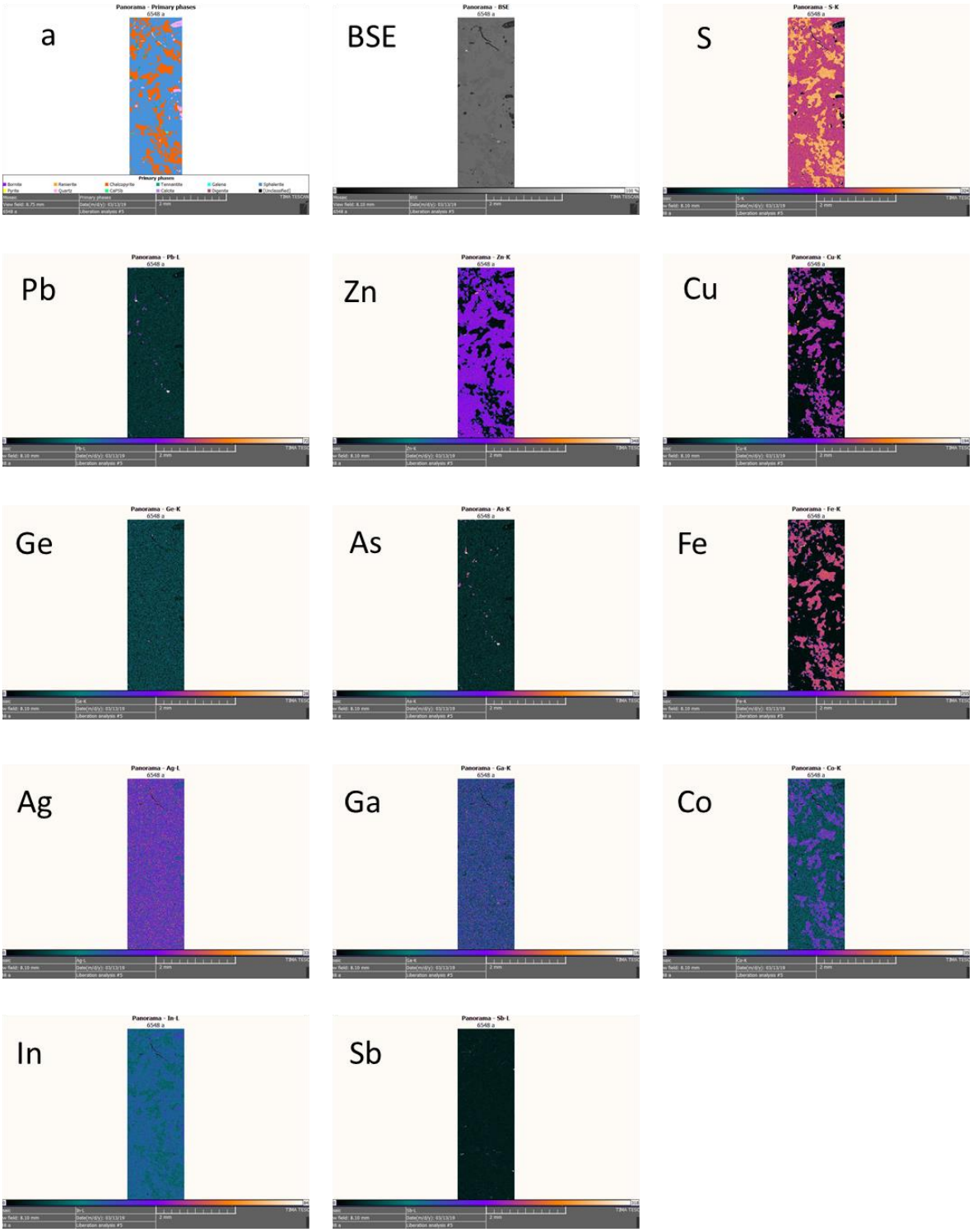

Figure 52: False colour phase map (a), backscatter image, and element maps of S, Pb, Zn, Cu, Ge, As, Fe, Ag, Ga, Co, In and Sb for a section of the polished thin section from thin section a from sample 6548.

Sample 1058

Three areas were chosen for scanning by the TIMA for this polished thin section. Figure 53, the first area, shows Ge concentration within the renierite, as seen on the primary phase map. The Ge also concentrates, to a lesser but still notable extent, into the galena. The galena is also rich in As and Ga. Co appears to concentrate into the chalcopyrite.

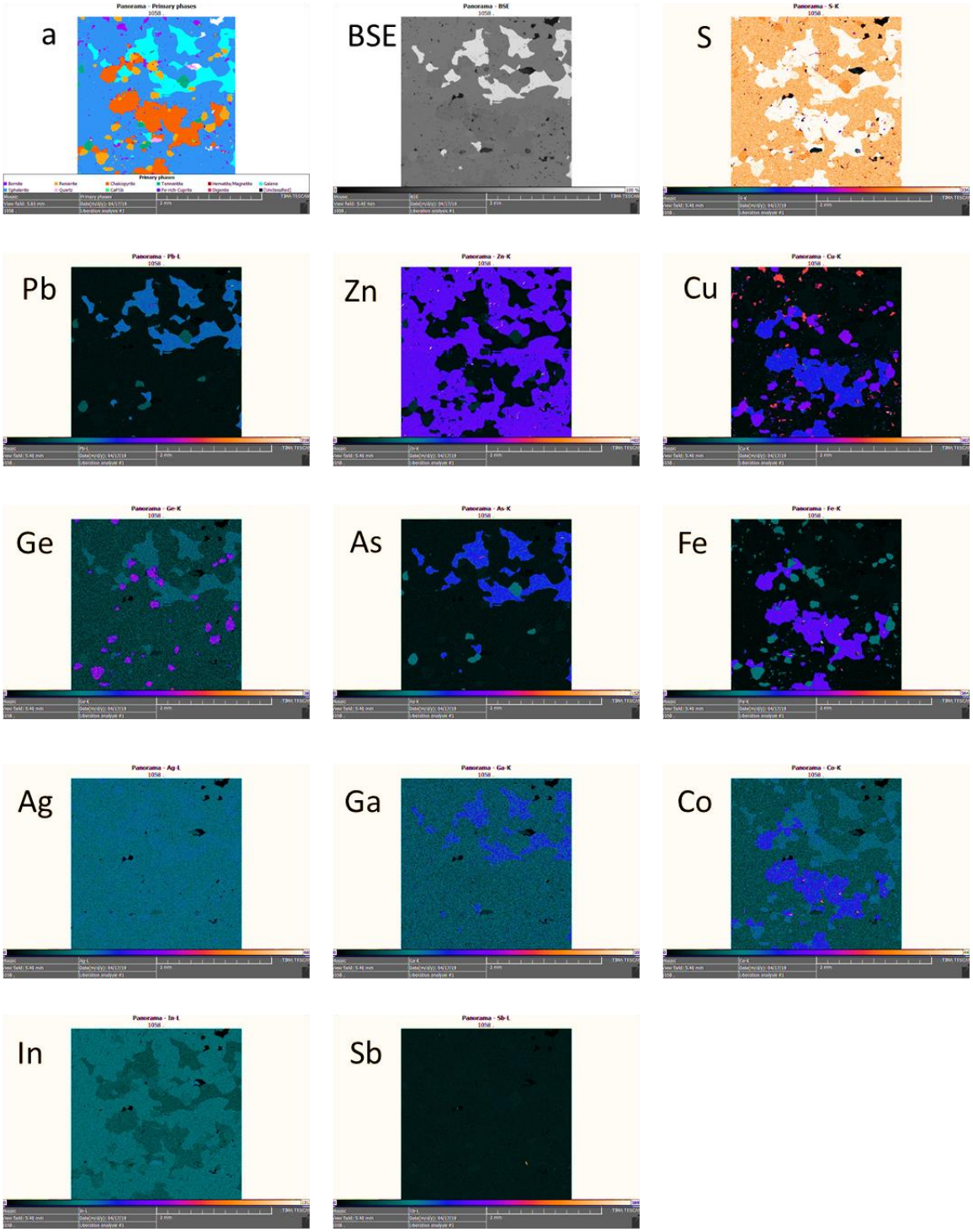

Figure 53: False colour phase map (a), backscatter image, and element maps of S, Pb, Zn, Cu, Ge, As, Fe, Ag, Ga, Co, In and Sb for a section of the polished thin section from sample 1058.

In Figure 54, Ge concentration is noted in the renierite. The rest of the Ge is concentrated into the galena. It can be noted that the galena also contains high concentrations of As and Ga. The chalcopyrite is rich in Co.

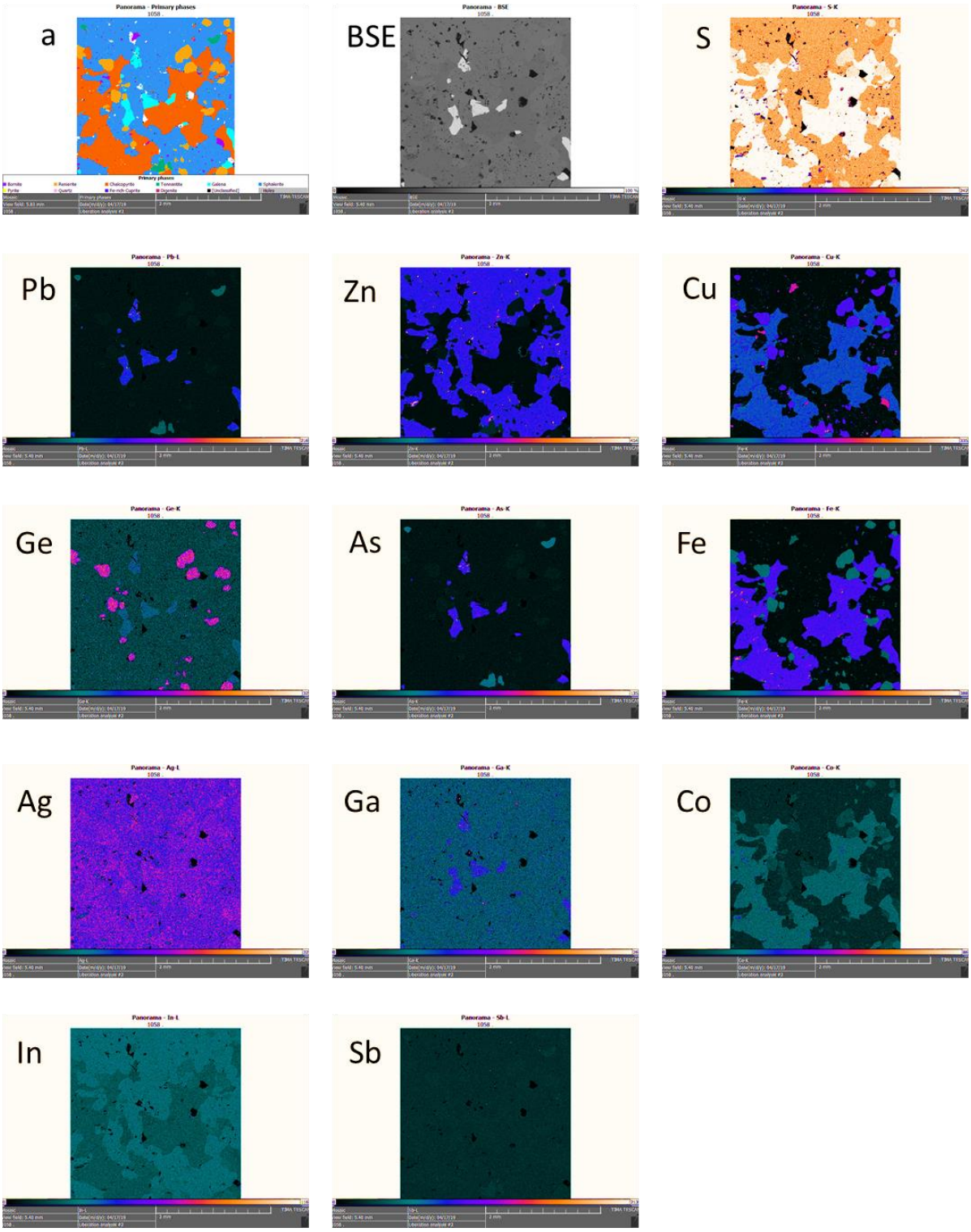

Figure 54: False colour phase map (a), backscatter image, and element maps of S, Pb, Zn, Cu, Ge, As, Fe, Ag, Ga, Co, In and Sb for a section of the polished thin section from sample 1058.

Figure 55 shows a high concentration of Ge in renierite, with a lesser concentration in galena. The galena contains As and Ga. Co is found within the chalcopyrite.

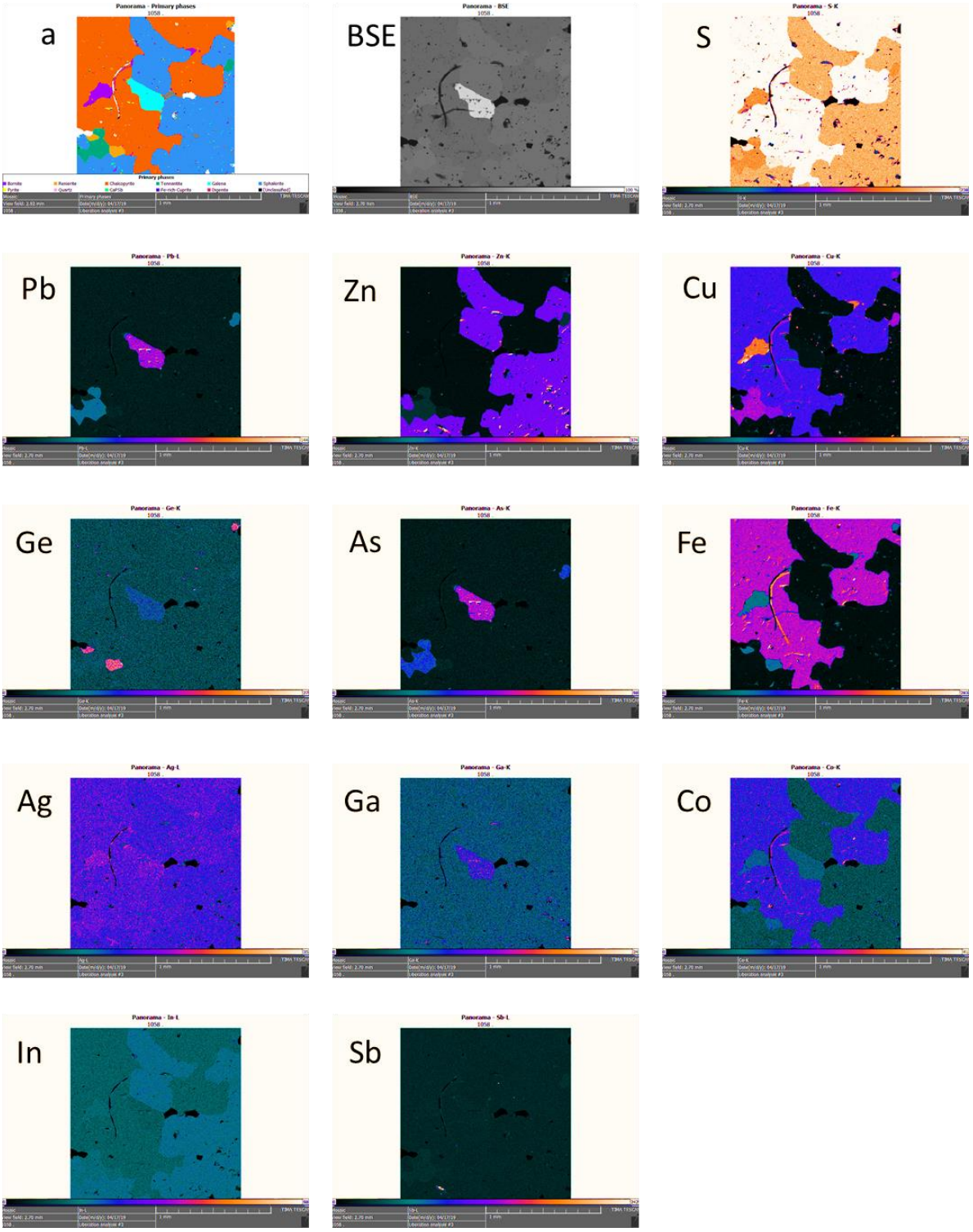

Figure 55: False colour phase map (a), backscatter image, and element maps of S, Pb, Zn, Cu, Ge, As, Fe, Ag, Ga, Co, In and Sb for a section of the polished thin section from sample 1058.

Sample 12492

Four areas were selected on thin section 12492 f for analysis. Figure 56 has insignificant amounts of Ge. The chalcopyrite is rich in Co. The quartz has a high concentration of In.

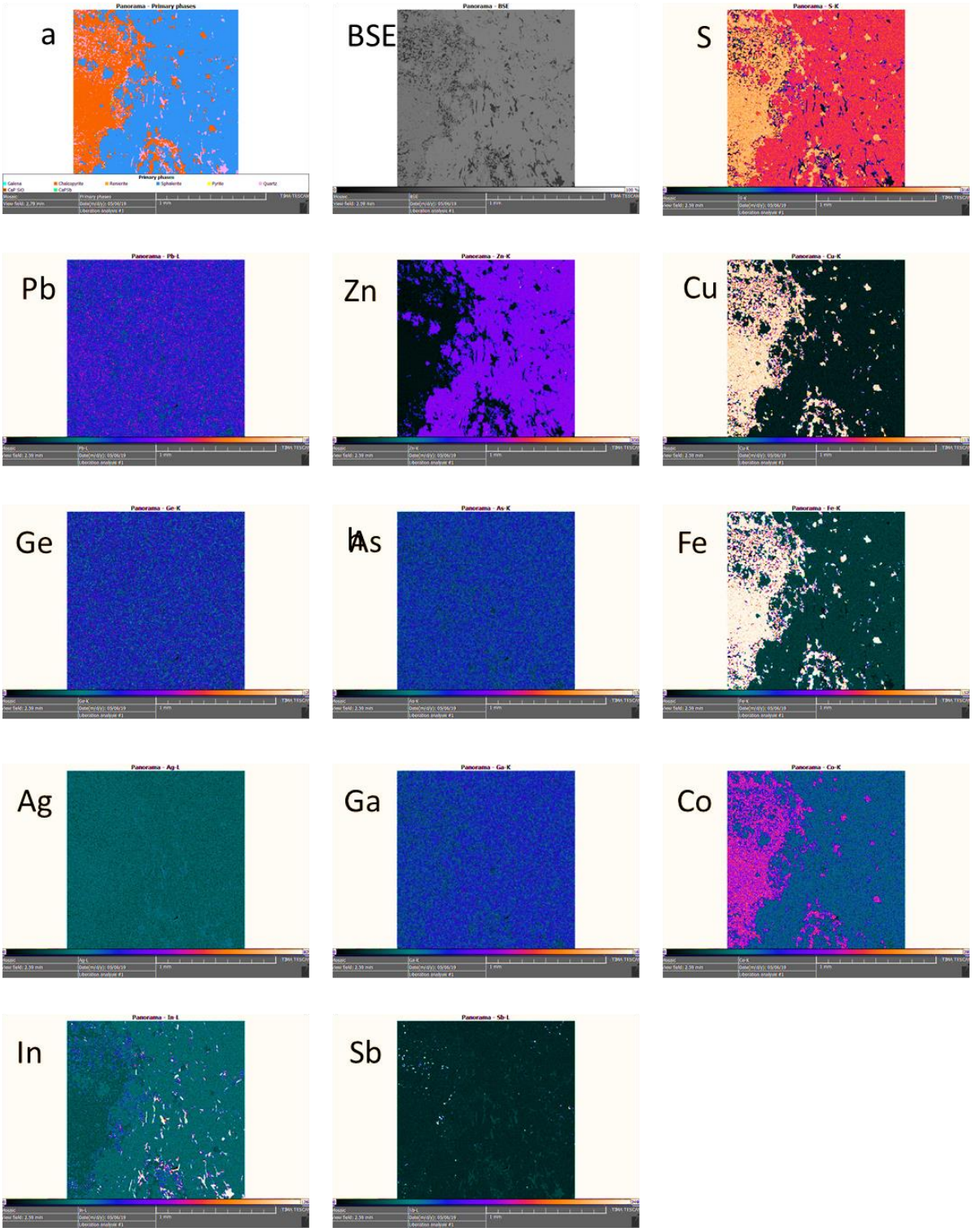

Figure 56: False colour phase map (a), backscatter image, and element maps of S, Pb, Zn, Cu, Ge, As, Fe, Ag, Ga, Co, In and Sb for a section of the polished thin section f from sample 12492.

The next area, Figure 57, shows the same lack of Ge, and Co rich chalcopyrite. There are some phases in the centre of this area that the TIMA was unable to scan as this phase had a BSE level less than 15 %. This leaves an unidentifiable mineral.

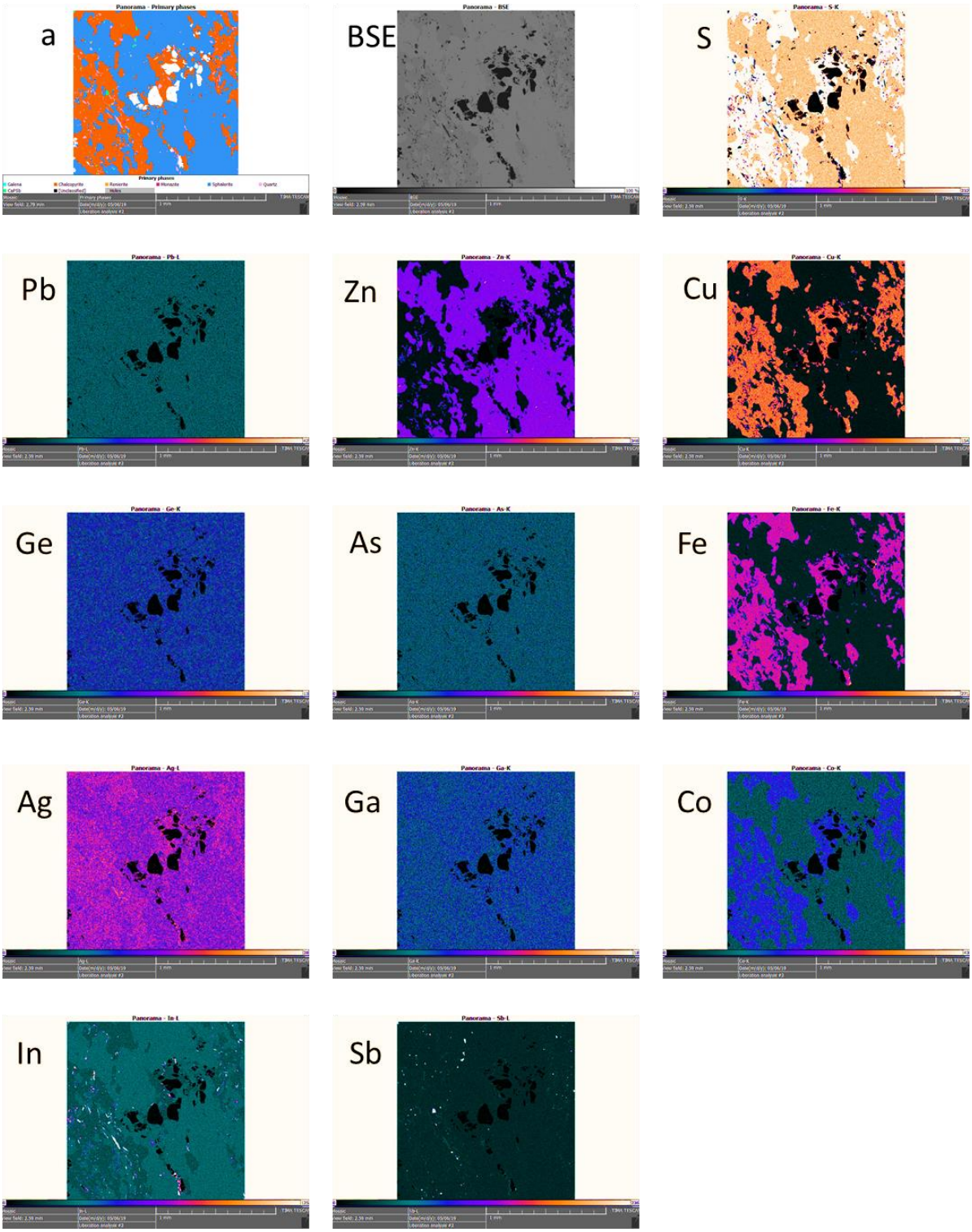

Figure 57: False colour phase map (a), backscatter image, and element maps of S, Pb, Zn, Cu, Ge, As, Fe, Ag, Ga, Co, In and Sb for a section of the polished thin section f from sample 12492.

Figure 58 also shows an unscanned mineral phase, and chalcopyrite with a high concentration of Co. The Ge is once again negligible. The quartz is rich in In.

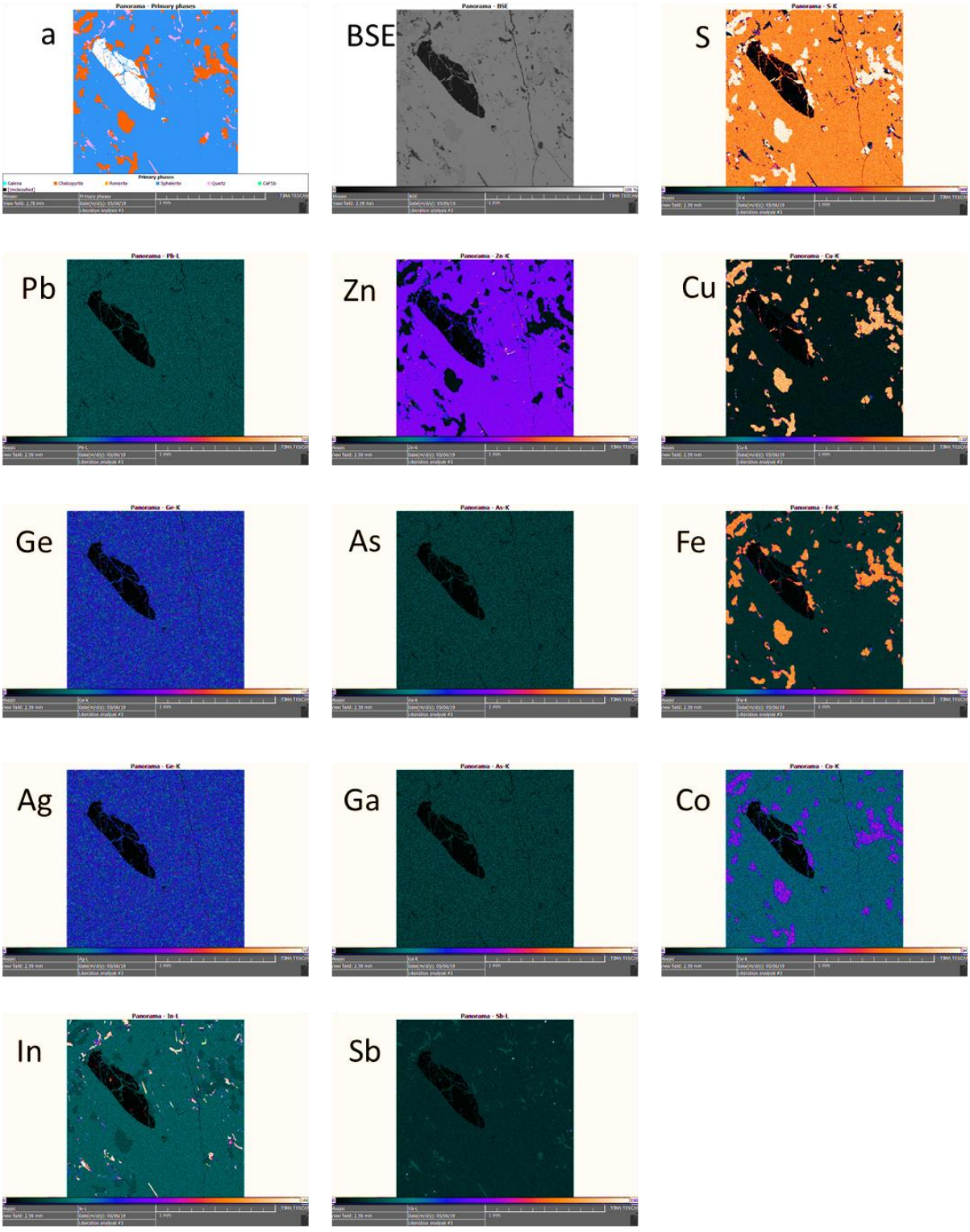

Figure 58: False colour phase map (a), backscatter image, and element maps of S, Pb, Zn, Cu, Ge, As, Fe, Ag, Ga, Co, In and Sb for a section of the polished thin section f from sample 12492.

The final area for this sample, Figure 59, shows insignificant Ge, Co rich chalcopyrite and In rich quartz.

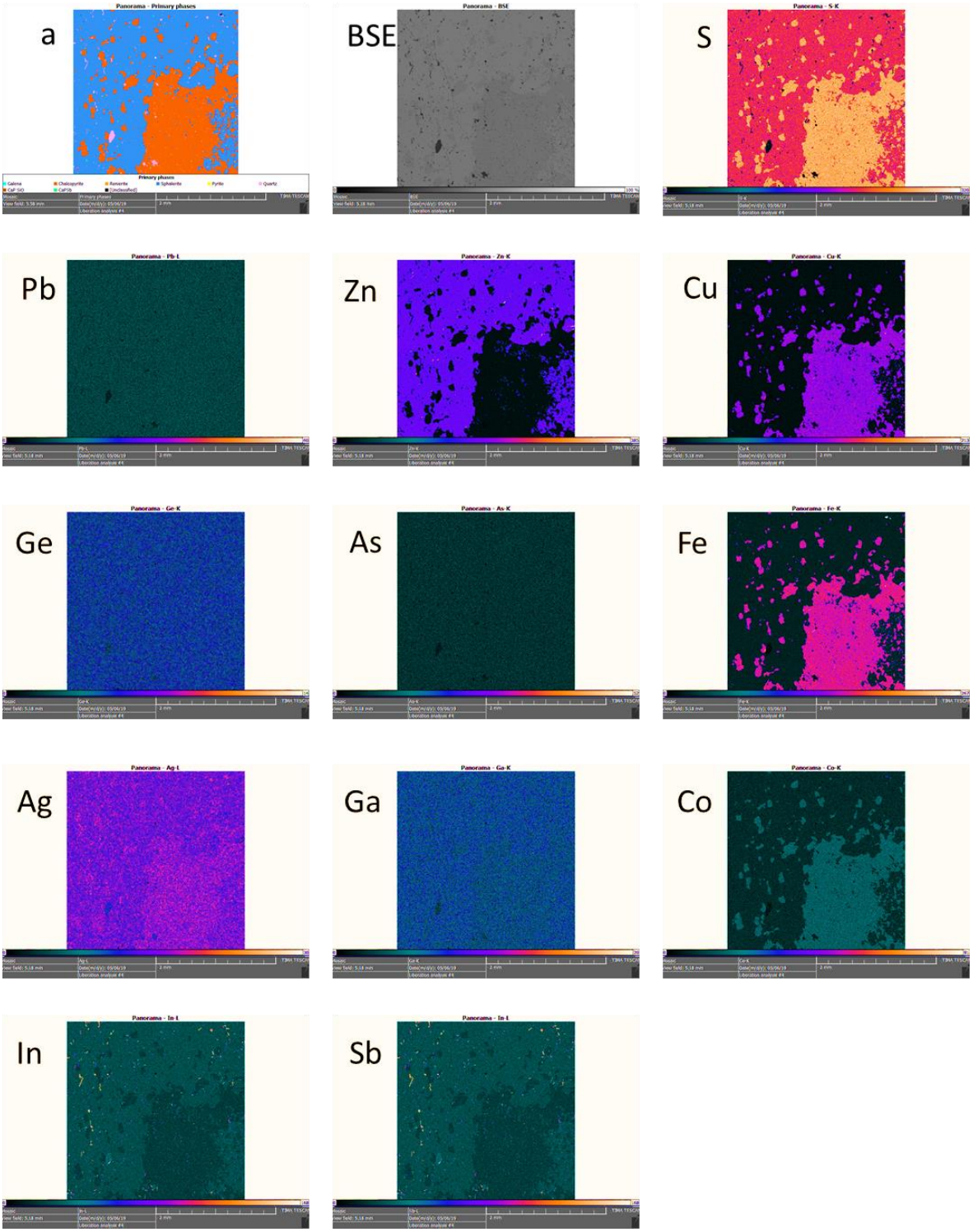

Figure 59: False colour phase map (a), backscatter image, and element maps of S, Pb, Zn, Cu, Ge, As, Fe, Ag, Ga, Co, In and Sb for a section of the polished thin section f from sample 12492.

C.2.6. Sphalerite-bornite-dominant assemblage

Sample 15452

Polished thin section 15452 b was chosen for this sample. Seven areas were scanned on this polished thin section using the TIMA. When comparing the BSE and primary phase map in Figure 60, the galena is shown to have high concentrations of Ge, As and Ga. The tennantite also contains some Pb. In is noted to concentrate within the quartz.

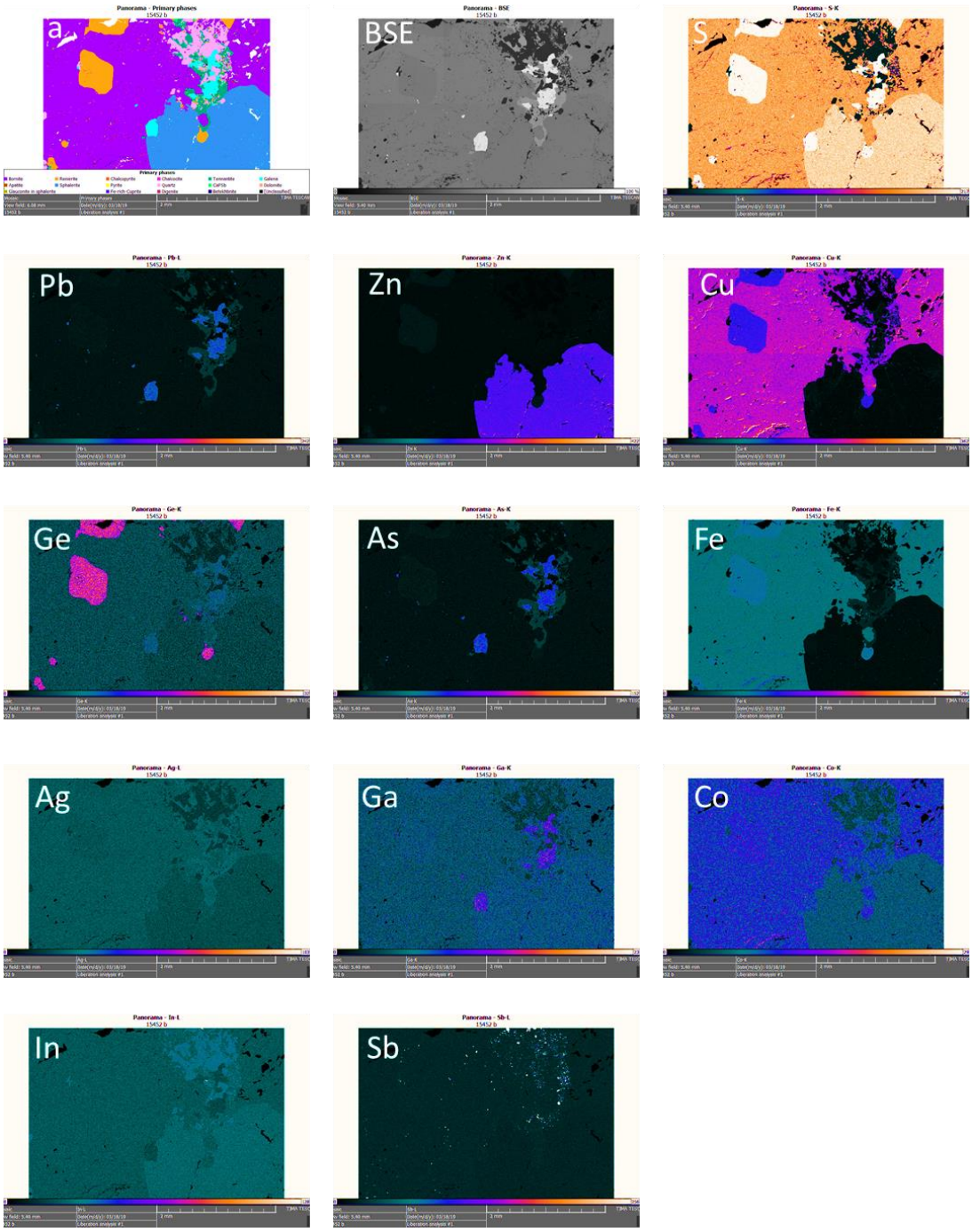

Figure 60: False colour phase map (a), backscatter image, and element maps of S, Pb, Zn, Cu, Ge, As, Fe, Ag, Ga, Co, In and Sb for a section of the polished thin section from thin section b from sample 15452.

Figure 61 shows that the Ge is found to concentrate within the renierite. The tennantite contains some Zn and Pb. Once again, the quartz has a high In concentration.

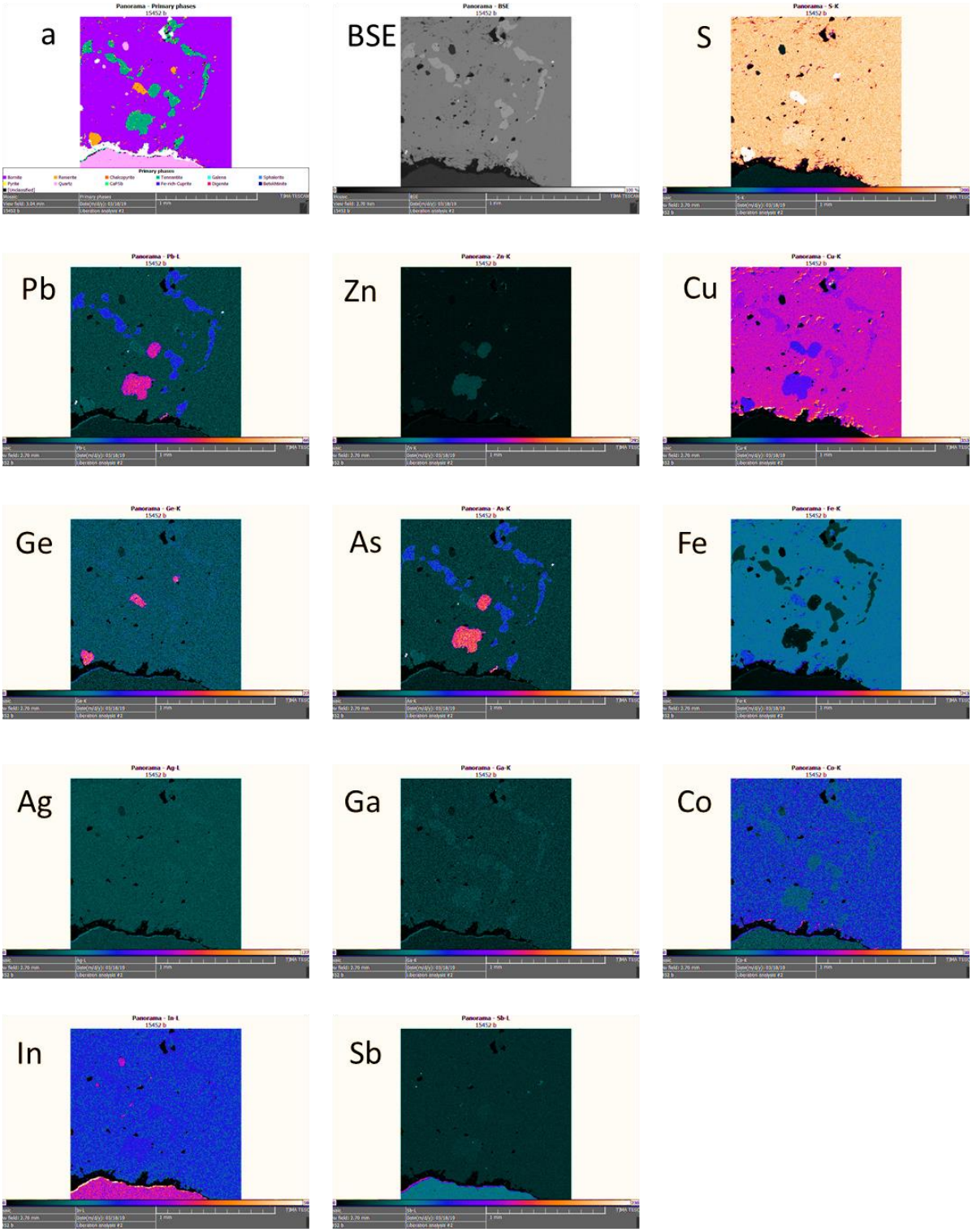

Figure 61: False colour phase map (a), backscatter image, and element maps of S, Pb, Zn, Cu, Ge, As, Fe, Ag, Ga, Co, In and Sb for a section of the polished thin section from thin section b from sample 15452.

In Figure 62, the Ge concentrates into the galena. The galena also shows high concentrations of Pb, As and lesser Ga. The chalcopyrite is seen to be enriched in Co. The quartz is In enriched.

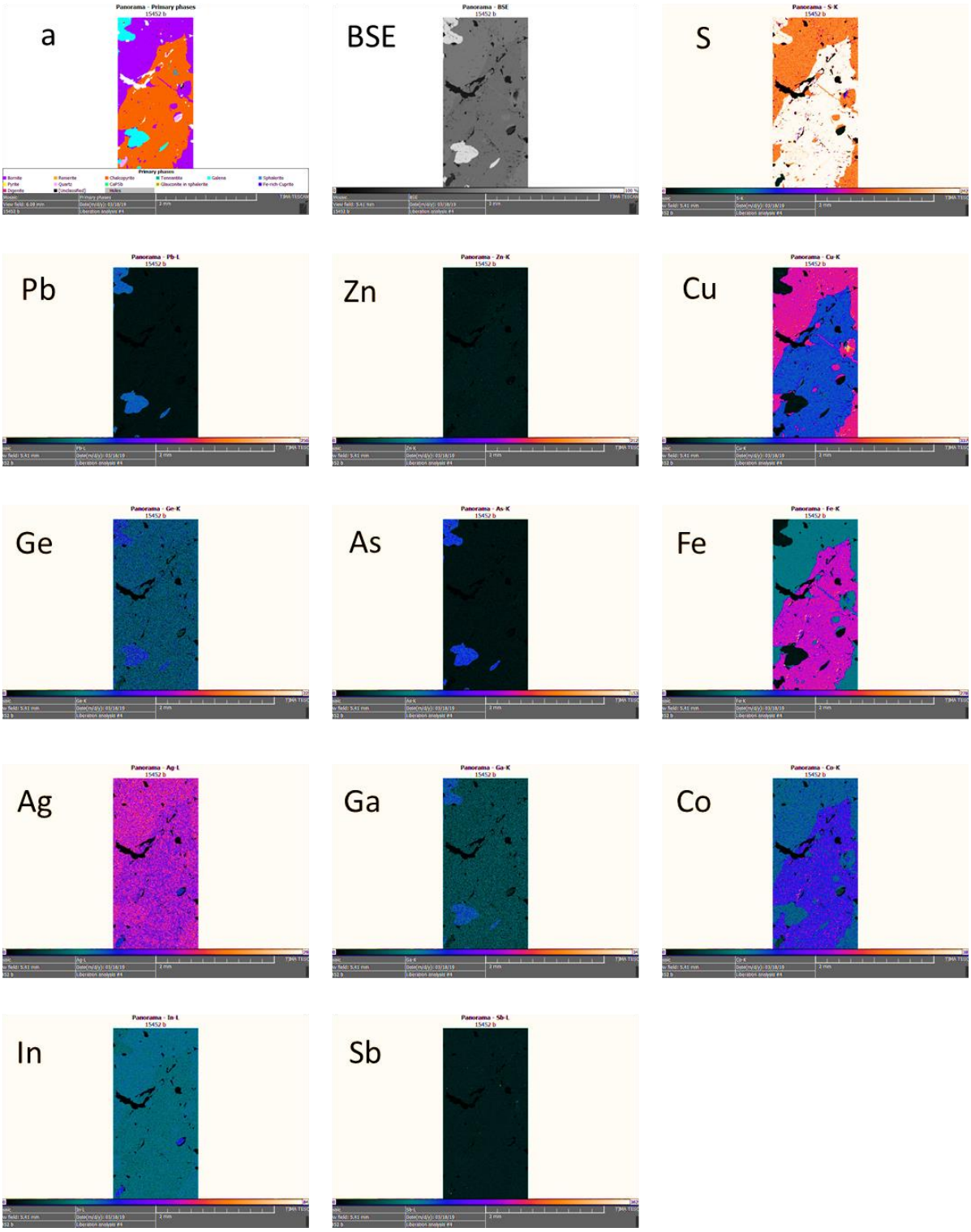

Figure 62: False colour phase map (a), backscatter image, and element maps of S, Pb, Zn, Cu, Ge, As, Fe, Ag, Ga, Co, In and Sb for a section of the polished thin section from thin section b from sample 15452.

The Ge concentrates into renierite in Figure 63. Galena has a high concentration of Pb and As, and lesser Ge and Ga. The bornite contains some Ag and Co.

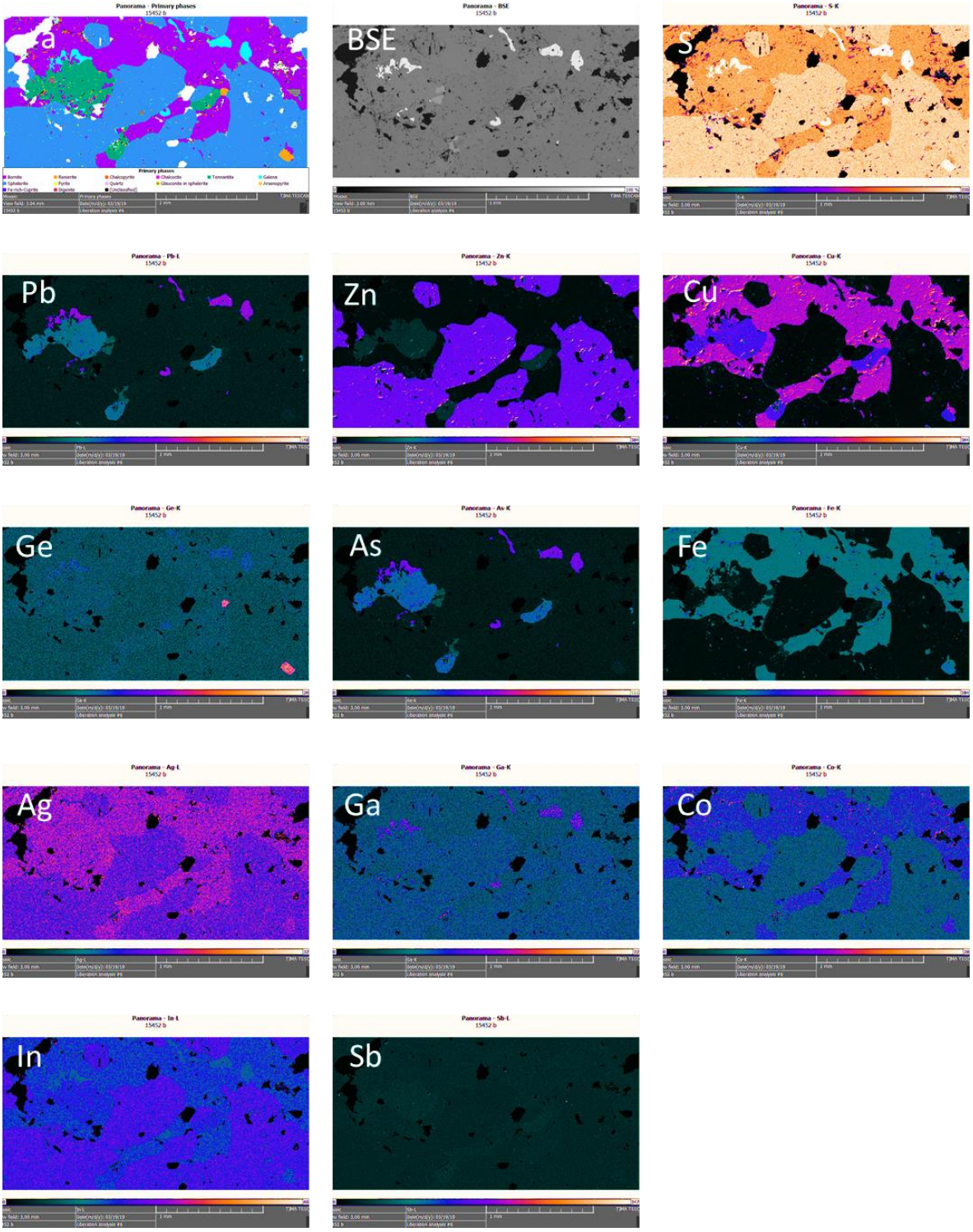

Figure 63: False colour phase map (a), backscatter image, and element maps of S, Pb, Zn, Cu, Ge, As, Fe, Ag, Ga, Co, In and Sb for a section of the polished thin section from thin section b from sample 15452.

The Ge in Figure 64 is seen to concentrate within two renierite blebs, as well as within the galena. The galena is also enriched in As and Ga. Quartz has a high In concentration.

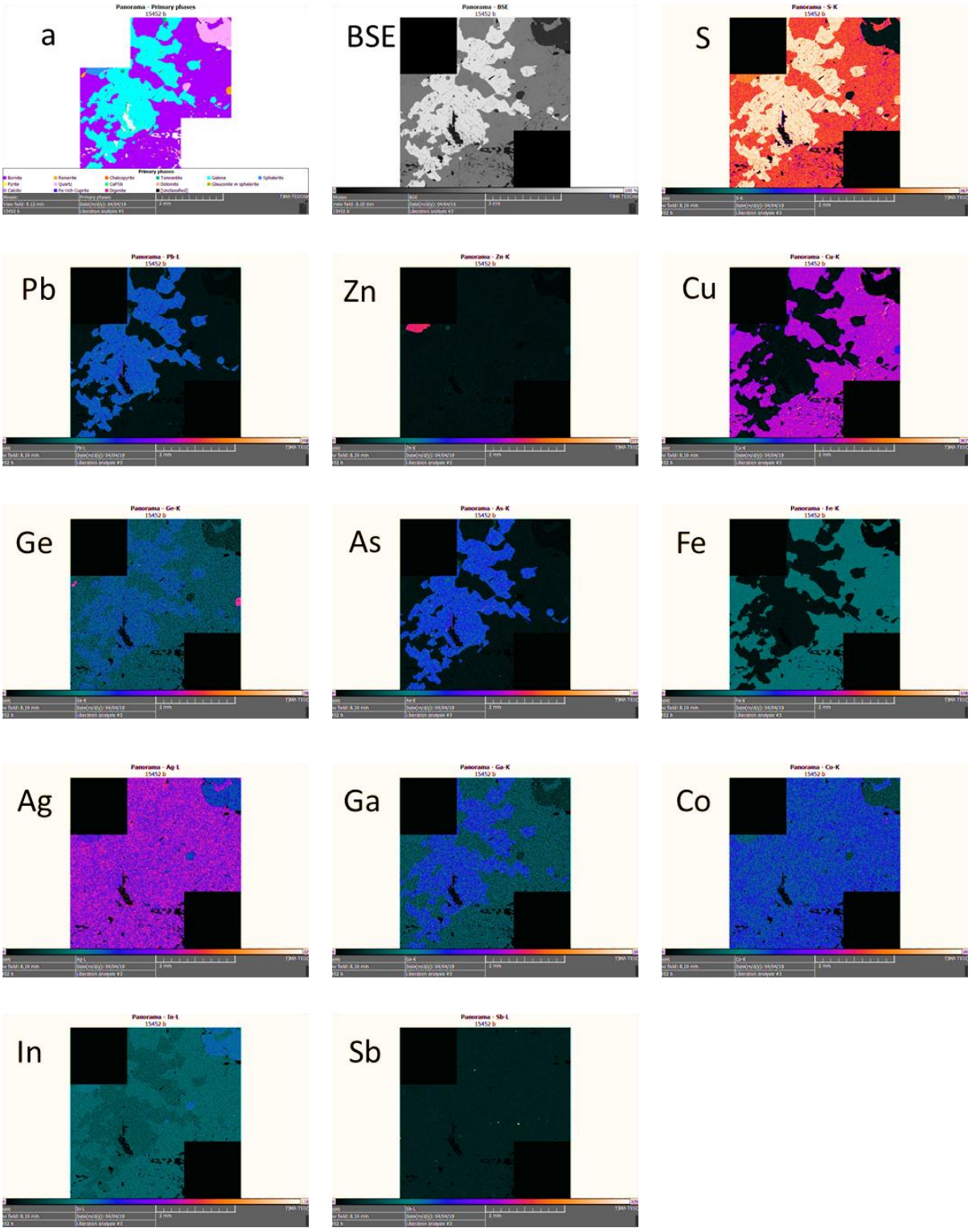

Figure 64: False colour phase map (a), backscatter image, and element maps of S, Pb, Zn, Cu, Ge, As, Fe, Ag, Ga, Co, In and Sb for a section of the polished thin section from thin section b from sample 15452.

In Figure 65, the Ge concentrates into the renierite and has a lesser concentration in galena and tennantite respectively. The galena is enriched in As and lesser Ga. The tennantite also contains a small concentration of Pb. The quartz is, once again, rich in In.

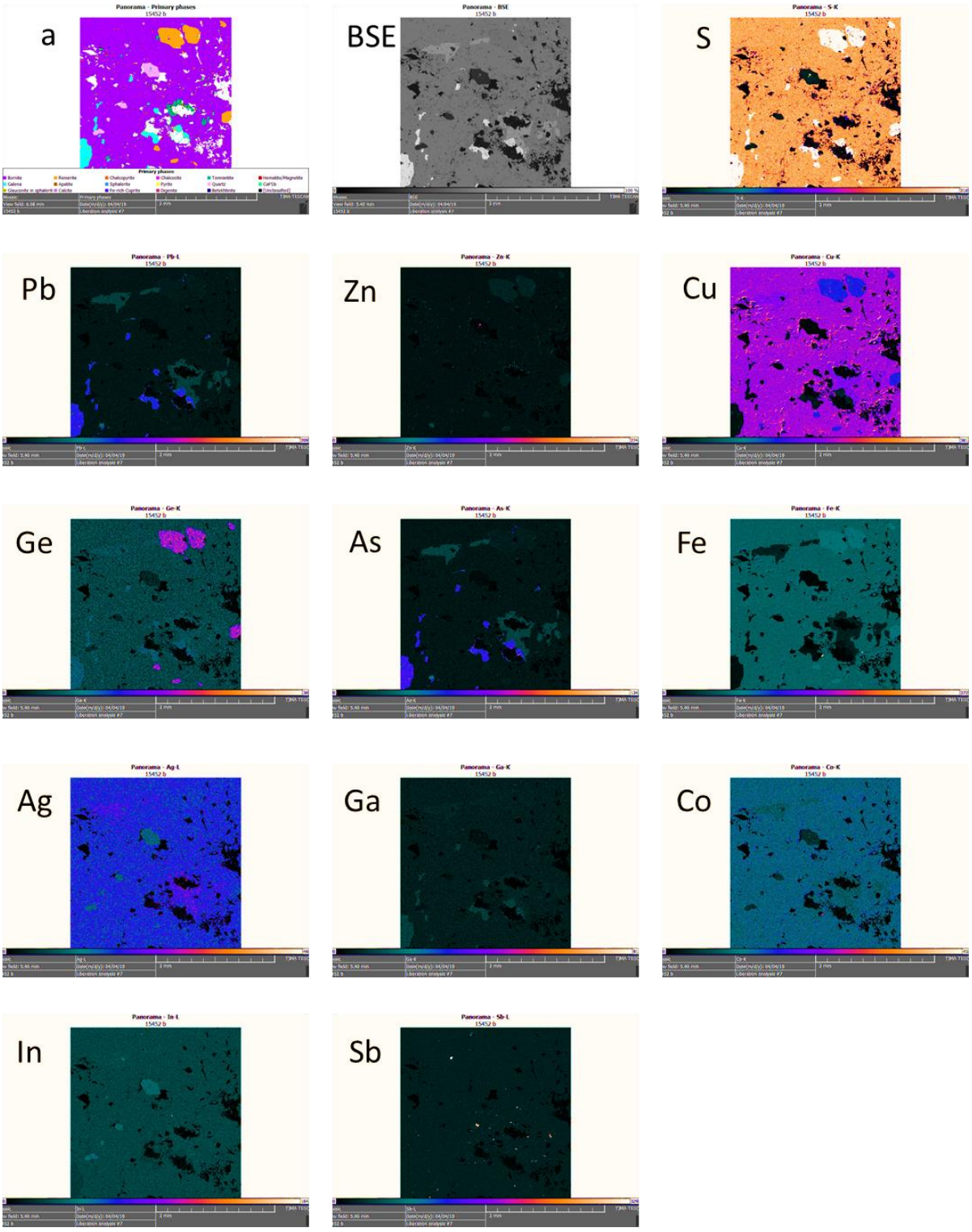

Figure 65: False colour phase map (a), backscatter image, and element maps of S, Pb, Zn, Cu, Ge, As, Fe, Ag, Ga, Co, In and Sb for a section of the polished thin section from thin section b from sample 15452.

Figure 66 shows Ge concentrating into the renierite. The rest of the Ge is concentrated into the galena in this area. The galena is also rich in As and Ga. The chalcopyrite has Co concentrated into it. In is most concentrated within the quartz, and interestingly, in the sphalerite.

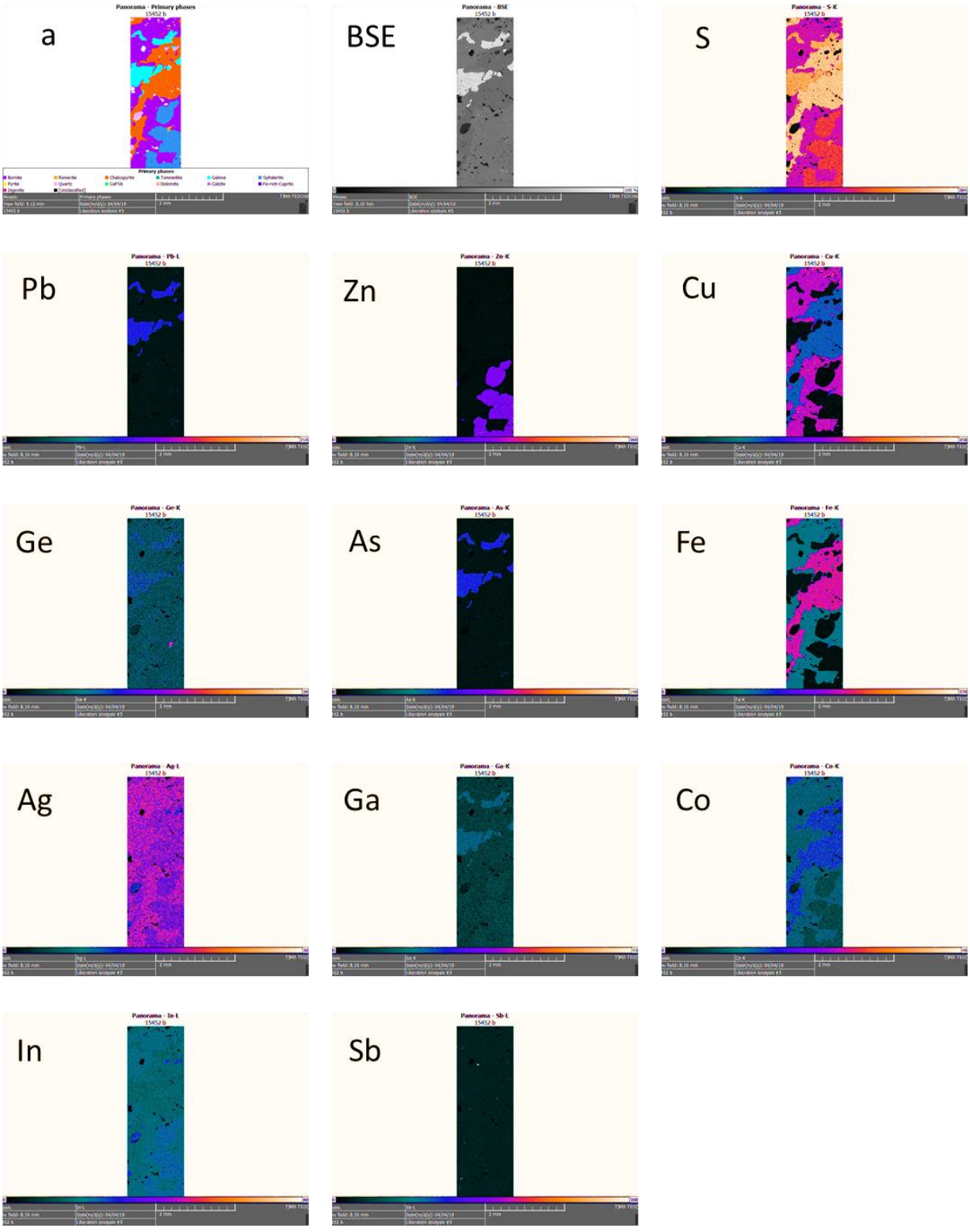

Figure 66: False colour phase map (a), backscatter image, and element maps of S, Pb, Zn, Cu, Ge, As, Fe, Ag, Ga, Co, In and Sb for a section of the polished thin section from thin section b from sample 15452.

Sample KP 2

Four areas were chosen to be scanned by the TIMA for this sample. The Ge concentrates into the renierite and galena in Figure 67. The galena is rich in As and Ga, and the tennantite is rich in Pb. Both the quartz and the sphalerite contain small concentrations of In.

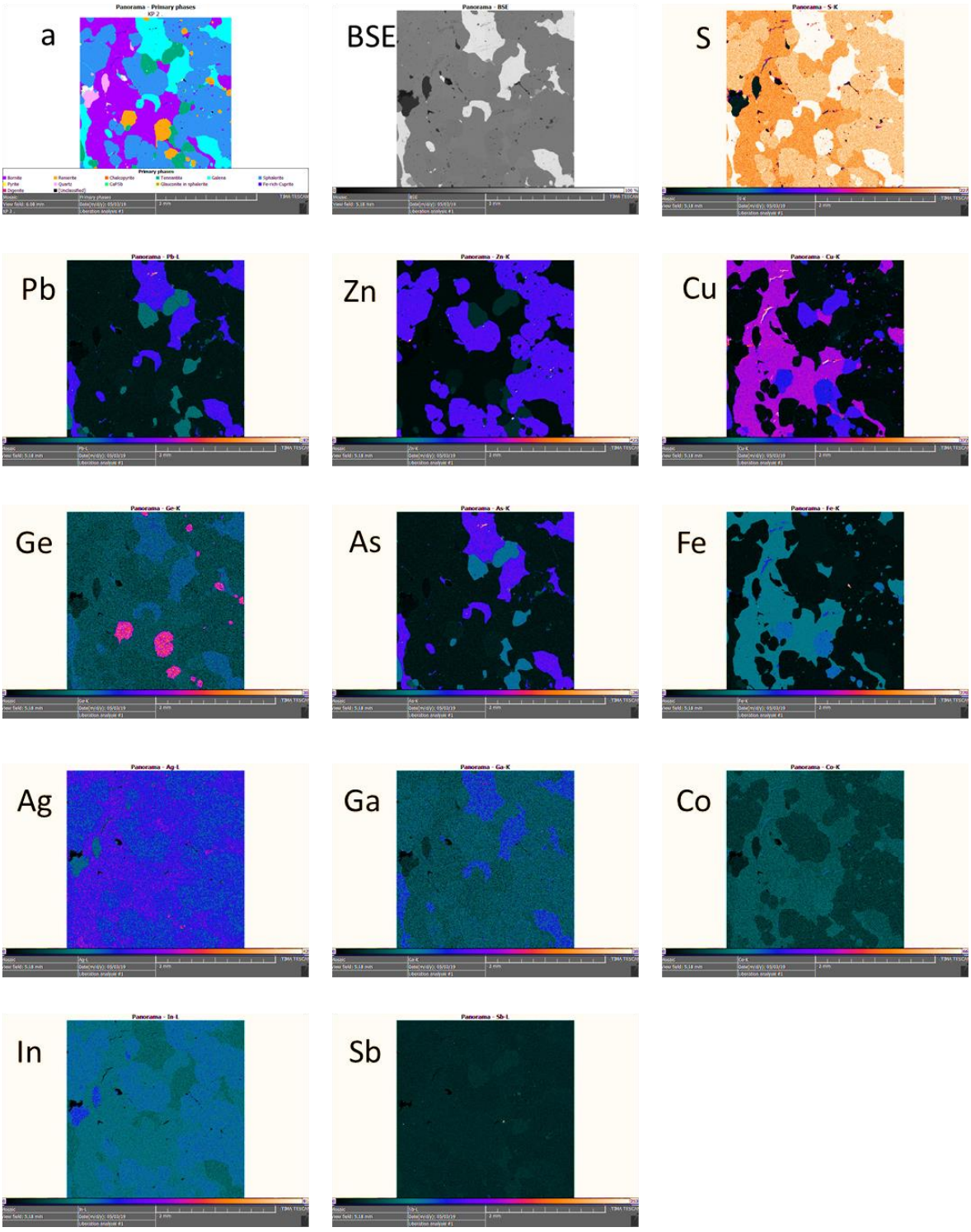

Figure 67: False colour phase map (a), backscatter image, and element maps of S, Pb, Zn, Cu, Ge, As, Fe, Ag, Ga, Co, In and Sb for a section of the polished thin section from sample KP 2.

Figure 68 shows the highest concentration of Ge to lie within the renierite, and lesser amounts into the galena. It also shows the galena is enriched with As and Ga. Co, interestingly, seems to concentrate into the chalcopyrite, galena, bornite and renierite. There appears to be a low concentration of Ag in the bornite and galena.

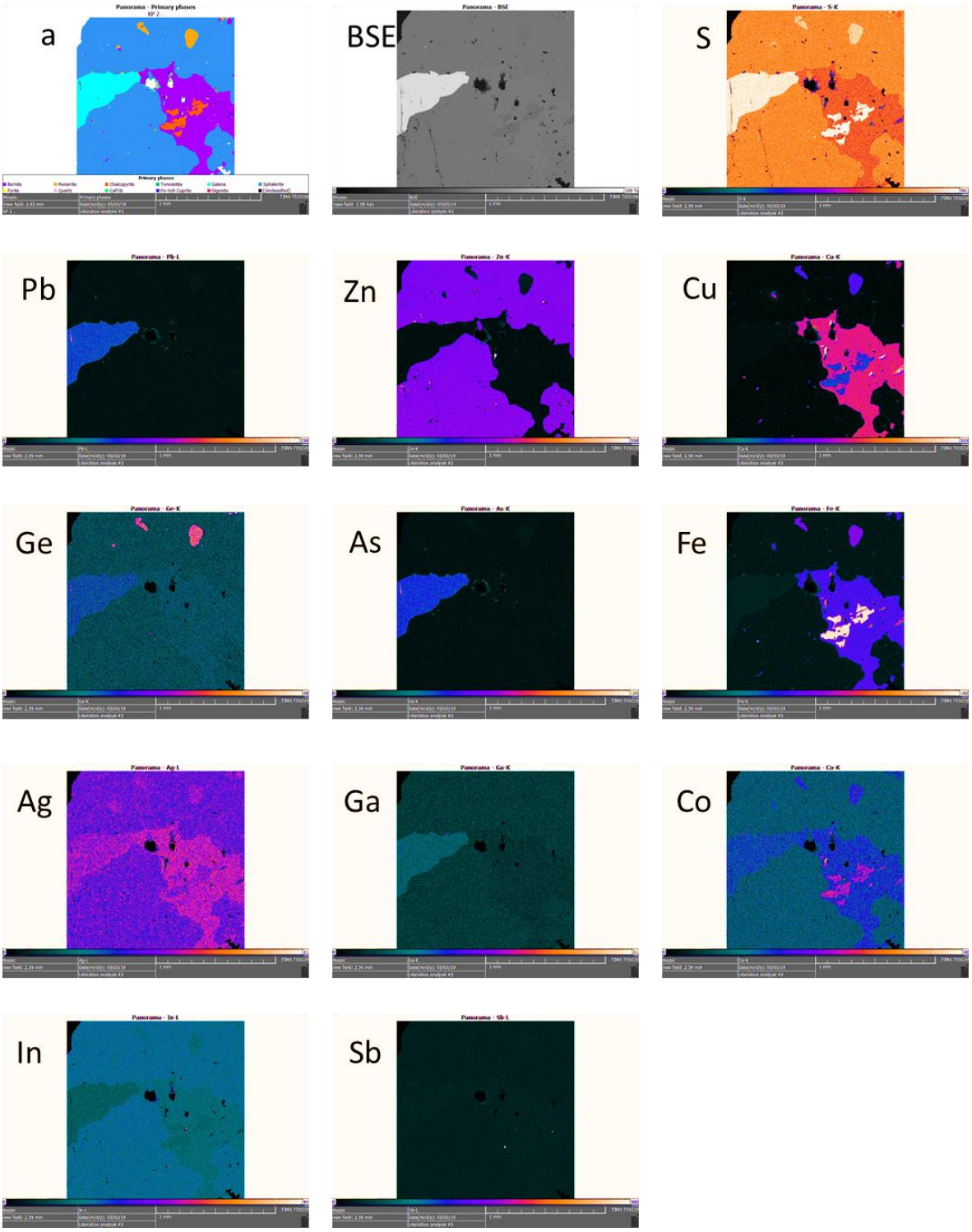

Figure 68: False colour phase map (a), backscatter image, and element maps of S, Pb, Zn, Cu, Ge, As, Fe, Ag, Ga, Co, In and Sb for a section of the polished thin section from sample KP 2.

Ge is seen to concentrate into renierite in Figure 69. Ge also concentrates into the galena. The galena is As and Ga enriched. There is a very low concentration of In in the sphalerite.

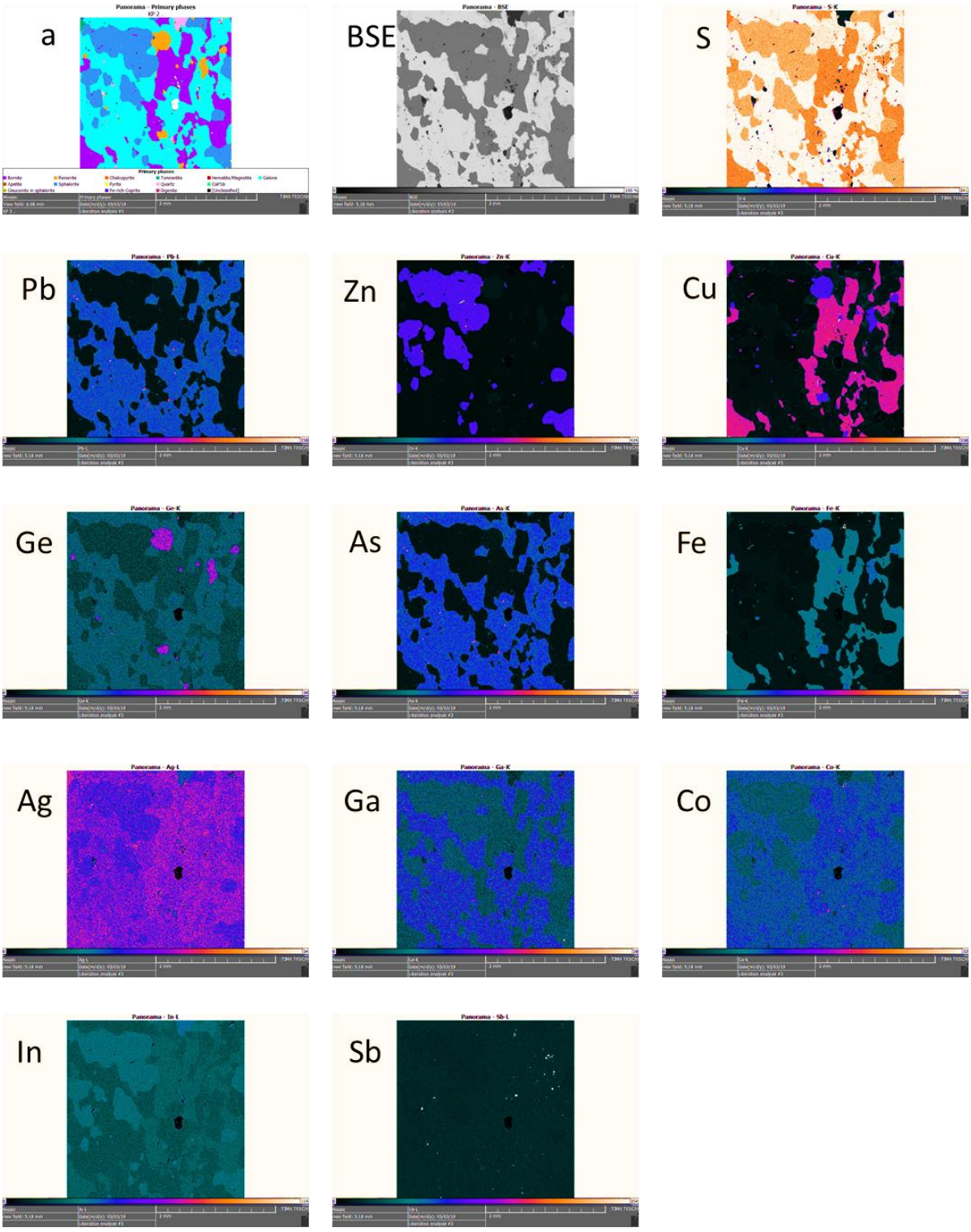

Figure 69: False colour phase map (a), backscatter image, and element maps of S, Pb, Zn, Cu, Ge, As, Fe, Ag, Ga, Co, In and Sb for a section of the polished thin section from sample KP 2.

Figure 70 shows the Ge is found to concentrate within the renierite and galena, respectively. The galena is As enriched and contains some Ga. The galena and bornite both seem to have Co concentrating into them.

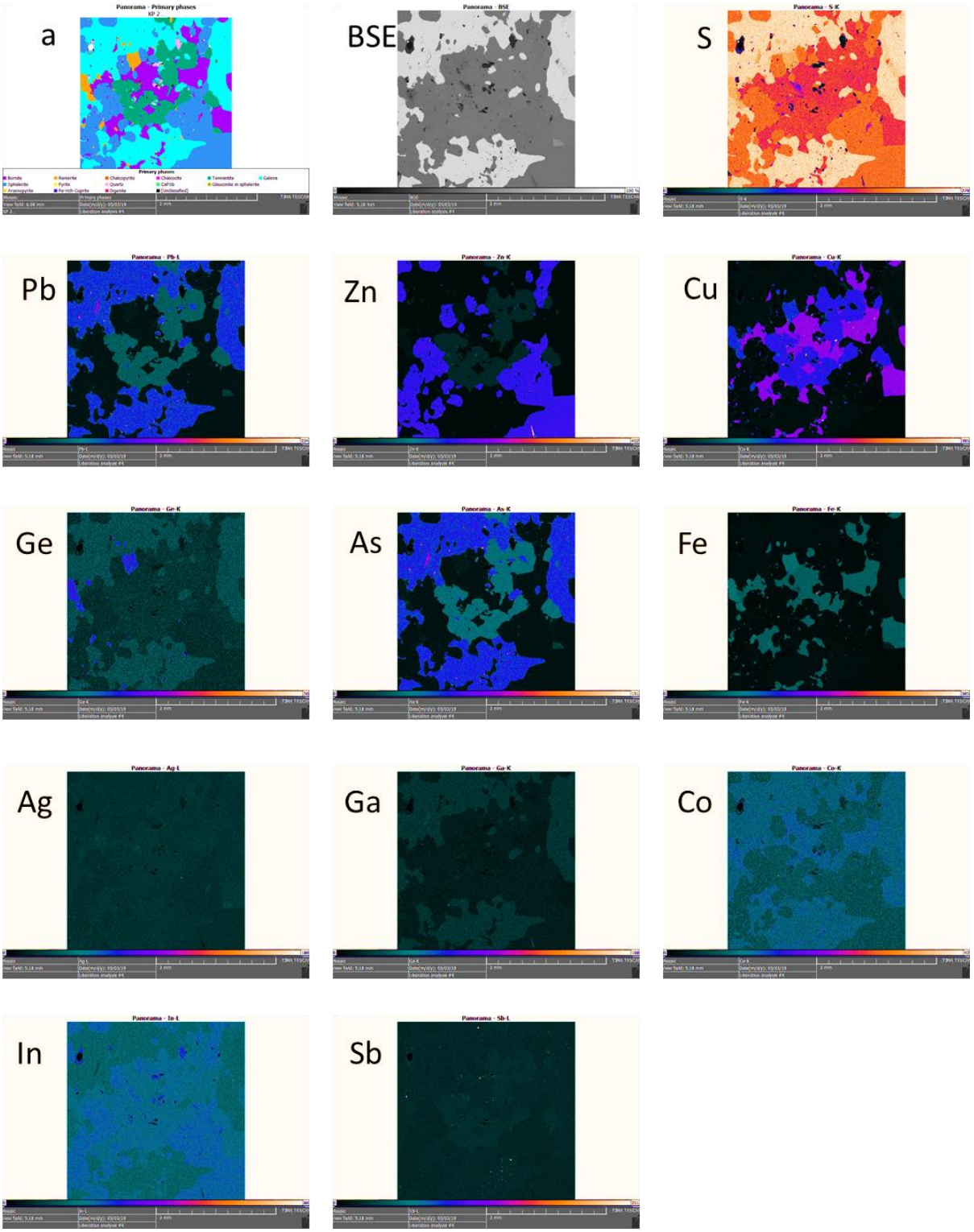

Figure 70: False colour phase map (a), backscatter image, and element maps of S, Pb, Zn, Cu, Ge, As, Fe, Ag, Ga, Co, In and Sb for a section of the polished thin section from sample KP 2.

Sample KP 17

Four areas on polished thin section KP 17 c were selected for analyses for this sample. Figure 71 shows renierite hosting the most of the Ge.

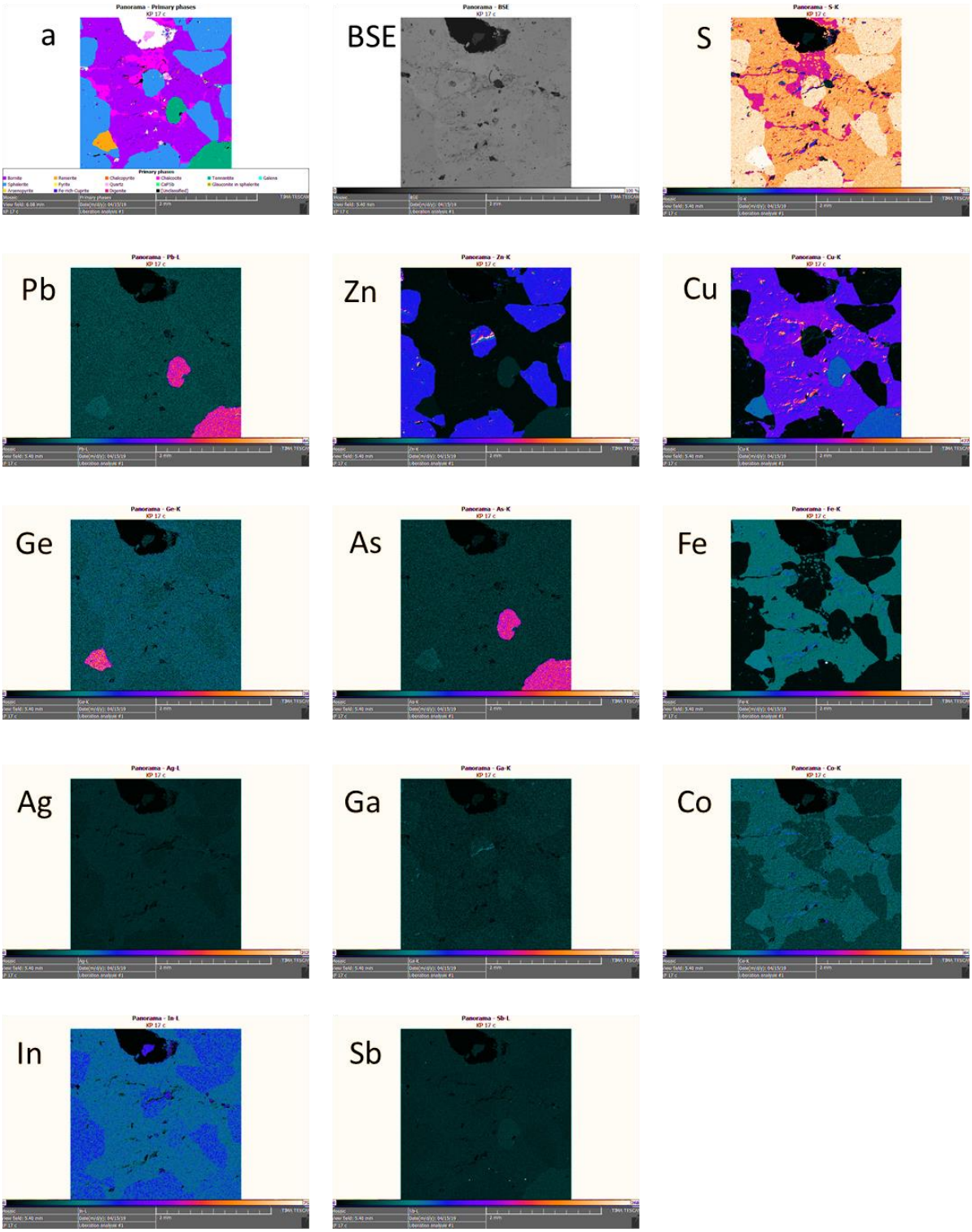

Figure 71: False colour phase map (a), backscatter image, and element maps of S, Pb, Zn, Cu, Ge, As, Fe, Ag, Ga, Co, In and Sb for a section of the polished thin section from sample KP 17.

The Ge concentration in Figure 72, the second area, is negligible.

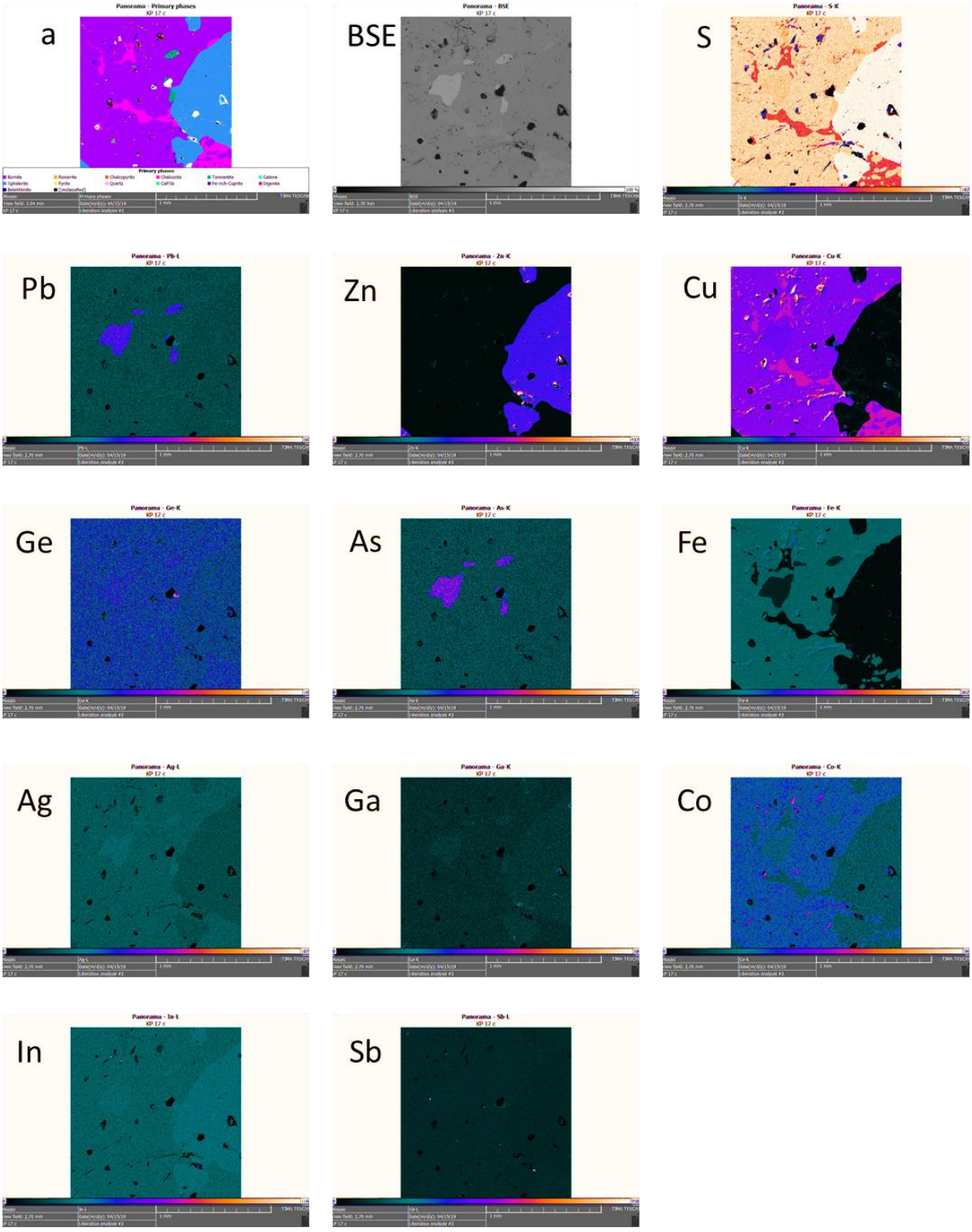

Figure 72: False colour phase map (a), backscatter image, and element maps of S, Pb, Zn, Cu, Ge, As, Fe, Ag, Ga, Co, In and Sb for a section of the polished thin section from sample KP 17.

Figure 73 shows insignificant Ge in this area. It does, however, show a new phase not noted in the previous scans. This Cu, Co and S rich phase is carrollite. The carrollite also contains some Ga. The sphalerite has a small concentration of In in it.

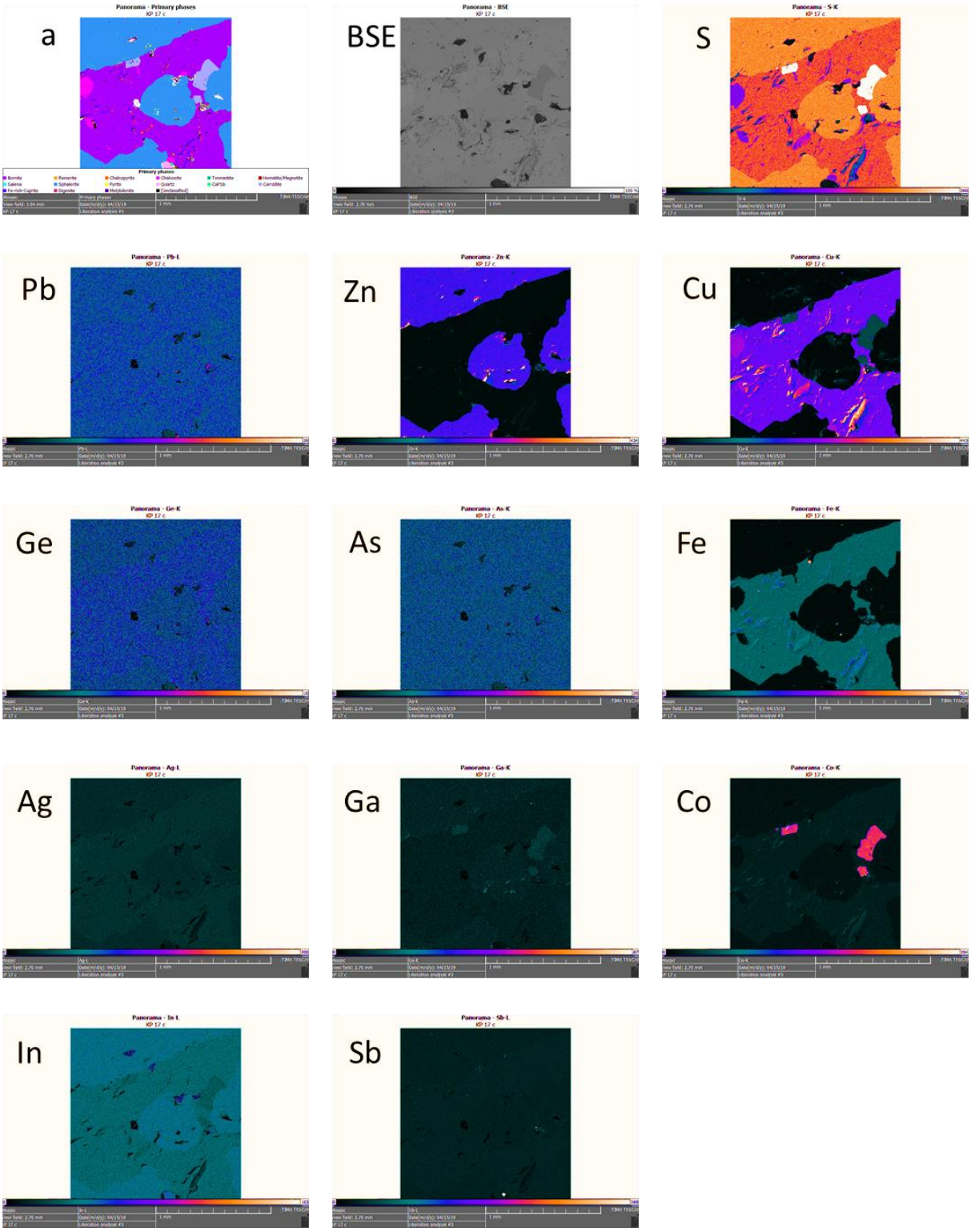

Figure 73: False colour phase map (a), backscatter image, and element maps of S, Pb, Zn, Cu, Ge, As, Fe, Ag, Ga, Co, In and Sb for a section of the polished thin section from sample KP 17.

Figure 74 shows a high concentration of Ge in renierite, and has a low concentration of Pb in it. One again, there is a small amount of In within the sphalerite.

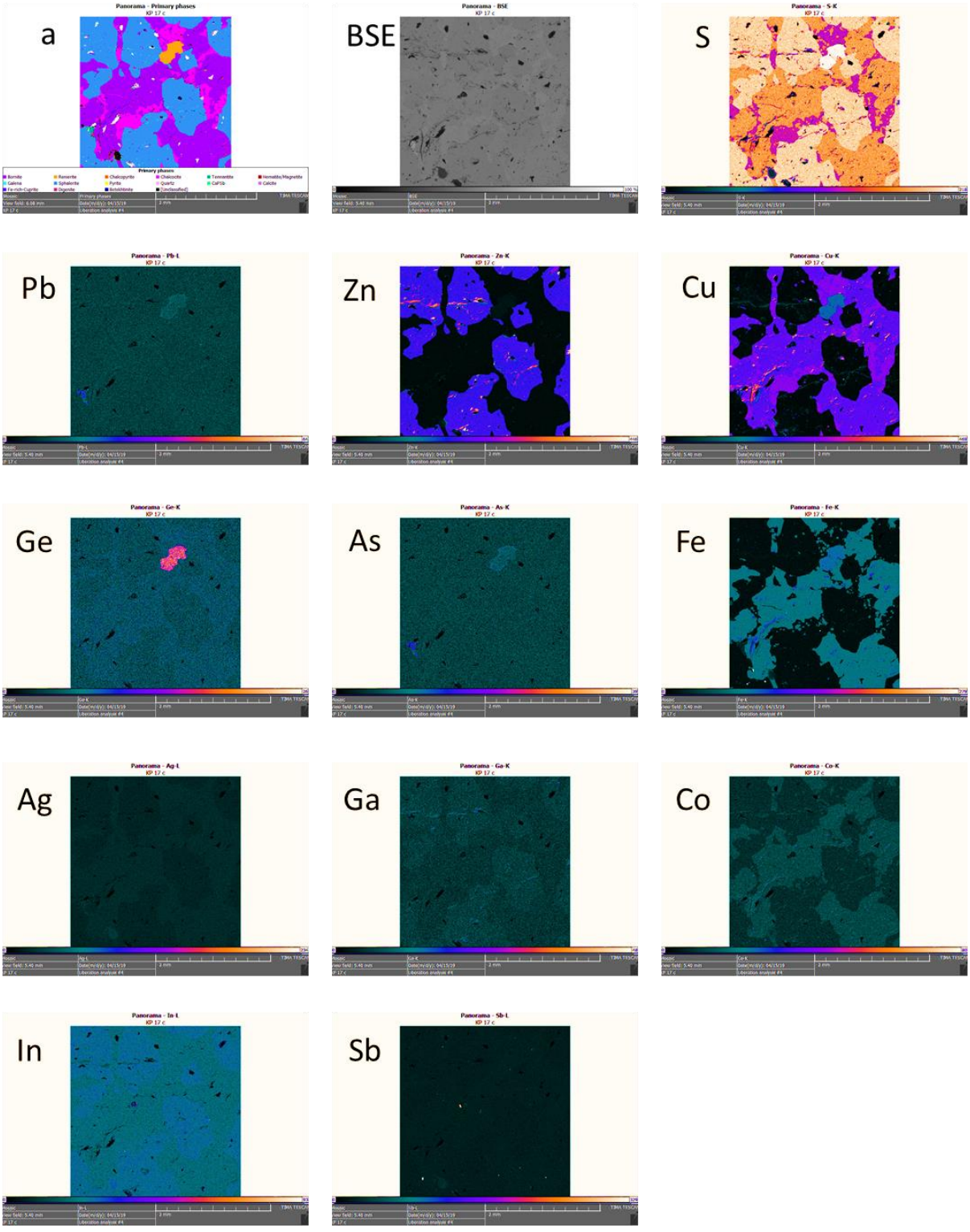

Figure 74: False colour phase map (a), backscatter image, and element maps of S, Pb, Zn, Cu, Ge, As, Fe, Ag, Ga, Co, In and Sb for a section of the polished thin section from sample KP 17.

Appendix D

Scanning electron microscopy and mineral analysis for the Tsumeb sample suite

D.1. Bornite-dominant-assemblage

Sample 125

Two areas were selected to create element maps for this sample. Figure 1 shows the false colour phase map, back scatter image and element maps for the first area of this sample. The Ge is shown to concentrate within the renierite. The renierite also has some Pb and As within it. The tennantite is enriched in Pb and Zn. The renierite, as well as the bornite, has a low concentration of Co.

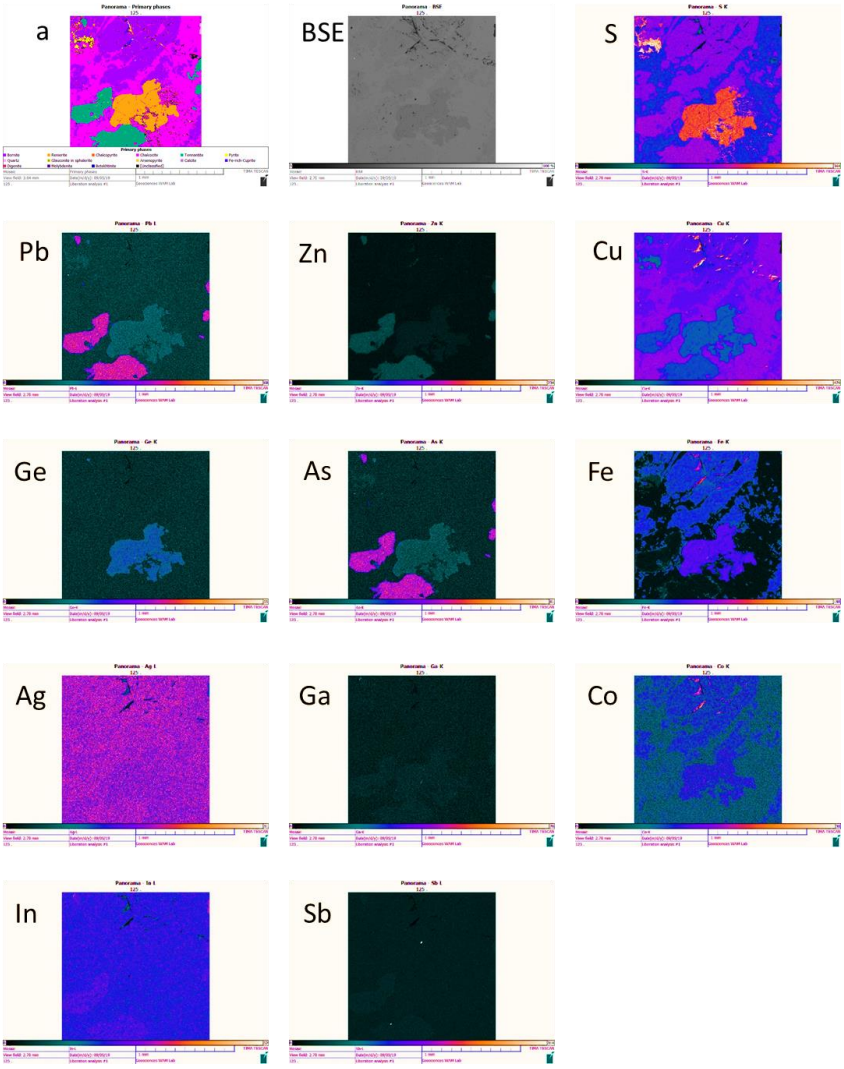

Figure 1: False colour phase map (a), backscatter image, and element maps of S, Pb, Zn, Cu, Ge, As, Fe, Ag, Ga, Co, In and Sb for an area on the polished ore block from sample 125.

The second area scanned for this sample can be seen in Figure 2. These element maps show the Ge concentrating into the renierite. The tennantite contains some Pb, Zn and Sb. The sphalerite has some In in it. The renierite and bornite are enriched in Co.

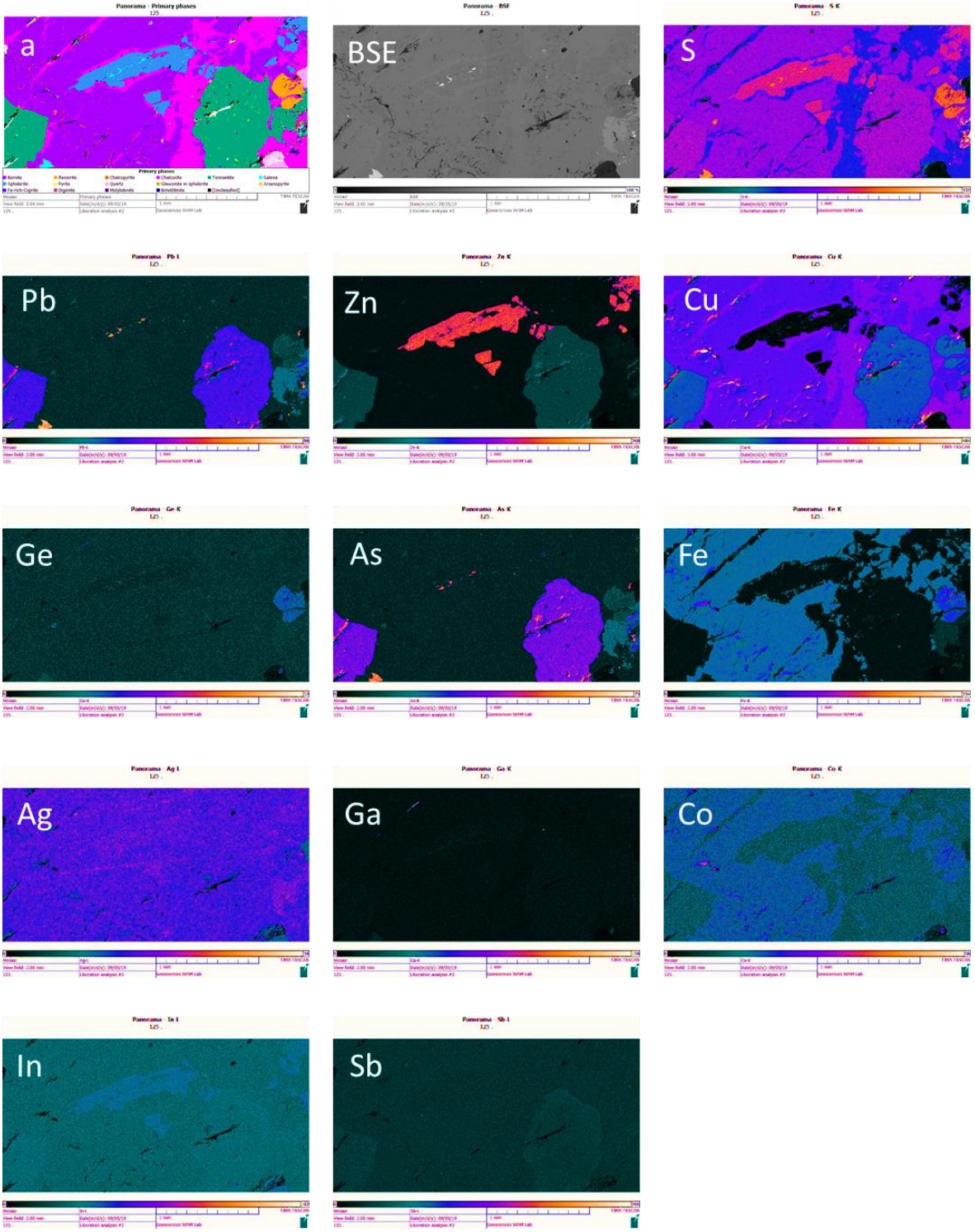

Figure 2: False colour phase map (a), backscatter image, and element maps of S, Pb, Zn, Cu, Ge, As, Fe, Ag, Ga, Co, In and Sb for an area on the polished ore block from sample 125.

Sample 253 b is shown in Figure 3. The Ge in this sample is found to concentrate within the galena. The galena is also enriched in As and Ga.

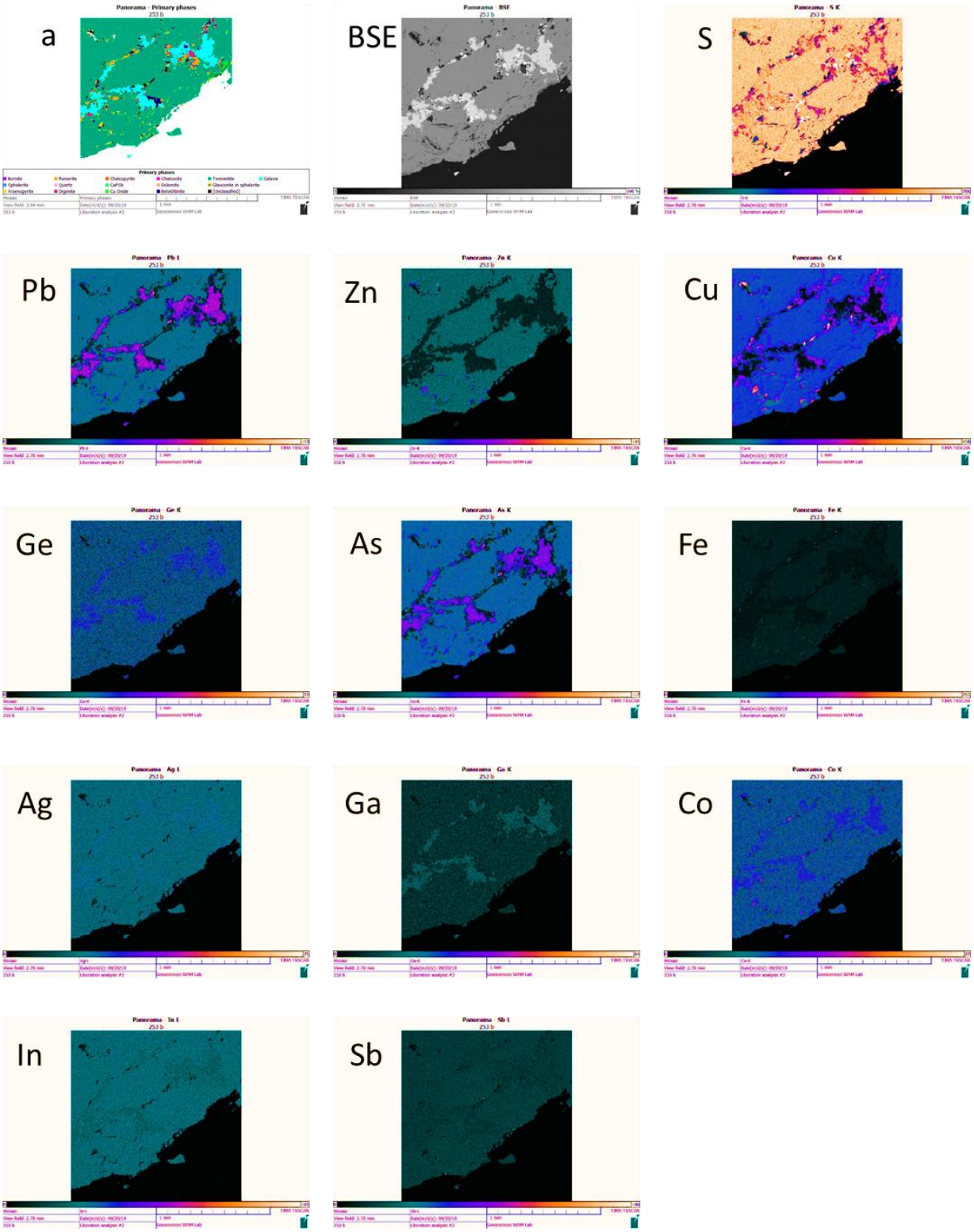

Figure 3: False colour phase map (a), backscatter image, and element maps of S, Pb, Zn, Cu, Ge, As, Fe, Ag, Ga, Co, In and Sb for an area on the polished ore block from sample 253 b.

Sample 717

One area was selected for this sample. The resultant maps can be seen in Figure 4. The Ge is found to concentrate within the galena, and to a lesser extent within the chalcocite. The galena is rich in As and Ga. The pyrite contains trace amounts of Co. The betekhtinite (the previously unidentified grey mineral) is rich in As.

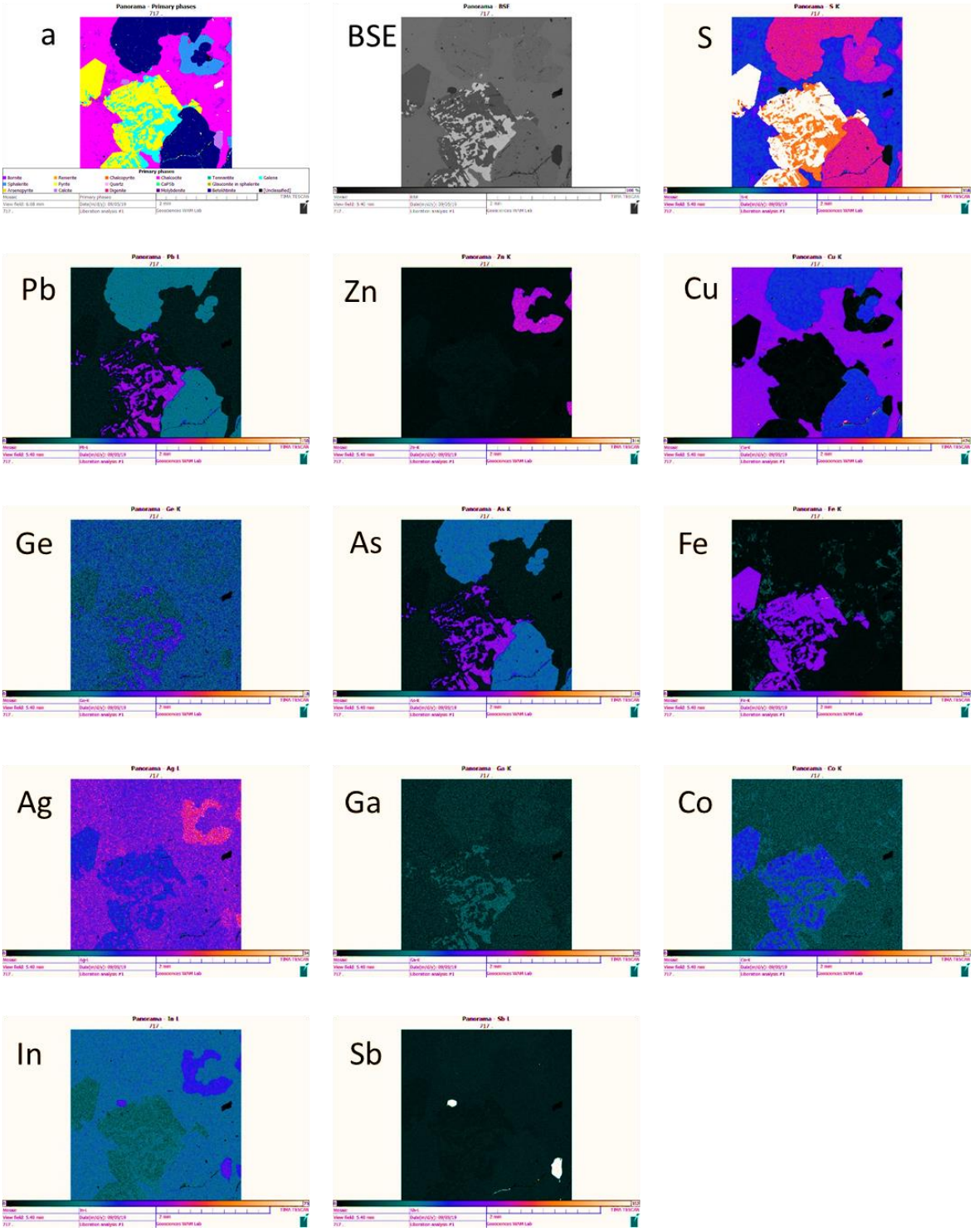

Figure 4: False colour phase map (a), backscatter image, and element maps of S, Pb, Zn, Cu, Ge, As, Fe, Ag, Ga, Co, In and Sb for an area on the polished ore block from sample 717.

Sample TS 3

Two areas were selected for this sample. Petrographic analysis of this sample shows a network of renierite and germanite. The element maps for the first area is shown in Figure 5. Here, the false colour primary phase map shows a large section of renierite, when in fact this area is a network of renierite and germanite. The TIMA software struggles to differentiate the two phases as they are very similar chemically. This network can be easily seen in the Ge map, the Ge is more highly concentrated in the germanite than the renierite. The tennantite in this sample is enriched with Pb and Zn. The calcite surrounding the renierite and germanite is falsely rich in Sb and In.

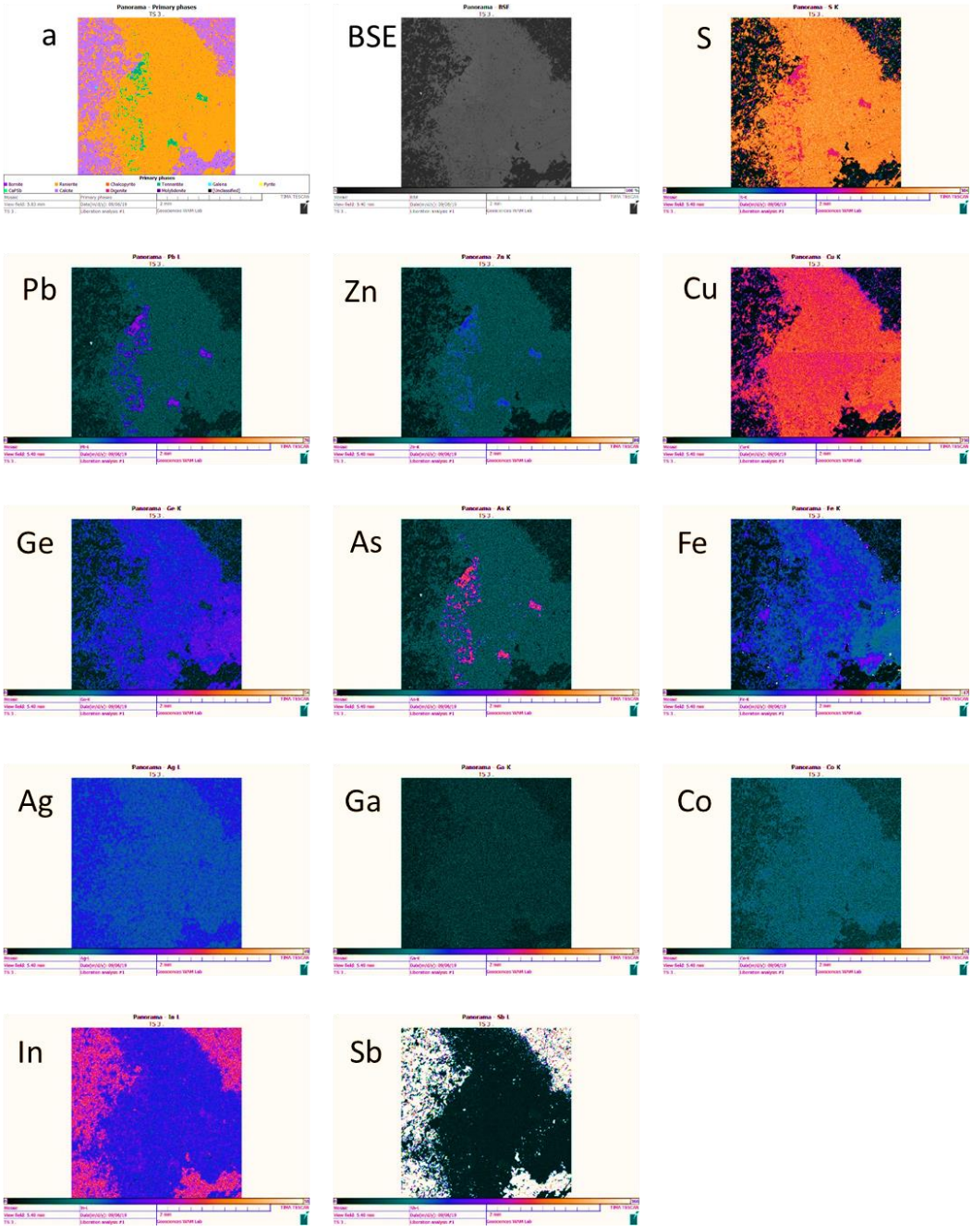

Figure 5: False colour phase map (a), backscatter image, and element maps of S, Pb, Zn, Cu, Ge, As, Fe, Ag, Ga, Co, In and Sb for an area on the polished ore block from sample TS 3.

The second area for sample TS 3 can be seen in Figure 6. The false colour primary phase map, again shows only renierite, when germanite should also be present. The germanite can be distinguished from the renierite by looking at the Ge element map. The germanite has a higher concentration of Ge than the renierite. Galena contains less Ge than the germanite and renierite. The galena also has high concentrations of As and Ga. The tennantite has some Pb in it. The pyrite has some Co concentrating into it. Once again, the surrounding calcite is falsely rich in Sb and In.

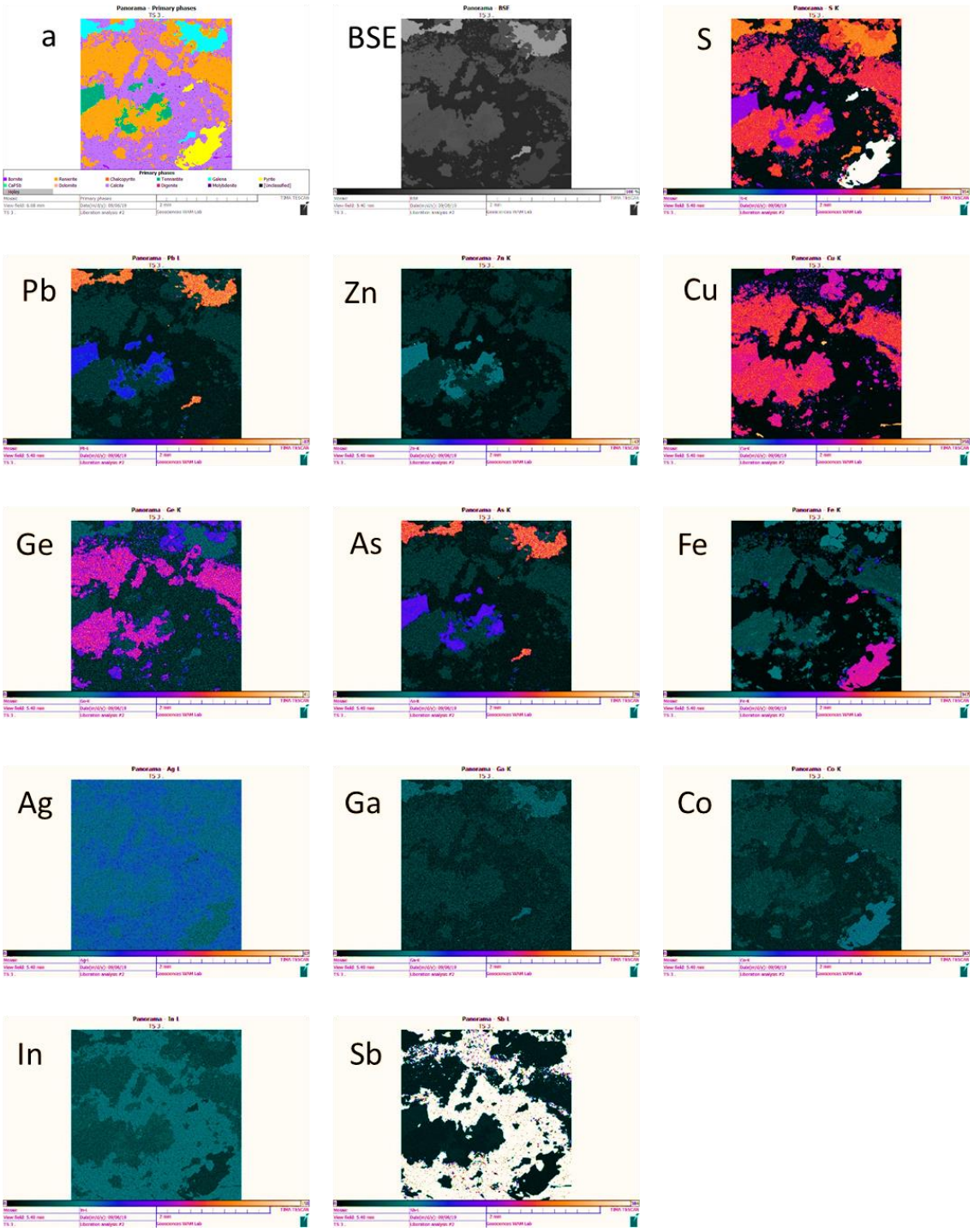

Figure 6: False colour phase map (a), backscatter image, and element maps of S, Pb, Zn, Cu, Ge, As, Fe, Ag, Ga, Co, In and Sb for an area on the polished ore block from sample TS 3.

Sample 263

Two areas were selected for TIMA scans from this sample. The results from the first scan can be seen in Figure 7. The Ge has concentrated into the galena, as has As and Ga. The tennantite contains Pb and Zn. The bornite and chalcocite are rich in Co. All the sulphides in this area appear to have some trace of Ag.

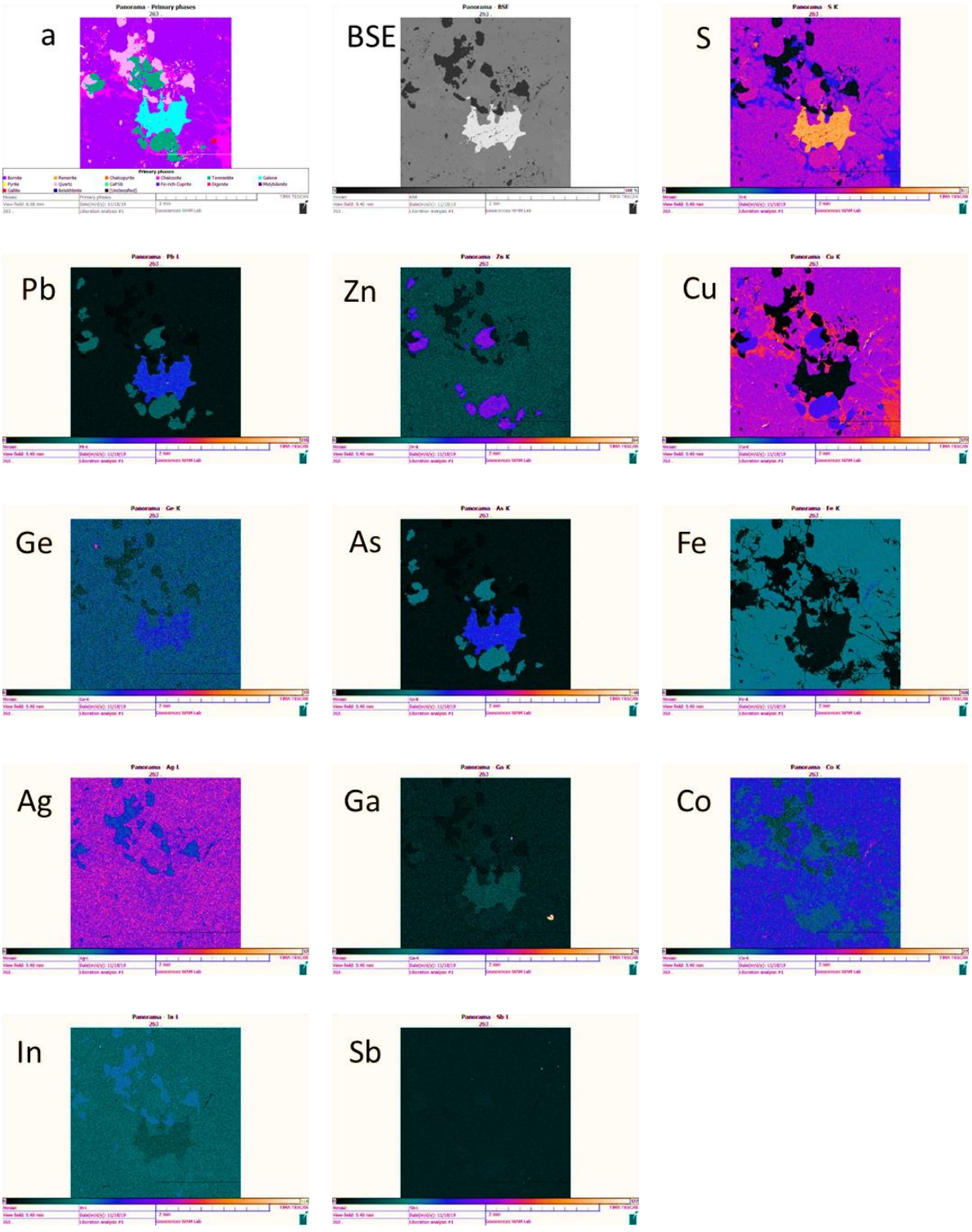

Figure 7: False colour phase map (a), backscatter image, and element maps of S, Pb, Zn, Cu, Ge, As, Fe, Ag, Ga, Co, In and Sb for an area on the polished ore block from sample 263.

The second area shows the Ge concentrating into the renierite (Figure 8). The tennantite is enriched in Pb.

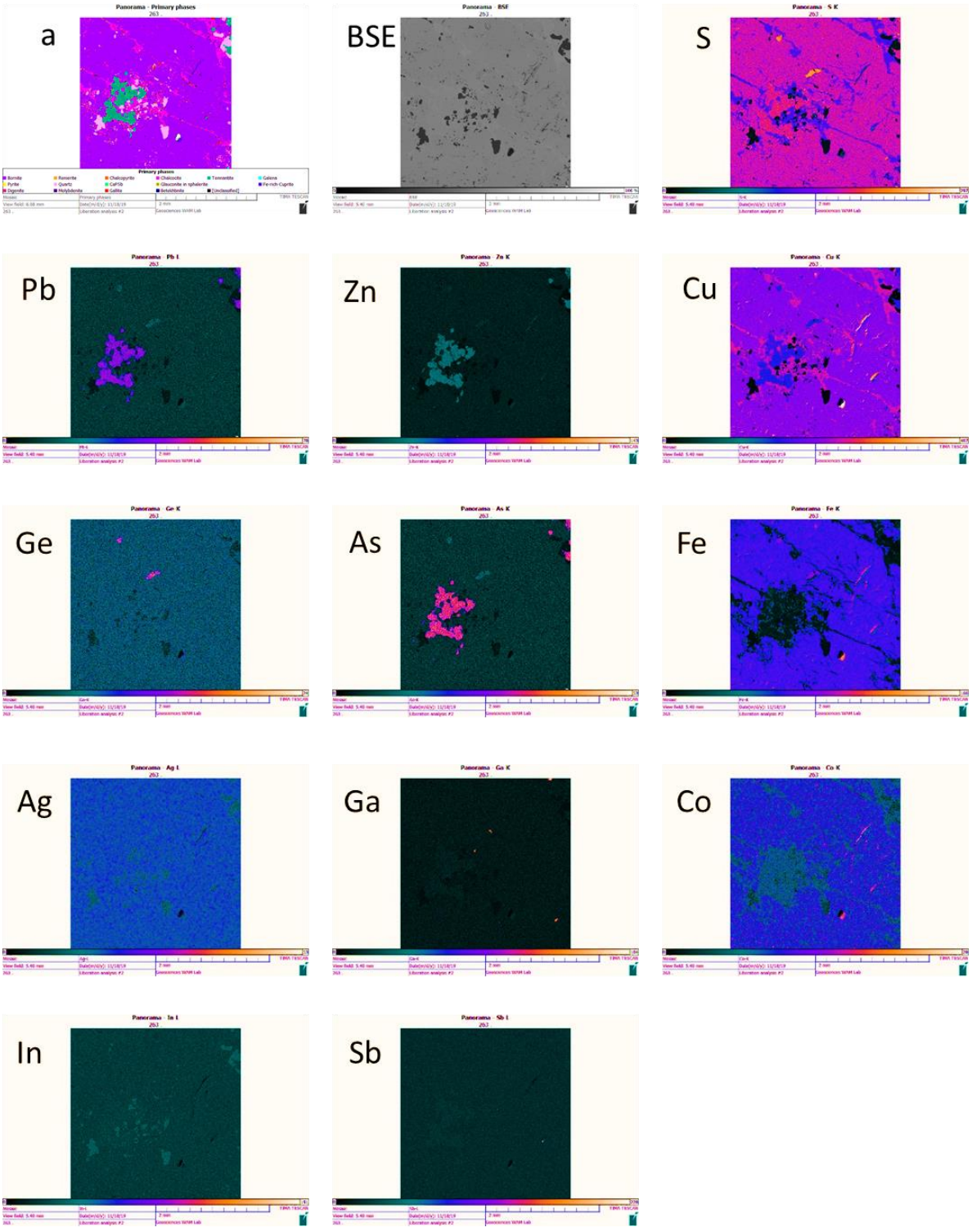

Figure 8: False colour phase map (a), backscatter image, and element maps of S, Pb, Zn, Cu, Ge, As, Fe, Ag, Ga, Co, In and Sb for an area on the polished ore block from sample 263.

Sample 333

Three areas were selected for this area. The first area is seen in Figure 9. It shows a slight Ge concentration in the sulphide phases. The tennantite, digenite, galena and betekhtinite have strong peaks of As and Pb.

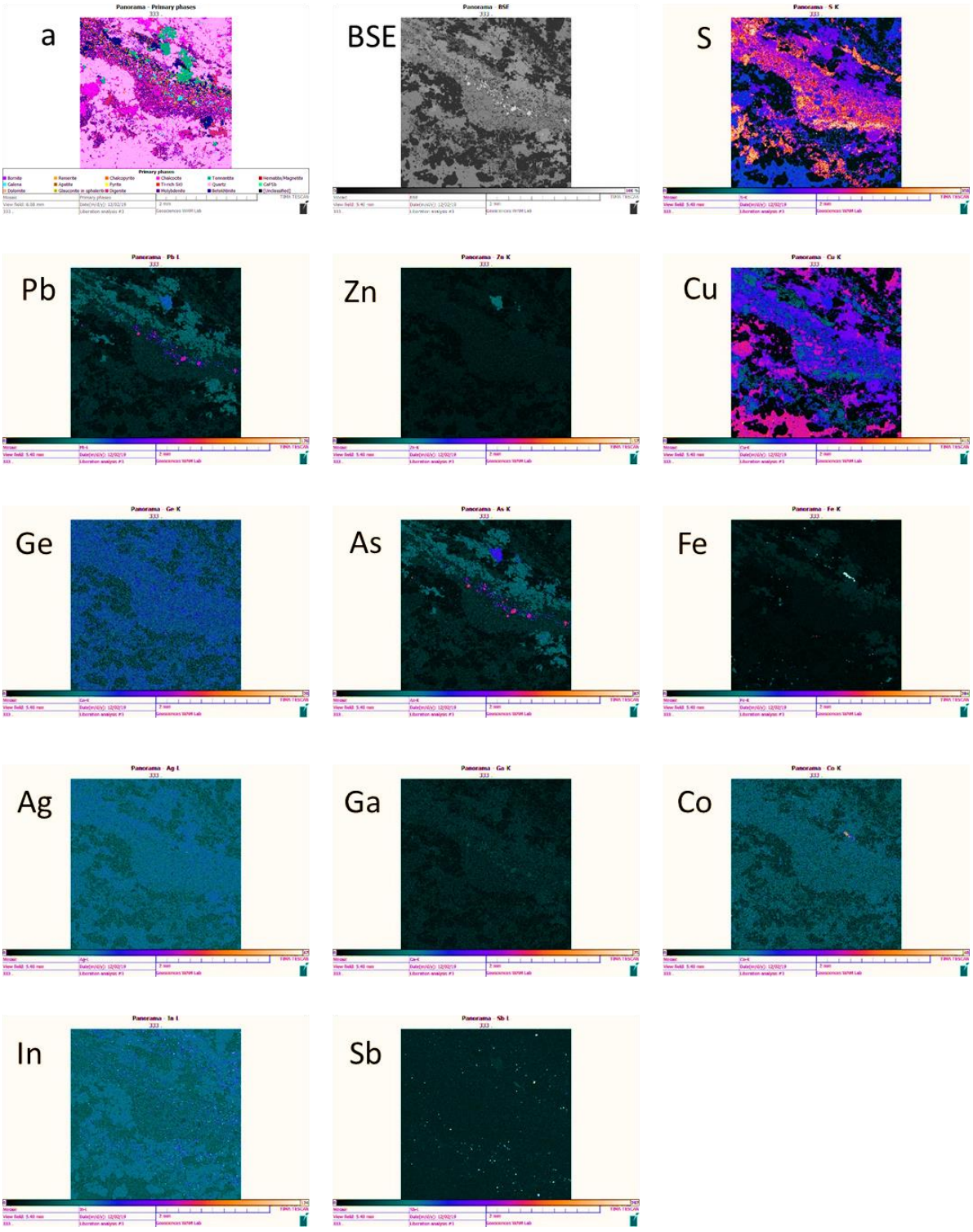

Figure 9: False colour phase map (a), backscatter image, and element maps of S, Pb, Zn, Cu, Ge, As, Fe, Ag, Ga, Co, In and Sb for an area on the polished ore block from sample 333.

The second area, Figure 10, shows a uniform concentration of Ge within the sulphide phases. The tennantite is enriched in Pb and Zn. The betekhtinite is enriched with As.

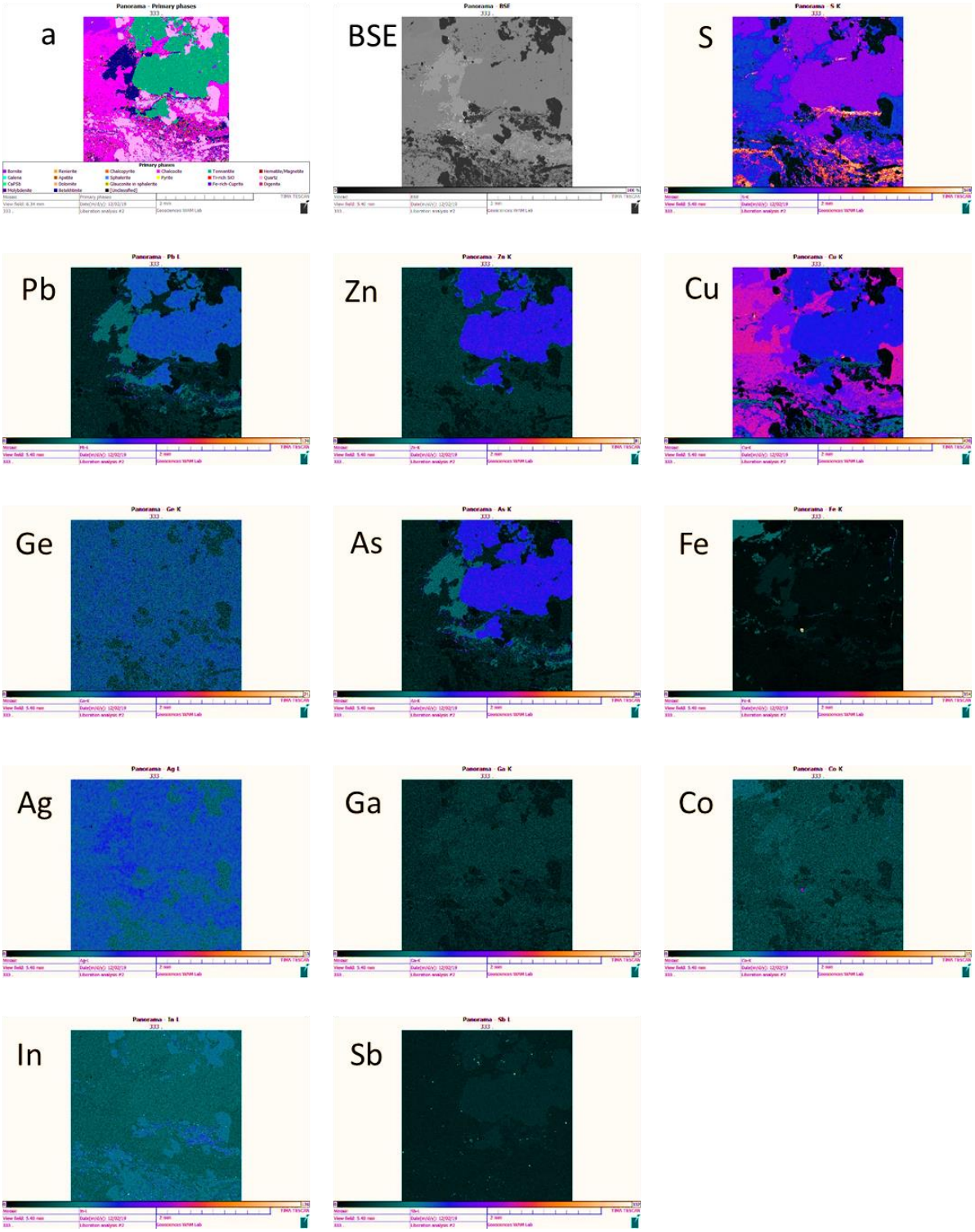

Figure 10: False colour phase map (a), backscatter image, and element maps of S, Pb, Zn, Cu, Ge, As, Fe, Ag, Ga, Co, In and Sb for an area on the polished ore block from sample 333.

The final area for this sample, Figure 11, shows the Ge concentrating into the galena, and to a lesser extent in the surrounding Cu-sulphides. The galena is also enriched in As and Ga. All the sulphides in this area contain some Co and Ag, with most of the Ag concentrating into the betekhtinite.

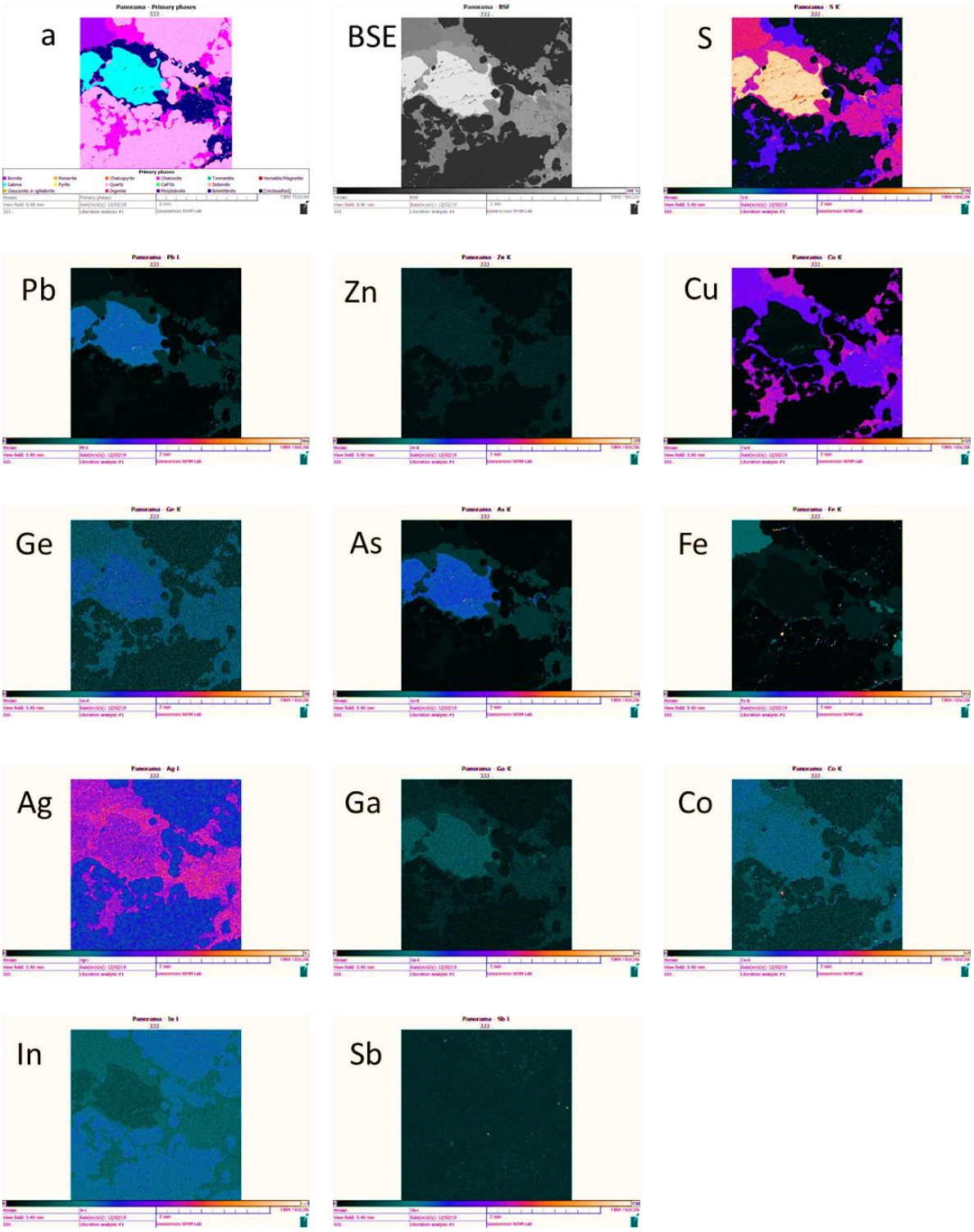

Figure 11: False colour phase map (a), backscatter image, and element maps of S, Pb, Zn, Cu, Ge, As, Fe, Ag, Ga, Co, In and Sb for an area on the polished ore block from sample 333.

D.2. Tennantite-dominant assemblage

Sample TS 7

Three areas were selected for this sample. Both germanite and renierite were visually identified in this sample. Figure 12 shows the first area. Here, the renierite in the false colour primary phase map is actually germanite, which is where most of the Ge concentrates. Ge, to a lesser extent, also concentrates into the galena. The galena also has As, Ga and Co concentrating into it.

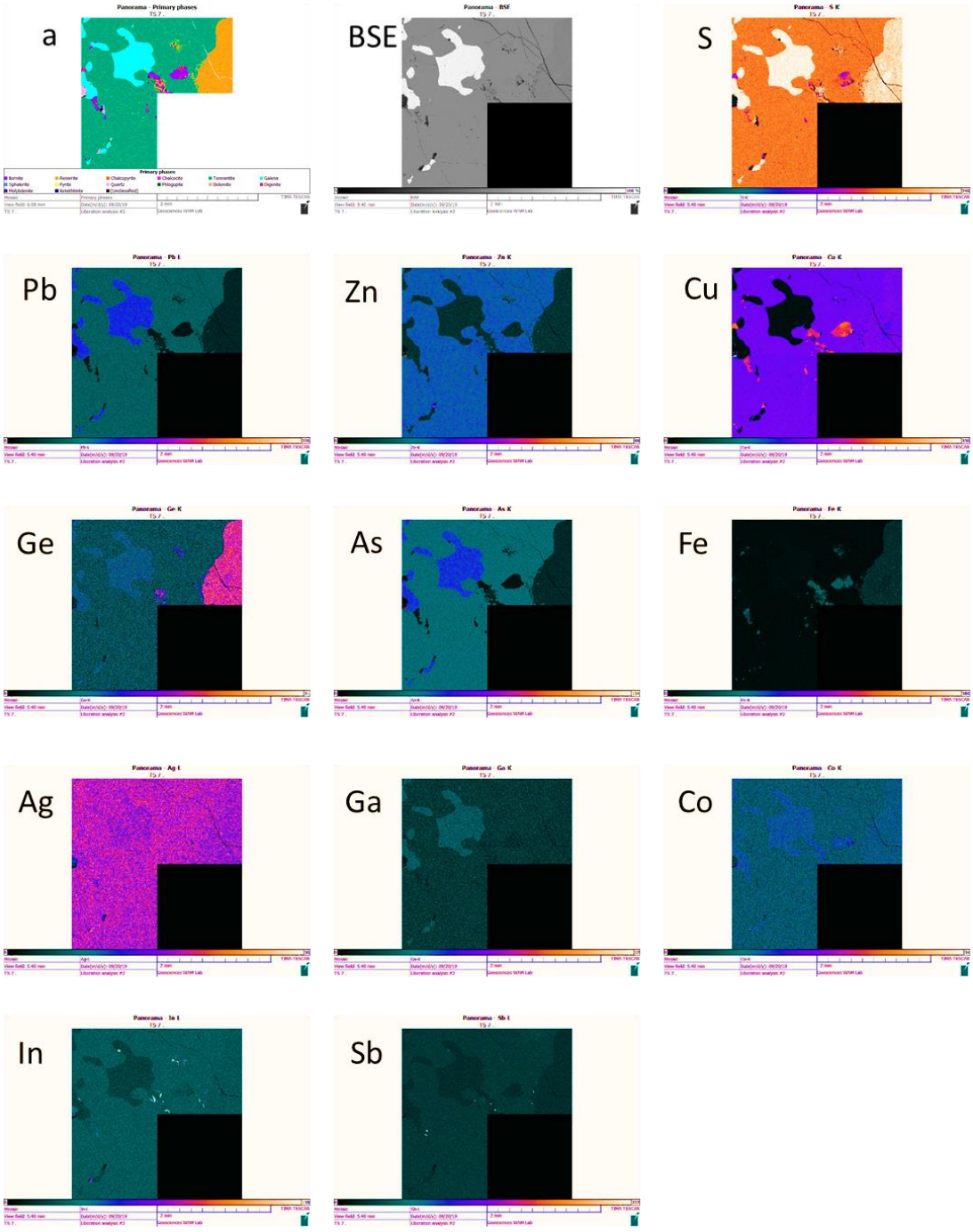

Figure 12: False colour phase map (a), backscatter image, and element maps of S, Pb, Zn, Cu, Ge, As, Fe, Ag, Ga, Co, In and Sb for an area on the polished ore block from sample TS 7.

Figure 13, the second area for this sample, once again shows renierite in the place of germanite in the false colour primary phase map. This germanite is where all the Ge concentrates. The tennantite has Pb concentrated into it. The bornite contains some Co. The dolomite is rich in Sb.

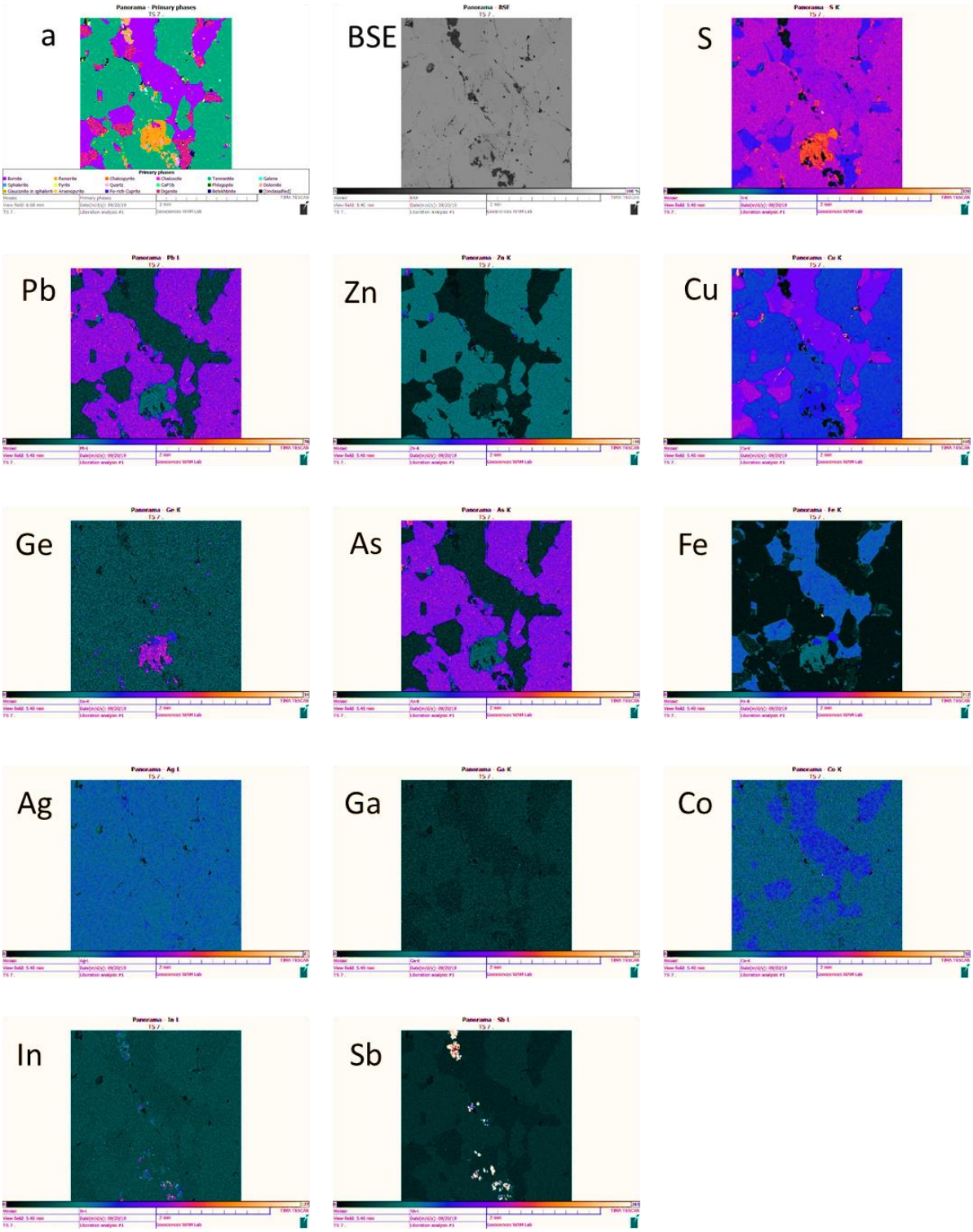

Figure 13: False colour phase map (a), backscatter image, and element maps of S, Pb, Zn, Cu, Ge, As, Fe, Ag, Ga, Co, In and Sb for an area on the polished ore block from sample TS 7.

Figure 14 shows the third area for this sample. Renierite is again in place of the germanite in the false colour primary phase map. The Ge all concentrates into the germanite. The tennantite is enriched in Pb.

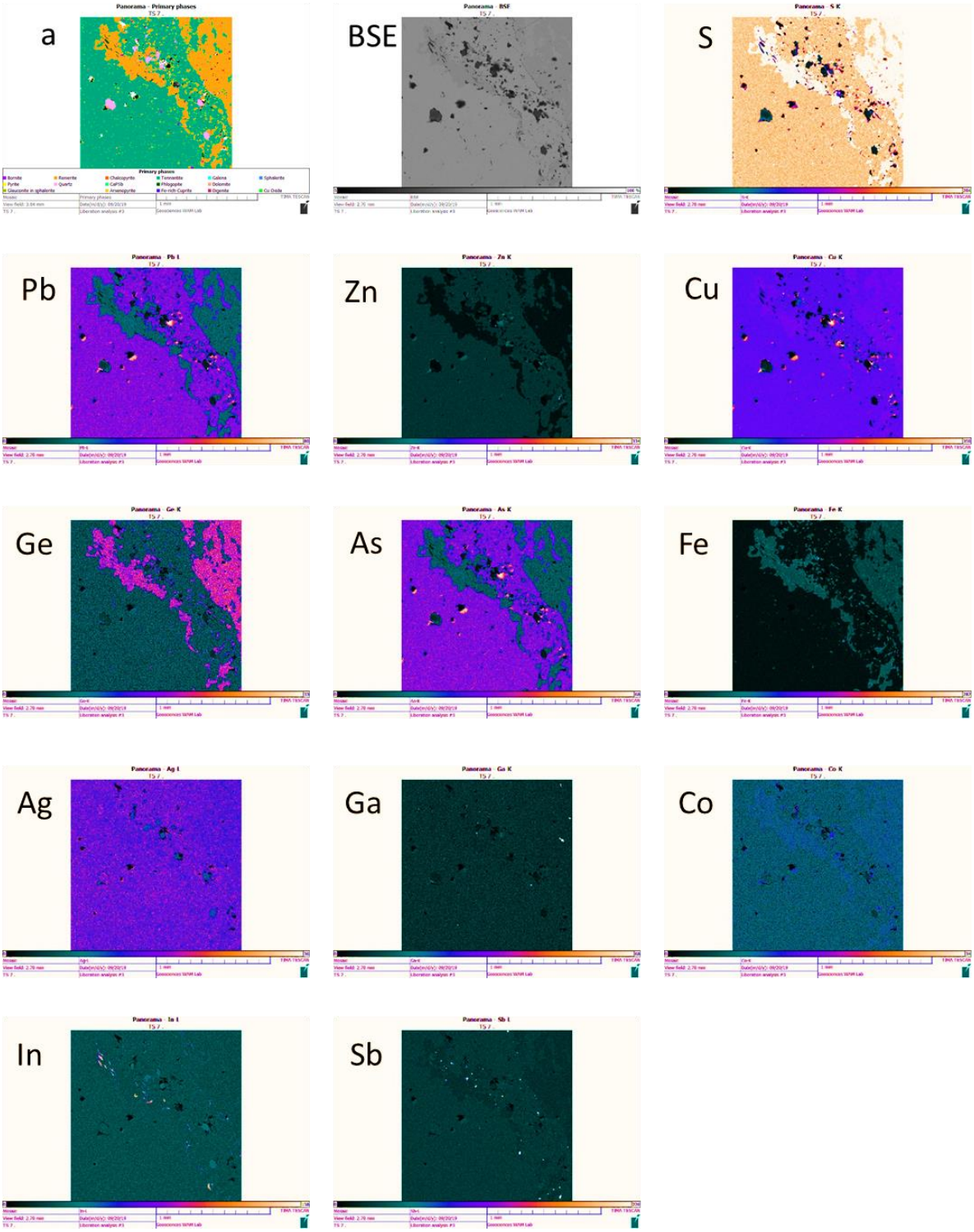

Figure 14: False colour phase map (a), backscatter image, and element maps of S, Pb, Zn, Cu, Ge, As, Fe, Ag, Ga, Co, In and Sb for an area on the polished ore block from sample TS 7.

Sample 99A b

Two areas were selected for this sample. The first area is represented in Figure 15. Here, the Ge is seen to concentrate into the galena, as does the As, Ga and Co. The quartz has some In within it.

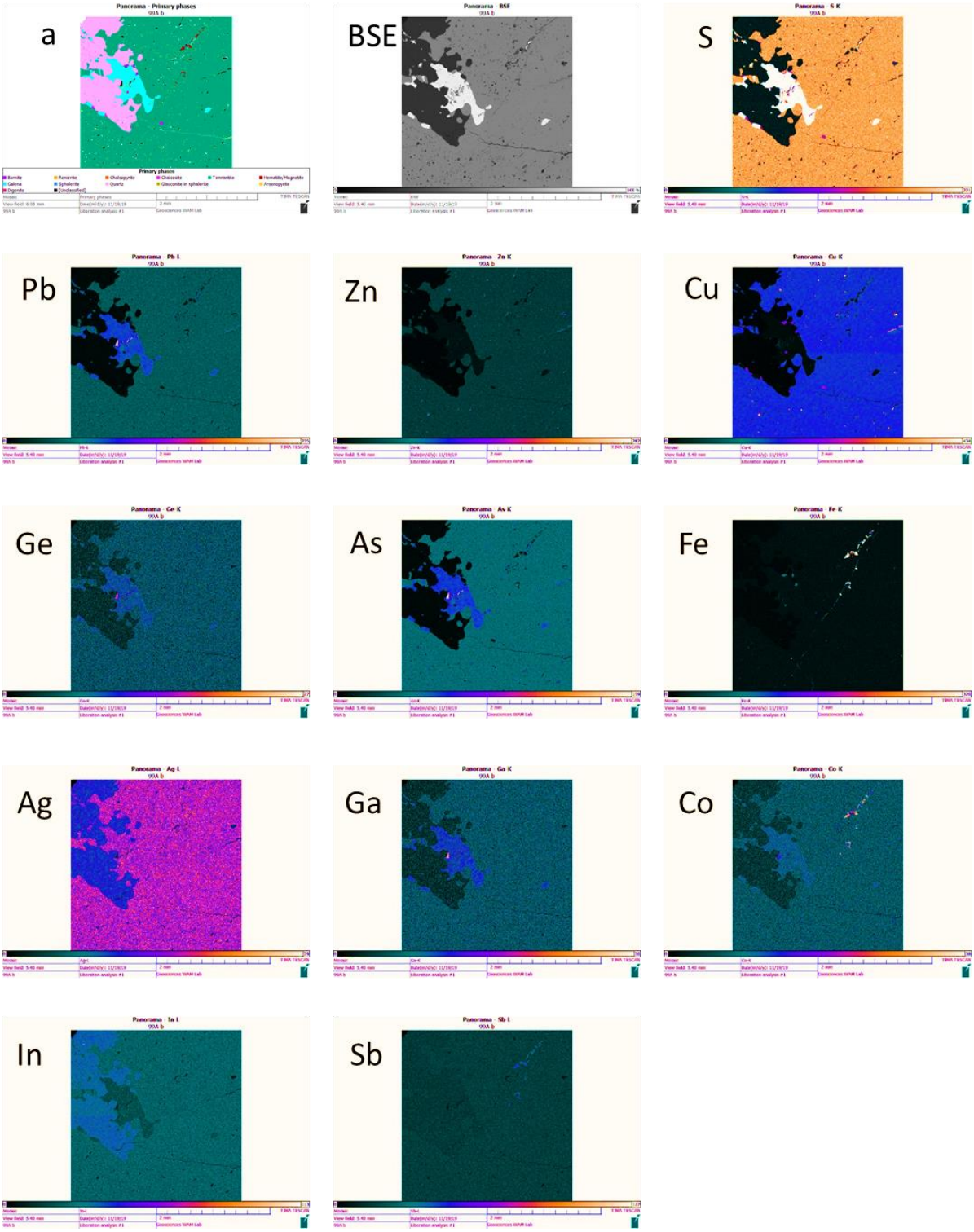

Figure 15: False colour phase map (a), backscatter image, and element maps of S, Pb, Zn, Cu, Ge, As, Fe, Ag, Ga, Co, In and Sb for an area on the polished ore block from sample 99A.

The second area for sample 99 A b is seen in Figure 16. There is minimal Ge within this area, however it can be noted there is more Ge within the tennantite than any of the other phases present. The tennantite has a high concentration of Pb. The dolomite is extremely rich in Sb and In.

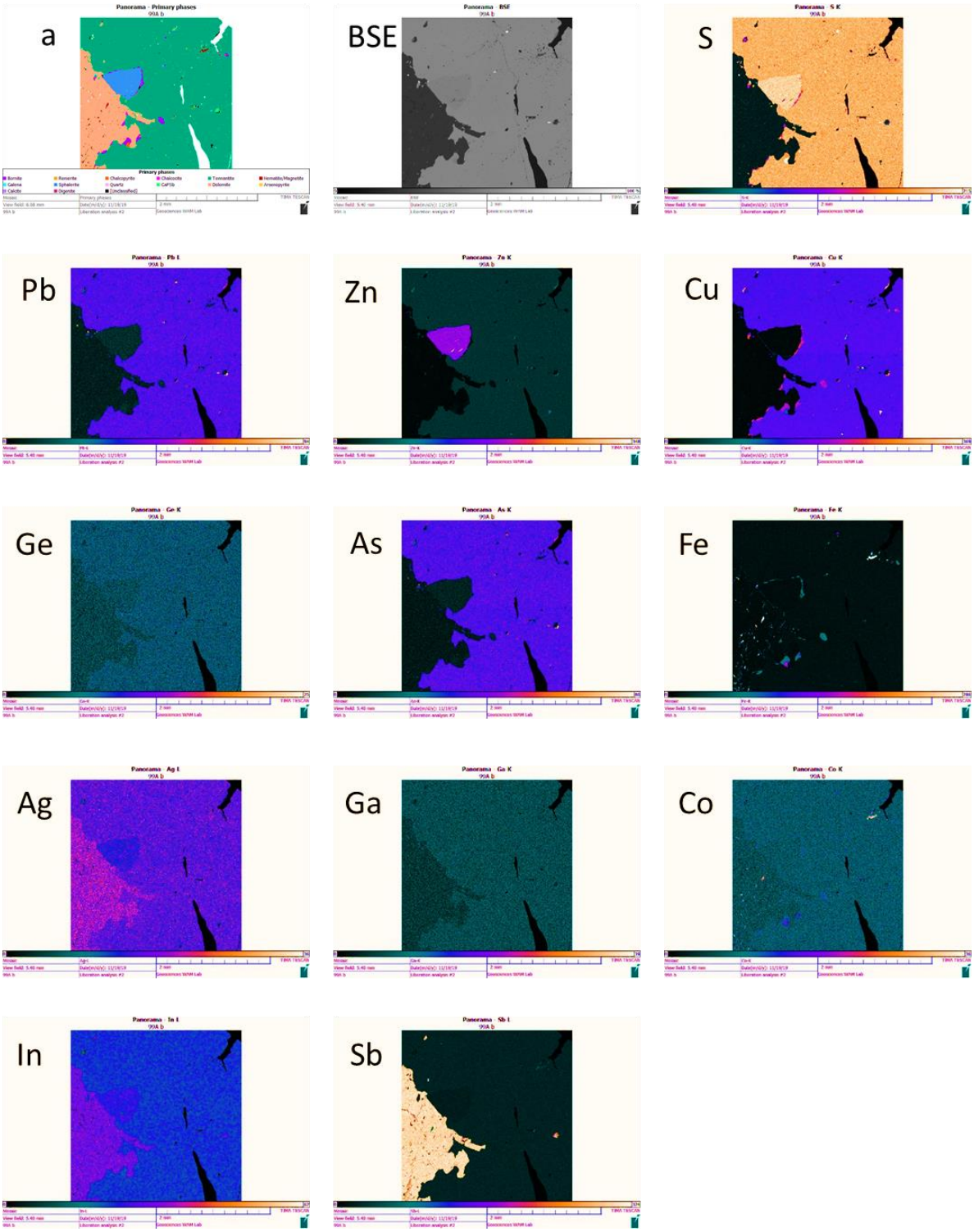

Figure 16: False colour phase map (a), backscatter image, and element maps of S, Pb, Zn, Cu, Ge, As, Fe, Ag, Ga, Co, In and Sb for an area on the polished ore block from sample 99A.

D.3. Galena-dominant assemblage

Sample 253 a

Figure 17 shows the false colour phase map, BSE image and elemental maps from the galena sample. The Ge is found to concentrate within the galena. The tennantite is enriched in Pb and In. The dolomite is falsely rich in Sb. The galena contains trace amounts of Ga.

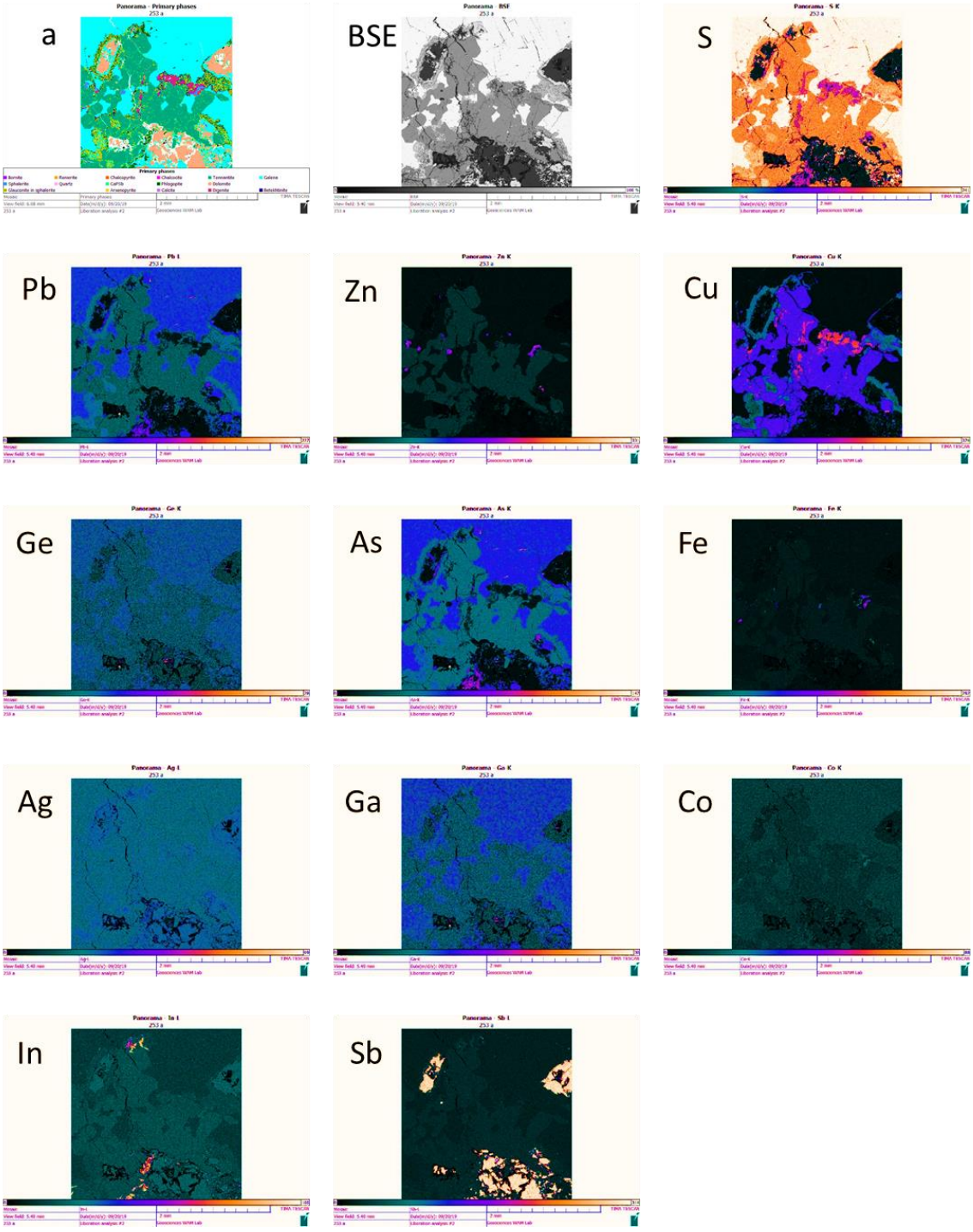

Figure 17: False colour phase map (a), backscatter image, and element maps of S, Pb, Zn, Cu, Ge, As, Fe, Ag, Ga, Co, In and Sb for an area on the polished ore block from sample 253 a.

Sample 423

One area was selected for element maps for this sample. Figure 18 shows these maps. The Ge is found to concentrate within the galena, as does As, Ga and Co. The tennantite has some In concentrating into it.

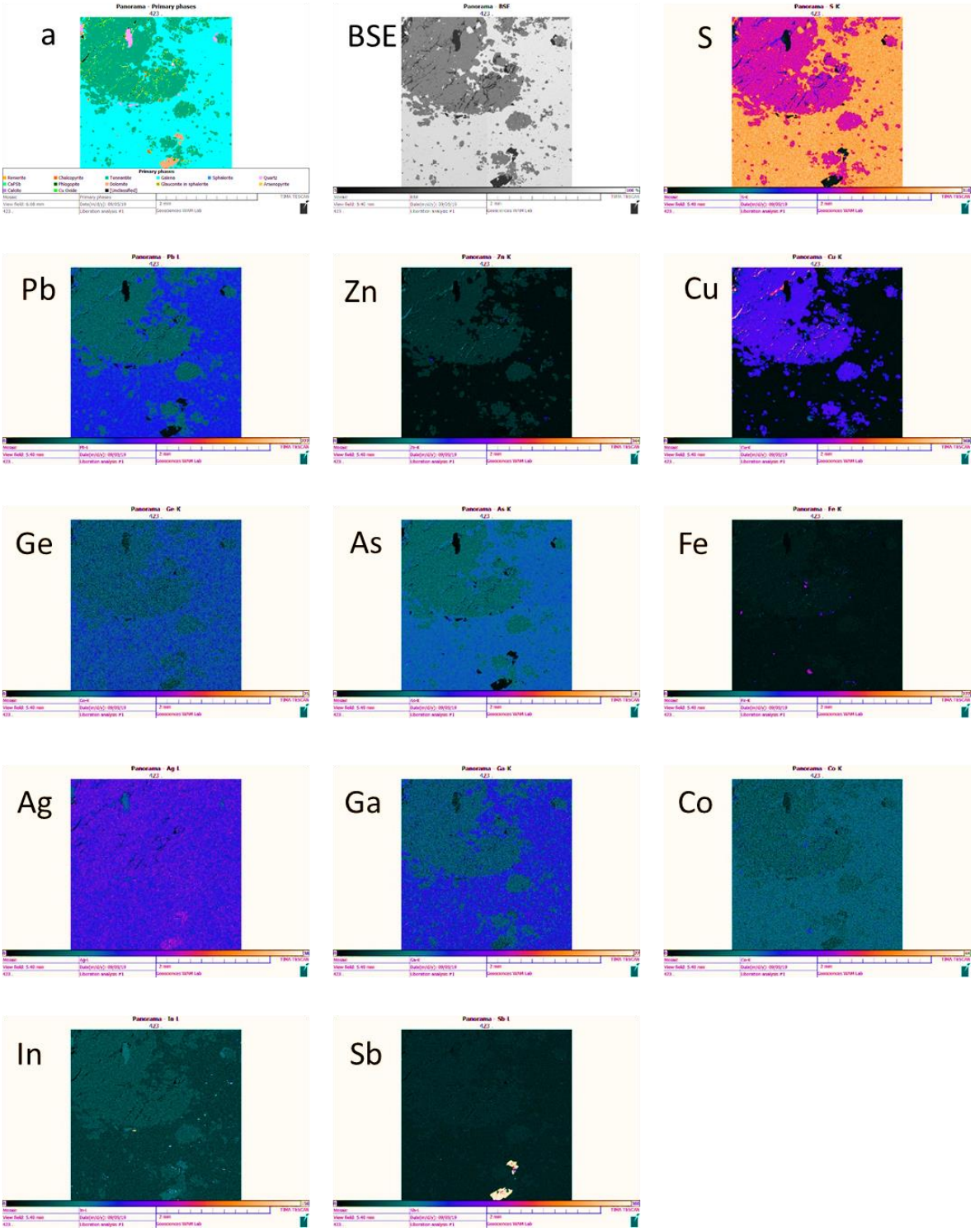

Figure 18: False colour phase map (a), backscatter image, and element maps of S, Pb, Zn, Cu, Ge, As, Fe, Ag, Ga, Co, In and Sb for an area on the polished ore block from sample 423.

Sample TS 5

Two areas were selected for this sample. Figure 19 shows the element maps for the first area. In this area the Ge is seen to concentrate into the galena. The galena also has As, Ga and Co concentrating into it. The tennantite is enriched in Pb and Sb. The sphalerite has In within it.

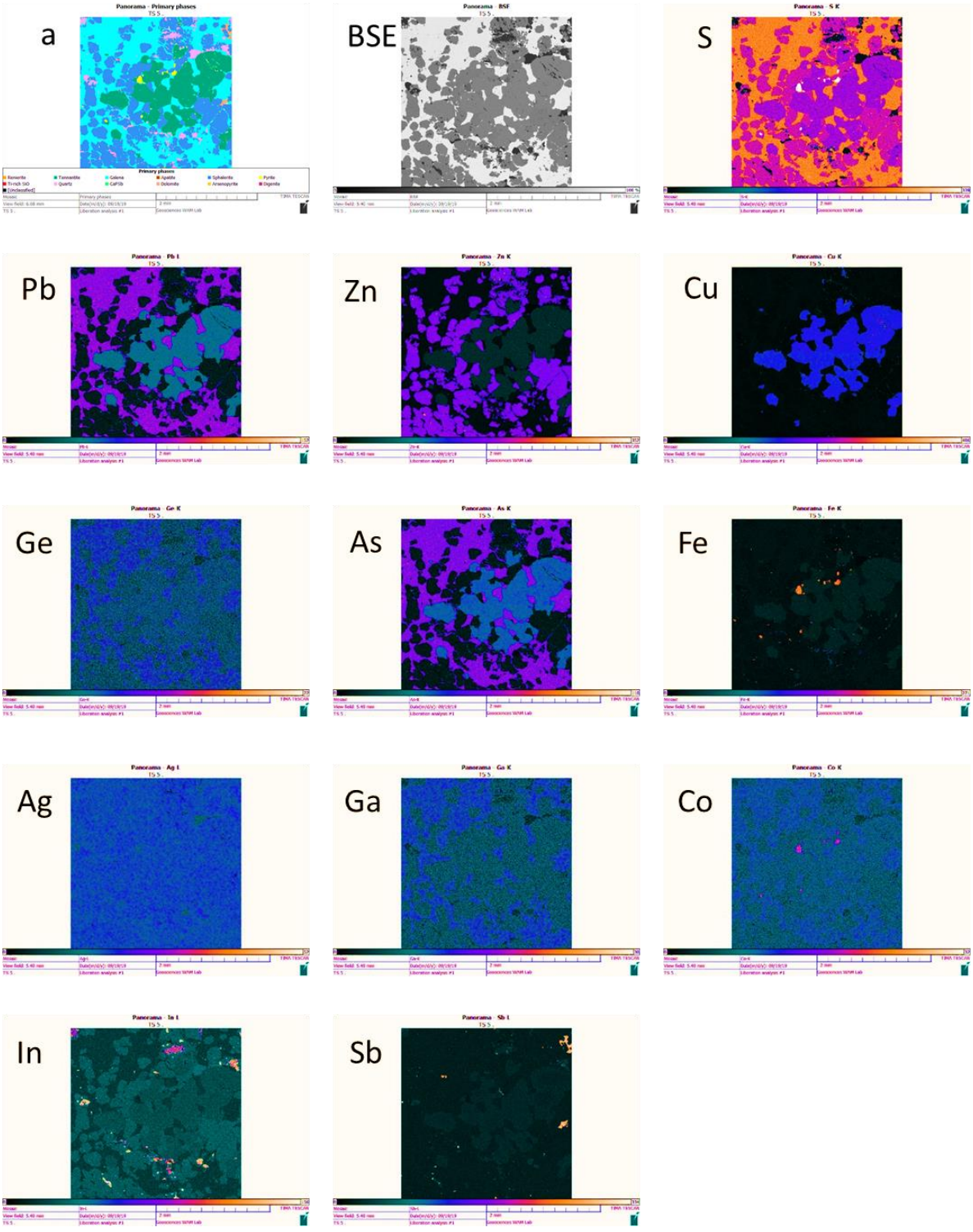

Figure 19: False colour phase map (a), backscatter image, and element maps of S, Pb, Zn, Cu, Ge, As, Fe, Ag, Ga, Co, In and Sb for an area on the polished ore block from sample TS 5.

Figure 20 shows the maps from the second area. Once again, the Ge is seen to be concentrated within the galena, as is As, Ga and Co. The tennantite is enriched in Pb. The quartz has a high concentration of In.

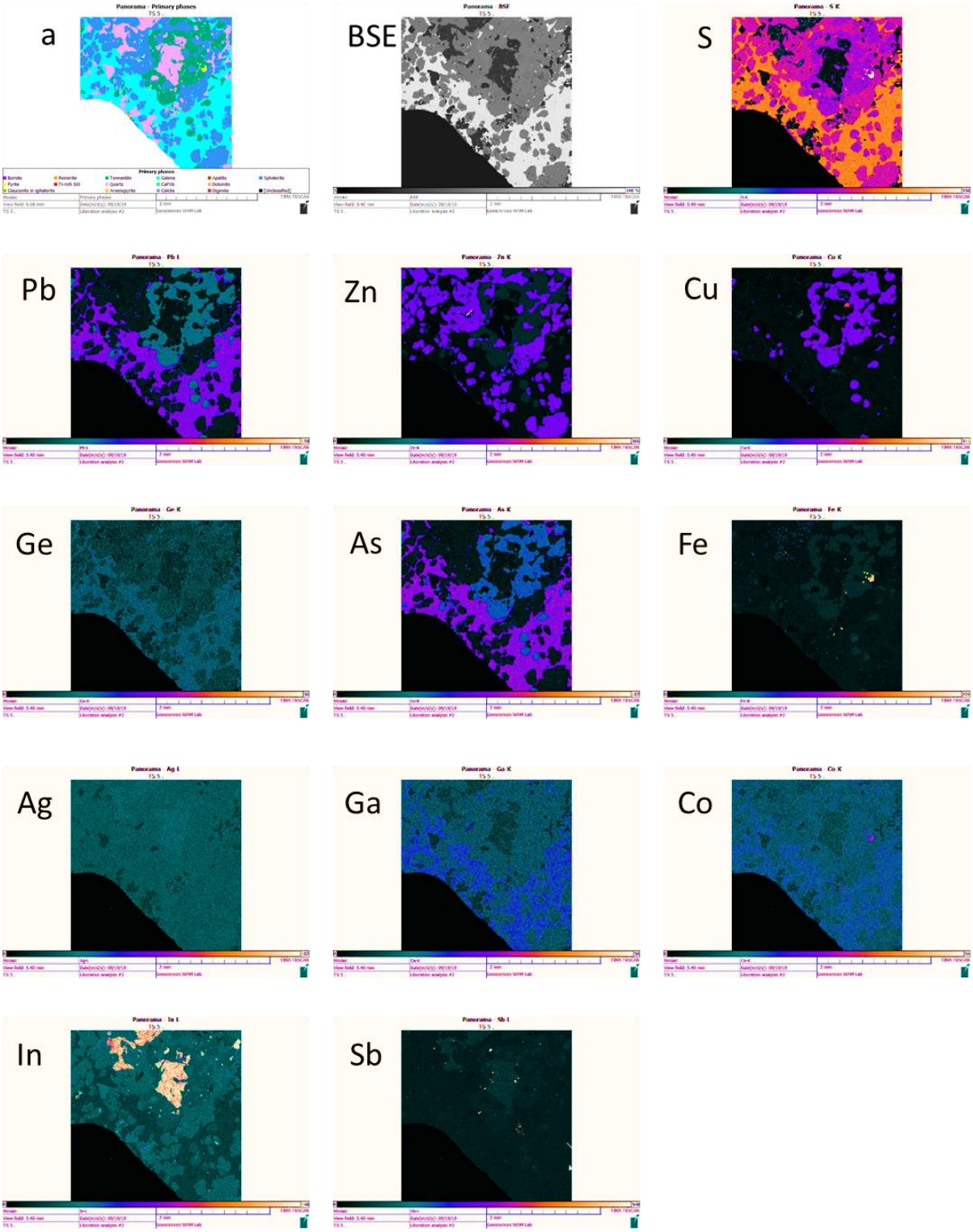

Figure 20: False colour phase map (a), backscatter image, and element maps of S, Pb, Zn, Cu, Ge, As, Fe, Ag, Ga, Co, In and Sb for an area on the polished ore block from sample TS 5.

Sample TS 11

Two areas were selected for this sample. Area one can be seen in Figure 21. Here, the Ge concentrates into the galena, as does As, Ga and Co. The tennantite is enriched in Pb, Zn and In. The pyrite has a high concentration of Co. All the sulphides, apart from pyrite, appear to contain some Ag.

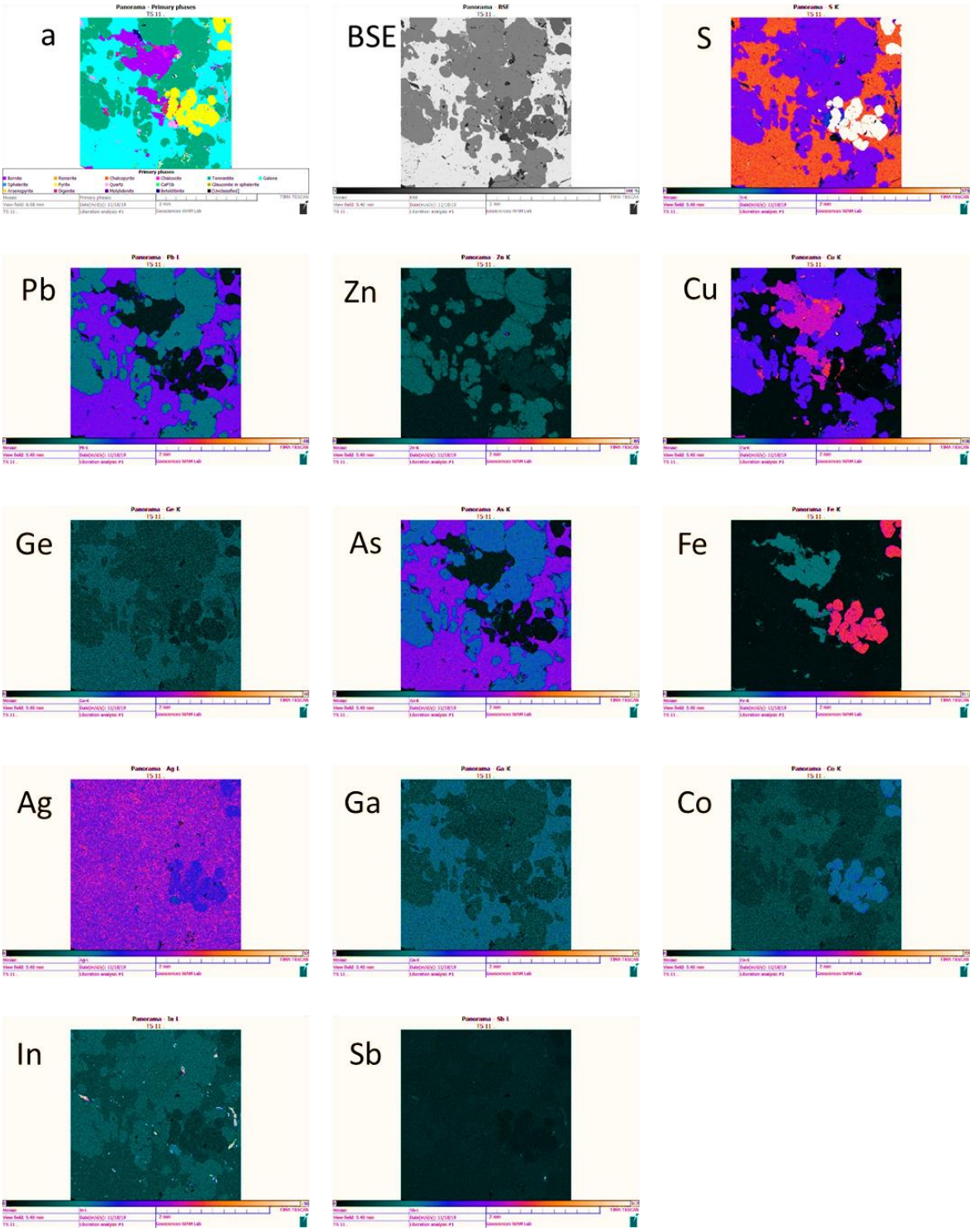

Figure 21: False colour phase map (a), backscatter image, and element maps of S, Pb, Zn, Cu, Ge, As, Fe, Ag, Ga, Co, In and Sb for an area on the polished ore block from sample TS 11.

The second area for this sample can be seen in Figure 22. The Ge is found to be concentrating into the galena, as does As, Ga and Co. The tennantite is enriched with Pb, Zn and In. There is some Ag contained within the betekhtinite.

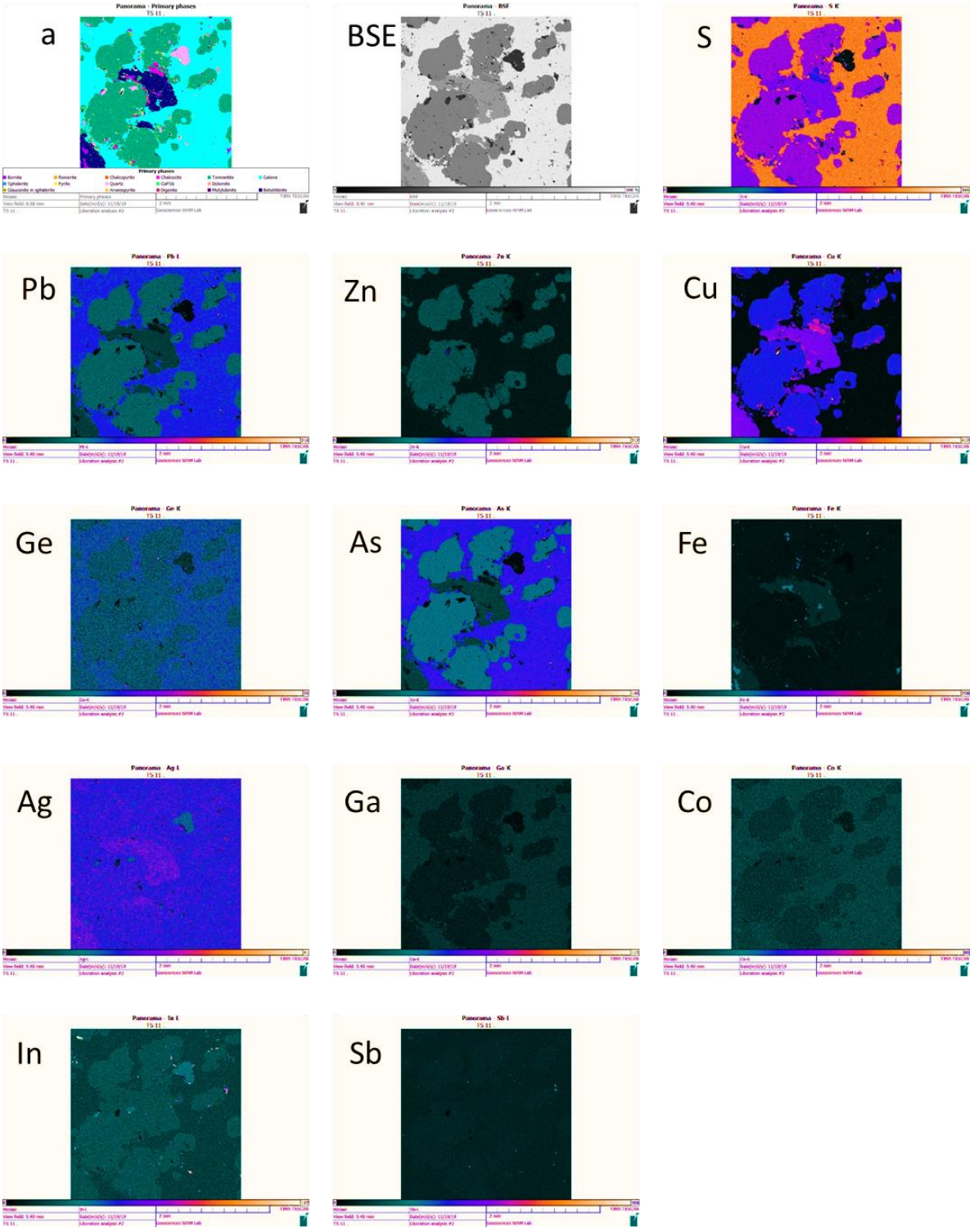

Figure 22: False colour phase map (a), backscatter image, and element maps of S, Pb, Zn, Cu, Ge, As, Fe, Ag, Ga, Co, In and Sb for an area on the polished ore block from sample TS 11.

Sample 259

Two areas were selected for this sample. Area one can be seen in Figure 23. Here the Ge is seen to concentrate within the galena, as does As, Ga and Co. In concentrates within the sphalerite.

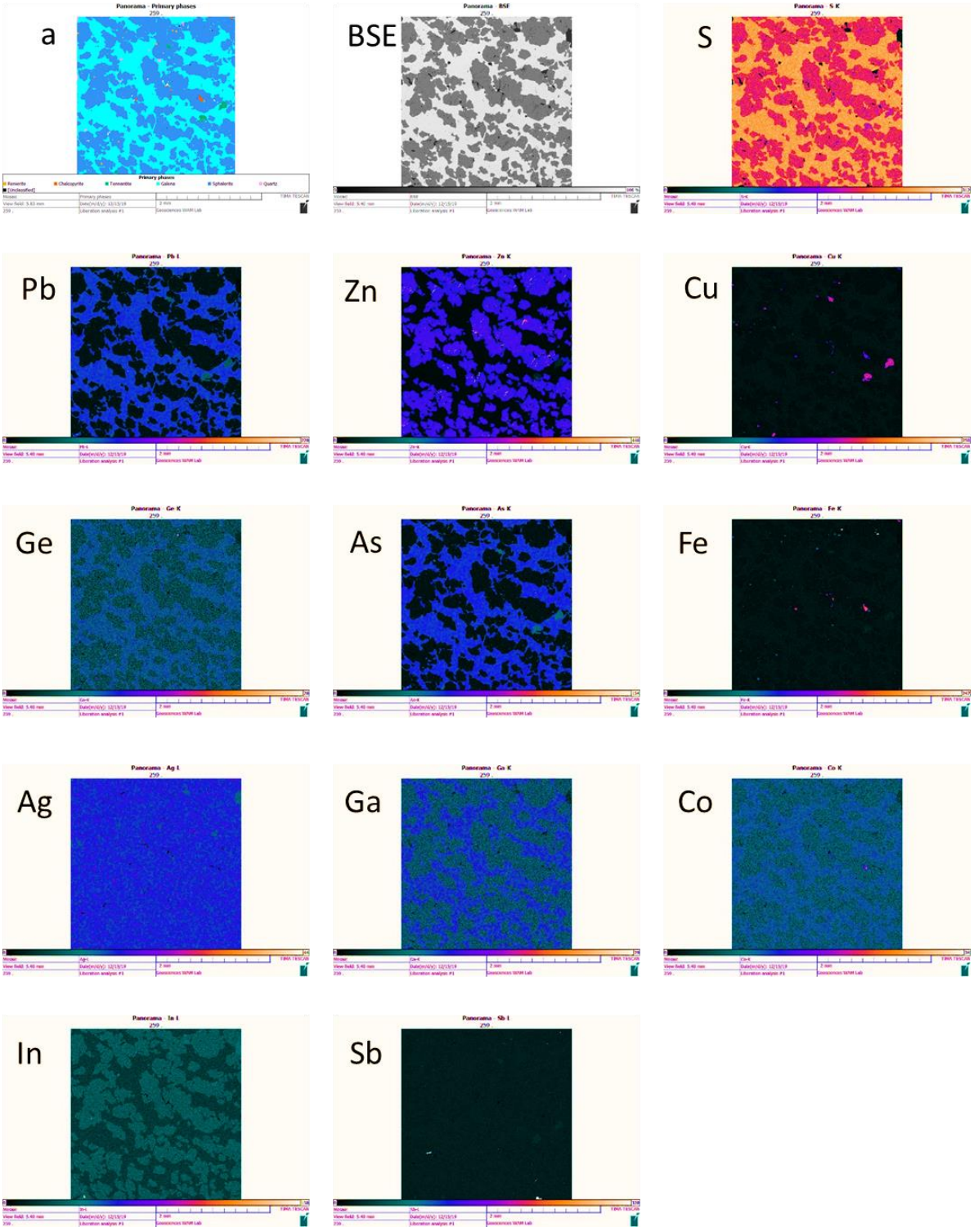

Figure 23: False colour phase map (a), backscatter image, and element maps of S, Pb, Zn, Cu, Ge, As, Fe, Ag, Ga, Co, In and Sb for an area on the polished ore block from sample 259.

Area two for sample 259 is shown in Figure 24. The Ge in this area is mostly strongly concentrated within the small blebs of renierite, followed by the galena. The galena also contains As and Ga. The pyrite contains Co. There are a few blebs of highly concentrated In in this area.

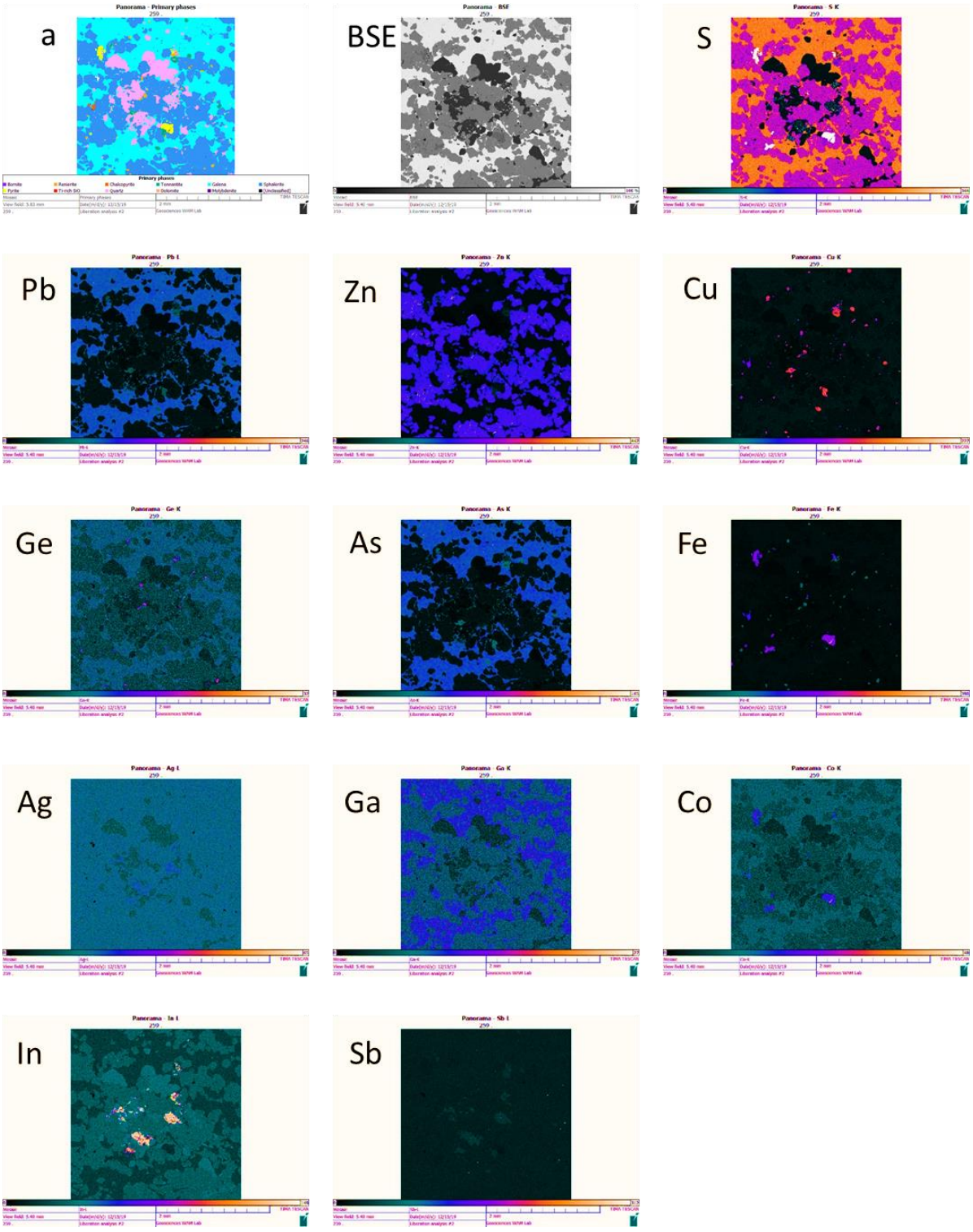

Figure 24: False colour phase map (a), backscatter image, and element maps of S, Pb, Zn, Cu, Ge, As, Fe, Ag, Ga, Co, In and Sb for an area on the polished ore block from sample 259.

D.4. Sphalerite-dominant assemblage

Sample 735

Two areas were chosen for this sample. The element maps from the first area can be seen in Figure 25. Here, the Ge is concentrated into the galena, as is As and Ga. The bornite is rich in Co. The sphalerite contains some In.

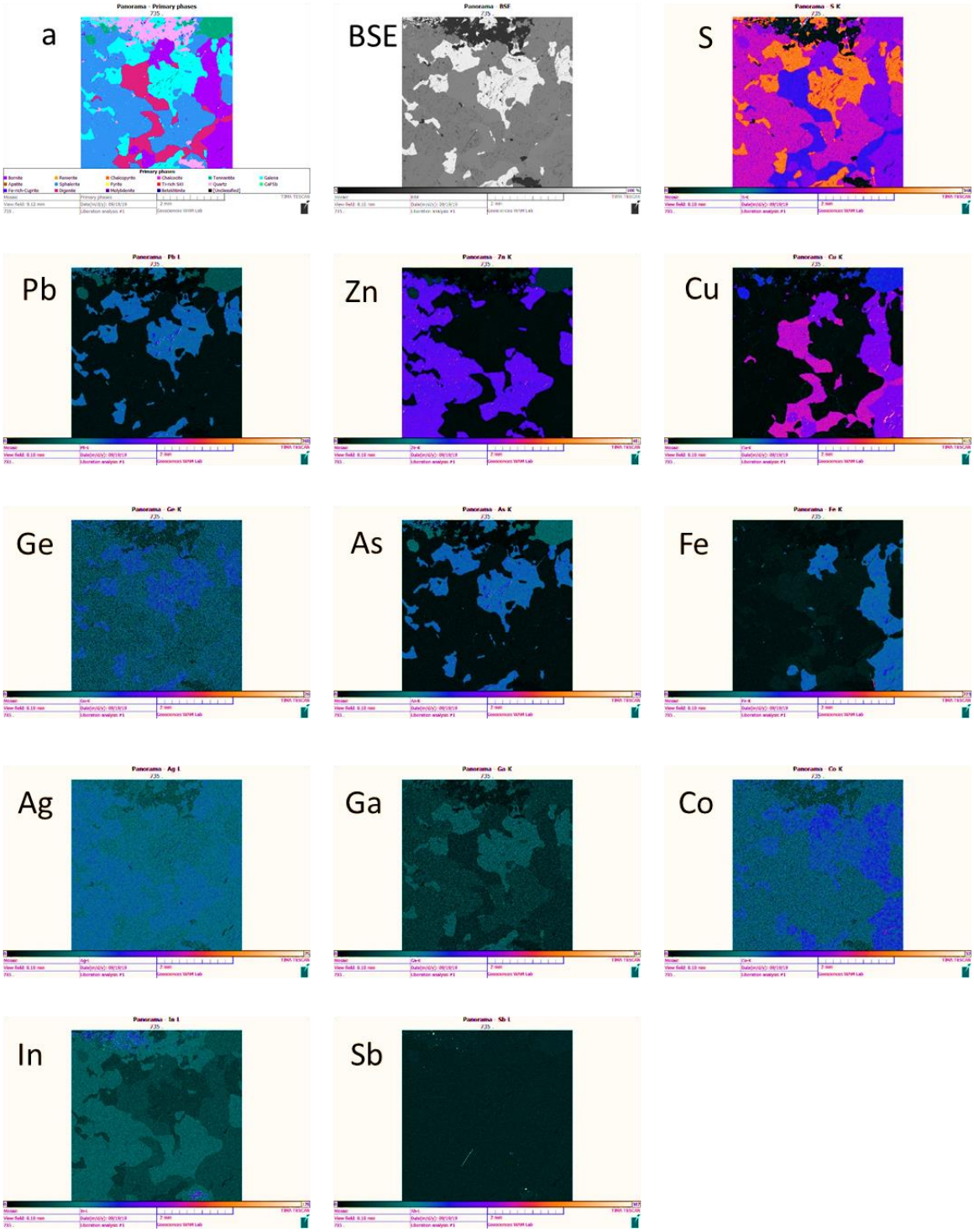

Figure 25: False colour phase map (a), backscatter image, and element maps of S, Pb, Zn, Cu, Ge, As, Fe, Ag, Ga, Co, In and Sb for an area on the polished ore block from sample 735.

The second area for sample 735 can be seen in Figure 26. The Ge is seen to concentrate into the galena once again, as does As, Ga and Co. The tennantite is also enriched in Pb.

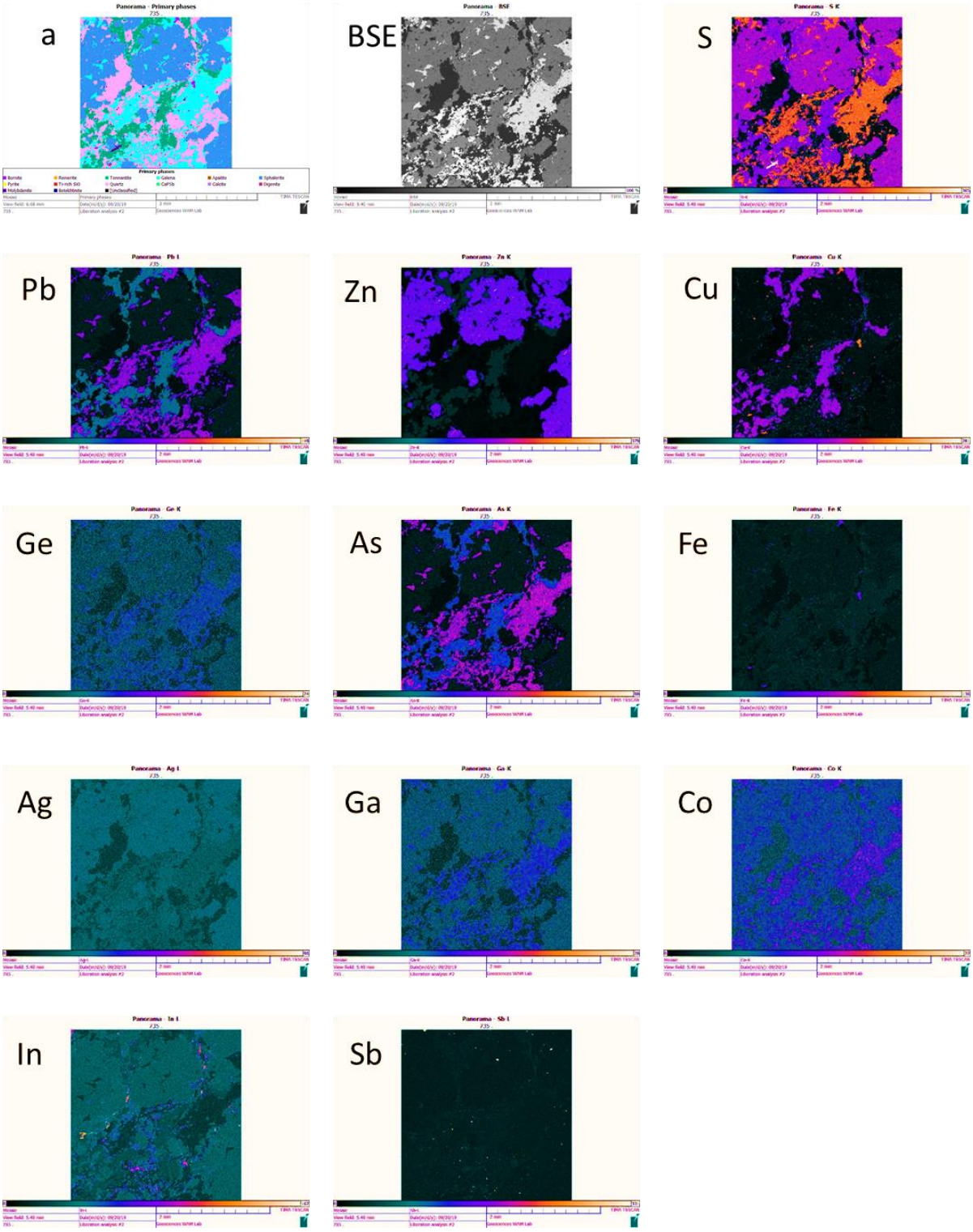

Figure 26: False colour phase map (a), backscatter image, and element maps of S, Pb, Zn, Cu, Ge, As, Fe, Ag, Ga, Co, In and Sb for an area on the polished ore block from sample 735.

Sample 110

Two areas were selected for this sample. The first area is seen in Figure 27. Here the Ge is seen to concentrate into the galena, and, to a lesser extent, into the tennantite. The galena also contains As, Ga and Co. The tennantite contains some Pb. The pyrite contains a high concentration of Co.

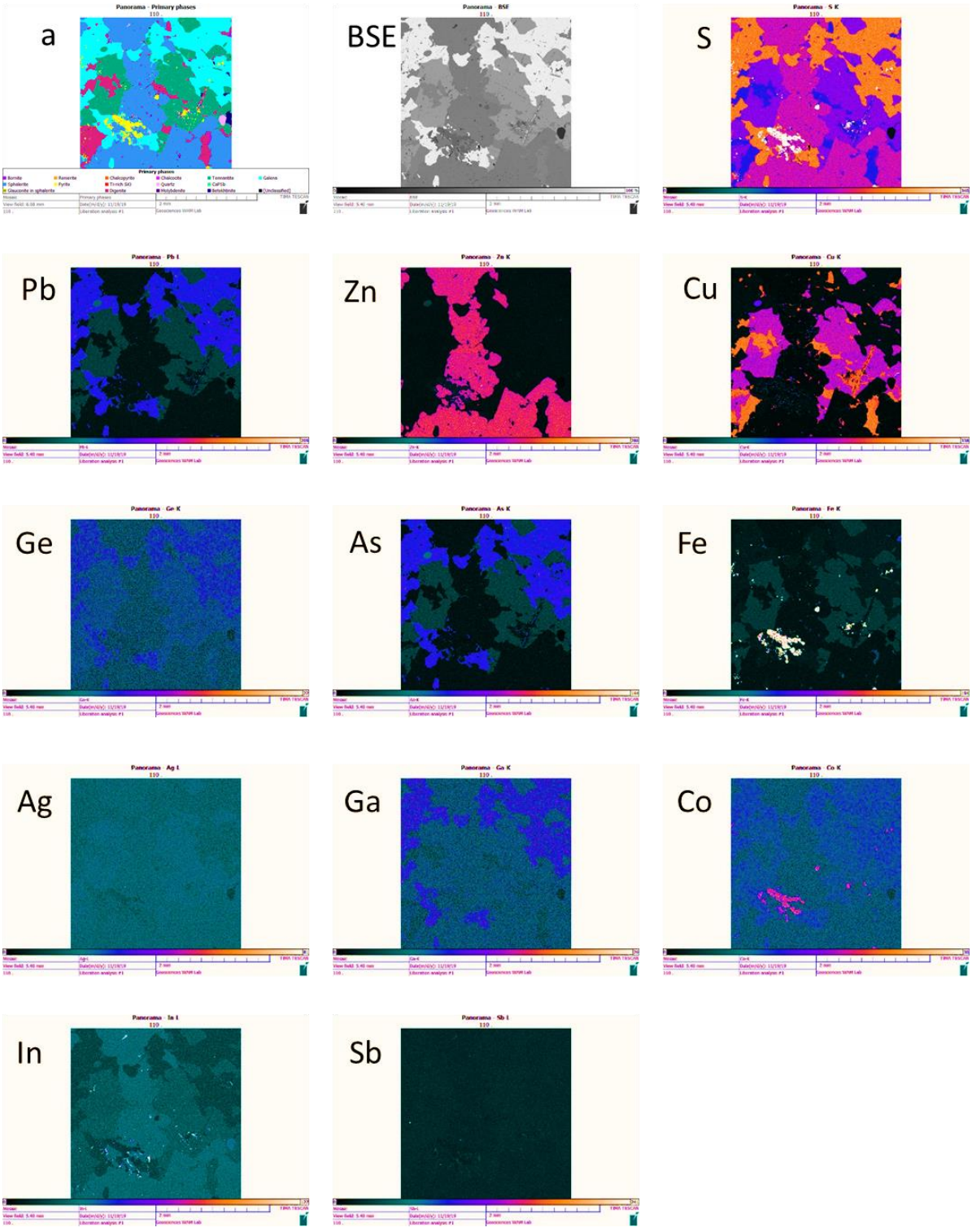

Figure 27: False colour phase map (a), backscatter image, and element maps of S, Pb, Zn, Cu, Ge, As, Fe, Ag, Ga, Co, In and Sb for an area on the polished ore block from sample 110.

Figure 28 shows the second area from sample 110. The Ge is concentrating into the galena in this sample. The galena also contains some As, Ga and Co. The tennantite contains Pb. The pyrite has a high concentration of Co. The quartz has a high concentration of In.

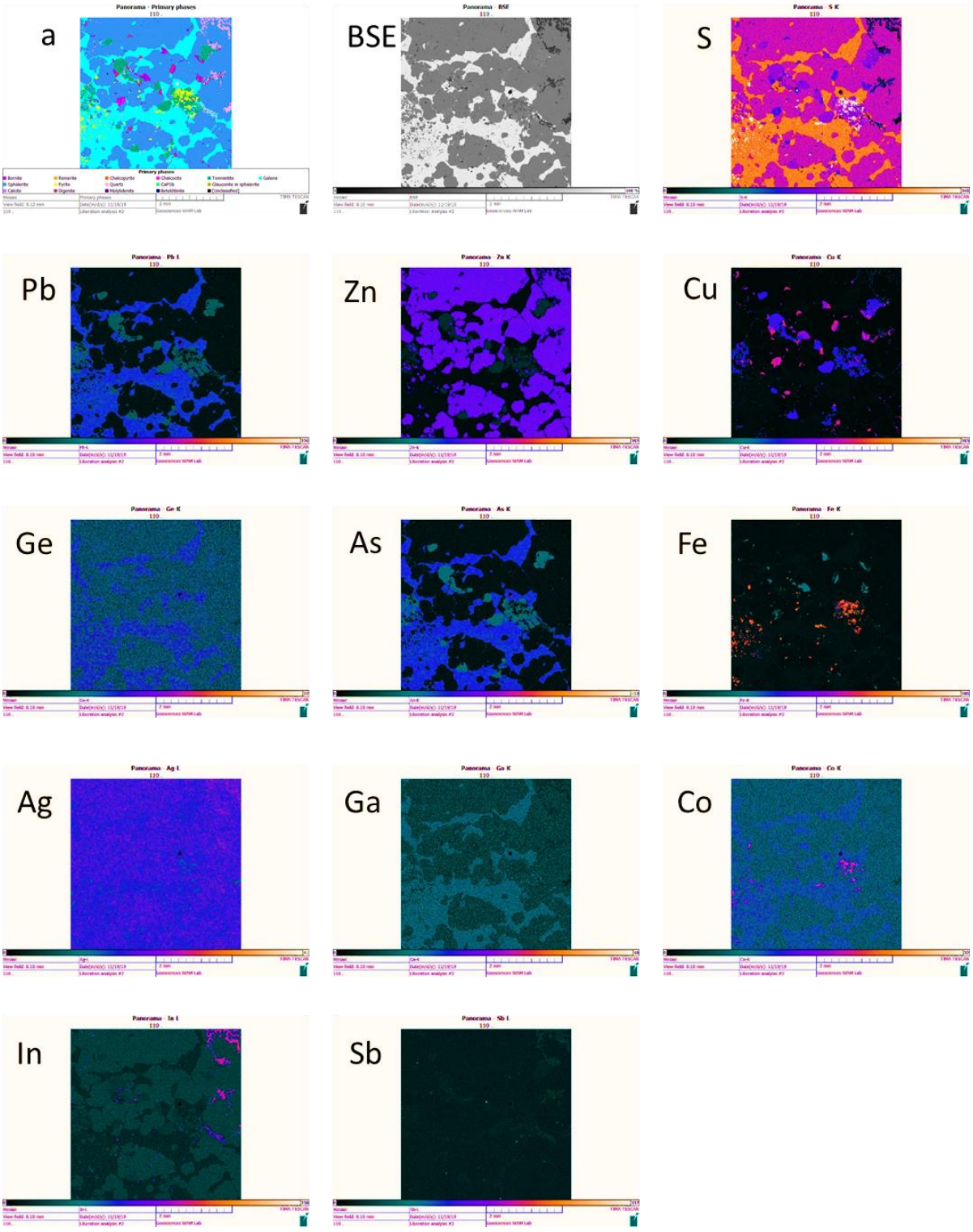

Figure 28: False colour phase map (a), backscatter image, and element maps of S, Pb, Zn, Cu, Ge, As, Fe, Ag, Ga, Co, In and Sb for an area on the polished ore block from sample 110.

Sample 272 A

One area was selected for sample 272 A. Figure 29 shows the resultant maps for this area. The Ge is located within the galena, as is As and Ga. The tennantite is enriched with Pb and Zn. The pyrite has a high concentration of Co. The quartz has In within it.

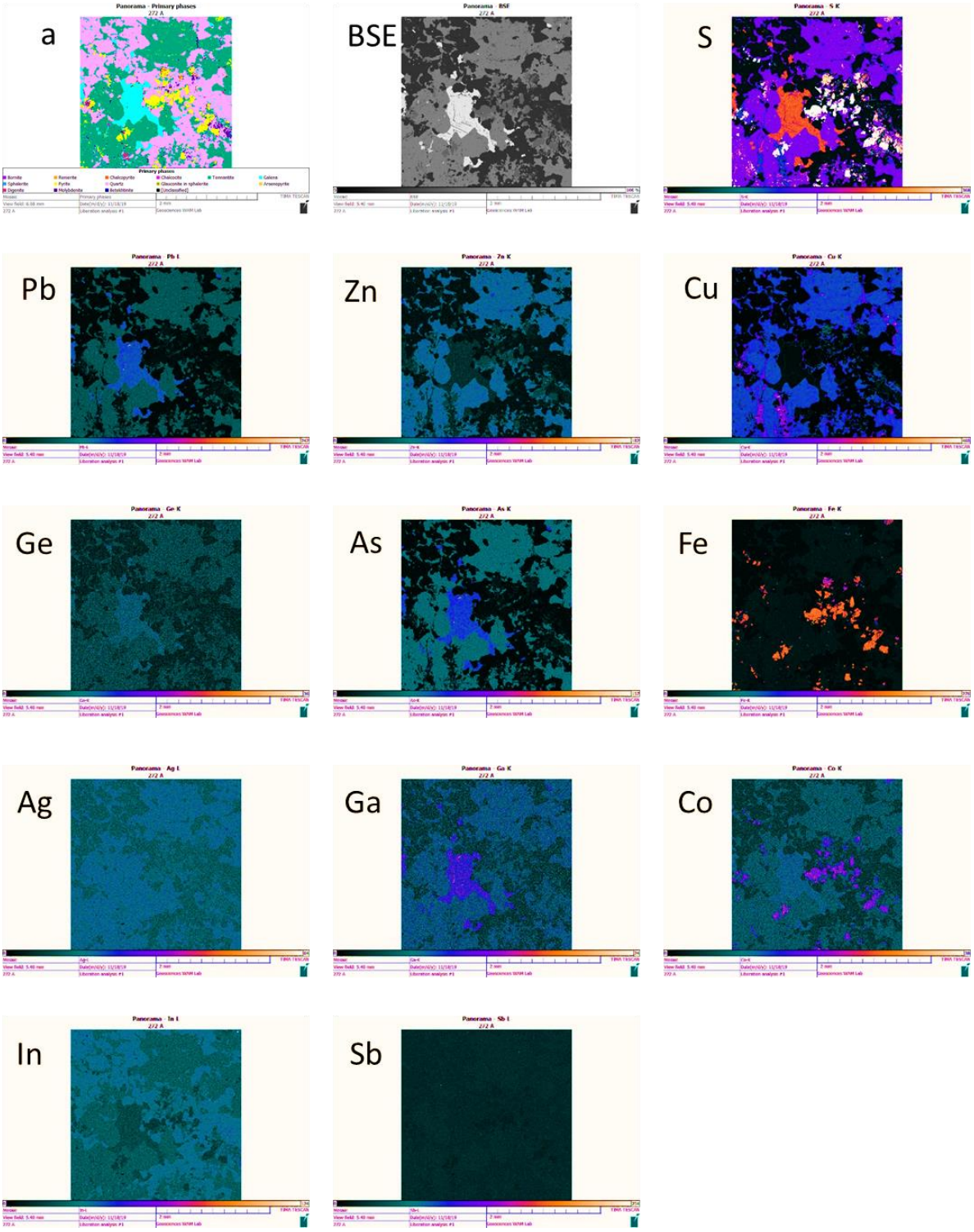

Figure 29: False colour phase map (a), backscatter image, and element maps of S, Pb, Zn, Cu, Ge, As, Fe, Ag, Ga, Co, In and Sb for an area on the polished ore block from sample 272 A.

Appendix E

Electron Microprobe Analyser

Standards used:

Element	Standard	Expected Composition	Achieved Composition
Ni	Pentlandite	S : 32.89%, Fe : 30.88%, Co : 0.43%, Ni : 35.61%	S : 32.89%, Fe : 30.88%, Co : 0.43%, Ni : 35.61%
Fe, As, S	Arsenopyrite	Fe : 34.16%, As : 46.1%, S : 19.28%, Co : 0.02%	Fe : 34.16%, As : 46.1%, S : 19.28%, Co : 0.02%
Co	Co	Co : 99.995%	Co : 100.%
Cu	Cuprite	Cu : 88.82%, O : 11.18%	Cu : 88.82%, O : 11.18%
Zn	Sphalerite	Zn : 67.0977%, S : 32.9023%	Zn : 67.0977%, S : 32.9023%
Ga	GaAs	Ga : 48.20%, As : 51.80%	Ga : 48.208%, As : 51.792%
Ge	Ge	Ge : 99.9999%	Ge : 100.%
Ag	Ag	Ag : 99.9985%	Ag : 100.%
In	InP	In : 78.76%, P : 21.24%	In : 78.7551%, P : 21.2449%
Pb	Galena	Pb : 86.34%, S : 13.51%	Pb : 86.34%, S : 13.51%

E.1. Kipushi data

Signals Used for samples: Ni Ka, Fe Ka, Co Ka, Cu Ka, Zn Ka, Ga Ka, Ge Ka, Ag La, In La, Pb La, As Kb, As Kb, As La, As La, S Ka.
Spectromers Conditions: Sp5 LLIF, Sp5 LLIF, Sp5 LLIF, Sp5 LLIF, Sp3 LLIF, Sp3 LLIF, Sp3 LLIF, Sp1 PET, Sp1 PET, Sp3 LLIF, Sp5 LLIF, Sp3 LLIF, Sp4 TAP, Sp2 TAP, Sp1 PET
Full Spectromers Conditions: Sp5 LLIF(2d= 4.0267,K= 0.000058), Sp5 LLIF(2d= 4.0267,K= 0.000058), Sp5 LLIF(2d= 4.0267,K= 0.000058), Sp5 LLIF(2d= 4.0267,K= 0.000058), Sp3 LLIF(2d= 4.0267,K= 0.000058), Sp3 LLIF(2d= 4.0267,K= 0.000058), Sp3 LLIF(2d= 4.0267,K= 0.000058), Sp1 PET(2d= 8.75,K= 0.000144), Sp1 PET(2d= 8.75,K= 0.000144), Sp3 LLIF(2d= 4.0267,K= 0.000058), Sp5 LLIF(2d= 4.0267,K= 0.000058), Sp3 LLIF(2d= 4.0267,K= 0.000058), Sp4 TAP(2d= 25.745,K= 0.00218), Sp2 TAP(2d= 25.745,K= 0.00218), Sp1 PET(2d= 8.75,K= 0.000144)
Column Conditions: Cond 1: 15keV -0.001nA

Table 1: Weight percent data from selected minerals for sample 15452 b.

Sample 15452 b													
Phase	**Ni**	**Fe**	**Co**	**Cu**	**Zn**	**Ga**	**Ge**	**Ag**	**In**	**Pb**	**As**	**S**	**Total**
Sphalerite	0.021694	0.02233	0.031167	0.020658	67.54086	0.00001	0.00001	0.00001	0.00001	0.00001	0.00001	34.82973	102.4665
	0.00001	0.01689	0.013345	0.043097	67.60099	0.00001	0.042464	0.00001	0.00001	0.243058	0.00001	34.91503	102.8749
	0.014417	0.00001	0.022157	0.051579	66.8961	0.018898	0.00001	0.00001	0.00001	0.00001	0.00001	35.53296	102.5362
	0.00001	0.00001	0.024318	0.041897	70.22292	0.00001	0.00001	0.073104	0.051871	0.00001	0.00001	35.14587	105.56
	0.033698	0.024918	0.022438	0.009506	70.26807	0.00001	0.00001	0.00001	0.025964	0.00001	0.007202	35.1573	105.5491
	0.005826	0.021284	0.030861	0.084463	70.3957	0.083659	0.00001	0.00001	0.00001	0.3858	0.027352	35.6384	106.6734
	0.00001	0.095359	0.000781	0.379664	62.19456	0.082634	0.00001	0.037679	0.00001	0.236581	0.00001	28.20772	91.23503
	0.00001	1.334746	0.00001	7.577704	52.69588	0.00001	0.00001	0.058449	0.048707	1.440268	0.00001	27.1962	90.35201
	0.01146	3.027074	0.00001	17.80206	39.13992	0.007283	0.00001	0.00001	0.006254	2.460143	0.005865	24.6553	87.11541
	0.00001	4.524651	0.00001	27.84509	26.42153	0.00001	0.00001	0.032838	0.00001	0.249514	0.00001	21.96371	81.0374
Galena	0.011794	0.00001	0.007827	0.015202	0.00001	0.014075	0.057312	0.00001	0.009339	89.94891	0.00001	13.98603	104.0505
	0.00001	0.000335	0.00001	0.041974	0.033166	0.138319	0.0168	0.108327	0.020239	90.03402	0.028978	14.17781	104.6
	0.046747	0.00001	0.00001	0.025313	0.020361	0.068564	0.217939	0.060059	0.00001	90.98994	0.025722	14.22577	105.6804
Tennantite	0.00001	4.078441	0.00001	40.24146	2.36412	0.03852	0.099268	0.161592	0.001579	24.01302	3.583521	19.95184	94.53337
	0.002625	2.37058	0.00001	34.15189	2.520337	0.00001	0.070575	0.082957	0.04128	37.93263	3.567863	18.66603	99.40679
	0.00001	1.475531	0.00001	30.77686	2.069582	0.00001	0.00001	0.186835	0.00001	44.24495	2.130893	17.49196	98.37666
Unknown	0.00001	7.647394	0.00001	30.94461	1.01306	0.141179	3.572153	0.109116	0.032004	24.8387	0.268967	22.42605	90.99326
	0.000907	6.869005	0.00001	26.55355	1.381286	0.025836	3.875216	0.096823	0.00001	27.47718	0.00001	22.83249	89.11232
	0.0227	5.604789	0.00001	19.59855	1.230555	0.00001	3.42134	0.00001	0.004864	36.58286	0.265359	21.16255	87.8936
	0.00001	5.060766	0.00001	17.48451	1.021947	0.00001	3.300585	0.101376	0.00001	43.82661	0.00001	20.16518	90.96103
	0.020564	4.188456	0.00001	13.69298	0.824265	0.168154	2.953357	0.00001	0.00001	51.07161	0.015089	19.03843	91.97294
	0.021619	2.652611	0.00001	8.161192	0.5471	0.00001	1.516022	0.00001	0.00001	62.10918	0.095127	16.27804	91.38093
	0.00001	6.560583	0.00001	44.21017	6.299	0.00001	0.106348	0.295716	0.00001	10.5721	0.676074	21.52229	90.24232
	0.014644	5.544282	0.00001	45.37308	1.713562	0.00001	0.078398	0.262698	0.054566	13.61839	2.395676	20.67715	89.73247

Details for samples KP 12 and KP 12492f

Table 2: Weight percent data from selected minerals for sample KP 12.

Sample KP 12													
Phase	**Ni**	**Fe**	**Co**	**Cu**	**Zn**	**Ga**	**Ge**	**Ag**	**In**	**Pb**	**As**	**S**	**Total**
Galena	0.020184	0.00001	0.034732	0.131527	0.098698	0.00001	0.00001	0.00001	0.00001	83.29203	0.00001	12.93758	96.51482
	0.00001	0.00962	0.007575	0.537071	0.14254	0.00001	0.00001	0.157836	0.00001	83.26611	0.024872	12.80279	96.94846
	0.00001	0.00001	0.00001	0.587045	0.086807	0.215648	0.305431	0.247036	0.00001	82.78494	0.00001	12.59546	96.82243
Sphalerite	0.00001	0.030624	0.016887	0.030744	65.03963	0.001243	0.00001	0.086033	0.00001	0.569498	0.004873	30.58436	96.36392
	0.013142	0.032617	0.018537	0.168776	64.87371	0.028688	0.00001	0.00001	0.00001	0.472027	0.008838	31.90878	97.52515
	0.016056	0.043108	0.007005	0.195354	57.3038	0.074488	0.00001	0.00001	0.04105	0.225341	0.006474	35.75348	93.66617
	0.00001	0.039646	0.028096	0.012044	57.24161	0.022762	0.0703	0.00001	0.00001	0.347694	0.00001	35.70744	93.46964
	0.00001	0.030872	0.00001	0.152626	57.32599	0.00001	0.037089	0.026268	0.00001	0.866097	0.00001	35.09145	93.53045
Renierite	0.00001	13.42727	0.00001	43.10903	2.805828	0.00001	7.058814	0.08076	0.00001	0.958735	0.364721	32.93702	100.7422
	0.00001	13.58295	0.00001	43.69401	2.422934	0.011503	6.725451	0.216619	0.068829	0.662486	0.341688	32.78049	100.507
	0.00001	13.55162	0.00001	43.0689	2.478712	0.00001	7.013561	0.119248	0.00001	1.753689	0.305956	33.98038	102.2721
Bornite	0.026911	10.54987	0.00001	68.12146	0.019004	0.00001	0.066463	0.285656	0.00001	1.390184	0.005706	26.85949	107.3248
Tennantite	0.011101	0.10869	0.001994	47.5984	7.012312	0.00001	0.135505	0.243497	0.00001	17.04731	8.003167	28.33261	108.4946
	0.00001	0.072741	0.004389	47.17858	6.967703	0.00001	0.139409	0.059862	0.00001	16.88749	8.12498	28.12831	107.5635
	0.008801	0.12133	0.00001	47.37524	6.985063	0.00001	0.028731	0.269123	0.00001	15.74425	7.978631	28.22987	106.7411
	0.020254	0.766793	0.00001	35.6165	11.80014	0.00001	0.005752	0.403528	0.037423	14.9738	5.124427	26.21065	94.95928
	0.005584	0.100924	0.00001	47.87324	6.71481	0.00001	0.00001	0.504947	0.00001	14.26828	7.925748	29.27402	106.6676
	0.00001	1.632355	0.00001	52.05227	5.466298	0.00001	0.227154	0.463464	0.037022	12.00153	6.567293	28.6392	107.0866
	0.000464	0.110858	0.010344	47.98705	6.49009	0.00001	0.053853	0.106696	0.011311	13.98669	8.056871	29.3122	106.1264

Table 3: Weight percent data from selected minerals for sample 12492 f.

Sample 12492 f													
Phase	**Ni**	**Fe**	**Co**	**Cu**	**Zn**	**Ga**	**Ge**	**Ag**	**In**	**Pb**	**As**	**S**	**Total**
Unknown	0.00001	0.037107	0.00001	0.036143	0.25914	0.004025	0.006525	0.00001	0.00001	0.020571	0.03354	0.86444	1.26153
	0.014036	0.062112	0.00001	0.025325	0.40838	0.00001	0.00001	0.00001	0.001689	0.486614	0.00001	0.449438	1.447643
	0.00001	1.017549	0.00001	0.4117	25.22438	0.00001	0.002058	0.02171	0.019565	0.00001	0.025828	15.39425	42.11707
	0.00001	0.01824	0.00001	0.022183	0.110458	0.00001	0.041058	0.019349	0.00001	0.033713	0.024015	0.666022	0.935078
	0.00001	0.026625	0.00001	0.009795	0.860042	0.003786	0.00001	0.00001	0.001687	0.095122	0.01629	0.845798	1.859185
Chalcopyrite	0.00001	29.24781	0.00001	33.93863	0.066041	0.00001	0.00001	0.00001	0.00001	0.00001	0.023737	33.49849	96.77479
	0.014152	29.07403	0.00001	33.70597	0.069533	0.00001	0.191232	0.00001	0.004777	0.722741	0.00001	34.10719	97.88967
	0.022803	29.40819	0.00001	33.84451	0.110808	0.054334	0.01648	0.04656	0.015978	1.013679	0.00001	34.50605	99.03941
Sphalerite	0.00001	2.197011	0.00001	0.250438	60.87565	0.00001	0.00001	0.00001	0.00001	0.47893	0.038822	34.2783	98.11921
	0.010491	17.96124	0.00001	19.99047	25.51578	0.00893	0.00001	0.00001	0.019211	0.00001	0.004917	33.6352	97.14627
	0.013088	1.943089	0.00001	0.00001	60.48928	0.00001	0.10085	0.112695	0.00001	0.00001	0.018741	33.24401	95.9218

Table 4: Weight percent data from selected minerals for sample KP 2.

Sample KP 2													
Phase	**Ni**	**Fe**	**Co**	**Cu**	**Zn**	**Ga**	**Ge**	**Ag**	**In**	**Pb**	**As**	**S**	**Total**
Tennantite	0.00001	0.111229	0.00001	43.02787	8.610985	0.00001	0.058864	0.110767	0.00001	20.79578	13.73713	24.13291	110.5856
	0.01065	0.096088	0.001429	42.75988	8.56922	0.00001	0.091091	0.015259	0.00001	18.96544	14.59737	24.52802	109.6345
	0.00001	0.075902	0.00001	42.93569	8.524146	0.00001	0.00001	0.015259	0.00001	18.93433	14.66019	24.37568	109.5213
	0.00001	0.059938	0.027963	46.2317	8.352301	0.00001	0.171206	0.288508	0.00001	9.934655	15.34073	26.78085	107.1879
	0.009048	0.095668	0.041825	45.72936	8.172945	0.00001	0.101104	0.030373	0.012925	12.74687	14.53521	26.64107	108.1164
Sphalerite	0.012337	0.005176	0.00536	0.070692	69.70385	0.00001	0.00001	0.06135	0.008646	0.00001	0.024788	30.97316	100.8654
	0.00001	0.022436	0.00001	0.09823	70.35431	0.00001	0.00001	0.00001	0.00001	0.00001	0.014464	30.20626	100.6958
	0.010129	0.00001	0.00001	0.038479	71.61066	0.016694	0.00001	0.00001	0.00001	0.700931	0.00001	28.99399	101.371
	0.00001	0.033064	0.011391	0.00001	72.17445	0.00001	0.00001	0.095811	0.005764	0.00001	0.00001	28.48735	100.8079
Galena	0.00001	0.01239	0.02837	0.031919	0.099136	0.00001	0.014589	0.087687	0.00001	90.36291	0.011903	12.69408	103.343
	0.00001	0.018463	0.026732	0.433099	0.059392	0.127306	0.302097	0.053414	0.045914	87.79437	0.00001	12.45252	101.3133
	0.00001	0.00001	0.00001	0.00001	0.00001	0.095364	0.002632	0.022806	0.00001	92.84299	0.034906	11.4276	104.4264
	0.021866	0.00001	0.00001	0.011719	0.103206	0.033959	0.00001	0.00001	0.00001	92.62789	0.00001	11.21338	104.0121
	0.002895	0.00001	0.004737	0.059157	0.054526	0.00001	0.047866	0.04196	0.02961	86.77105	0.00001	13.26913	100.281
	0.015227	0.00001	0.027806	0.015808	0.110514	0.065422	0.071974	0.122185	0.00001	85.95619	0.018633	13.68887	100.0927
	0.002898	0.005417	0.00001	0.123723	0.059444	0.00001	0.00001	0.057276	0.00001	86.83734	0.00001	13.31596	100.4021
Bornite	0.015115	10.88957	0.00001	64.09959	0.00001	0.00001	0.00001	0.269927	0.033525	0.00001	0.00001	23.59736	98.90517
	0.004316	10.94386	0.00001	63.34626	0.00001	0.00001	0.039882	0.439554	0.00001	0.00001	0.00001	23.40556	98.1795
Renierite	0.030147	13.55143	0.00001	42.33354	3.038687	0.00001	8.905006	0.060703	0.00286	0.727126	0.757792	29.99099	99.3983
	0.01571	13.53386	0.00001	42.20974	3.162746	0.00001	8.713546	0.094824	0.00001	1.295138	0.700733	29.5561	99.28244
	0.00001	13.38294	0.00001	44.29301	2.778073	0.00001	8.635705	0.159332	0.00001	0.361086	0.681095	31.4336	101.7249
	0.00001	13.27009	0.00001	44.34654	3.044261	0.007983	8.312526	0.109656	0.00001	0.00001	0.733184	31.22538	101.0497
	0.00001	12.92612	0.00001	44.21525	3.155764	0.00001	8.958414	0.041529	0.00001	1.156277	0.623283	31.02412	102.1008

E.2. Tsumeb data

Signals Used for samples: Ni Ka, Fe Ka, Co Ka, Cu Ka, Zn Ka, Ga Ka, Ge Ka, Ag La, In La, Pb La, As Kb, As Kb, As La, As La, S Ka.
Spectromers Conditions: Sp5 LLIF, Sp5 LLIF, Sp5 LLIF, Sp5 LLIF, Sp3 LLIF, Sp3 LLIF, Sp3 LLIF, Sp1 PET, Sp1 PET, Sp3 LLIF, Sp5 LLIF, Sp3 LLIF, Sp4 TAP, Sp2 TAP, Sp1 PET
Full Spectromers Conditions: Sp5 LLIF(2d= 4.0267,K= 0.000058), Sp5 LLIF(2d= 4.0267,K= 0.000058), Sp5 LLIF(2d= 4.0267,K= 0.000058), Sp5 LLIF(2d= 4.0267,K= 0.000058), Sp3 LLIF(2d= 4.0267,K= 0.000058), Sp3 LLIF(2d= 4.0267,K= 0.000058), Sp3 LLIF(2d= 4.0267,K= 0.000058), Sp1 PET(2d= 8.75,K= 0.000144), Sp1 PET(2d= 8.75,K= 0.000144), Sp3 LLIF(2d= 4.0267,K= 0.000058), Sp5 LLIF(2d= 4.0267,K= 0.000058), Sp3 LLIF(2d= 4.0267,K= 0.000058), Sp4

TAP(2d= 25.745,K= 0.00218), Sp2 TAP(2d= 25.745,K= 0.00218), Sp1 PET(2d= 8.75,K= 0.000144)
Column Conditions: Cond 1: 15keV -0.001nA

Original weight percent data from Tsumeb samples

Table 5: Original weight percent data from selected minerals for sample 253 a.

Sample 253a													
Phase	**Ni**	**Fe**	**Co**	**Cu**	**Zn**	**Ga**	**Ge**	**Ag**	**In**	**Pb**	**As**	**S**	**Total**
Galena	0.00001	0.03355	0.009237	0.044538	0.00001	0.069318	0.280405	0.025122	0.00001	80.0195	0.021606	12.32711	92.83042
	0.00001	0.00001	0.004463	0.05283	0.042223	0.007092	0.062613	0.003593	0.051608	82.24863	0.00001	12.55062	95.0237
	0.050105	0.00001	0.021986	0.368677	0.00001	0.071776	0.00001	0.00001	0.057095	78.67733	0.021284	12.33208	91.60036
Unknown	0.019502	0.020178	0.007627	32.24871	0.00001	0.00001	0.018911	0.00001	0.00001	35.77721	0.021455	14.80262	82.91624
	0.004101	0.00001	0.00001	30.09623	0.00001	0.014682	0.00001	0.17157	0.00001	35.9749	0.069363	13.39944	79.73032
	0.009948	0.00001	0.00001	40.5269	0.018609	0.05355	0.00001	0.26933	0.00001	31.10572	0.00001	17.88283	89.86693
Betekhtinite	0.00001	0.00623	0.003903	1.463129	0.009671	0.031176	0.06826	0.055154	0.00001	62.4612	0.00001	0.376441	64.4752
	0.00001	0.00001	0.041456	1.423312	0.00001	0.00001	0.067114	0.144798	0.00001	63.23887	0.00001	0.45698	65.37259
	0.00001	0.00001	0.009963	2.428106	0.048757	0.029981	0.009507	0.103638	0.00001	62.17862	0.00001	0.830037	65.63865
Digenite	0.00001	0.00001	0.00001	0.00001	0.00001	0.011296	0.00001	0.013313	0.016965	0.049472	0.00001	0.003397	0.094513
	0.00596	0.00001	0.00001	0.00001	0.025894	0.015035	0.00001	0.00001	0.00001	0.00001	0.00001	0.00001	0.04698
	0.010146	0.005981	0.00001	0.005935	0.02371	0.018006	0.00001	0.028048	0.022617	0.00001	0.00001	0.00001	0.114493

Table 6: Original weight percent data from selected minerals for sample TS 5.

Sample TS 5													
Phase	**Ni**	**Fe**	**Co**	**Cu**	**Zn**	**Ga**	**Ge**	**Ag**	**In**	**Pb**	**As**	**S**	**Total**
Galena	0.026761	0.008049	0.00001	0.041029	0.254151	0.00001	0.00001	0.067974	0.00001	83.83062	0.00001	11.65683	95.88547
	0.00001	0.00001	0.034593	0.002875	0.322796	0.153042	0.037416	0.053715	0.00001	83.10522	0.00001	11.76226	95.47196
	0.03295	0.00001	0.00001	0.037451	0.422306	0.042456	0.221185	0.00001	0.023633	80.71093	0.012654	11.97039	93.47398
Tennantite	0.00785	2.056137	0.00001	39.72788	5.625813	0.00001	0.00001	0.028682	0.00001	9.446507	13.89864	23.87103	94.66258
	0.035483	2.056777	0.00001	39.09719	5.560575	0.00001	0.096152	0.017914	0.021711	13.90129	13.47998	23.68714	97.95424
	0.00001	2.071744	0.00001	40.18124	5.78394	0.00001	0.034418	0.00001	0.004065	8.015924	14.24648	24.68049	95.01833
Sphalerite	0.03015	0.103828	0.015974	0.265307	62.30761	0.00001	0.01378	0.039967	0.00001	0.660122	0.015932	29.87686	93.32955
	0.024909	0.105538	0.00001	0.092594	62.79965	0.045403	0.00001	0.00001	0.00001	0.00001	0.00001	30.12691	93.19508
	0.016965	0.119914	0.009857	0.068511	61.9366	0.009491	0.183084	0.021809	0.00001	0.00001	0.00001	30.30735	92.67361

Weight percent data adjust by Alexander Ziegler

Table 7: Adjusted weight percent data from selected minerals for sample 253 a.

Sample 253a													
Phase	**Ni**	**Fe**	**Co**	**Cu**	**Zn**	**Ga**	**Ge**	**Ag**	**In**	**Pb**	**As**	**S**	**Total**
Galena	0.00001	0.033428	0.009202	0.044361	0.00001	0.069027	0.279198	0.025061	0.00001	86.53195	0.021504	12.31439	99.32815
	0.00001	0.00001	0.004446	0.052621	0.042053	0.007063	0.062345	0.003585	0.051502	88.83882	0.00001	12.53873	101.6012
	0.049882	0.00001	0.021892	0.367016	0.00001	0.071431	0.00001	0.00001	0.056963	85.12955	0.021169	12.31732	98.03526
Unknown	0.019373	0.020104	0.007606	32.01268	0.00001	0.00001	0.018721	0.00001	0.00001	39.50726	0.021208	14.68215	86.28912
	0.004073	0.00001	0.00001	29.87723	0.00001	0.014531	0.00001	0.17135	0.00001	39.72723	0.068564	13.28885	83.15188
	0.009891	0.00001	0.00001	40.24727	0.018464	0.05305	0.00001	0.269125	0.00001	34.40348	0.00001	17.74934	92.75067
Betekhtinite	0.00001	0.006227	0.003901	1.462527	0.009663	0.031143	0.068189	0.055148	0.00001	68.51809	0.00001	0.376116	70.53104
	0.00001	0.00001	0.041432	1.422626	0.00001	0.00001	0.067041	0.144778	0.00001	69.35103	0.00001	0.456595	71.48357
	0.00001	0.00001	0.009953	2.426172	0.048685	0.029927	0.00949	0.103612	0.00001	68.17223	0.00001	0.828906	71.62901
Digenite	0.00001	0.00001	0.00001	0.00001	0.00001	0.011296	0.00001	0.013313	0.016965	0.049472	0.00001	0.003397	0.094513
	0.00596	0.00001	0.00001	0.00001	0.025894	0.015035	0.00001	0.00001	0.00001	0.00001	0.00001	0.00001	0.04698
	0.010146	0.005981	0.00001	0.005935	0.02371	0.018006	0.00001	0.028048	0.022617	0.00001	0.00001	0.00001	0.114493

Table 8: Adjusted weight percent data from selected minerals for sample TS 5.

Sample TS 5													
Phase	**Ni**	**Fe**	**Co**	**Cu**	**Zn**	**Ga**	**Ge**	**Ag**	**In**	**Pb**	**As**	**S**	**Total**
Galena	0.026485	0.007972	0.00001	0.040599	0.251447	0.00001	0.00001	0.067536	0.00001	90.4848	0.00001	10.12657	101.0055
	0.00001	0.00001	0.034243	0.002844	0.319317	0.151333	0.036986	0.053365	0.00001	89.73894	0.00001	10.21714	100.5542
	0.032594	0.00001	0.00001	0.037038	0.417589	0.041963	0.218547	0.00001	0.023497	87.24319	0.012489	10.396	98.42294
Tennantite	0.00001	2.147216	0.00001	42.66721	5.635607	0.00001	0.00001	0.058266	0.007296	0.00001	19.69898	31.53912	101.7537
	0.00001	1.923171	0.00001	43.25601	5.650783	0.025563	0.043363	0.080801	0.00001	0.00001	20.71856	28.00053	99.69883
	0.00001	2.122617	0.00001	43.67234	5.61684	0.002233	0.061668	0.011569	0.00001	0.00001	19.54265	27.93793	98.96789
Sphalerite	0.029893	0.103268	0.015868	0.264192	66.96446	0.00001	0.013744	0.03979	0.00001	0.658049	0.015886	29.87221	97.97738
	0.024698	0.104967	0.00001	0.092199	67.4619	0.045256	0.00001	0.00001	0.00001	0.00001	0.00001	30.11801	97.8471
	0.016819	0.119261	0.009791	0.068217	66.54833	0.00946	0.182579	0.021712	0.00001	0.00001	0.00001	30.29838	97.27458

Appendix F

X-Ray Diffraction (XRD)

Samples from both Kipushi and Tsumeb were selected for XRD. A total of 17 samples were sent for analysis to XRD Analytical and Consulting. The rock samples were then pulverised using a Cr-steel milling pot in a swing mill, and underwent the back loading preparation method. Diffractograms were obtained by means of a Malvern Panalytical Aeris diffractometer with a PIXcel detector as well as slits with Fe filtered Co-Kα radiation. The mineral phases were then identified using X'Pert Highscore plus software. The weight % of each phase was determined using the Rietveld method.

Table 1: Various phases detected in samples from Kipushi and Tsumeb, and the weight % of each phase. 0 represents no detection of phase above the detection limit of 0.5 – 3 weight%.

Kipushi	Dolomite	Bornite	Tennantite	Quartz	Renierite	Chalcopyrite	Galena	Sphalerite	Bornite high	Pyrite	Total
1058	0	3.6	5.8	1.9	6.2	14.6	6.1	60	1.9	0	100.1
1213	0	6.5	0.2	8.5	3.4	65.2	0	3.1	10.9	2.3	100.1
12492	0	0	0.8	2	0	97.1	0	0.2	0	0	100.1
12492A	0	84.2	1	13.1	0	0	0	1.8	0	0	100.1
15453	0	7.8	16.8	2.1	0	25.3	0	5.6	42.3	0	99.9
6548	0	2.9	0.3	2.8	4.9	5.8	0	81.1	2.2	0	100
15452	0	8.1	1.1	5.2	0	0.4	0.3	31.1	53.7	0	99.9
586	0	7.1	4	12.8	0	0.3	0.9	21.7	53.2	0	100
KP1	0	13.8	0	0	0	0	0	1.7	81.2	3.3	100
KP11	0	3.8	0	9.4	6.2	0.7	0	76.1	3.9	0	100.1
KP7	87.5	2.9	1	1.4	0	0	0.7	2.3	3.1	1	99.9
S2801	0.8	0	0.4	2.3	0	94.5	0	0.2	0	1.7	99.9

Tsumeb	Dolomite	Bornite	Tennantite	Quartz	Renierite	Chalcopyrite	Galena	Sphalerite	Bornite high	Pyrite	Total
110	0	4.2	5.8	0.4	3.3	0	21.4	57.5	1.1	6.3	100
125	0.6	18.8	0.2	76.9	0.4	0	0.1	0	2.8	0	99.8
340	0	0	0	15.6	0	1.9	72.4	1.8	0	8.2	99.9
477	0	3.7	2.6	13.9	0.1	0.1	9.3	6.4	63.9	0	100
99A	0	1	24.7	12.7	0	0.1	31.8	17.1	4.8	7.8	100

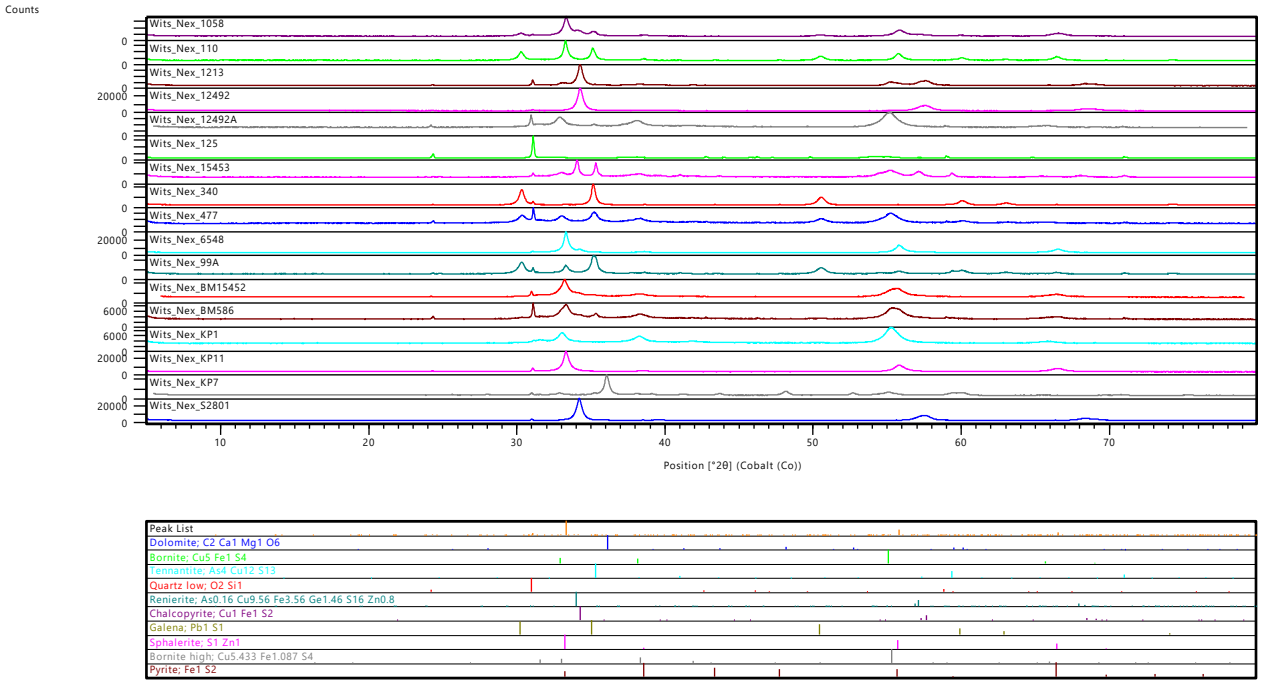

Figure 1: Counts and their position for the detection of each phase for each sample using Co.